

Study of protein-bacteriochlorophyll and
protein-lipid interactions of natural and
model light-harvesting complex 2 in
purple bacterium *Rhodobacter*
sphaeroides

DISSERTATION
DEPARTMENT OF BIOLOGY I
BOTANIC
LUDWIG-MAXIMILIANS-UNIVERSITÄT MÜNCHEN

Submitted
by
Lee Gyan KWA

March 2007

1. Referee: PD. Dr. P. Braun

2. Referee: Prof. Dr. H. Scheer

Date of oral defence: 1 June 2007

Acknowledgements

I am grateful to my supervisor PD. Dr. Paula Braun, who shared her experience in light-harvesting complex with me and for her advice throughout the years and during the preparation of this dissertation.

I would like to express my gratitude to Brigitte Strohmann and Prof. Dr. Hugo Scheer for sharing their expertise with me.

Many thanks to Prof. Dr. Gerhard Wanner (LMU, Biology Department I, Munich) for providing the EM facilities; Dr. Dominik Wegmann and PD. Dr. Britta Brügger (University of Heidelberg, Germany) for the ESI-MS measurements; Dr. Wolfgang Doster and Dr. Ronald Gerhardt (Technical University Munich, Germany) for light scattering and high pressure measurements; Ulrike Oster for her help with the TLC analyses; Silvia Dobler for the EM preparations and Dr. Alexander Pazur for his help with the PS statistical analyses.

Sources of bacteria, Prof. Dr. Neil Hunter (University Sheffield, UK) is gratefully acknowledged.

For fruitful and valuable discussions, I would like to thank my colleagues in the laboratory and institute; who have contributed to this work with their technical advices and their friendships.

My special thanks are devoted to Kee Ping Wee, Han Ting How, Jörg Naydek, Ralf Kaiser, everyone in the small group and in MICC for their wonderful friendship, encouragement and for providing me with their time.

I thank my family and all the people that have supported, encouraged and motivated me over the years.

Thanks to Chong Yew for being the light of my days.

Above all, I give praise to HIM!

Summary

The natural design of the photosystems of plants and photosynthetic bacteria using chlorophylls (Chls) or bacteriochlorophylls (BChls) as photoreceptors are robust. The basic principles of the biological system of light-harvesting complex 2 (LH2) are studied with the use of natural and model sequences expressed *in vivo* in modified *Rhodobacter (Rb) sphaeroides* strains. Three aspects have been explored in the thesis: (1) BChl's macrocycle-protein interactions, (2) BChl's phytol-protein interactions underlying the structural and functional assembly of the pigment-protein complexes, and (3) LH2-lipid interactions and the role of these interactions in photosynthetic membrane morphogenesis.

BChls' macrocycle-protein interactions: Residues at the immediate BChl-B850/protein interface are found to have little effect on specifying the BChl-B850 array, and their light-harvesting activity in LH2. Nevertheless, these residues are important for the structural thermal stability. With the use of 'rescue' mutagenesis of the model BChl binding site, the hydrogen-bond between α Ser -4 and the C13¹ keto carbonyl group of β BChl-B850 is shown to be a crucial motif for driving the assembly of model LH2 complex. Possibilities for residue modifications are limited in the β -subunits as compared to the α -subunits, which suggests that the two polypeptides have distinct roles in complex assembly. In the β -subunits, there are residues detected adjacent to the BChl-B850 site which are critical for the assembly of LH2.

BChls' phytol-protein interactions: Mutagenesis of residues closely interacting with the BChl-B850 phytol moiety result in the pronounced loss of BChl-B800 from LH2. Dephytylation of bound BChls within assembled LH2 to BChlides also resulted in the loss of BChl-B800 and destabilisation of LH2 structural assembly. Thus, the phytol chains were shown to be important for optimal pigment binding, especially for BChl-B800; which appears to be highly sensitive to the proper packing of the phytols. The pattern of phytol interactions with their surrounding environments are significantly different for α - and β -ligated (B)Chls. The phytols of β -ligated (B)Chls, as opposed to α -ligated (B)Chls, have ample and specific

interactions with residues of the binding helix which may contribute to the tertiary interactions of helices.

LH2-lipids interactions: Phospholipid determination of LH2 only expressing strains of *Rb sphaeroides* shows that the nonbilayer-forming phospholipid, phosphatidylethanolamine (PE) is present in elevated amounts in the intracytoplasmic membranes and in the immediate vicinity of the LH2 complex. In combination with β Glu -20 residue and the carotenoid headgroup at the N-terminus of the transmembrane β -helices is shown to influence the composition of lipids surrounding LH2. Specific local interactions between LH2 protein and lipids not only promote LH2 protein stability but appear to modulate the morphology of intracytoplasmic membranes. Based on these findings, the presence of LH2-lipid specificity is postulated.

The approach of using model $\alpha\beta$ -sequences with simplified pigment binding sites allows us to study the underlying factors involved in LH2 assembly and function. This gives rise to a better understanding of the interplay between BChl, apoproteins and membrane lipids in the assembly of a highly efficient light-harvesting complex in its native lipid-environment.

TABLE OF CONTENTS**Chapter 1: Introduction**

1.1	The photosynthetic machinery of purple non-sulphur bacteria	1
1.1.1	<i>Rhodobacter sphaeroides</i> as a model organism for photosynthetic studies	3
1.1.1.1	The characteristic of LH complexes of <i>Rb sphaeroides</i>	4
1.1.1.2	Energy transfer in the photosystem of <i>Rb sphaeroides</i>	6
1.1.1.3	Biogenesis of the photosynthetic membrane of <i>Rb sphaeroides</i>	7
1.2	Purple non-sulphur bacterial light-harvesting complexes	9
1.2.1	Structures of light-harvesting complexes	9
1.2.1.1	The structure of light-harvesting complex 2	10
1.3	Photosynthetic pigments: bacteriochlorophyll and carotenoid	14
1.3.1	Bacteriochlorophylls: structures and functions	14
1.3.1.1	BChl-protein interactions in LH2 complex of <i>Rb sphaeroides</i>	17
1.3.2	Carotenoids: structures and functions	18
1.3.2.1	Carotenoid-protein interactions in LH2 complex of <i>Rb sphaeroides</i>	19
1.4	The photosynthetic membrane in <i>Rb sphaeroides</i>	23
1.4.1	Membrane morphology of <i>Rb sphaeroides</i>	23
1.4.2	Membrane phospholipid composition	24
1.5	Summary and approaches	27
1.5.1	Summary	27
1.5.2	Approaches	28
1.6	Thesis objectives and organisation of chapters	30

Chapter 2: Materials and methods

2.1	Materials	31
2.1.1	Bacterial strains	31
2.1.2	Plasmids and vectors	32
2.1.3	Buffers and solutions	32
2.1.4	Column materials and solutions	35
2.1.5	Enzymes, chemicals and kits	35
2.1.5.1	Antibiotics	35
2.1.5.2	Phospholipids	36
2.1.5.3	Markers	36
2.1.5.4	Others	36
2.1.6	Technical devices	37
2.1.6.1	Centrifugation	37
2.1.6.2	Spectrophotometers	37
2.1.6.3	Others	37
2.2	Methods	38
2.2.1	Media and growth conditions	38
2.2.2	General molecular biological methods	38
2.2.3	Mutagenesis	38
2.2.3.1	Primers design	39
2.2.3.2	Polymerase chain reaction (PCR)	39
2.2.4	Agarose gel electrophoresis	40
2.2.5	Conjugation	40
2.2.6	Bacterial cultivation	41
2.2.7	LH2 intracytoplasmic membrane isolation	41
2.2.8	LH2 isolation	42
2.2.9	Sodium dodecyl sulphate polyacrylamide (SDS-PAGE) gels	43
2.2.10	Chlorophyllase experiment	44
2.3	Analytical methods	45
2.3.1	Absorption spectroscopy	45
2.3.2	Electron microscopy (EM) analysis	45

TABLE OF CONTENTS

2.3.3	Electrospray ionization mass spectroscopy (ESI-MS)	45
2.3.4	Circular dichroism (CD) spectroscopy	47
2.3.5	Fluorescence spectroscopy	48
2.3.6	Protein quantification	48
2.3.7	Thin layer chromatography (TLC)	48
2.3.7.1	Phospholipids extraction	49
2.3.8	Statistic analysis of pigment-protein interactions in PSI	49
2.3.9	Structural modelling	49
2.3.10	Websites	50
 RESULTS		
PART I: Protein-bacteriochlorophyll interactions in model and native light-harvesting complex 2		
Chapter 3: Bacteriochlorophylls' macrocycle-protein interactions underlying LH2 assembly and function		
3.1	Introduction	53
3.2	Results and discussion	60
	Simplification of the BChl-B850 binding site: model sequences in the TMH of the β -subunit	60
	Design of the model LH2 α WT/ β AL	60
	The functional and structural characteristics of α WT/ β AL	61
	Study of interaction motifs at the model and native BChl-protein interface: H-bonding between the hydroxyl of serine and the keto carbonyl of BChl-B850	66
	H-bond donor residue at position -4 of α -subunit	67
	H-bond donor residue at position -4 of β -subunit	71
3.3	Conclusions	77

Chapter 4: Bacteriochlorophylls' phytol chain-protein interactions underlying LH2 assembly and function		
4.1	Introduction	79
4.2	Results and discussion	84
	Study of the role of BChls phytol by mutating protein binding residues	84
	Removal of the BChl phytol tails in assembled LH2 by enzymatic digestion	96
	Statistical analyses of α - and β -ligated (B)Chls	103
	Analysis of phytol-protein interactions in PSI	106
	Analysis of phytol-amino acid contacts	108
 PART II: Protein-lipid and pigment-lipid interactions in model and native light-harvesting complex 2		
Chapter 5: Study of the relationship between <i>Rb sphaeroides</i> LH2 protein-phospholipids interactions and ICM morphology		
5.1	Introduction	117
5.2	Results and discussion	128
	Study of the relationship between LH2 and ICM morphology	128
	Phospholipid composition of <i>Rb sphaeroides</i> expressing LH2 WT and model LH2 α AL _{S-4} / β AL	132
	Phospholipid headgroup compositions	132
	Phospholipid hydrocarbon chain compositions	134
	Phospholipid composition of <i>Rb sphaeroides</i> LH2 WT depending on temperature	137
	Phospholipid headgroup compositions	137
	Phospholipid hydrocarbon chain compositions	138

Phospholipid composition of isolated LH2 complex	140
Phospholipid headgroup compositions	140
Phospholipid hydrocarbon chain compositions	141
Study of the molecular interactions between LH2 complex and PE	144
Point mutation of β Glu -20: effects on LH2 protein	148
Modification of carotenoid's polar group and/or β Glu -20: effects on LH2 protein	150
Effects of delipidation on LH2 WT and β Glu -20 complexes	153
Membrane protein contents	155
Phospholipid composition of <i>Rb sphaeroides</i> expressing LH2 WT or LH2 α WT/ β WT _{-20A} in DD13 and DG2 strains	156
Phospholipid headgroup compositions	156
Phospholipid hydrocarbon chain compositions	158
Phospholipid composition of isolated DD13 α WT/ β WT _{-20A}	161
Modifications of ICM morphology in mutants DD13 α AL _{S-4} / β AL and α WT/ β WT _{-20A}	164
5.3 Conclusions	167

Chapter 6: Discussion

Part I: Protein-bacteriochlorophyll interactions in model and native light-harvesting complex 2

Bacteriochlorophylls' macrocycle-protein interactions underlying LH2 assembly and function (Chapter 3)

Simplification of the BChl-B850 binding site: model sequences in the TMH of the β -subunit	170
Putative H-bonding between β Ser -4 and α BChl-B850	172

Bacteriochlorophylls' phytol chain-protein interactions underlying LH2 assembly and function (Chapter 4)	176
Study of the role of BChls phytol by mutating protein binding residues	176
Removal of BChl phytol tails in assembled LH2 by enzymatic digestion	178
Statistical analyses of α - and β -ligated (B)Chls	180
 Part II: Protein-lipid and pigment-lipid interactions in model and native light-harvesting complex 2	
 Study of the relationship between <i>Rb sphaeroides</i> LH2 protein-phospholipids interactions and ICM morphology (Chapter 5)	182
 Additional notes	192
 References	195
 Appendices	
 Curriculum vitae	

LIST OF FIGURES

(Titles abbreviated)

Chapter 1

Figure 1-1	Schematic illustration of a photosystem	3
Figure 1-2	Model for the organisation of the bacterial photosystem	5
Figure 1-3	Schematic representation of the sequence of morphological changes in the CM and ICM	8
Figure 1-4	Schematic presentation of LH2 complex	12
Figure 1-5	Typical absorbance spectrum of LH2	13
Figure 1-6	Bacteriochlorophyll <i>a</i> structure	15
Figure 1-7	Carotenoid biosynthesis pathway	20
Figure 1-8	Carotenoid absorption spectra	22
Figure 1-9	Chemical structures of carotenoids	22
Figure 1-10	Schematic representation of how lipid shapes affect their curvature preferences	25

Chapter 2

Figure 2-1	<i>Rb sphaeroides</i> culture	41
Figure 2-2	Sucrose gradient	41
Figure 2-3	SDS-PAGE gel	43
Figure 2-4	Negative ion mass spectrum	47

Chapter 3

Figure 3-1	Structure of BChl <i>a</i>	55
Figure 3-2	Illustration of the elementary subunit of LH2 complex	57
Figure 3-3	Model LH2 α WT/ β AL	61
Figure 3-4	Absorption and CD spectra of LH2 WT and α WT/ β AL	62
Figure 3-5	Fluorescence excitation spectra of LH2 WT and α WT/ β AL	64
Figure 3-6	Thermal denaturation spectra of LH2 WT and α WT/ β AL	64
Figure 3-7	Schematic illustration of model LH2	66
Figure 3-8	Thermal denaturation of LH2 α WT/ β AL, α AL/ β WT and	

	α AL _{S-4} / β WT	68
Figure 3-9	Resonance Raman spectra of LH2 WT and α WT _{-4A} / β WT	69
Figure 3-10	Critical role of α Ser -4 in model LH2 assembly and stability	71
Figure 3-11	Amino acid alignment of TMH of β -subunits	72
Figure 3-12	Putative H-bonding between α - and β -serine -4 and keto carbonyl group of BChl-B850	74
Figure 3-13	LH2 assembly and stability of LH2 WT and α WT/ β AL _{-4S}	75
Chapter 4		
Figure 4-1	Isoprenoid esterifying alcohols of (B)Chls	80
Figure 4-2	The initial step of Chl degradation	80
Figure 4-3	NIR absorption spectra of LH2 WT, α WT/ β AL, α WT/ β AL _{-7A} and α WT/ β AL _{-9A}	84
Figure 4-4	Contacts between BChls' phytols and -7 and -9 residues of β -subunits	85
Figure 4-5	Absorption and fluorescence excitation spectra of LH2 WT, α WT/ β WT _{-9A} and α WT/ β WT _{-7-9A}	87
Figure 4-6	CD and thermal denaturation spectra of LH2 WT, α WT/ β WT _{-9A} and α WT/ β WT _{-7-9A} chromatophores	89
Figure 4-7	CD and thermal denaturation spectra of isolated LH2 WT, WT/ β WT _{-9A} and α WT/ β WT _{-7-9A}	91
Figure 4-8	Contacts between the phytol of β BChl-B850 and its surrounding molecules	94
Figure 4-9	NIR absorption spectra of isolated LH2 WT in acetone	97
Figure 4-10	NIR absorption spectra of isolated LH2 WT with Chlase	98
Figure 4-11	Optical densities of BChl-B850 and -B800 during 120 minutes of incubation	99
Figure 4-12	TLC of LH2 pigment	100
Figure 4-13	CD and thermal denaturation spectra of Chlase treated and non-treated isolated LH2 WT	101
Figure 4-14	The α - and β -diastereoisomers of (B)Chls	105

Figure 4-15	Analysis of contacts of the α - and β -ligated (B)Chl's phytyl and protein environment	106
Figure 4-16	Distribution of amino acids residues around the Chl's phytyl chains in PSI	109
Figure 4-17	The contacts between α -ligated Chls' phytol moieties and amino acid residues within a radius of ≤ 5 Å in PSI	112
Figure 4-18	The contacts between β -ligated Chls' phytol moieties and amino acid residues within a radius of ≤ 5 Å in PSI	112
Chapter 5		
Figure 5-1	General depiction of 3 types of amphipathic phospholipids molecules	118
Figure 5-2	Illustration of the spatial relationship between lipids and integral membrane proteins	119
Figure 5-3	Phospholipid biosynthetic pathway in bacteria	121
Figure 5-4	ICM of <i>Rb sphaeroides</i> harbouring the bacterial photosystems	123
Figure 5-5	Major phospholipids in <i>Rb sphaeroides</i>	125
Figure 5-6	Functional assembly of DD13 WT and α AL _{S-4} / β AL	130
Figure 5-7	Comparison of the ultrastructure of <i>Rb sphaeroides</i> cells	131
Figure 5-8	Relative changes in percentage of fatty acids in PE of α AL _{S-4} / β AL and DD13 WT	135
Figure 5-9	Comparison of phospholipid composition in <i>Rb sphaeroides</i> cells containing LH2 WT at different growth temperature	138
Figure 5-10	Changes of PC and PE fatty acyl compositions at different temperatures	139
Figure 5-11	Relative changes of fatty acids in PE of isolated LH2 and DD13 WT cells	142
Figure 5-12	Alignment of β -subunits	145
Figure 5-13	Schematic illustration of β Glu -20 interacts with its surrounding lipid environment	146
Figure 5-14	Illustration of LH2 protein-lipid interface	147

Figure 5-15	Absorption, CD and fluorescence excitation spectra of DD13 -20 mutants	148
Figure 5-16	Thermal denaturation spectra of DD13 -20 mutants	149
Figure 5-17	Modelling of the interactions of β Glu -20 with carotenoid	150
Figure 5-18	Chemical structures of carotenoids	151
Figure 5-19	Absorption, CD and fluorescence excitation spectra of DG2 -20 mutants	152
Figure 5-20	Thermal denaturation spectra of DG2 -20 mutants	152
Figure 5-21	Thermal denaturation spectra of isolated LH2 WT and α WT/ β WT _{-20A} in DD13 and DG2 strains	154
Figure 5-22	Ultrastructure of bacterial cells	166
 Chapter 6		
Figure 6-1	NIR absorbance spectra of LH2 WT and model complexes	173
Figure 6-2	Modelling of putative H-bonding between α BChl-B850 C13 ¹ keto carbonyl group and β His 0 and β Ala -4	174
Figure 6-3	Illustration of interactions between β BChl-B850 and BChl-B800	178
Figure 6-4	Illustration of LH2 protein-lipid interface	187

LIST OF TABLES

(Titles abbreviated)

Chapter 1

Table 1-1	Major absorption maxima of chlorins	16
-----------	-------------------------------------	----

Chapter 2

Table 2-1	Buffers and solutions	32
Table 2-2	Column materials and solutions for LH2 isolation	35
Table 2-3	Antibiotics and their concentrations	35

Chapter 3

Table 3-1	Amino acid sequences of model LH2 used in Chapter 3	78
-----------	---	----

Chapter 4

Table 4-1	Alignment of amino acid sequence of β -polypeptides	86
Table 4-2	Contacts of BChls' phytol within LH2 complex	93
Table 4-3	List of residues within ≤ 5 Å in PSI of the α -ligated Chl phytol tail	110
Table 4-4	List of residues within ≤ 5 Å in PSI of the β -ligated Chl phytol tail	111
Table 4-5	Amino acid sequences of model LH2 used in Chapter 4	114

Chapter 5

Table 5-1	Percentage of phospholipids of DD13, DD13 WT and α AL _{S-4} / β AL	133
Table 5-2	PE fatty-acyl chain length of DD13, DD13 WT and α AL _{S-4} / β AL	135
Table 5-3	Phospholipid composition of LH2 WT and DD13 WT	140
Table 5-4	PE fatty-acyl chain length of DD13 WT	142
Table 5-5	PC fatty-acyl chain length of DD13 WT	143
Table 5-6	Comparison of total protein concentrations of LH2 WT and	

	mutants	155
Table 5-7	Percentage of major phospholipids of LH2 WT and α WT/ β WT _{-20A} in DD13 and DG2 strains	157
Table 5-8	PE fatty-acyl chain length of LH2 WT and α WT/ β WT _{-20A}	158
Table 5-9	PC fatty-acyl chain length of LH2 WT and α WT/ β WT _{-20A}	159
Table 5-10	Percentage of major phospholipids of isolated LH2 WT and α WT/ β WT _{-20A}	161
Table 5-11	PE fatty-acyl chain length of isolated LH2 WT and α WT/ β WT _{-20A}	162
Table 5-12	Summary of LH2 vesicles ultrastructure in WT and mutants	165
Table 5-13	Amino acid sequences of model LH2 used in Chapter 5	168
Chapter 6		
Table 6-1	Summary of LH2 and α WT/ β WT _{-20A} thermal stabilities and phospholipids compositions	188

ABBREVIATIONS AND UNITS

Å	Ångström
ADP	Adenosin diphosphate
APS	Ammonium persulphate
ATP	Adenosin triphosphate
ATPase	ATP synthase
a.u.	Arbitrary unit
(B)Chl	(Bacterio)chlorophyll
BChlide	Bacteriochlorophyllide
BSA	Bovine serum albumin
bp	Base pairs
CD	Circular dichroism
Chlase	Chlorophyllase
CL	Cardiolipin
DEAE	Diethylaminoethyl
DNA	Deoxyribonucleic acid
DNase	Deoxyribonuclease
dNTP	Deoxynucleotide triphosphate
ds	Double stranded
<i>E. coli</i>	<i>Escherichia coli</i>
EDTA	Ethylendiamine tetraacetate
ESI-MS	Electrospray ionisation mass spectroscopy
FMO	Fenna Matthews Olson
g	Gramm (analogously: mg and µg)
H-bond	Hydrogen-bond
ICM	Intracytoplamic membrane
kb	Kilobase
kDa	KiloDaltons
Km ^R	Kanamycin resistance
l	Liter (analogously: ml and µl)
LHC	Light-harvesting complex

M	mol·l ⁻¹ (analogously: mM, μM and nM)
Mdeg	Millidegree
MGDG	Monogalactosyl diglyceride
MHz	Megahertz
MS	Mass spectroscopy
MW	Molecular weight
m/z	Mass per charge
n.d.	Not detected
NIR	Near infrared
nm	Nanometre
NMR	Nuclear magnetic resonance
OD	Optical density
P _i	Inorganic phosphate
PCR	Polymerase chain reaction
PC	Phosphatidylcholine
PDB	Protein data bank
PE	Phosphatidylethanolamine
PG	Phosphatidylglycerol
PL	Phospholipid
PSI	Photosystem I
Rb	Rhodobacter
RC	Photosynthetic reaction centre
Rps	Rhodopseudomonas
Rsp	Rhodospirillum
SDS-PAGE	Sodium dodecyl sulphate polyacrylamide gel electrophoresis
Sm ^R	Streptomycin resistance
Tc ^R	Tetracycline resistance
TEMED	N, N, N', N'-Tetramethylethylenediamine
TLC	Thin layer chromatography
T _m	Mid-point of denaturation transition
TMH	Transmembrane helix
Tris	Tris-hydroxymethylaminomethane

ABBREVIATIONS AND UNITS

TritonX-100	Alkylphenyl polyethylenglycol
v/v	Volume / volume
w/v	Weight / volume
WT	Wild type
β OG	n-octyl- β -D-glycopyranoside
ϵ	Extinction coefficient ($M^{-1}\cdot cm^{-1}$)

CHAPTER 1

INTRODUCTION

Photosynthesis is the fundamental process for the production of biomass on Earth and oxygen is released as a by-product. During the process, solar energy is captured and converted into useful chemical energy which most living forms on Earth depend on. Naturally, it is vital to understand this process, and apply this knowledge for the benefit of our global environment.

1.1 The photosynthetic machinery of purple non-sulphur bacteria

Photosynthesis is carried out in plants, algae and photosynthetic bacteria. The primary processes of photosynthesis involve absorption of photons by light-harvesting complexes (LHC), transfer of excitation energy from LHC to the photosynthetic reaction centres (RCs), and the primary charge separation across the photosynthetic membrane (Fleming & van Grondelle, 1997; van Grondelle *et al.*, 1994).

Generally, photosynthetic organisms are grouped into two classes, oxygenic and anoxygenic. The general principles of energy transduction are similar in both the types. Photosynthesis in eukaryotic plant organisms and cyanobacteria is oxygenic, i.e. water is used as an electron donor and oxygen is generated during the process. They contain two photosystems (PS); each is an assembly of RC and LH complexes which contain chlorophylls and carotenoids (Cogdell *et al.*, 1996; Prince *et al.*, 1997; Scheuring *et al.*, 2004b). The two PS work in tandem within chloroplast (or membrane-bound organelles), thus making the eukaryotes capable of splitting water and producing oxygen.

Most prokaryotic photosynthetic organisms contain only one PS; they are anoxygenic, i.e. they do not produce oxygen during the photosynthetic process. The anoxygenic photosynthetic apparatus does not reside within distinct organelles but within invaginations of the inner membranes. Prokaryotic photosynthetic organisms are divided into six different groups: heliobacteria, green sulphur and non-sulphur bacteria, purple sulphur and non-sulphur bacteria and cyanobacteria. The latter group, the cyanobacteria, operate oxygenic photosynthesis and have eukaryotic-like photosynthetic properties, similar to those found in higher plants and green algae.

Prokaryotic photosynthetic organisms use molecules such as hydrogen (H_2), hydrogen sulphide (H_2S), sulphur (S) and organic molecules as an electron source. Purple non-sulphur bacteria (*Rhodospirillaceae*) have been subdivided from purple sulphur bacteria (*Chromatiaceae*) based on their electron donors for carbon dioxide (CO_2) reduction (Imhoff, 1995). Purple non-sulphur bacteria are unable to oxidise sulphides and are intolerant to high concentration of H_2S ; they use organic molecules such as succinate or malate as their electron source (Imhoff, 1995).

In all photosynthetic organisms, the photosynthetic process involves LHC in which the light is harvested by (bacterio)chlorophylls ((B)Chls) and carotenoids. These pigments funnel the excited-state energy down a “gradient” to the RC. In the RC, the primary charge separation is achieved across the membrane and a cyclic electron transport chain is formed. Ultimately, this results in the production of adenosine triphosphate (ATP) that is used to fuel cellular processes (figure 1-1).

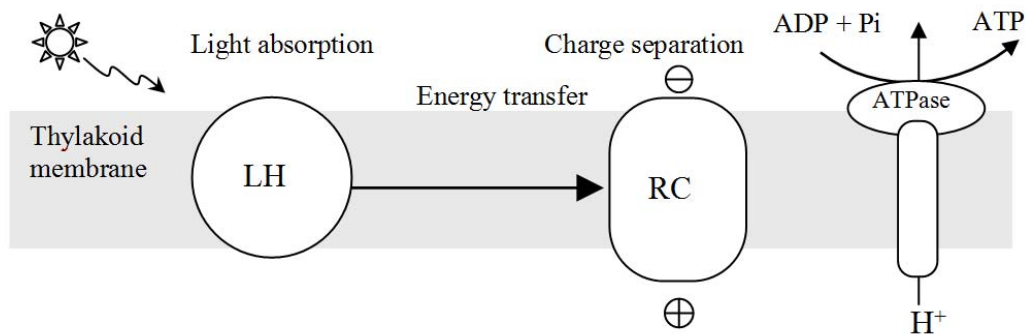


Figure 1-1: Schematic illustration of the photosynthetic process and production of ATP. The photosystem consists of LH which harvests light and transfers excitation energy to the RC. In turn, this energy is used to create a charge separation which is harnessed for ATP generation. The pill shape represents polypeptides which either span the membrane or are soluble.

1.1.1 *Rhodobacter sphaeroides* as a model organism for photosynthetic studies

Purple non-sulphur bacteria such as *Rhodobacter (Rb) sphaeroides*, *Rb capsulatus*, *Rhodospseudomonas (Rps) viridis* and *Rps acidophila* have been the source of intensive study of photosynthesis due to their relatively simple structure and handling procedures (Cogdell *et al.*, 2003; Geyer & Helms, 2006). Their light-harvesting systems function by using only one major type of bacteriochlorin-photopigment and the resonance absorption bands arising from these chromatophores are well-resolved. The pigments of different LH complexes can be excited independently by light and thus transfer of the excitation energy from one LHC to another can be conveniently studied. These characteristics have made the bacterial systems relatively straightforward and an ideal model to study photosynthesis. The photosynthetic apparatus of bacteria can therefore be regarded as a “natural model system”.

The good genetic accessibility of some of the purple non-sulphur bacteria allowed the production of mutant strains. There are deletion mutants deficient in one, two or three pigment-proteins (e.g. Coleman & Youvan, 1990; Jones *et al.*, 1992; Fowler *et al.*, 1995). The potential to construct ‘partial’ photosystems has made valuable

contributions to advancing our knowledge of assembly and function of the photosynthetic systems (for details see Hunter, 1995).

Rb sphaeroides is one of the most studied photosynthetic organisms. It belongs to the gram-negative bacteria of the Proteobacteria group (Verméglio & Joliot, 1999) and has been renamed from *Rhodospseudomonas sphaeroides* (Imhoff *et al.*, 1984). This bacterium possesses an extensive range of metabolic capabilities and can switch between aerobic respiration, anaerobic respiration, fermentation and anoxygenic photosynthesis depending on external triggers which can be activated under laboratory conditions (Kiley & Kaplan, 1988).

In my thesis, *Rb sphaeroides* is used as a model system for the study of photosynthesis; in particular, its light-harvesting machinery. The following sections introduce the light-harvesting machinery and its individual components.

1.1.1.1 The characteristic of LH complexes of *Rb sphaeroides*

The PS of *Rb sphaeroides* is composed of two light-harvesting complexes with varying spectral characteristics and a particular structural organisation (Hu *et al.*, 2002; Scheuring *et al.*, 2004a, 2004b) (figure 1-2). The assembly of the components is highly organised to ensure the efficiency of light harvesting and energy transfer. The first type of light-harvesting antenna complex is designated LH1; it has a single strong near-infrared (NIR) BChl *a* absorption band at 875 nm, therefore also known as B875 antenna complex. BChl *a* in LH1 occurs in a fixed stoichiometry with the RC at a constant molar ratio of ~25:1 (Cogdell *et al.*, 1996, 2003). A core-complex is formed with the RC in the middle of an LH1 antenna ring (Miller, 1979). This core complex is present in all purple bacteria species studied so far (Cogdell *et al.*, 1996). Hitherto, all LH1 structures which have been studied at sufficiently high resolution exhibit 16 paired $\alpha\beta$ -apoproteins in circular arrangement (Karrasch *et al.*, 1995; Roszak *et al.*, 2003).

The second type of LHC is designated LH2. LH2 is not present in all purple non-sulphur bacteria, for example, they are absent in *Rhodospirillum (Rsp) rubrum* and *Rps viridis* (Sistrom, 1978; Stark *et al.*, 1984). Typically LH2 has two strong NIR absorption peaks at 800 nm and 850 nm; therefore it is also known as B800-850 antenna complex. LH2 is also known as the peripheral light-harvesting complex. It is not in direct contact with the RC but transfers energy to RC via LH1 (van Grondelle *et al.*, 1994). In contrast to LH1, LH2 does not occur in a fixed stoichiometry with the RC; instead, the amount of LH2 in the membrane depends on the growth conditions such as temperature and light intensity (Zuber & Cogdell, 1995; Cogdell & Lindsay, 2000). The variable content of LH2 allows the bacteria to regulate the size of their photosynthetic unit and optimise their light harvesting capacity to adapt to the prevailing light intensity. During low illumination, the amount of LH2 can increase to three times the amount of LH1 (Cogdell & Hawthornthwaite, 1993). LH2 structures are also constructed differently from LH1 and exhibit a smaller ring arrangement than LH1; approximately half of LH1's ring size (see section 1.2).

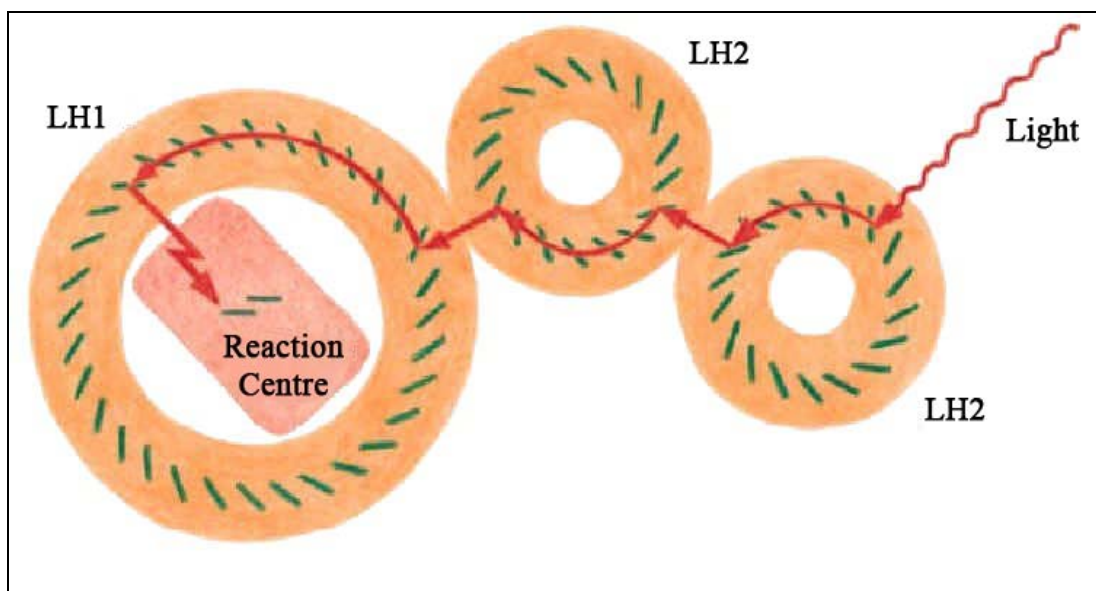


Figure 1-2: Model for the organisation of the bacterial photosystem in the plane of membrane. The small donut shape represents the LH2 rings with BChl-B850 molecules within the rings in green colour. The bigger donut represents LH1 rings with BChl-B875 and RC in the middle. The light capturing pathway from LH2 to RC is illustrated (figure is taken from Branden & Tooze, 1999).

1.1.1.2 Energy transfer in the photosystem of *Rb sphaeroides*

In the bacterial PS of *Rb sphaeroides*, the direction of energy transfer is determined by an energy gradient in the absorption maxima of the light-harvesting active BChl. The direction is from LH2 to LH1 (B800→ B850→ B875) and then to the RC (figure 1-2). In this process, the light-harvesting system acts as a ‘funnel’ to capture excitation energy and transfer it to RC with more than 95 % efficiency and little energy dissipation (Fleming & van Grondelle, 1997; Verméglio & Joliot, 1999; Sundström *et al.*, 1999; Schubert *et al.*, 2004). Within the LH2 complex, the excited energy is absorbed and transferred by the light-harvesting pigments, carotenoids and bacteriochlorophylls. The energy is absorbed and transferred from carotenoids to BChl-B800, alternatively to BChl-B850 and subsequently from BChl-B800 to BChl-B850 molecules. The whole process occurs in picoseconds time frame ($<10^{-10}$ s) (Kennis *et al.*, 1996; Cogdell & Lindsay, 2000; MacPherson *et al.*, 2001; Ritz *et al.*, 2001) (see section 1.2).

The high efficiency of energy transfer is governed by parameters such as the distance between pigments, the relative geometric arrangement of the transition dipole moments of the pigments, the excited state lifetimes, and the spectral overlap between the fluorescence emissions of the donor pigment with the absorption of the acceptor pigment (Law *et al.*, 2004; Scheuring *et al.*, 2004b). Evidently, these parameters are highly dependent on the interactions between the pigments and the protein scaffold (Hess *et al.*, 1995; Freer *et al.*, 1996). Studying the underlying principles of the arrangements of photopigments within the protein complex is vital for our understanding of light-harvesting.

1.1.1.3 Biogenesis of the photosynthetic membrane of *Rb sphaeroides*

In the presence of oxygen, the *Rhodobacter* cells tend to be unpigmented and have a smooth cell membrane morphologically similar to most other gram-negative bacteria (Drews & Oelze, 1981; Chory *et al.*, 1984). When *Rhodobacter* is grown photoheterotrophically using organic compounds as both the carbon and the reducing source, without the presence of oxygen, the bacteria switches to photosynthetic mode and develops the photosynthetic apparatus *de novo* (Cohen-Bazire *et al.*, 1959; Kiley & Kaplan, 1988).

Formation of the photosynthetic apparatus involves the synthesis and assembly of LHC and RC together with the emergence of a third membrane (Chory *et al.*, 1984). This third membrane, the intracytoplasmic membrane (ICM), is distinct from the cytoplasmic membrane and the outer membrane. The photosynthetic apparatus and activities are housed within the ICM, which are invaginations of the CM (Lascelles & Szilagyi, 1965; Lascelles, 1968; Niederman *et al.*, 1976; Drews & Oelze, 1981) (figure 1-3). Thereby, the surface of membrane available for use by membrane-bound energy-yielding machineries is increased, similar to the enlargement of the thylakoid membranes in chloroplasts. The interior of ICM is accessible from the periplasmic space while the exterior is in contact with the cytoplasm (Francis & Richards, 1980; Sturgis & Niederman, 1996). The developmental changes of these photosynthetic membranes are tightly regulated and respond to environmental conditions such as oxygen tension, temperature and light intensity (Sistrom, 1978; Evans, 1989).

The formation of ICM is affected not only by these external factors but also by additional factors such as the pigment-proteins complexes. Mutants that are devoid of one or more of the pigment-protein complexes (Hunter *et al.*, 1988) and mutants with repressed BChl *a* or carotenoid (Penfold & Pemberton, 1994) have shown an alteration in their ICM morphology. The specialised photosynthetic membrane and pigment-protein components are dependent on each another and interact together to build the highly efficient photosystem. Exactly how these two components interact and influence membrane morphology is not fully understood.

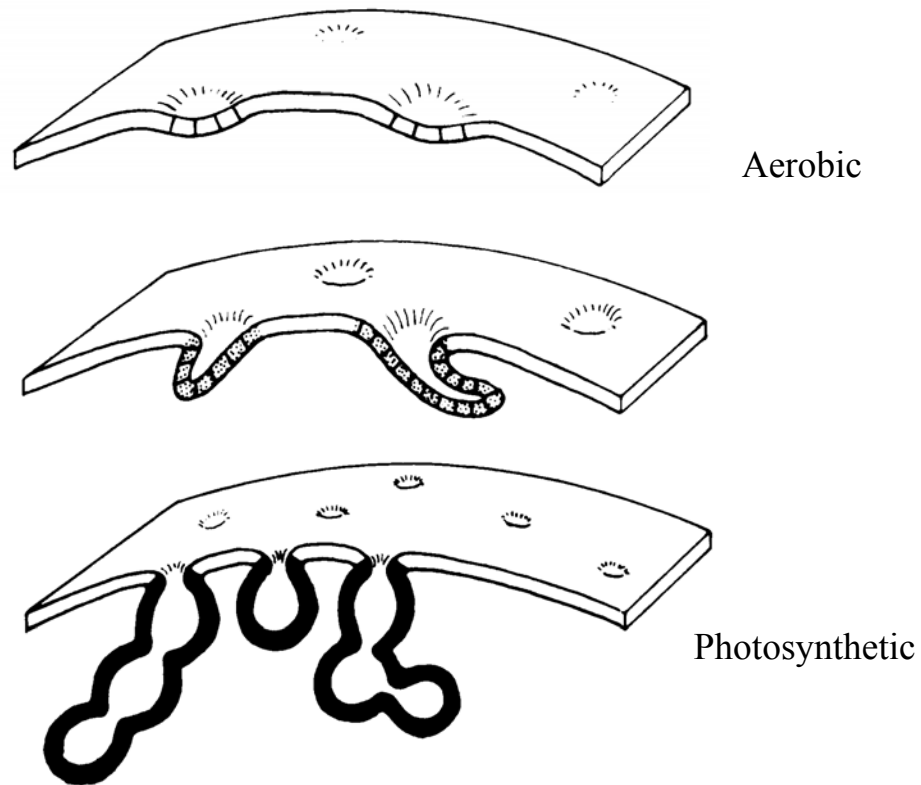


Figure 1-3: Schematic representation of the sequence of morphological changes in the CM and ICM of *Rb sphaeroides* when aerobic cells are shifted to anaerobic conditions. The process of ICM induction is shown as progressing from the assembly of small tubular membrane to fully mature ICM invagination present in the photosynthetic cells. The location of the photosynthetic machinery is indicated by the bold lines (figure is adapted from Chory *et al.*, 1984).

1.2 Purple non-sulphur bacterial light-harvesting complexes

1.2.1 Structures of light-harvesting complexes

The understanding of membrane proteins in general and in particular, of the photosynthetic ones was greatly enhanced with the resolution of the structure of bacterial RC from *Rps viridis*ⁱ at 3.0 Å (Deisenhofer *et al.*, 1985). The RC structure was not only the first X-ray crystallographic determination of the structure of an integral membrane protein but was also the first to reveal the structural basis of the primary photochemical redox reaction. This was followed by a burst of high-resolution crystal structures of transmembrane proteins which includes the RC structure of *Rb sphaeroides* (Chang *et al.*, 1986; Allen *et al.*, 1987; Ermler *et al.*, 1994), the atomic structures of LH1 *Rsp rubrum* (Karrasch *et al.*, 1995; Jamieson *et al.*, 2002) and *Rps palustris* (Roszak *et al.*, 2003) and high-resolution structures of LH2 (*Rps acidophila*, McDermott *et al.*, 1995; Papiz *et al.*, 2003) and *Rsp molischianum*ⁱⁱ (Koepke *et al.*, 1996) (for review, see Fyfe & Cogdell, 1996; Cogdell *et al.*, 2003).

Apart from crystal structure determinations, the basic structure of photosystems and its individual components have also been elucidated by techniques such as cryo-electron microscopy (Kühlbrandt *et al.*, 1994; Koepke *et al.*, 1996; Walz *et al.*, 1998; Jungas *et al.*, 1999), atomic force microscopy (AFM) (Scheuring *et al.*, 2001, 2003, 2004a, 2004b; Bahatyrova *et al.*, 2004) and nuclear magnetic resonance (NMR) (Kikuchi *et al.*, 1999; Conroy *et al.*, 2000; Sorgen *et al.*, 2002).

The availability of these novel methods has not only confirmed some of the early biophysical evidences of pigment proteins (Cogdell *et al.*, 1983; Robert & Lutz, 1985) but also enhanced the progress in structural, genetic and other biochemical studies about the organisation of protein complexes within the photosynthetic membrane.

ⁱ *Rhodopseudomonas viridis* has been renamed *Blastochloris viridis* (Hiraishi, 1997).

ⁱⁱ *Rhodospirillum molischianum* has been renamed *Phaeospirillum molischianum* (Imhoff *et al.*, 1998).

However, as the former names have been widely used; for the convenience of readers, the former names are used in the thesis.

All known LH complexes of purple bacteria are constructed on the same modular design (Zuber & Brunisholz, 1991; Zuber & Cogdell, 1995). Both the LH2 and LH1 antenna complexes display a similar ring-shaped architecture with the peptides and pigments cyclically arranged (Cogdell *et al.*, 1996; Prince *et al.*, 1997). The elementary unit is a heterodimer of two very short hydrophobic polypeptides (α and β) with 50 to 60 amino acids each and to which the pigments (bacteriochlorophylls and carotenoids) are non-covalently attached. The number of $\alpha\beta$ -heterodimer varies from 16 units in LH1 to 8 or 9 units in LH2. LH2 complexes can be subdivided into two families: the nonameric family includes *Rps acidophila* (McDermott *et al.*, 1995), *Rhodovulum sulfidophilum* (Montoya *et al.*, 1995; Savage *et al.*, 1996), *Rb sphaeroides* (Walz *et al.*, 1998), and *Rhodocyclus gelatinosus* (Ranck *et al.*, 2001), while the octameric family is represented to date by *Rsp molischianum* only (Koepke *et al.*, 1996).

1.2.1.1 The structure of light-harvesting complex 2

Before the elucidation of detailed high-resolution structures for the light-harvesting antenna complexes, a significant amount of indirect structural information was obtained from extensive comparative analysis of the amino acid sequences of LHC apoproteins. The primary structures were analysed from seven different species of purple bacteria and more than 20 of the α - and β -polypeptides have been sequenced (Brunisholz & Zuber, 1988; Zuber & Brunisholz, 1991). Conspicuously, they all showed a strong tripartite character; a hydrophobic core of 20-24 amino acids, a polar N-terminus and a polar C-terminus. The hydrophobic core spans the membrane as a single α -helix. At either ends of the transmembrane protrude short surface-lying helices and extended structures; the N- and C-termini. Among these conserved primary structural features, a highly conserved histidine residue is found on both the α - and β -polypeptide (Brunisholz & Zuber, 1988; Zuber & Cogdell, 1995).

In 1995, the crystal structure of the LH2 complex from *Rps acidophila* strain 10050 has been solved (McDermott *et al.*, 1995). Although the LH2 structure of *Rb*

sphaeroides has not yet been determined by X-ray crystallography, current evidence would suggest that it is analogous to that found in *Rps acidophila*. The electron microscopy data from Walz *et al.*, (1998) indicate that the LH2 complex from *Rb sphaeroides* is also a nonamer instead an octamer. Furthermore, the α - and β -apoprotein of *Rb sphaeroides* exhibit a close homology to the LH2 subunits of *Rps acidophila* (α -apoprotein has 45 % sequence homology and β -apoprotein has 65 % sequence homology with *Rps acidophila*). Therefore, the LH2 crystal structure from *Rps acidophila* is generally used as a structural template for *Rb sphaeroides*.

LH2 complex from *Rps acidophila* is a nonameric aggregate of $\alpha\beta$ -heterodimers. The inner ring is formed by α -polypeptides, with an internal radius of ~ 18 Å, while the outer ring is formed by β -polypeptides, with an external radius of ~ 34 Å. All the pigments are arranged between the $\alpha\beta$ -polypeptides (figure 1-4A). Each $\alpha\beta$ -subunit binds a total of three BChl *a* and one or two carotenoid molecules (McDermott *et al.*, 1995; Papiz *et al.*, 2003; Prince *et al.*, 2003), giving a total of 27 BChl *a* and 9 or 18 carotenoid molecules in the LH2 complex. In each $\alpha\beta$ dimer unit, two of the three BChl molecules are arranged near the periplasmic surface of the complex as a closely coupled dimer. The nine coupled dimers in LH2 forms a nearly circular excitonically coupled BChl-ring; the distance between the central Mg^{2+} atoms within a pair is ~ 9.5 Å and between pairs is ~ 8.9 Å. These BChl dimers have their bacteriochlorin rings lying perpendicular to the membrane plane, with their central Mg^{2+} atoms ligated to the highly conserved histidine residues of their respective polypeptides. This was confirmed by resonance Raman studies (Robert & Lutz, 1985). In addition, site-directed mutagenesis of these histidine residues showed that this residue is strictly required for the assembly of LH2 (Olsen *et al.*, 1997). The absorption maximum of monomeric BChl *a* in organic solvents is about 770 nm, but when present as a dimer within the LH2 complex, this red-shifts to about 850 nm due to excitonic as well as pigment-protein interactions. Hence, these pigments are known as BChl-B850.

There is a second group of BChls located on the N-terminal (cytoplasmic) side of the LH2 complex. Unlike the BChl-B850, their central Mg^{2+} ions are not ligated to a histidine residue but rather to a carboxylate moiety on the N-terminal amino group

of α Met 1 (Papiz *et al.*, 2003). These molecules have an absorption maximum at 800 nm and are identified as BChl-B800. The bacteriochlorin rings of this group of BChls lie parallel to the plane of the membrane. Each BChl-B800 is considered monomeric as the distance between the central Mg^{2+} of neighbouring BChl-B800 is about 20 Å. This results in significantly weaker excitonic coupling than the case of BChl-B850. A typical absorbance spectrum of the photopigments in the LH2 complex of *Rb sphaeroides* is shown in figure 1-5.

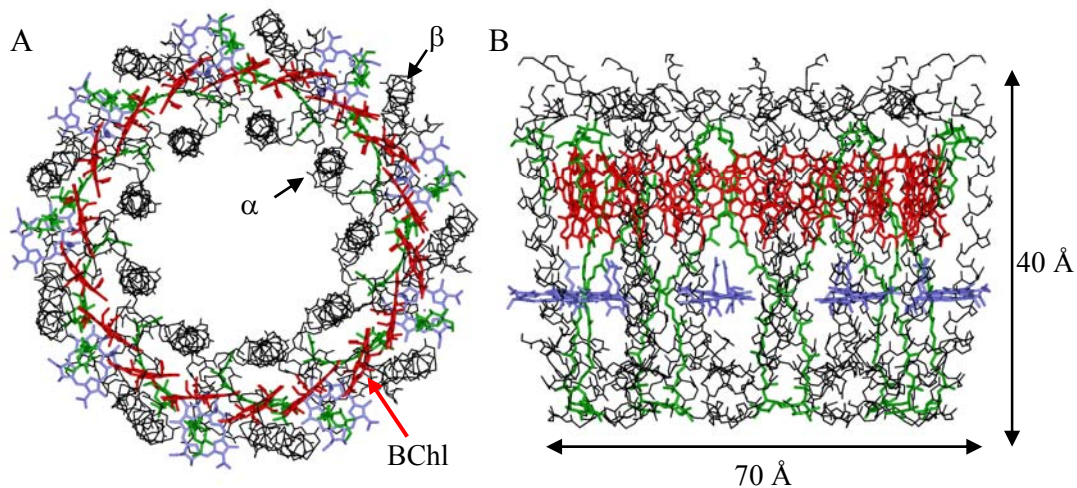


Figure 1-4: Schematic presentation of the overall structure of the LH2 complex based on the 2.0 Å crystal structure of *Rps acidophila* (Papiz *et al.*, 2003).

(A) Top view of the complex. (B) Side view of the complex.

The dimensions of the complex are ~ 70 Å in diameter by ~ 40 Å for the transmembrane width. The $\alpha\beta$ -polypeptides are displayed in black, BChls-B850 displayed in red, BChls-B800 displayed in blue and carotenoids are displayed in green.

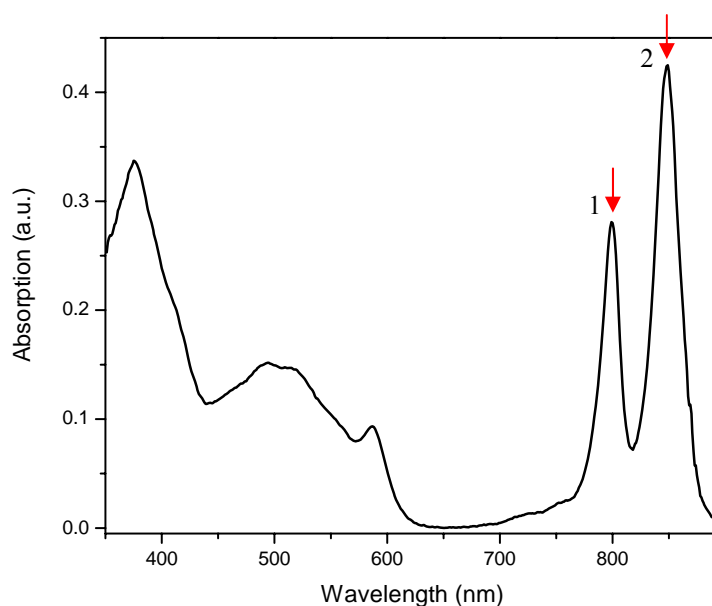


Figure 1-5: Typical absorbance spectrum of LH2 isolated membranes. The two arrows indicate the near-infrared absorption maxima associated with BChls Q_y transition at 800 nm (1) and 850 nm (2), BChls Q_x transition at 580 nm and Soret band at ~380 nm. The peak from 450-550 nm is of the carotenoids.

The overall LH2 structural arrangement of *Rps acidophila* provides a model template for the arrangement of LH2 in *Rb sphaeroides* used in my thesis. The individual photosynthetic components within the LH2 complex are strategically arranged and influence one another. Site-directed mutagenesis of the amino acid residues can be performed to study the interactions and the role of the protein moiety. The potential interactions of individual components, bacteriochlorophylls, carotenoids and membrane lipids, with one another and with the protein will be described in the following sections.

1.3 **Photosynthetic pigments: bacteriochlorophyll and carotenoid**

To capture light for photosynthesis, phototrophic organisms employ three classes of pigment molecules: magnesium porphyrins (chlorophylls and bacteriochlorophylls, also called chlorins), open-chain tetrapyrrole bilin pigments (phycobilins) and carotenoids (Scheer, 1991). The major light-absorbing pigments in purple bacteria are BChls *a* and carotenoids. Generally, they appear not to exist within the cells in a free state, but are bound non-covalently to hydrophobic membrane proteins (Hawthornthwaite & Cogdell, 1991). In LH2 complex, the interactions of the pigments with each other and the protein environments modulate their spectroscopic characteristics and thereby their function.

1.3.1 **Bacteriochlorophylls: structures and functions**

BChl *a* is structurally very similar to Chl *a* found in higher plants (figure 1-6). It consists of two units: the macrocycle and the C20 isoprenoid alcohol chain (Scheer, 1991). The magnesium-containing chlorin molecules are the major photosynthetic pigments found in all photosynthetic organisms in nature (Scheer, 1991). So far, zinc-containing BChl *a* is only observed in aerobic photosynthetic bacterium *Acidiphilium rubrum* (Wakao *et al.*, 1996). Minor alterations in the chlorin structure are also found in nature that allows organisms to adapt to various environments. Modifications found in the BChls' tetrapyrrole structures include changes in the hydration state of the ring structures and alterations of various side groups (Smith, 1991). These modifications also result in spectral changes which allow the organisms to absorb light over a broad range of wavelengths (table 1-1).

In addition to the modifications found within the conjugated ring structure, there are also variations found within the esterifying alcohol chains (Rüdiger & Schoch, 1991). In nature, this alcohol component varies considerably; phytol tail (C₂₀H₃₉OH) is the most common esterified alcohol of Chl *a* in plants and BChl *a* in photosynthetic bacteria (Rüdiger & Schoch, 1991). Other esterifying alcohols such as geranylgeraniol are found in BChl *a* of *Rsp rubrum* (Katz *et al.*, 1972) and farnesol in BChls *c* of *Chlorobium limicola* (Caple *et al.*, 1978). The roles of these

variations of the esterifying alcohols in diverse species are not known. The alcohol contribution to the spectral properties appear to be marginal (Fiedor *et al.*, 2003) but they are likely to have distinct roles in the structure, function and assembly of LH2.

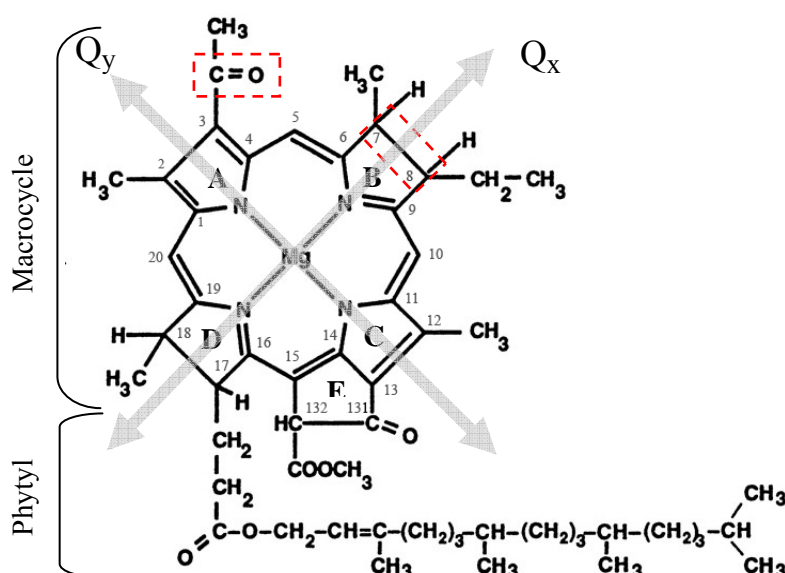


Figure 1-6: Bacteriochlorophyll *a* structure showing the Mg tetrapyrrole and phytol chain moieties. Red lined boxes indicate the two differences between BChl *a* and Chl *a*. Firstly, in ring A, instead of the acetyl carbonyl group in BChl, a vinyl group is found in Chls. Secondly, Chl has an addition double bond in ring B. The arrows indicate the direction of the Q_y and Q_x transition dipole moment. Nomenclature is according to International Union of Pure and Applied Chemistry (IUPAC).

Groups of organisms	Chlorin	<i>In vivo</i> absorption maxima
Cyanobacteria	Chl <i>a</i>	670-675
α -, β - and γ - Proteobacteria	BChl <i>a</i>	375, 590, 800-810, 830-890
β -Proteobacteria	BChl <i>b</i>	400, 605, 835-850, 986-1035
Green coloured Chlorobiaceae and Chloroflexus sp.	BChl <i>c</i>	457-460, 745-755
Green coloured Chlorobiaceae	BChl <i>d</i>	450, 715-745
Brown coloured Chlorobiaceae	BChl <i>e</i>	460-462, 710-725
Heliobacteriaceae	BChl <i>g</i>	375, 419, 575, 788

Table 1-1: Major absorption maxima of chlorins in whole cells of phototropic bacteria (Glaeser, 2003).

1.3.1.1 BChl-protein interactions in LH2 complex of *Rb sphaeroides*

BChl *a* is the only BChl present in *Rhodospirillaceae* (Scheer, 1991). In organic solvent, BChl *a* has its NIR absorption band at ~770 nm. When it is non-covalently bound within LHC, its NIR absorption band will be red-shifted by up to several hundreds of nanometres depending upon the complex type. This characteristic red-shift in absorption band arises from pigment-pigment and pigment-protein interactions within the native antenna complex.

In *Rb sphaeroides*, there are BChls-B800 and -B850 in LH2 complex. The structural arrangement of the BChls is determined by interactions among each another and within the proteins binding pocket (Cogdell *et al.*, 2003; Law *et al.*, 2004). Distortion of these interactions will affect the spectroscopic properties which have been used as a sensitive probe for the study of the structure-function relationships in antennae proteins.

The precise orientation of BChl-B850 molecules in the LH2 assembled protein is controlled to a large extent by its surrounding proteinaceous environment. Apart from the main coordination between the central Mg²⁺ atoms in BChl-B850 to the conserved histidine residues of each of the α - and β -polypeptides, additional interactions between the BChls and the protein exist. For example, peripheral H-bonding interactions between the aromatic residues and the carbonyl groups of the BChl have been shown (e.g. Olsen *et al.*, 1997; Gall *et al.*, 1997). The complete details and the role of the polypeptide in the pigment binding pocket still require clarification.

The specificity of the interactions between BChls' macrocycle and the polypeptides has been investigated in my thesis, described in chapter 3. Factors responsible for the spectral properties of LH2 complex are studied. Structural and functional amino acid residues at the BChl-protein interface; in particular, the tetrapyrrole ring and its immediate polypeptide environment are addressed.

On the other hand, the alcohol moiety of BChl *a* is very hydrophobic; it varies in length and saturation. It has been shown that it does not affect the spectral properties significantly (Rüdiger & Schoch, 1991; Fiedor *et al.*, 2003) but participates in light-

harvesting (Addlesee & Hunter, 2002) and may be of structural significance (Agostiano *et al.*, 2000). The structural role of the alcohol chain is addressed in my thesis, described in chapter 4.

1.3.2 Carotenoids: structures and functions

Carotenoids represent a class of isoprenoid pigments present in all photosynthetic organisms. They share a similar basic structure consisting of a polyene chain (generally 40 carbon atoms). In some, a tertiary hydroxyl or methoxy group(s) is present at the terminal end of the molecule (Jensen *et al.*, 1958, 1961; Singh *et al.*, 1973). A number of secondary modifications such as dehydrogenation, hydroxylation and cyclisation result in the presence of a large diversity of carotenoid molecules (Frank & Cogdell, 1993, 1997; Takaichi, 1999). The light-harvesting active carotenoids have about 10 to 11 conjugated C=C bonds and are usually in *trans* configuration (Jensen *et al.*, 1961; Koyama, 1991). These conjugated π -electron systems are responsible for most of the spectroscopic properties of carotenoids (Frank & Cogdell, 1993, 1997).

Carotenoids probably first emerged in prokaryotic *Archaea* (formerly known as archaeobacteria) as lipids reinforcing cell membranes. Carotenoids share the common first stages of biosynthesis with cholesterol (Bramley & Mackenzie, 1988). It has been suggested by Rohmer *et al.*, (1979) that in Prokaryota, which do not contain cholesterol or other sterols in their membranes, carotenoids serve as cholesterol equivalents and have similar effects as cholesterol on the structure and dynamics of lipid bilayer membranes (Subczynski *et al.*, 1992, 1993; Wisniewska & Subczynski, 1998). In particular, polar carotenoids have been shown to segregate into carotenoid rich domains and preferentially interact with specific lipids (Wisniewska & Subczynski, 1998).

In the photosynthetic reactions, carotenoids have several different functions. Firstly, they harvest light in the blue-green region where (B)Chls do not absorb light very efficiently (Gillbro *et al.*, 1988; Koyama, 1991). Secondly, they serve as photo-protecting pigments that scavenge e.g. triplets or singlet oxygen and dissipate excess

(light) energy (Conn *et al.*, 1991). Finally, they have a structural role in pigment-protein complexes (Kühlbrandt *et al.*, 1994; Frank & Cogdell, 1997). The first two roles of the carotenoids in the photosynthetic bacteria have been well studied; however, much less is known about their structural role, hence their contribution to the assembly and stability of the LHC (Lang & Hunter, 1994).

1.3.2.1 Carotenoid-protein interactions in LH2 complex of *Rb sphaeroides*

In the high-resolution structure of LH2 complexes of *Rps acidophila* (McDermott *et al.*, 1995), a single carotenoid molecule is shown per $\alpha\beta$ -subunit. This carotenoid, rhodopin glucoside, has a typical all *trans* conformation (Ohashi *et al.*, 1996; Robert, 1996). It runs perpendicular to the macrocycle of BChl-B800 (at a closest distance of 3.42 Å), progresses into the neighbouring $\alpha\beta$ -heterodimer, and then passes over the face of the macrocycle of the α BChl-B850 (at a closest distance of 3.57 Å). A second carotenoid located peripheral at the C-terminal region of the LH2 complex was revealed in an improved crystal structure at a resolution of 2.0 Å (Papiz *et al.*, 2003). This second carotenoid is severely bent and this distortion very likely does not reflect its *in vivo* conformation. In fact, the existence of this carotenoid is still disputed, as this molecule may be a lipid or detergent as well. In a recent resonance Raman spectroscopy and crystallisation studies, only one carotenoid per $\alpha\beta$ -heterodimer is found (Gall *et al.*, 2006, Cherezov *et al.*, 2006).

The transmembrane carotenoid molecule makes many van der Waals contacts with both the B800 and B850 BChls while linking the $\alpha\beta$ polypeptides together (McDermott *et al.*, 1995; Law *et al.*, 2004). It is postulated that they are likely to have a role in LH2 complex assembly and in the arrangement of protein α -helices within the membrane (Lang & Hunter, 1994). The stabilisation and structural role played by carotenoids have been demonstrated in the studies of carotenoid depletion mutants of purple bacteria (Lang & Hunter, 1994; Liu Y *et al.*, 2004). However, there are reports of mutants defective in carotenoid biosynthesis that are still capable of forming RC, LH1 and LH2 complexes (Crouse *et al.*, 1963).

In *Rb sphaeroides*, carotenoid biosynthesis produces spheroidene under aerobic condition which is subsequently converted to spheroidenone. Spheroidenone, a red pigment, is a keto derivative of spheroidene; both of them are native carotenoids present in *Rb sphaeroides*. Their relative proportion depends on the growth conditions; in particular, at relatively high partial pressure of oxygen, predominantly spheroidenone is accumulated (Jensen *et al.*, 1961; Shneour, 1962) (Figure 1-7). In turn, spheroidene accumulates in low oxygen partial pressure and is bound to LH2 under native conditions.

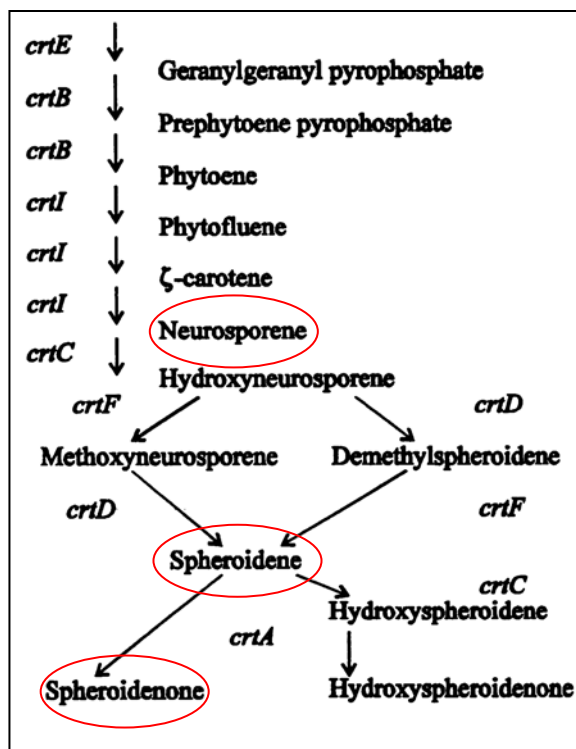


Figure 1-7: Outline of the carotenoid biosynthesis pathway in *Rb sphaeroides*. Carotenoid genes (*crt*) are indicated. The carotenoids used in the thesis are circled in red (figure is adapted from Hunter *et al.*, 1997).

The biosynthetic pathway has been explored by mutation studies *in vivo*. When the *crtC* gene in the carotenoid synthesis pathway is mutated, the bacteria accumulate neurosporene, instead of the native spheroidenone/spheroidene (Hunter *et al.*, 1997; figure 1-7).

Figure 1-8 shows the typical absorption spectra of spheroidenone and neurosporene in a range of 400 to 550 nm. Neurosporene has three distinct peaks at 430 nm, 457 nm and 490 nm; whereas, spheroidenone produces a relatively featureless absorption in the visible region. Neurosporene having such well-defined spectral peaks is well suited for monitoring minute alterations in its spectra. Furthermore, the energy transfer efficiency from carotenoid to BChls is similar for these two carotenoids (Olsen & Hunter, 1994; Hunter, 1995). To exploit this advantage, the native spheroidenone is substituted when advantageous with neurosporene in my thesis.

Structurally, differences are found between the two carotenoids. In spheroidenone, there are 11 π -electron-conjugated double bonds while in neurosporene there are only 9 (Frank & Brudvig, 2004). In addition, there are no polar carboxy or methoxy groups in the latter (figure 1-9). The higher number of conjugated bonds in spheroidenone results in a more rigid conformation than neurosporene.

In the LH2 structure from *Rps acidophila* (McDermott *et al.*, 1995), rhodopin glucoside is the main carotenoid. The structure of rhodopin glucoside is similar to the carotenoids present in *Rb sphaeroides* LH2 complex, except for the glucosyl head group (figure 1-9). In my thesis, the carotenoid-protein interactions are studied based on the template model structure of *Rps acidophila*.

1.4 The photosynthetic membrane in *Rb sphaeroides*

1.4.1 Membrane morphology of *Rb sphaeroides*

Anaerobic growth of photosynthetic purple bacteria (*Rhodospirillaceae*, *Chromatiaceae*) induces the development of the photosynthetic apparatus and is accompanied by the development of thylakoids membrane. These membranes are formed by invaginations of the cytoplasmic membranes (CM) and are associated with alteration in the membrane lipid composition (Niederman *et al.*, 1976; Drews & Oelze, 1981).

The pigment-protein complexes are inserted and assembled within the continuous cytoplasmic networks of ICM (Lascelles & Szilagyi, 1965). The morphology of the ICM within the purple photosynthetic bacteria varies considerably between different genera (Drews & Oelze, 1981). There are vesicles (found in *Rb sphaeroides*, *Rb capsulatus*) (Drews & Golecki, 1995; Sturgis & Niederman, 1996), tubules or stacks of flat membranes sacs (found in *Rps palustris*, *Rsp photometricum*, *Rps acidophila*) (Varga & Staehelin, 1983; Scheuring *et al.*, 2004b; Sturgis & Niederman, 1996). The morphogenetic factors of these membrane formations have been proposed to be at least in part governed by the photosynthetic proteins. However, these factors are still not understood (Varga & Staehelin, 1983; Drews & Golecki, 1995). In addition, the coordination of the biosynthesis of lipid membrane and protein complexes has as not yet been clarified. Some of these issues have been addressed by deletion of distinct components of the photosystem unit and its impact on membrane development. For example, in *Rb sphaeroides* and *Rb capsulatus*, a fully pigmented cell contains spherical or near-spherical invaginations. It has been shown that the absence of the LH1-RC core complex has no effect on the presence of the spherical invaginations (Kiley *et al.*, 1988; Hunter *et al.*, 1988). In contrast, the sole absence of LH2 complex induces a tubular ICM formation (Hunter *et al.*, 1988; Kiley *et al.*, 1988; Golecki *et al.*, 1989). These results suggest that LH2 is critical for ICM morphology. In apparent contradiction to these findings, wild type *Rsp rubrum* which entirely lacks LH2 but has (normal) LH1-RC, are able to develop spherical ICM. Furthermore, Golecki *et al.* (1989, 1991) have shown in mutant cells of *Rb sphaeroides* and *Rb capsulatus* that spherical ICM formation is achievable without

the incorporation of LH2 complexes. The reason for these contradictions is not known; therefore, it will be necessary to construct further mutants in order to define the relationship between LH2 biosynthesis and membrane morphology.

1.4.2 Membrane phospholipid composition

Biological membranes are bilipid layers, principally composed of lipids, primarily phospholipids, glycolipids, sulfolipids and sterols (except for prokaryotic organism, which do not synthesise sterols) (Rohmer *et al.*, 1979; Quinn & Chapman, 1980; Rao & Mayor, 2005). Phospholipids are the major components of bacterial cell membranes but also play a role in various processes in the cells (for recent review see Lee, 2003, 2004). (1) They provide the matrix for the assembly and function of a wide variety of membrane proteins; (2) they act as molecular signals in metabolic processes and (3) they also participate in the synthesis of macromolecules and are vital for proper folding and activity of numerous membrane proteins (Fyfe *et al.*, 2001; Cronan, 2003).

The major phospholipids in *Rb sphaeroides* include: phosphatidylethanolamine (PE), phosphatidylglycerol (PG), phosphatidylcholine (PC), and a minor proportion of cardiolipin (CL) and phosphatidic acid (PA) (Lechevalier, 1977; Birrell *et al.*, 1978; Imhoff & Bias-Imhoff, 1995; Fang *et al.*, 2000). The acyl chains of the lipids are characteristically rich in saturated and monounsaturated fatty-acyl chains such as C16:0, C16:1, C18:0 and C18:1 (Wood *et al.*, 1965; Kenyon, 1978; Russell *et al.*, 2002).

The properties of a particular phospholipid are largely determined by its chemical structure. This in turn is dependent on the structure of its head group and of its acyl chains (fatty acyl chain length and degree of saturations) (Cronan, 2003; Mukherjee & Maxfield, 2004; Liu F *et al.*, 2004). For example, cone-shaped lipids (with a headgroup area smaller than the acyl chain area) favour a negative membrane curvature whereas inverted cone lipids (with a headgroup area larger than the acyl chain area) favour a positive membrane curvature (Lee, 2004) (figure 1-10). Similarly, cylindrical-shaped lipids (with headgroup area proportional to acyl chain

area) favour a planar membrane. In contrast to cylindrical-shaped lipids which stabilise bilayer/planar membranes, the lipids that deviates from cylindrical shapes disfavour planar layer.

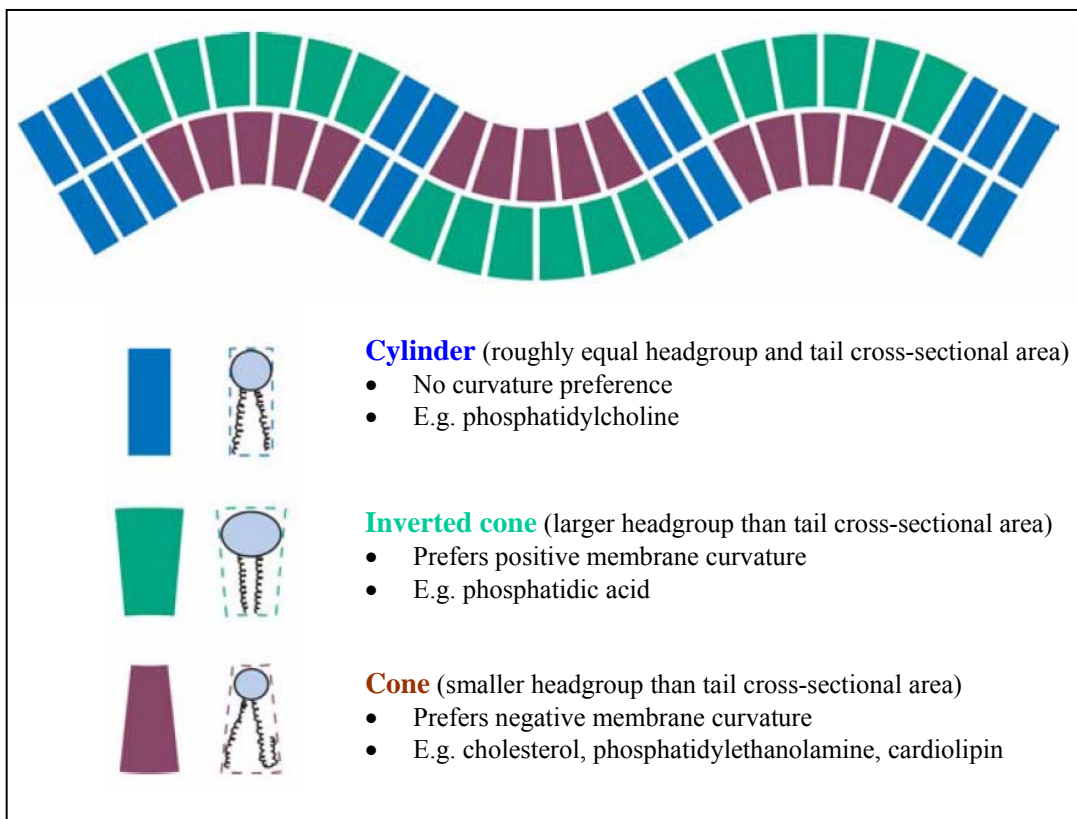


Figure 1-10: Schematic representation of how lipid shapes affect their curvature preferences. The direction of monolayer curvature is defined from the point of view of an observer in the fatty acyl chain region of the bilayer looking out towards the lipid headgroup region. A concave curvature for the monolayer is defined as being positive and a convex curvature is defined as being negative (Lee, 2004) (figure is taken from Mukherjee & Maxfield, 2004).

Specific types of phospholipid often join together in clusters and are distributed asymmetrically as lipid domains within the membrane (Rao & Mayor, 2005). This lateral phase separation gives rise to lateral asymmetry within a leaflet of a bilayer (Cronan, 2003). On a larger-scale, such asymmetry can result in morphological changes in the membrane. These include bud formation, vesicularisation and fusion of membrane vesicles (Mukherjee & Maxfield, 2004; McMahon & Gallop, 2005); all of which are biologically important events. For example, ICM formations, which

can be visualised as bud formation in purple bacteria, are induced to maximise the amount of membrane available for the membrane-bound energy-yielding apparatus. However, phospholipids coexist with other membrane determinants and thus do not solely contribute to the occurrence of lipid phase separation and membrane curvature. As discussed in section 1.4.1, membrane proteins may also play a crucial role in the formation of specific membrane structures. The exact involvement of membrane proteins in this process is, however, still not known.

Membrane proteins can potentially interact with and modulate membrane properties through interfacial electrostatic interactions with the polar headgroups of membrane phospholipids (Tocanne & Teissié, 1990; Mukherjee & Maxfield, 2004). Much less is known about the interactions between the membrane proteins and acyl-chain (Dumas *et al.*, 1999). To date, the interactions of membrane lipids and membrane proteins have been studied by the (i) examination of the effects of removal and/or addition of lipids to purified membrane protein complexes (e.g. Stamouli *et al.*, 2003), (ii) analysis of lipids bound to the purified complexes (e.g. Fyfe *et al.*, 2001; Jones *et al.*, 2002; Russell *et al.*, 2002), and (iii) characterisation of the membrane functions of mutants defective in a particular lipid biosynthesis (e.g. Bogdanov & Dowhan, 1998). The former two strategies accumulated substantial information on the possible roles of protein bound lipid. However, these studies owing to substantial influences of detergents in *in vitro* experiments may not reflect the actual *in vivo* conditions. The last method has been used to obtain *in vivo* evidence regarding lipid functions (Sato *et al.*, 2000). The biogenesis of ICM in *Rb sphaeroides* provides a suitable system for the study of relationship of protein-membrane *in vivo*. Under photosynthetic conditions, pigments-proteins interact with membrane lipids and induced specialised membrane invaginations. Putative protein-lipid interaction sites can be studied by using site-directed mutagenesis. This approach is used in the chapter 5 of my thesis.

1.5 Summary and approaches

1.5.1 Summary

Photosynthesis is the most vital process on Earth, most living organisms depend on it. The photosynthetic light reactions can be divided into two parts; harvesting light energy and conversion of light energy into chemical energy. Photosynthesis in eukaryotes is complex, but a simpler and equally representative model can be found in prokaryotic photosynthetic bacteria.

Genetic manipulations of non-sulphur purple bacteria (Fowler *et al.*, 1992, 1997; Olsen & Hunter, 1994; Hunter, 1995) have provided the opportunity to study the light-harvesting complexes on its native lipid environment without the complication of overlapping signals. Furthermore, the availability of high-resolution LH2 structures (McDermott *et al.*, 1995; Papiz *et al.*, 2003) provides a model to study potential interactions between various components within the light-harvesting complex, and the surrounding environment.

The understanding of LH2 pigment-protein complex assembly and function is still incomplete; the following areas require further clarification:

- (a) The specificity of interactions at the BChl macrocycle/protein interface and its structural and functional role.
- (b) The structural and functional role of BChls alcohol chain in LH2 complex.
- (c) The molecular basis for the role of LH2 membrane proteins in the ICM invagination process.
- (d) The elucidation of interactions between carotenoids and membrane lipids as well as LH2 protein.

1.5.2 Approaches

In order to answer the above questions, interactions within the LH2 complex and its surroundings are studied with the assistance of the available high-resolution LH2 structures (McDermott *et al.*, 1995; Papiz *et al.*, 2003).

Protein-BChls, protein-carotenoids and protein-membrane interactions can be explored by mutating the $\alpha\beta$ -apoproteins. The modified novel LH2 proteins are re-introduced into genetically customised *Rb sphaeroides* strains; DD13 and DG2. In both the modified strains, the peripheral LH2 complex and the core LH1-RC complex have been genetically deleted (Fowler *et al.*, 1992, 1994; Jones *et al.*, 1992; Hunter, 1995), this results in a featureless but a valuable null background for the re-introduction of novel LH2 protein. The absence of other LH complexes, permits the examination of the novel LH2 protein in the ‘near-native’ membrane environment even when the expression levels are low (Braun *et al.*, 2002, 2003; Kwa *et al.*, 2004; Garcia-Martin *et al.*, 2006a, 2006b). The ‘fitness’ of the complexes can be conveniently monitored by spectroscopic analysis as the complexes are present in a spectroscopically pure state in its native lipid environment without interference of overlapping signals from other BChl-proteins.

Interactions that are vital for the light harvesting process, when altered by mutations of amino acids, are likely to give rise to spectroscopic changes due to the sensitivity of the spectra to excitonic coupling between the pigments. Similarly, any interactions that are vital for the stability of the LH2 complex, when altered, will result in a destabilisation of the pigment-protein complex.

Such changes can be studied by routine spectroscopic procedures such as optical absorption (e.g. Katz *et al.*, 1968, 1978; Goldman & Youvan, 1992), fluorescence spectroscopy (e.g. Gall *et al.*, 1997; Maxwell & Johnson, 2000) and circular dichroism (CD) (e.g. Koolhaas *et al.*, 1998; Hu *et al.*, 1998). Particularly informative are the Q_y absorption and CD spectra of the closely coupled BChl-B850, which are sensitive to changes in the environment (pigment as well as protein) of these BChls. Energy transfer between photopigments within the LH2 complex can be studied by excitation fluorescence spectroscopic measurements. In my thesis, these

spectroscopic techniques have been used for the determination of the BChl binding and functional assembly in the novel LH2 mutants. Together with the available high-resolution data, inferences can be made on how each mutation affects the pigments, and hence the function of each amino acid can be deduced.

The protein-carotenoid interactions can be further assessed by using *Rb sphaeroides* with different carotenoid contents. The DD13 and DG2 strains differ by their major carotenoid, with spheroidenone present in the DD13 and neurosporene in the DG2 strain (Fowler *et al.*, 1992; Jones *et al.*, 1992; Braun *et al.*, 2002) (section 1.3.2.1). Thereby, the protein-carotenoid interactions are modulated and further information on the role of the carotenoids in LH2 assembly and function may be obtained.

For the elucidation of the relationship between lipid compositions, ICM morphology and LH2 complex in response to the protein modifications, the phospholipid composition of the membrane may be analysed by electron ionisation mass spectroscopy (ESI-MS). Thus, the effect of protein-membrane interactions on membrane composition can be studied. The involvement of LH2 membrane protein in lipid membrane invaginations can be examined by studying ICM morphology under electron microscopy (EM).

1.6 Thesis objectives and organisation of chapters

The challenge in the study of photosynthesis is to understand the structural basis of the light-harvesting efficiency in native membranes; more precisely, the relationship between the different components of the system that ensure efficient energy and electron transfer. The aim of the thesis is to understand the inter-component interactions and their relationship to (1) the assembly and function of LH2 complex and (2) the biogenesis of the membrane housing the photosynthetic machinery. The thesis is divided in two major sections:

Part I is aimed at the elucidation of the interactions between the light-harvesting active BChl-B850 and the LH2 proteins, particularly input of the amino acid residues of the β -polypeptides. This part is divided into two chapters. In *Chapter 3*, interactions between the BChl-B850's macrocycle and the binding pocket, in particular the β -subunit is examined. Model LH2-like complexes are created to study the assembly, function and stability of the LH2 protein in dependence of particular interaction motifs at the BChl-protein interface. The results from chapter 3 were published in Kwa *et al.*, 2004.

In *Chapter 4*, the study of pigment-protein interactions are extended towards the alcohol moiety of the BChl. The structural contributions of the alcohol moiety, in particular, its impact on the stability and assembly of LH2 complex is explored by enzymatic, mutagenetic and statistical approaches in this chapter.

In Part II, the biogenesis of the *Rb sphaeroides* photosynthetic membrane in relation to the LH2 complex is addressed. In *Chapter 5*, the effect of novel LH2 proteins on ICM morphology and lipids compositions are analysed by electron microscopy and electrospray ionisation mass spectroscopy as follows: (1) Lipid composition (head group and acyl chain length), (2) ICM morphology and (3) structural stability of LH2 complex is analysed in dependence of variable amino acid residues and carotenoid composition.

Finally, the main results of the chapters are discussed in *Chapter 6* and the summary and some future plans are included.

CHAPTER 2

MATERIALS AND METHODS

2.1 MATERIALS

2.1.1 Bacterial strains

Rb sphaeroides DD13 and DG2 strains were kindly provided by Prof. N.C. Hunter, University of Sheffield, United Kingdom. Both the *Rhodobacter* strains had *pucBA*ⁱ (coding for the LH2 β and α subunits) and *pufBALMX* genes (coding for the LH1 β and α and reaction centre L and M subunits, respectively) deleted which results in the absence of endogenous BChl-proteins, RC, LH1 and LH2 complexes. Streptomycin (Sm^R) and kanamycin (Km^R) resistance genes were inserted for selection (Burgess *et al.*, 1989; Jones *et al.*, 1992; Olsen & Hunter, 1994; Hunter, 1995). The DG2 strain carries a mutation in the *crtC* and *crtD* genes that alters the normal pathway of carotenoid synthesis in wild type (WT) *Rb sphaeroides*, preventing the completion of spheroidenone synthesis, and resulting in the presence of neurosporene as the major carotenoid (Lang & Hunter, 1994; Olsen *et al.*, 1997). The *Rhodobacter* strains can easily be differentiated by their distinct colours which arise from their carotenoid. During cell cultivation, the DD13 strain has a ruby red colour and the DG2 strain a brown-yellow colour.

E. coli strains S17-1 (*thi pro hsdR⁻ hsdM⁺ recA RP4-2 (Tc::Mu Km::Tn7)*) (Simon *et al.*, 1983) was used for the conjugation of *Rb sphaeroides*.

Competent cells included *E. coli* DH5 α , JM109 and One Shot[®] TOP10 (Invitrogen, GmbH, Karlsruhe, Germany) strains.

ⁱ A second set of *pucBA* operon has been identified in the genome of *Rb sphaeroides* 2.4.1 (Zeng *et al.*, 2003). The relevance of this finding will be discussed in chapter 6.

2.1.2 Plasmids and vectors

Topo-TA (Invitrogen GmbH, Karlsruhe, Germany) pCRII-TOPO, 4.0 kb is used for cloning of PCR products. By using an engineered *KpnI* site at the upstream of start codon *pucB* and *BamHI* site at the downstream of *pucA* coding region.

pRKCBC1 as mobilisable plasmid (tetracycline resistance (Tc^R) derivative of pRK415; insertion of a 4.4 kb fragment encompassing *pucBAC*) contains the *pucBA* genes as a 420 bp *KpnI-BamHI* insert (Burgess *et al.*, 1989; Jones *et al.*, 1992). For *pRKCBC1* sequence see appendix 1. The modified transmembrane helices (TMH) were expressed in genetically engineered *Rb sphaeroides* DD13 and DG2 strains which lack the operons encoding the apoproteins of the photosynthetic apparatus but provide the assembly factors, pigments, and membranes that are required to test the fitness of the model proteins to function as a light harvesting unit within a nearly native system (Braun *et al.*, 2002, 2003; Kwa *et al.*, 2004).

2.1.3 Buffers and solutions

Table 2-1: Buffers and solutions:

Buffers and solutions	Composition	
LB medium (10x concentrate)	100 g	Tryptone peptone
	50 g	Yeast extracts
	50 g	NaCl
Filled up to 1 litre with deionised water and adjusted to a pH of 7.5 with NaOH.		
M22 medium (10x concentrate)	30.6 g	KH_2PO_4
	23 g	$K_2HPO_4 \cdot 3H_2O$
	19 ml	Sodium Lactate, DL-lactic acid (60 % syrup)
	5 g	$(NH_4)_2 SO_4$
	5 g	NaCl
	43.43 g	Di-sodium succinate hexahydrate
	27 g	$C_5H_8NNaO_4 \cdot H_2O$
	0.4 g	DL-aspartic acid
	200 ml	Solution C (50x concentrate)

Table 2-1: Buffers and solutions (continue):

Buffers and solutions	Composition	
Filled up to 1 litre with deionised water and adjusted to a pH of 7.6 with KOH, stored at -20 °C. Dilute to 1x concentrate prior use.		
Solution C (50x concentrate)	10 g	Nitriloacetate (Titriplex I)
	24 g	MgCl ₂
	3.35 g	CaCl ₂ .2H ₂ O
	125 mg	EDTA (Titriplex III)
	250 mg	ZnCl ₂
	250 mg	FeCl ₂ .4H ₂ O
	90 mg	MnCl ₂ .4H ₂ O
	9.25 mg	(NH ₄) ₆ MO ₇ O ₂₄ .4H ₂ O
	7.75 mg	CuCl ₂
	12.5 mg	Co(NO ₃) ₂
	5.75 mg	Boric acid
Filled up to 1 litre and adjusted to a pH of 6.8-6.9 with KOH and stored at -20 °C.		
SDS-PAGE electrode buffer (10x concentrate)	121 g	Tris base
	179 g	Tricine
	100 ml	10 % (w/v) SDS solution
Filled up to 1 litre with deionised water, dilute to 1x prior to use.		
SDS-PAGE sample buffer	2.5 ml	0.5 M Tris-HCl, pH 6.8
	2 ml	Glycerol
	4 ml	10 % (w/v) SDS solution
	0.5 ml	0.1 % (w/v) bromophenol blue
	0.5 ml	2-Mercaptoethanol
SDS-PAGE gel (2 gels) [7 x 8.5 cm (HxW)]	Stacking gel 14 %:	
	1.8 ml	ProSieve 50 solution
	1.6 ml	Tris-HCl 1.5 M, pH 8.8
	3 ml	H ₂ O
	65 µl	10 % (w/v) SDS
	65 µl	10 % (w/v) APS
	2.6 µl	TEMED
	Separating gel 5 %:	
	300 µl	ProSieve 50 solution
	390 µl	Tris-HCl 1 M, pH 6.8
	2.3 ml	H ₂ O
	30 µl	10 % (w/v) SDS
	30 µl	10 % (w/v) APS

Table 2-1: Buffers and solutions (continue):

Buffers and solutions	Composition	
		3 μ l
SDS gel staining	10 ml	Coomassive Blue
	10 ml	Methanol
	30 ml	H ₂ O
SOC medium	2 g	Tryptone
	0.5 g	Yeast extracts
	200 μ l	5 M NaCl
	250 μ l	1 M KCl
	1 ml	1 M MgCl ₂
	1 ml	1 M MgSO ₄
	1.8 ml	20 % Glucose
Filled up to 100 ml with deionised water, pH 6.8-7.5.		
Electrophoresis buffer: TAE buffer (50x concentrate)	242 g 57.1 ml 100 ml	Tris base Glacial acetic acid 0.5 M EDTA
Filled up to 1 litre with deionised water, pH 8.0. Dilute to 1x concentrate prior to use; with a final concentration of 40 mM Tris-acetate, 1 mM EDTA.		
TBE buffer (5x concentrate)	54 g 27.5 g 20 ml	Tris base Boric acid 0.5 M EDTA
Filled up to 1 litre with deionised water, pH 8.0. Dilute to 1x concentrate prior to use; with a final concentration of 45 mM Tris-borate, 1 mM EDTA.		
TE buffer	10mM Tris-HCl and 1 mM EDTA, pH 8.0	
Vitamins (1000x concentrate)	100 mg 50mg 10 mg 1 mg	Nicotin acid Thiamine para-Aminobenzosäure Biotin

2.1.4 Column materials and solutions

Table 2-2: Column materials (Amersham Biosciences, Sweden) and solutions for LH2 isolation:

Column materials	Sizes (WxH)	Properties	Washing buffers	Elute buffers
DEAE sepharose fast flow-ion exchange	1x 8 cm	Ion-exchange	50 mM NaCl, 10 mM Hepes and 0.8 % β OG	300 mM NaCl, 10 mM Hepes and 0.8 % β OG
Superdex 200	1x 20 cm	Sizes exclusion	-	10 mM Hepes and 0.8 % β OG

2.1.5 Enzymes, chemicals and kits

All chemicals were purchased from Sigma-Aldrich (München, Germany), Roth (Karlsruhe, Germany), Pharmacia (Uppsala, Sweden), Serva (Heidelberg, Germany) and Merck (Darmstadt, Germany).

Plasmid isolation, PCR purification and gel purification kits were from Qiagen (Hilden, Germany). Protein quantification kits were from Pierce BCATM (Bonn, Germany) and Roche (Penzberg, Germany). Restriction enzymes were purchased from MBI Fermentas (St. Leon-Rot, Germany), New England Biolabs (Frankfurt/Main, Germany), Promega (Madison, USA) and Invitrogen GmbH (Karlsruhe, Germany).

2.1.5.1 Antibiotics

Table 2-3: Antibiotics and their concentrations used in the thesis:

Antibiotics	Company	Concentration (μ g/ml)	
		<i>E .coli</i>	<i>Rb sphaeroides</i>
Ampicillin	Roth	50	-
Kanamycin	Sigma-Aldrich	30	-
Neomycin	Sigma-Aldrich	-	20
Streptomycin	Sigma-Aldrich	-	30
Tetracycline	Sigma-Aldrich	10	1

2.1.5.2 Phospholipids

CL	Cardiolipins
PA	L- α -phosphatidic acid (sodium salt) P-9511 from egg yolk lecithin
PC	3-sn-phosphatidylcholine from fresh egg yolk
PE	1,2-Diacyl-sn-glycero-3-phosphatidylethanolamine from bovine brain ~98 % TLC
PG	L- α -Phosphatidyl-DL-glycerol ammonium salt from egg yolk lecithin
PI	Phosphatidylinositol from soy bean

All the phospholipids are obtained from Sigma-Aldrich, München, Germany and were used without further purification.

2.1.5.3 Markers

DNA	GeneRuler™ 1000 bp DNA ladder (MBI Fermentas, St. Leon-Rot, Germany) Lambda DNA restricted with <i>EcoRI</i> and <i>HindIII</i> (MBI Fermentas, St. Leon-Rot, Germany) GeneRuler™ 100 bp DNA ladder (MBI Fermentas, St. Leon-Rot, Germany)
Protein	Polypeptide SDS-PAGE molecular weight standards (Biorad) Kaleidoscope polypeptide standards (Biorad)

2.1.5.4 Others

Casamino acid	BD Biosciences-Difco, Germany
DNA ligase	T4 DNA ligase Invitrogen GmbH, Germany
DNase I	Roth (use in LH2 cells prior French press to avoid viscosity)
ExoSap-It	Amersham Biosciences, Freiburg, Germany
Lysozyme	Serva, Heidelberg, Germany (use in LH2 cells prior French press to break intracellular membrane)
β OG	Calbiochem, Merck, Germany

2.1.6 Technical devices

2.1.6.1 Centrifugation

Beckman Optima™ TLX bench top Ultra-centrifuge CO-TLX120 (Ramsey, Minnesota, USA), rotor: 100.3

Sigma 3K18C bench top refrigerate centrifuge (Braun, Melsungen), rotors: 12154, 12155

Sorvall Discovery 90 ultracentrifuge (Thermo, Waltham, MA, USA), rotors: Beckman SW40Ti, Beckman 70Ti (Ramsey, Minnesota, USA)

Sorvall RC-5B (Thermo, Waltham, MA, USA), rotor: F9S (Piramoon, Santa Clara, CA, USA)

2.1.6.2 Spectrophotometers

Ocean Optics fibre-optic spectrophotometer model SD2000 (Ostfildern, Germany)

Shimadzu spectrophotometer UV-2401PC (Duisburg, Germany)

Perkin Elmer Lambda 25 (Jügesheim, Germany)

CD6 dichrograph spectrometer (Horiba Jobin Yvon InC., Edison, USA)

Jasco J715 spectropolorimeter (Gross-Umstadt, Germany)

EM 912 electron microscope (Zeiss, Oberkochen, Germany)

Perkin Elmer LS55 spectrofluorometer (Jügesheim, Germany)

Spex FluoroLOG spectrofluorometer (Horiba Jobin Yvon Inc., Edison, USA)

2.1.6.3 Others

Biorad constant voltage power supply 1000/500 and Mini Protein III dual slab cell (Biorad, Munich, Germany)

Pharmacia electrophoresis power supply EPS 3500 for DNA gels

Biometra model Tpersonal PCR machine

Laminar flow (Büttner Schilde Haas, Bad Hersfeld, Germany)

Speed Vac Eppendorf Concentrator 5301 (Eppendorf, Hamburg)

2.2 METHODS

2.2.1 Media and growth conditions

Rb sphaeroides strains were cultivated under semi-aerobic/dark conditions in M22⁺ medium at ~34 °C as described by Hunter & Turner, 1988. Cultures were grown in Erlenmeyer flasks, filled to ~30 % of its nominal capacity covered with aluminium foil and plugged lightly with cotton wool. The flasks were continuously shaken at 180-200 rpm in the dark. Neomycin and tetracycline were added to cultures at the final concentration of 20 µg/ml and 1 µg/ml respectively to maintain selection for the expression vector *pRKCBCI* and its derivatives. Liquid cultures were supplemented with vitamins and 0.1 % casamino acids for growth. *E. coli* strains were grown in Luria broth and tetracycline was used at a concentration of 10 µl/ml.

Cell densities were monitored by the cultures' turbidity measured with spectroscopy; optical density (OD) at 650 nm. A conversion factor was used to estimate cell density: $OD_{650 \text{ nm}} \times 10^9 = \text{number of viable cells per millilitre}$ (Sambrook *et al.*, 1989).

2.2.2 General molecular biological methods

General molecular biological methods such as growing conditions of bacteria, restriction endonuclease digestion, DNA ligation, agarose gel electrophoresis, transformation of *E. coli* and recombinant DNA procedures were carried out according to standard procedures as described in Sambrook *et al.*, (1989). Plasmid DNA isolation, PCR and gel purification were prepared using Qiagen (Hilden, Germany) according to manufacturer's protocols.

2.2.3 Mutagenesis

Single substitutions in the $\alpha\beta$ -polypeptides to simplified Ala-Leu sequences were constructed by site-directed mutagenesis using the Quick-Change protocol from Strategene (La Jolla, CA, USA) according to manufacturer's protocol. Mutations were carried out either by direct mutation of the *pucBA* in *pRKCBCI* using the XL-

Quick change kit or on a 420 bp fragment of *pucBA* genes on cloning vector, TOPO-TA pCRII (Invitrogen GmbH, Germany). After PCR mutagenesis, the native methylated DNA templates were digested with DpnI (Promega, Madison, WI) for 1 hour at 37 °C. The mutations were subcloned into *pRKCBCI* using an engineered *KpnI* site at the upstream of start codon *pucB* and *BamHI* site at the downstream of *pucA* coding region. The mutations were confirmed by DNA sequencing. The resultant DNA was purified by Qiagen gel purification kit, digested with *KpnI* and *BamHI* and purified on an agarose gel prior to the ligation into *KpnI-BamHI* digested *pRKCBCI* vector.

2.2.3.1 Primers design

Primers were designed primarily according to Strategene mutagenesis kit (La Jolla, USA). All primers used for the mutagenesis were purchased from Thermo Electron Corporation (U.K.) with reversed phase HPLC as standard purification and have more than 38 bp. The melting temperature of the designed primers should be more than 75 °C and has been calculated by using the following formula:

$$\text{Melting temperature} = 81.5 + 0.41(\% \text{ GC}) - 675/N - (\text{mismatch } \%)$$

2.2.3.2 Polymerase Chain Reaction (PCR)

DNA fragments for cloning into plasmid vectors and sequencing were generated by PCR carried out as recommended by protocols. DNA fragments are amplified by PCR Beads ready to go (Amersham Pharmacia, Germany) in a reaction mixture of 25 µl. The PCR were performed with the following steps: (1) 94 °C denaturation, 3 min, (2) 94 °C denaturation, 30 sec, (3) 55 °C annealing, 30 sec, (4) 72 °C elongation, 1 min per 1 kb DNA, (5) 72 °C termination, 10 min and (6) 4 °C cooling. The amplification cycles (steps 2- 4) were repeated 30 times.

DNA mutageneses were performed using thin-wall PCR tubes in a total of 50 µl reaction mixture. The PCR were performed with the following steps: (1) 95 °C

denaturation, 1 min, (2) 95 °C denaturation, 50 sec, (3) 60 °C annealing, 50 sec, (4) 68 °C elongation, 2 min per 1 kb DNA, (5) 68 °C termination, 10 min and (6) 4 °C cooling. The amplification cycles (steps 2- 4) were repeated 18 times.

2.2.4 Agarose gel electrophoresis

All the plasmid DNA, PCR reaction products and DNA digestion fragments were analysed by 1 % or 2 % agarose gels and 1 µg/ml ethidium bromide with 1x TAE or 1x TBE running buffers. Samples were mixed with loading buffer provided with the markers prior to the run. The markers employed in all the gels were either lambda DNA (for 1 % agarose gel) or 100 bp DNA markers (for 2 % agarose gel). The DNA of the gel electrophoresis were visualised by UV light illumination (302 nm).

2.2.5 Conjugation

Modified plasmids were introduced into LH2⁻ LH1⁻ RC⁻ double deletion *Rb sphaeroides* DD13 and DG2 strains (Jones *et al.*, 1992), by the transformation of S17 *E. coli* strain (Simon *et al.*, 1983). Mating was performed as described in Hunter and Turner (1988). Transconjugants were grown aerobically in the dark at 34 °C on plate of M22⁺ medium supplemented with neomycin and tetracycline at 20 µg/ml and 5 µg/ml respectively. Screening for expression of the mutant genes was done approximately 2 days following conjugative transfer, and the presence or absence of LH2 complex are directly screened on Whatson filter paper by using reflection spectroscopy (Ocean Optic model SD200 fibre-optic spectrophotometer). The positive mutants were grown up from 10 ml start culture into 1.5 litre M22⁺ liquid culture containing 0.1 % casamino acids with antibiotics and temperature stated as before.

2.2.6 Bacterial cultivation

The 1.5 l semi-aerobically cultures of *Rb sphaeroides* cells were harvested during their mid-logarithmic phase of growth when the OD_{650 nm} is between 1.2-1.6 (within 1-2 days) (figure 2-1). Cells were centrifuged by low-speed centrifugation in Sorvall F9S 4x1000Y ml rotor at 5,000 g for 10 min and resuspended in 25 ml of chilled TE buffer (10 mM Tris, 1 mM EDTA, pH 8.0). Again, the cells were centrifuged at 7,000 g in Sigma 3K18C refrigerated bench top centrifuge for 10 min to obtain pellets which is then stored at -80 °C until use.



Figure 2-1: 1.5 l cultures of WT *Rb sphaeroides* DD13 strain after incubation and before harvest.

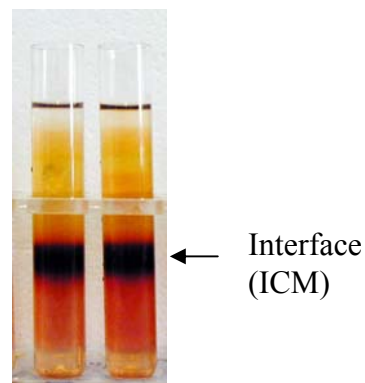


Figure 2-2: Chromatophores after sucrose gradient centrifugation. The interface rings were collected and recovered in Tris buffer.

2.2.7 LH2 intracytoplasmic membrane isolation

The ICM were prepared as described in Olsen *et al.*, 1994. Cell-free ICM fractions of *Rb sphaeroides* were isolated from the pelleted cells of the 1.5 l cultures (~10 g wet weight) which are first thawed on ice in dark, a few crystals of DNase I and a

small amount of lysozyme were then added into the cells for ~30 min for cellular extraction. The cells were disrupted by passage twice through a French pressure cell at 18,000 lb/in² (psi) and centrifuged at 10,000 g for 10 min in Sigma 3K18C bench top centrifuge to remove any unbroken cells and cellular debris.

The broken cells (supernatant) were layered on to 15/40 % (w/w) discontinuous sucrose gradients (made up in 1 mM Tris, 1 mM EDTA, pH 8.0 TE buffer) and centrifuged in a Beckman SW40Ti rotor at 39,000 rpm for 13 h. The ICM fraction was recovered from the interface (figure 2-2) and was collected and sedimented by centrifugation in a Beckman 70Ti rotor at 47,000 rpm for 3 h. The pellet was then suspended in small volume of buffer containing 1 mM EDTA, 10 mM Tris pH 8.0.

2.2.8 LH2 isolation

Approximately $OD_{850\text{ nm}} = 20\text{ cm}^{-1}$ of the ICM sample was solubilised with ~1 ml of 100 mM β OG, 10 mM Hepes and 50 mM NaCl, pH 7.5, leave on ice for at least 20 min in dark and then centrifuged in Beckman OptimaTM TLX at 52,000 rpm (150,000 g) for 25 min. The supernatant was loaded onto a pre-equilibrated ion-exchange DEAE-Sepharose column (1 cm x 5 cm, WxH). The column was pre-washed with two column volumes of 30 mM NaCl, 10 mM Hepes and 1 % β OG at a flowing rate of 1 ml/min before loading the sample. The unbound proteins were removed by washing the column with more than 10 times the column volumes of 30 mM NaCl, 10 mM Hepes and 30 mM β OG (pH 7.5) and eluted by 300 mM NaCl, 10 mM Hepes and 30 mM β OG. Several fractions were collected and their absorption spectra were recorded. The whole procedure was carried out in the dark at ~8 °C. When necessary, the fractions were pooled and concentrated using Amicon Ultra centrifugal filter concentrators with 10 kDa cut-off (Millipore corporation, Bedford USA) in a Sigma 3K18C bench top centrifuge before application to a size-exclusion gel chromatography Superdex G200 column for further purification. The purity of LH2 fractions were determined by the ratio of the absorbance at 850 nm (due to BChl *a*) to 280 nm (due to aromatic amino acids). Ratios of $OD_{850\text{ nm}}/OD_{280}$

$n_{\text{nm}} > 2$ are considered spectrally pure (Walz *et al.*, 1998). Purity of the samples is also monitored by running onto SDS-polyacrylamide gels (figure 2-3).

2.2.9 Sodium dodecyl sulphate polyacrylamide (SDS-PAGE) gels

The electrophoresis was performed essentially as described by Laemmli system (1970) employing a 5 % acrylamide (w/v) stacking gel and a 14 % acrylamide (w/v) separating gel. Samples (10 μ l) were mixed with equal volumes of sample buffer containing 0.125 M Tris, pH 7.0, 8 % SDS, 4 % 2-mercaptoethanol and 20 % glycerol (v/v) and were heated at 100 °C for 5 min. Samples were centrifuged at 13,000 g for 15 min prior to loading into wells. Electrophoresis was conducted using Biorad model 1000/500 Power Supply (50 V for 30 min, 75 V for 130 min). Gels were stained by Coomassie Brilliant Blue R250. As the size of the polypeptides is small, typically 5-6 kDa, it is difficult to obtain a good resolution in standard SDS gels of the polypeptide bands.

Markers (Biorad Kaleidoscope polypeptide standards) consist of 36400, 26600, 16000, 8400 and 3800 kDa protein and are coloured violet, orange, red, blue and blue respectively.

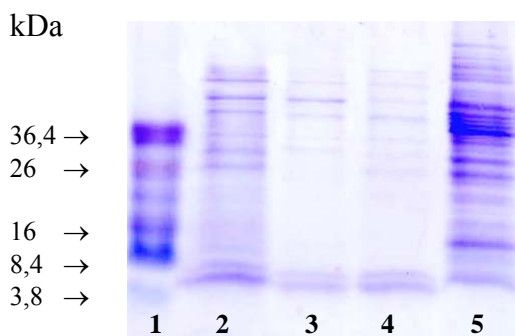


Figure 2-3: SDS-PAGE gel. Lane 1: Biorad Kaleidoscope polypeptide standards; lane 2: WT LH2 complex after ion-exchange column, lanes 3 & 4: isolated WT LH2 after size-exclusion gel; lane 5: WT LH2 complex before the columns.

2.2.10 Chlorophyllase experiment

The chlorophyllase (Chlase) was isolated from the chloroplasts (acetone powder) of *Franxinus excelsior* leaves as described in Chiba *et al.*, (1967) and Fiedor *et al.*, (1992).

37 mg of Chlase acetone powder was dissolved in 1 ml of Chlase buffer which consists of 0.5 M NaCl, 10 mM MgCl₂ and 20 mM Tris HCl (pH 8.0). The mixture was incubated at 4 °C in dark, overnight under constant shaking. 240 µl of the extracted Chlase was added with 320 µl of acetone and 5.6 µl of 1 M MgCl₂ (in order to achieve the end concentration of 40 % acetone and 10 mM MgCl₂). The Chlase mixture was then added into 240 µl of isolated WT LH2 in 30 mM Hepes and 10 mM βOG with the OD_{850 nm} at ~5 cm⁻¹. The final mixture was incubated at 34 °C in the dark for one to two hours with constant shaking. Absorption spectra were recorded throughout the incubation period. After two hours of incubation, acetone was removed by a flow of argon for >5 min. The sample was divided into two equal portions (240 µl each); one portion was used for the circular dichroism measurement while another portion was used for pigments analysis on TLC. Control experiment was included without the present of Chlase under the same conditions.

2.3 ANALYTICAL METHODS

2.3.1 Absorption spectroscopy

UV visible absorption spectra at room temperature were measured on Shimadzu UV-2401PC or Perkin Elmer Lambda 25 using a 1 cm or 1 mm path length cuvette.

2.3.2 Electron microscopy (EM) analysis

Cells were fixed immediately after collection with 2.5 % (v/v) glutardialdehyde (Fisher Scientific Co., Fair Lawn, N.J.) in 75 mM sodium cacodylate, 2 mM MgCl₂, pH 7.0, for 1 h at room temperature; rinsed several times in fixative buffer and post-fixed for 1 h with 1 % osmium tetroxide in fixative buffer at room temperature. After two washing steps in distilled water, the cells were stained *en bloc* with 1 % uranyl acetate in 20 % acetone for 30 min. Dehydration was performed with a graded acetone series. Samples were then infiltrated and embedded in Spurr's low-viscosity resin (Spurr, 1969). After polymerisation, ultra thin sections with thickness between 50 and 70 nm were cut with a diamond knife and mounted on uncoated copper grids. The sections were post-stained with aqueous lead citrate (100 mM, pH 13.0). All micrographs were taken with an EM 912 electron microscope (Zeiss, Oberkochen, Germany) equipped with an integrated OMEGA energy filter operated in the zero loss mode. All electron microscopy was performed in collaboration with Prof. Dr. Wanner G (LMU, Munich, Germany).

2.3.3 Electrospray Ionisation mass spectroscopy (ESI-MS)

Identification of phospholipids present in LH2 protein was carried out by electrospray ionisation mass spectroscopy (ESI-MS) in collaboration with Dr. D. Wegmann and PD. Dr. B. Brügger (Heidelberg University, Germany) (for measurement data, see appendix 4).

Chromatophores, cells and isolated LH2 WT and mutants were diluted in water. Small sample aliquots (1-10 µl) were added to 110 µl of 5 mM ammonium acetate in

methanol in a Sarstedt 1.5 ml tube. Before addition of the sample, the buffer was spiked with a mixture of lipid standards (PE/PC/PG). Without prior mixing, the samples were sonicated for 5 min at room temperature in a water bath. After mixing, precipitated proteins were pelleted at 16000 x g in a table top centrifuge at 4 °C. The supernatant was transferred to another microtube and subjected to mass spectroscopic analysis.

Microflow-ESI-MS/MS analysis was performed on a Micromass QII triple-stage quadrupole tandem mass spectrometer equipped with a microflow-ESI source (Z spray) from Micromass (Manchester, UK). Argon was used as collision gas at a nominal pressure of 2.5×10^{-3} millibar. The cone voltage was set to 50 V for PC, 45 V for PG and to a cone ramp of 40-65 V in a mass range of mass/charge (m/z) 600-1000 for PE respectively. Resolution of Q1 and Q3 was set to achieve isotope resolution.

Quantification of PE was performed by neutral loss scanning, selecting for a neutral loss of 141 (positive ion mode) at a collision energy of 27 eV ($1 \text{ eV} = 1.602 \times 10^{-19}$ J). PC quantification was performed by precursor ion scanning for fragment ion m/z 184 (positive ion mode, collision energy of 32 eV). PG quantification was performed by precursor ion scanning for fragment ion m/z 171 (negative ion mode) with a collision energy of 37 eV. Unsaturated PE and PG standards were synthesized and purified via HPLC as described (Koivusalo *et al.* 2001). Quantitative analyses were performed as described (Brügger *et al.*, 2000, 2004). Phosphate determination was performed according to Rouser *et al.* (1970). The significance of data was tested by analysis of variance with repeated measures.

Figure 2-4 shows the intense ions of the $[M-H]^-$ ions of PE, PG and PC. No other phospholipids such as cardiolipin, PA and PI were detected. Due to different ionisation efficiencies, the relative signal intensities of the ions of different phospholipid calluses do not directly represent their molar abundances. The quantitative determinations of phospholipids were performed with the addition of internal lipid standards.

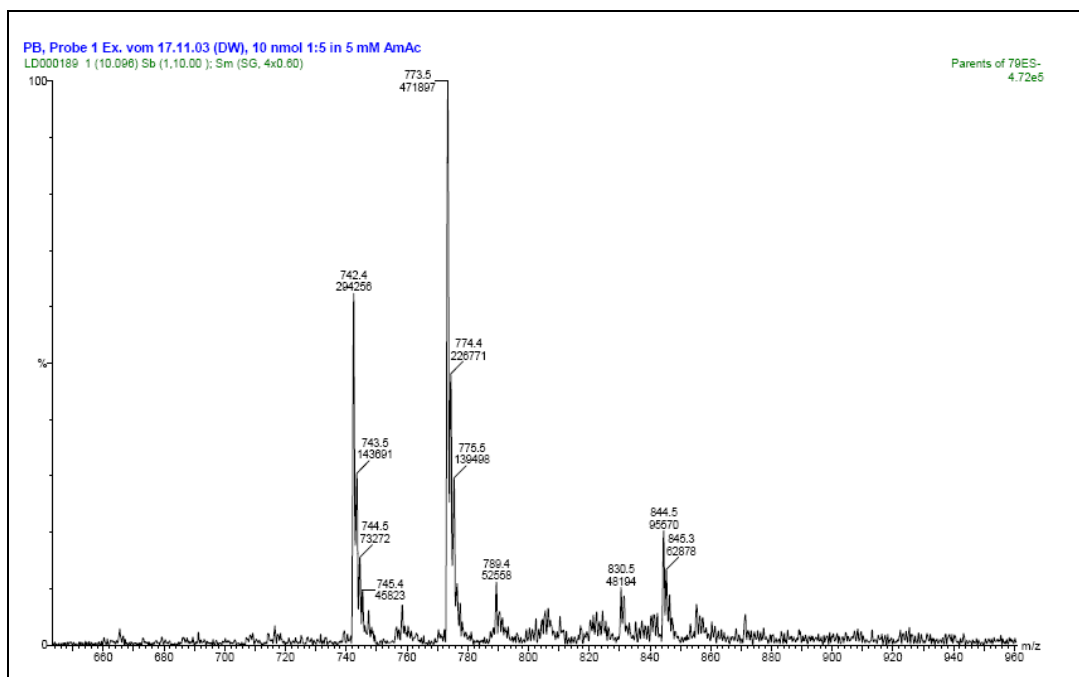


Figure 2-4: Negative ion mass spectrum by ESI-MS of total lipid extract from *Rb sphaeroides*. The main peaks 742, 773 and 844 m/z represent PE, PG and PC respectively.

2.3.4 Circular dichroism (CD) spectroscopy

Circular dichroism measurements were performed on a Dichrograph CD6 (Jobin Yvon, Division Instruments, USA) in 1 mm or 1 cm cylindrical Quartz cuvette or Jasco J715 spectropolarimeter in 1 mm rectangular Quartz cuvette (Hellma, Mühlheim, Germany). Purified LH2 membranes were adjusted to $OD_{850\text{ nm}} = \sim 4\text{ cm}^{-1}$ in TE buffer (10 mM Tris, 1 mM EDTA, pH 8.0) and measured in thermo stated quartz cuvette. CD spectra were recorded with 1 nm per sec scan rate under temperature control. During temperature experiments, the heating rate was 2 °C per min, recorded from 15 °C to 95 °C with integration time of 0.2 s at 845 nm. Data acquisition is done by spectra manager software, analysed, plotted, or smoothed by data analysis software Origin 7.0 (OriginLab Cooperation, Northampton, MA, USA).

2.3.5 Fluorescence spectroscopy

The excitation fluorescence spectra of *Rb sphaeroides* chromatophores were recorded by Spex FluoroLOG spectrofluorometer (NJ, USA). Excitations were scanned from 300 to 850 nm with the emission wavelength of 880 nm.

2.3.6 Protein quantification

Protein concentrations were determined either by protein assay kits from Fluka advance (Seelze, Germany), Roche ESL (Basel, Switzerland), Pierce BCATM (Rockford, USA) or with spectroscopy measurement using absorption at 280 nm. For more information see appendix 2.

2.3.7 Thin layer chromatography (TLC)

Identification of lipids and photopigments present in isolated LH2 complex was carried out by one- or two-dimensional TLC (see appendix 3). For photopigments (especially BChls) investigation, the extraction solvent is ethylesteracetate: water (4:1), the running solvent is methanol: acetone: water (30:20:2).

The extracted pigments were dried under argon, re-dissolved in a small volume (~5 µl) of acetone and run at the start position of the TLC plate. The TLC plates were pre-run with the similar running solvent before applying samples to remove any unwanted particles. 10 cm x 10 cm pre-coated silica gel 60 plates (Merck, Germany) were used for both phospholipids and pigments identification.

Image intensities were determined densitometrically using AIDA (Advanced Image Data Analyzer, Raytest, Straubenhardt, Germany) version 3.52 software.

2.3.7.1 Phospholipids extraction

0.5 ml sample + 1 ml methanol were vortexed thoroughly and left on ice for at least 5 min. Then 3 ml of chloroform and 3 ml of water were added, mix well and vortexed. This mixture was centrifuged at 3000 g for 15 min at ~ 4 °C, the bottom phase was collected carefully and transferred to a clean tube and dried under stream of argon. The samples could be stored at -20 °C before further analysis.

2.3.8 Statistic analysis of pigment-protein interactions in PSI

Statistic analysis of phytyl-binding pockets in PSI from *Thermosynechococcus elongatus* (Jordan *et al.*, 2001) were determined by use of the molecular simulation program WebLab ViewerPro 3.7 (Cambridge, UK). Every atom of the phytyl chains have been analysed for contacts with the surrounding environment at a radius ≤ 4 Å. Comparison of the contacts of α - and β -positioned Chls under different variance was performed with standard Chi-Square test using Microsoft Excel 2003. In all the cases, significance was assumed only if the P value is less than 0.005.

2.3.9 Structural modelling

Structural modelling of LH2 protein was based on the high resolution structures of *Rhodospseudomonas acidophila* (McDermott *et al.*, 1995; Papiz *et al.*, 2003) using the molecular simulations program WebLab ViewerPro 3.7 (Cambridge, UK) or PyMol Viewer version 0.98 (DeLano Scientific LLC, South San Francisco, California, USA).

2.3.10 Websites

Protein sequences were taken from sequence database Swiss-Prot, TrEMBL (<http://www.expasy.org>) and National Centre for Biotechnology Information (NCBI) (<http://www.ncbi.nlm.nih.gov>).

Sequences alignments were done by using BLAST (<http://www.expasy.org/tools/blast/>) or CLUSTAL W (<http://www.ebi.ac.uk/clustalw>).

3D biological macromolecular structures were downloaded from RCSB PDB protein databank (<http://www.rcsb.org>).

PDB ID **1JB0**: Photosystem I from cyanobacteria *Thermosynechococcus elongatus* at 2.5 Å (Jordan *et al.*, 2001)

PDB ID **1KZU**: LH2 from *Rhodospseudomonas acidophila* 10050 at 2.5 Å (McDermott *et al.*, 1995)

PDB ID **1NKZ**: LH2 from *Rhodospseudomonas acidophila* 10050 at 2.0 Å (Papiz *et al.*, 2003)

RESULTS

PART I:

Protein-bacteriochlorophyll interactions in
model and native light-harvesting complex 2

CHAPTER 3

Bacteriochlorophylls' macrocycle-protein interactions underlying LH2 assembly and function

3.1 INTRODUCTION

(Bacterio)chlorophyll ((B)Chl) is composed of a (bacterio)chlorin macrocycle and a long esterifying alcohol chain which is usually a phytol tail (Scheer, 1991). In protein complexes, the metal-containing chlorin macrocycles of hemes, Chls and BCHls have at least one protein ligand to the central metal atom of the macrocycle. Most of the BChl and Chl in photosynthetic proteins have a histidine as a ligand (Deisenhofer *et al.*, 1985; Goldsmith *et al.*, 1996); however, many other ligands have also been found. For instance, in LH2 of *Rps acidophila*, the BChl-B800's Mg atom is ligated to the N-terminal of the carbonyl oxygen of α Met 1ⁱ (McDermott *et al.*, 1995; Papiz *et al.*, 2003); similarly in *Rsp molischianum*, the BChl-B800 is ligated to the carboxylate of α Asp 6ⁱⁱ (Koepeke *et al.*, 1996). Other examples are found in photosystem I (PSI) from thermophilic cyanobacterium *Thermosynechococcus elongatus*, which comprises nearly 100 Chls *a* (Jordan *et al.*, 2001). Approximately 30 % of the Chls *a* in PSI have ligands other than histidine; frequently, the residues are Gln, Asp, Glu, Tyr, but also peptide groups, water and even phospholipids serve as the ligands for the Chls' central Mg atom (Jordan *et al.*, 2001).

In light-harvesting complexes of anoxygenic photosynthetic bacteria, a histidine which is defined as position 0 (His 0) is generally known to provide the coordinating

ⁱ The numbering of this residue is referred from the beginning of the N-terminus of the polypeptide. When counting from the conserved central histidine, it becomes position -30 of the α -polypeptide.

ⁱⁱ The numbering of this residue is referred as footnote i. When referring from the central histidine of the subunit, it becomes position -28 of the α -polypeptide.

ligand to the central Mg-atom of the dimeric BChl, as evidenced by resonance Raman data (Robert & Lutz, 1985; Chang *et al.*, 1990), high-resolution structure of LH2 (McDermott *et al.*, 1995) and mutagenesis studies (Bylina *et al.*, 1988). Mutation of His 0 to other amino acids has been shown not to severely hamper LH1 complexes formation (Bylina *et al.*, 1988, Olsen *et al.*, 1997). Moreover, replacing His 0 with Gln, Ser or Thr in bacterial RC, has also been shown to have no effect on the function of the RC (Coleman & Youvan, 1990; Goldsmith *et al.*, 1996). In contrast, LH2 complex formation in *Rb sphaeroides* is found to be abolished when His 0 of LH2 is mutated (Olsen *et al.*, 1997).

The ligation to the central Mg atom is often regarded as the most important factor for the binding of (B)Chl (Coleman & Youvan, 1990; Davis *et al.*, 1996; Olsen *et al.*, 1997). Nevertheless, various peripheral interactions exist between the (B)Chls' macrocycle and surrounding protein residues. Studies of reconstitution with modified BChl, site-directed mutagenesis and resonance Raman have been used to evaluate these interactions in details.

Peripheral substituents of the (bacterio)chlorin, such as the acetyl group at the C3 position, the carbomethoxy and keto carbonyl groups at C13 of ring E (Gudowskanowak *et al.*, 1990; Sturgis *et al.*, 1995; Scheer & Hartwich, 1995; Davis *et al.*, 1996) (for numbering system, see figure 3-1) have been found to play an important role in determining (B)Chl attachment and functional assembly of (B)Chl. The oxo-group of these substituents often partake in hydrogen (H)-bonding with the polypeptide residues in their close vicinity (e.g. Davis *et al.*, 1996; Braun *et al.*, 2003; Garcia-Martin *et al.*, 2006b; Rutkauskas *et al.*, 2006). It has been shown that the interactions with C3 acetyl oxo group modulate the electronic properties, and possibly the redox potential (Ivancich *et al.*, 1998). The aromatic residues Tyr +13 and Tyr +14 (figure 3-2) of the α -polypeptides of *Rb sphaeroides* LH2 have been found to participate in H-bonding with the C3¹-acetyl carbonyl group of one of the BChl-B850; breakage of this interaction results in a blue-shift of more than 10 nm of the BChl-B850 red-most absorption band (Fowler *et al.*, 1992, 1995). Similarly, disruption of the H-bonding between C3¹-acetyl and β Arg -10 of LH2 induces a ~10 nm red-shift in the Q_y absorbance maximum of BChl-B800 (Gall *et al.*, 1997). H-

bonding interactions with the C13 oxo groups have less or no effect on the electronic properties (Mattioli *et al.*, 1995; Ivancich *et al.*, 1998; Braun *et al.*, 2003). It is still not well understood whether these interactions contribute to the structural stability of the membrane-embedded (B)Chl proteins.

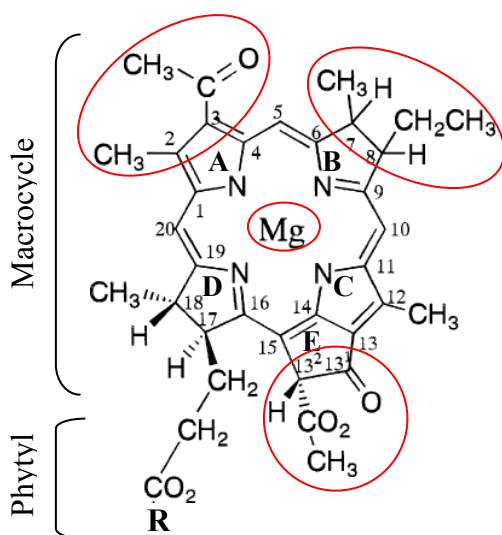


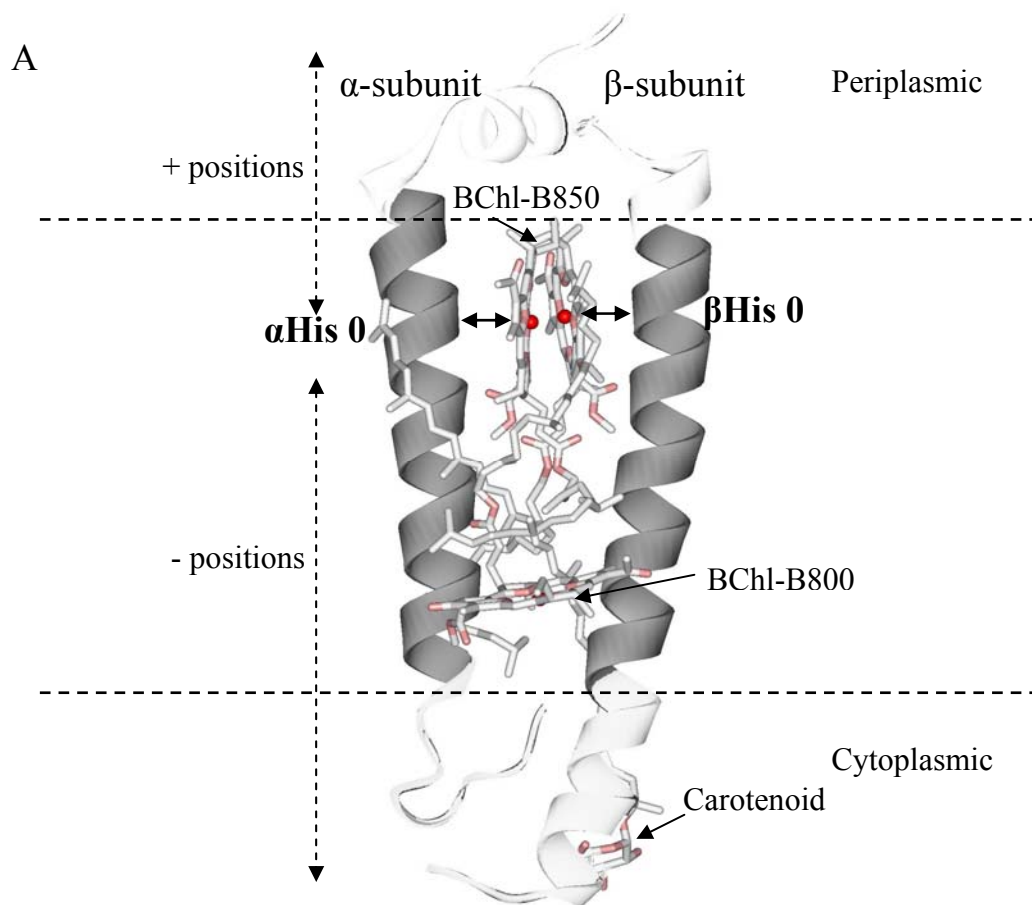
Figure 3-1: Structure of BChl *a*. It consists of a Mg tetrapyrrole macrocycle and a phytol chain (R). The important sites of interactions between BChl and proteins are circled in red. Nomenclature is according to IUPAC system.

In this chapter, peripheral interactions between pigment and protein, particularly with the BChl's macrocycle and their impact on LH2 assembly are investigated. Interactions between BChls' alcohol chains and protein are discussed in chapter 4.

Light-harvesting complex 2 (LH2) of *Rb sphaeroides* serves as a model system for the study of BChls-protein interactions. As described in Chapter 1 (section 1.2.1.1), the LH2 elementary subunit consists of three BChls, one or two carotenoids, and multiple copies of two relatively short (~50 amino acids each) α - and β -polypeptides (McDermott *et al.*, 1995). The primary structure of the α - and β -polypeptides is found to be highly homologous within the *Rhodospirillaceae* genus and even within the α -proteobacteria family (Zuber, 1985; Zuber & Brunisholz, 1991). Two common structural features are observed in LH2 polypeptides. Firstly, the polypeptides have a three-domain arrangement, namely the hydrophobic core (non-polar) region, the polar N- and C-termini. The transmembrane hydrophobic core region spans the

membrane once as an α -helix (McDermott *et al.*, 1995). Secondly, both the α - and β -polypeptides contain a highly conserved histidine residue. This residue is located on the C-terminal part of the hydrophobic domain and is ligated to the BChl central Mg-atom (McDermott *et al.*, 1995; Prince *et al.*, 1997) (figure 3-2).

The α - and β -polypeptides carry the information required for LH2 complex assembly and the optimum arrangement of light-harvesting pigments. They determine the relative position, orientation and environment of the pigment molecules, and thereby modulate their spectral properties. In numerous high-resolution structures of membrane proteins, H-bonding networks are shown to stabilise helix-helix association, and thereby contribute to the assembly of the final folded 3D structure. Participating in these bonds are the polypeptides' backbone keto carbonyl groups, as well as the polar side chain groups (Theiler *et al.*, 1984; Adamian & Liang, 2002). In cofactor binding proteins, the interactions between cofactor and polypeptide have been shown to critically contribute to the assembly and function of these proteins (e.g. Fowler *et al.*, 1992, 1995; Choma *et al.*, 2000; Zhou *et al.*, 2001).



B

N-terminal -15... -10... -5... 0... +5... +10 C-terminal

α : TNGKIWL VVKPTVGVPLFLSA AVIASVVIHAAVL TTTT WLPAYY QGSA AVAAE

β : TDDL NKVWPSGLTVAEAE EVHKQLILGTRVFGGMALIAHFLAAA ATPWLG

Figure 3-2: (A) An illustration of the elementary subunit of LH2 complex (McDermott *et al.*, 1995). Illustrated in side view are $\alpha\beta$ -polypeptides, three BChls and one carotenoid. The hydrophobic stretches in the transmembrane helices (TMHs) are displayed in grey; the N- and C-terminal (polar region) are displayed in white. BChls and carotenoid are sandwiched in between the $\alpha\beta$ -subunit and are displayed in stick style. The central Mg-atoms of BChl-B850 are displayed in red, ligated (solid arrows) to the histidine residue at position 0; for clarity the His 0 are not shown.

(B) The amino acid sequences of α - and β -polypeptides of LH2 complex from *Rb sphaeroides*. The hydrophobic region is marked in grey. The numbering specifies the amino acid position relative to the histidine, designated His (0) which binds the central Mg^{2+} atom of BChl-B850. Residues located on the N-terminal side of His 0 are defined as minus positions and residues on the C-terminal side of His 0 are defined as positive positions (this numbering system is used throughout the thesis, unless stated otherwise).

In order to fully understand the structure-function relationships underlying the assembly of pigment binding proteins, it is important to evaluate the contributions made by specific binding elements. In this chapter, the BChl-polypeptide interactions within the BChls-B850 binding pockets of LH2, in particular, the macrocycle binding sites have been investigated in their native lipid environment by the use of simplified model sequences (Braun *et al.*, 2002, 2003; Kwa *et al.*, 2004; Garcia-Martin *et al.*, 2006b). Our strategy is to design simplified polypeptides that are still able to assemble an antenna-like complex, i.e. a BChl-protein complex with characteristic red-shifted absorption bands and able to function in light-harvesting, i.e. to absorb and transfer light among the photopigments. Critical motifs (such as H-bonds) may be detected within the context of the destabilised model system, which may easily go unnoticed in the wild type sequence context due to multiple, compensating native interactions.

Our approach is to replace the native amino acids of the BChl binding sites flanking His 0 with simplified alanine-leucine (Ala-Leu) sequences. The use of model transmembrane helix (TMH), frequently poly-Leu or Ala-Leu stretches has been employed in several membrane proteins studies (e.g. Braun & von Heijne, 1999; von Heijne 1999; Braun *et al.*, 2002, 2003; Liu F *et al.*, 2004; Garcia-Martin *et al.*, 2006b). His 0 was kept for maintaining the ligation to the central Mg²⁺ atom (figure 3-2). Alternating Ala and Leu residues were chosen for several reasons. Small and hydrophobic residues are found frequently in well-packed regions of the TMH, particularly, in purple non-sulphur bacteria (Zuber & Cogdell, 1995). Furthermore, the relatively short side-chain of alanine facilitates the pigments accommodation in the binding pocket without major disturbances by steric hindrance. The hydrophobic leucine residue is frequently present in transmembrane proteins, in particular at lipid exposed stretches (von Heijne, 1999). Using such simplified model sequences, the complexity of BChl-protein interactions may be reduced by the reduction or elimination of multiple native interactions. Distinct interactions may be studied by the re-introduction of wild type residue(s) into such a simplified model sequence and thereby interaction motifs at the BChl-protein interface may be identified.

The assembly and function of these modified LH2 complexes have been examined *in vivo* by introducing plasmid-borne LH2 genes into a LH2⁻ LH1⁻ RC⁻ background (DD13 strain, Jones *et al.*, 1992; see chapter 1). The assembly of the LH2 complexes is monitored spectroscopically, as alterations in the BChl-BChl and BChl-polypeptide association in the membrane will result in spectroscopic changes.

3.2 RESULTS AND DISCUSSION

SIMPLIFICATION OF THE BCHL-B850 BINDING SITE: MODEL SEQUENCES IN THE TMH OF THE β -SUBUNIT

Design of the model LH2 α WT/ β AL

The factors contributing to the assembly and function of LH2 are explored by the use of a simplified Ala-Leu model sequences in the TMHs replacing the BChl-B850's binding site of the β -subunits. Specifically, the amino acid residues of the β -subunits in the close vicinity of the macrocycle of BChl-B850 are replaced by Ala or Leu residues. The resulting mosaic model β -subunits are then expressed with either wild type α -subunits (α WT) or model α -subunits (α AL) (Braun *et al.*, 2002) in the native membrane environment of modified *Rb sphaeroides* DD13 strain (LH2⁻ LH1⁻ RC⁻, for details see chapter 1 section 1.5.2 and chapter 2).

A contiguous stretch of 13 residues from β Phe -8 to β Ala +5 in the TMH of LH2 β -subunits has been replaced with a simplified Ala-Leu sequence (figure 3-3). In LH2 β WT, this stretch includes all residues that are proposed to interact with the macrocycles of α - and β -BChls-B850 at distances less than 4.5 Å, except for β Thr +7 and β Trp +9 which lie outside of the β -TMH domain (figure 3-3). When screening LH2- β sequences for overall Ala-Leu content in other purple non-sulfur bacteria, it was found that the Ala and Leu content is relatively high in this stretch of 13 residues. For example, a total of seven Ala and Leu residues were found in *Rb sphaeroides*, *Rps acidophila* and *Rb sulphidophilus* and a total of six were found in *Rb capsulatus* and *Rb gelatinus*. Except for Ala at position -4, Ala and Leu do not occupy identical positions in various species but are distributed randomly over this stretch of TMH (Zuber, 1985; Zuber & Cogdell, 1995; Braun *et al.*, 2002).

From residues β Phe -8 to β Ala +5, five amino acids have been replaced. Residues at positions -7, -6, -2 and +1 were replaced with Leu and the residue at position -5 was replaced with isoleucine (figure 3-3). Residues at position -4, -1, +3, +4 and +5 happened to be Ala already and the residues at position -3 and +2 were Leu in the

WT sequence. β His 0 has not been replaced in order to retain the ligation with the central metal of the BChl. In addition, β Phe -8 was not replaced because it is relatively conserved and in close proximity of the C13 groups of the BChl-B850 molecules (McDermott *et al.*, 1995; Papiz *et al.*, 2003). In previous studies, the importance of the C13 substituents for BChl-binding and assembly have been demonstrated (Scheer & Hartwich, 1995; Davis *et al.*, 1996). Thus, a total of five “new” residues are contained in the stretch of 13 alternating Ala-Leu residues. This mosaic β -subunit is expressed with the complement of α WT or α AL (Braun *et al.*, 2002).

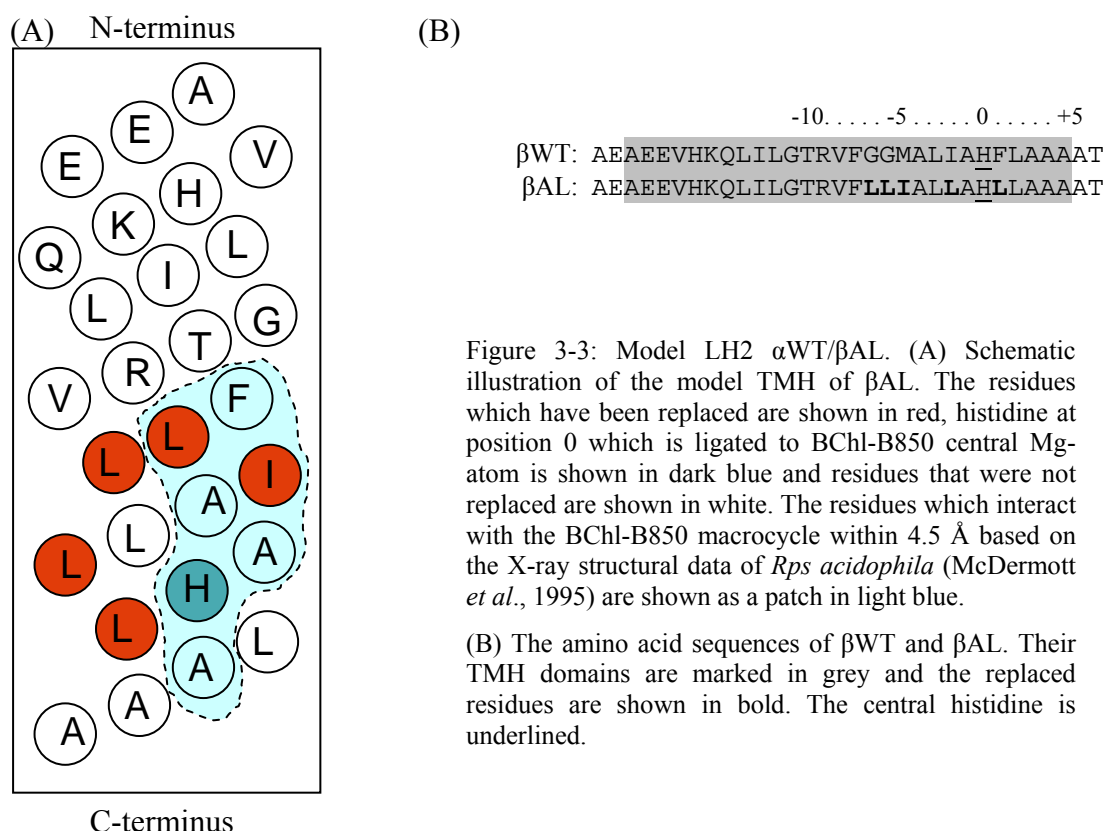


Figure 3-3: Model LH2 α WT/ β AL. (A) Schematic illustration of the model TMH of β AL. The residues which have been replaced are shown in red, histidine at position 0 which is ligated to BChl-B850 central Mg atom is shown in dark blue and residues that were not replaced are shown in white. The residues which interact with the BChl-B850 macrocycle within 4.5 Å based on the X-ray structural data of *Rps acidophila* (McDermott *et al.*, 1995) are shown as a patch in light blue.

(B) The amino acid sequences of β WT and β AL. Their TMH domains are marked in grey and the replaced residues are shown in bold. The central histidine is underlined.

The functional and structural characteristics of α WT/ β AL

The assembly of model LH2 α WT/ β AL is monitored by absorption spectroscopy (figure 3-4). The absorption spectrum of α WT/ β AL is largely similar to the spectrum

of WT LH2 complexes. In particular, the red-shift of the BChl-B850 red-most transition is retained with no significant alteration in the absorption maximum. This indicates that the BChl assemble to typical 'BChl-B850'. On the other hand, the red-most transition of the BChl-B800 band of α WT/ β AL is slightly reduced and broadened. In addition, there is a high level of scattering in the blue-region of the spectrum, which suggests that less α WT/ β AL is assembled in the membrane as compared to WT LH2.

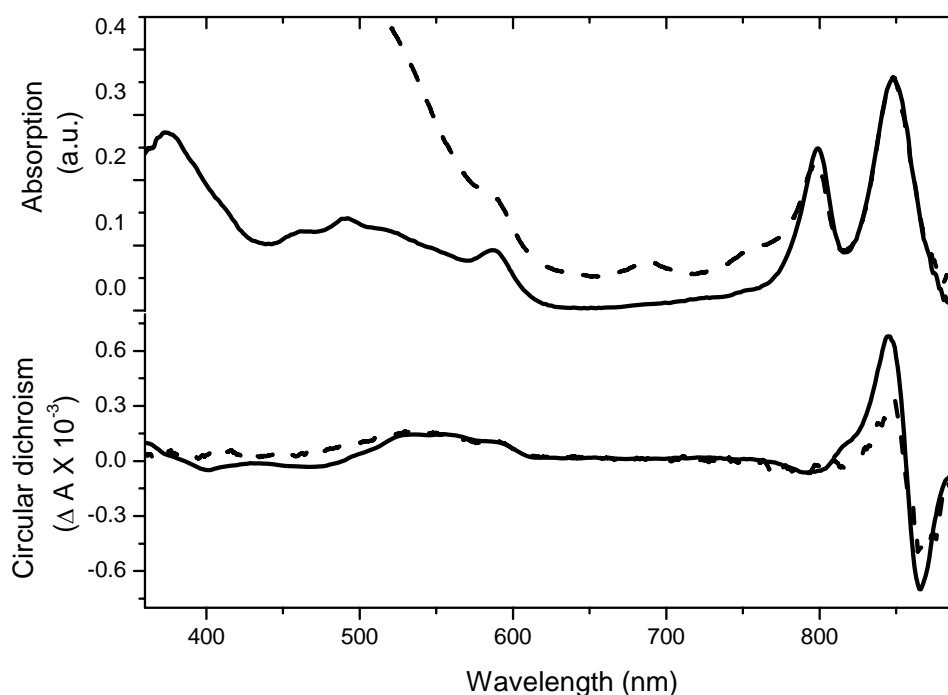


Figure 3-4: Absorption (upper panel) and circular dichroism spectra (lower panel) of LH2 with WT (solid line) and α WT/ β AL (dash line). Spectra are taken of membranes prepared from *Rb sphaeroides* DD13 strain. Note the elevated absorption in the blue region of α WT/ β AL.

The CD signals from the BChl-B850 may serve as a fingerprint of the pigment arrangement within LH2 protein. The CD signals of WT and α WT/ β AL LH2 complexes are shown in the lower panel of figure 3-4. The signal at ~ 795 nm is assigned to the BChls-B800 and the lowest exciton of BChl-B850 (Cogdell & Scheer, 1985; Koolhaas *et al.*, 1998). The CD signal of the BChl-B800 is relatively weak as the distance between the macrocycles of BChls-B800 is rather large (~ 20 Å

between their Mg atoms) and thus there are no strong excitonic interactions among these pigments in the complex (van Grondelle, 1985; McDermott *et al.*, 1995). The contributions of the strong S-shaped CD signal originates from the BChl-B850 macrocycles, which are strongly coupled due to their relative closeness and geometrical arrangements (see chapter 1, figure 1-4). The CD signal of BChl-B850 has extrema at 846 nm (+) and at 869 nm (-) with the zero crossing at ~855 nm; which is largely similar in LH2 α WT/ β AL and WT (Cogdell & Scheer, 1985). In α WT/ β AL, the strength of the BChl-B850 appears to be weaker as compared to the strength of WT, which may reflect some rearrangements and/or loss of pigments from this site. Nevertheless, the re-designed α WT/ β AL is able to support the binding of BChl molecules and the assembly into LH2-like complexes. However, the observed changes, in particular, the appearance of 760 nm shoulder and the high level of signal in the blue region of the spectrum, suggests that the expression level of assembled complex in mutant is weaker compared to WT LH2.

The function of LH2 complex is assessed by monitoring the excitation energy transfer, i.e. the efficiency of energy transfer within photopigments of the complex. In the fluorescence excitation spectra (figure 3-5), the typical broad excitation band from 450-550 nm is derived from the major carotenoid of *Rb sphaeroides*, spheroidenone. In α WT/ β AL, the intensity of the carotenoid is slightly reduced relative to that in WT LH2. Moreover, the intensity of the BChl-B800 excitation band is also decreased relative to the WT. Otherwise, the excitation spectrum of α WT/ β AL is largely similar to WT, and thus its functionality is largely retained.

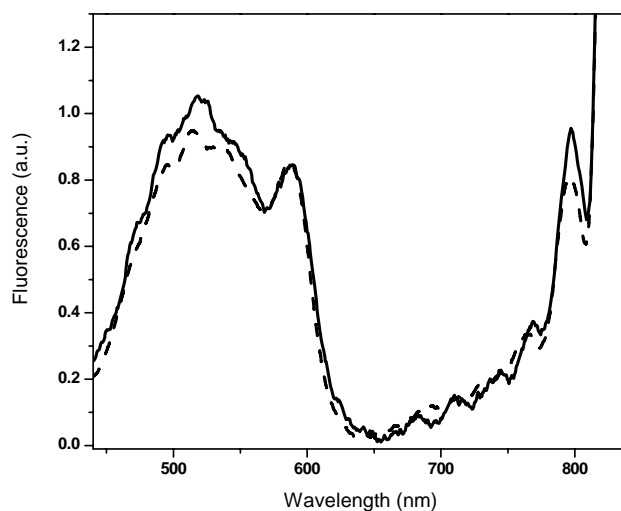


Figure 3-5: The fluorescence excitation spectra of LH2 WT (solid line) and α WT/ β AL (dash line). The bands at 800 nm arise from BChl-B800; at \sim 580 nm from the Q_x -transition of the BChls, and between 450 and 550 nm from carotenoid spheroidenone. The spectra are normalised to the BChl Q_x -transition at 590 nm. $\lambda_{\text{emission}} = 860$ nm.

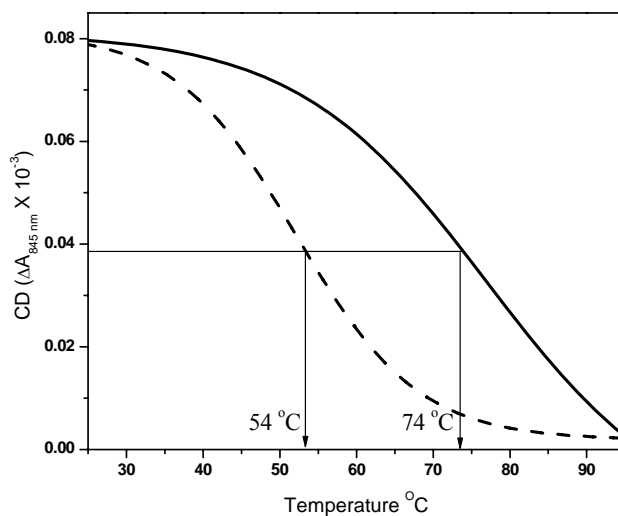


Figure 3-6: Thermal denaturation of LH2 WT (solid line) and α WT/ β AL (dash line). Changes of the CD signal at 845 nm during constant heating of LH2 membranes. The T_m values are indicated by arrows, heating rate is 2 $^{\circ}\text{C}$ per min.

Possible interactions contributing to the stabilisation of the LH2 complex might include: (1) coordination of the ligand to the Mg atom of the BChl, (2) H-bonding between the protein and BChl, (3) H-bonding between amino acid side chains of the polypeptides, (4) ion-pair interactions between the polypeptides and (5) packing interactions between polypeptide helices (Dunker & Jones, 1978). In order to

explore whether the simplification of the BChl-B850 binding site affected these stabilising interactions, the structural stability of pigment-protein complexes is assessed by monitoring the decay of the CD signal at ~845 nm of BChl-B850 during thermal denaturation of LH2 α WT/ β AL in the native lipid environment (figure 3-6). The mid-point of denaturation transition (T_m) of LH2 α WT/ β AL is shifted to a lower temperature (from ~74 °C in WT to ~54 °C). Thus, the thermal stability of this simplified model LH2 is significantly reduced.

In summary, LH2 α WT/ β AL retained a near native-like assembly of the photoactive BChl pigments in the complex. Minor losses and/or rearrangements of pigment binding are observed in the absorption, CD and the fluorescence excitation spectra. However, the overall arrangement of BChls pigments in the LH2 of α WT/ β AL is highly similar to WT. Taken together, these results indicate that by simplifying the binding site of the BChl-B850 around the β His 0 residue, pigment binding and/or arrangement are insignificantly altered and the complex assembly and function are largely retained.

The thermal stability of LH2 α WT/ β AL complex is greatly reduced in comparison to WT. This suggests that the immediate protein environment at the BChl/protein interface is of little importance for pigments function but of critical importance for the stable assembly of LH2 complex. Subsequent attempts have been made to further simplify the model β -subunit (for all amino acid sequences attempted see table 1-1). In all these further modifications, no formation of LH2-like complexes is observed (this investigation is presented in chapter 4). This suggests that the simplified β -polypeptide of LH2 is at its limit of tolerance to further modifications in the vicinity of the BChl-B850 binding site. α WT/ β AL model LH2 is marginally stable as further attempts at modifying the BChls-B850 binding site of β AL has been unsuccessful.

From these observations, the following may be concluded: (1) the five residues modified in α WT/ β AL (-7, -6, -5, -2 and +1) have little impact on the assembly and functionality of BChl-B850. (2) These residues have a significant impact on the stability of LH2 protein.

STUDY OF INTERACTION MOTIFS AT THE MODEL AND NATIVE BCHL-PROTEIN INTERFACE: H-BONDING BETWEEN THE HYDROXYL OF SERINE AND THE KETO CARBONYL OF BCHL-B850

The study of α WT/ β AL suggests that the residues at the BChl-B850/protein interface are of little importance for the pigment spectral and functional properties but of critical importance for stable assembly. The intolerance of β -subunits to further mutation is rather surprising. Based on the available LH2 x-ray structure from *Rps acidophila* (McDermott *et al.*, 1995) which closely resembles the LH2 from *Rb sphaeroides* (Walz *et al.*, 1998), the outer ring of the LH2 complex is formed by β -polypeptides, while the inner ring by α -polypeptides. The internal radius of the LH2 ring is ~ 18 Å and the external radius is ~ 34 Å (figure 3-7). It has been proposed that the outer ring of the complex, formed by the β -polypeptides is not as tightly packed as the α -polypeptides and therefore would permit more flexibility in its interactions than the inner ring made by α -polypeptides (Olsen *et al.*, 1997). Yet, our studies suggest otherwise.

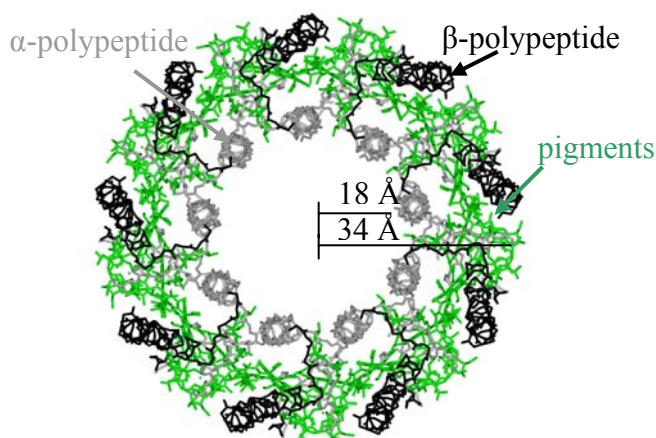


Figure 3-7: Schematic illustration of LH2 complex from the crystal structure of *Rps acidophila* (McDermott *et al.*, 1995). The α -polypeptides are displayed in grey, β -polypeptides displayed in black and photosynthetic pigments displayed in green. The internal radius of LH2 ring is ~ 18 Å and the external radius is ~ 34 Å.

A stretch of 14 amino acid residues in the BChl-B850 binding site of LH2 α -polypeptide from residues α Val -7 to α Thr +6, was successfully replaced by a

simplified Ala-Leu sequence, α AL/ β WT (Braun *et al.*, 2002; Kwa *et al.*, 2004) (figure 3-8). This simplified sequence includes a total of eight ‘new’ residues, as some residues were already Ala or Leu and some of the residues which are critical for assembly were not changed. This modified α AL/ β WT is still able to assemble to LH2-like complexes with little effects on its light-harvesting activity (Braun *et al.*, 2002; Kwa *et al.*, 2004). This suggests that LH2 functional assembly is less susceptible to alterations of the α -subunit than the β -subunit. Clearly, more residues may be mutated in the α -polypeptides which make up the BChl-B850 binding pocket than in the β -polypeptides. It appears that the amino acids surrounding His 0 of α -subunit play a subordinate role in LH2 assembly. This provides new insight into the factors that determine the assembly of LH2. Obviously, there are residues in the β -subunits, adjacent to the BChl-B850 site which is critical for the assembly of this complex. It appears that the two subunits have distinct roles in the make up of LH2 complex.

H-bond donor residue at position -4 of α -subunit

In the model LH2, α WT/ β AL, only 5 out of 28 residues of the β -TMH region, specifically in the BChl-B850 binding site, has been replaced by Ala or Leu residues. Any additional attempts to further modify the residues towards the N- and C-terminus lead to the loss of LH2-like complex from the membrane. In contrast, in model LH2, α AL/ β WT, 8 out of 25 residues of the α -TMH region have been replaced by Ala or Leu without the loss of light-harvesting active complexes (Braun *et al.*, 2002; Kwa *et al.*, 2004; Garcia-Martin *et al.*, 2006b). In α AL/ β WT, assembly of LH2-like complex is supported, but the expression level is low and the T_m of α AL/ β WT is much reduced (~ 34 °C against ~ 70 °C in WT).

The distinct contribution of individual residues to protein assembly and stability can be studied by the re-introduction of wild type amino acid residues into the model sequence. It has been noted that the residue at position -4 is relatively conserved, in α -subunit of photosynthetic bacteria being either serine or alanine residues (Zuber, 1985). In *Rb sphaeroides*, when α Ser -4 was re-introduced into the model sequence

of LH2 α AL_{-4S}/ β WT, the stability of α AL/ β WT complex is dramatically increased (from ~ 34 °C to ~ 57 °C) (figure 3-8).

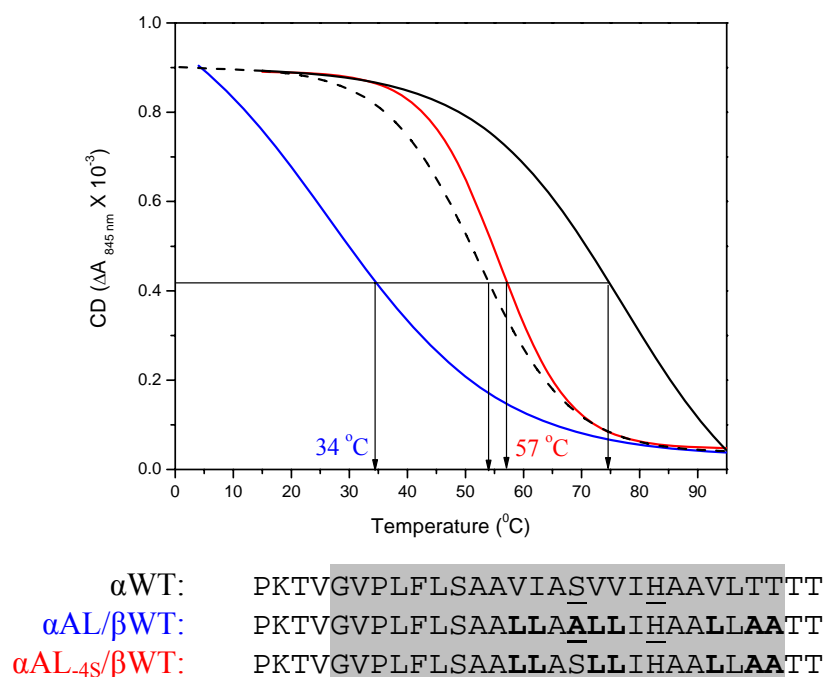


Figure 3-8: Thermal denaturation of LH2 WT (black solid line), α WT/ β AL (dash line), α AL/ β WT (blue line) and α AL_{-4S}/ β WT (red line). Changes of the CD signal at 845 nm during constant heating of suspended membranes. The T_m values are indicated by arrows. The heating rate is 2 °C per min. The amino acid sequences of the α -subunit of WT, α AL/ β WT and α AL_{-4S}/ β WT are shown underneath the graph. Their TM helical domains are marked in grey and the replaced residues are shown in bold. The central histidine and residue at position -4 are underlined.

It is important to note that the exchange of serine with alanine in WT sequence context (α WT_{-4A}/ β WT), does not significantly affect the stability, assembly and function of the complex (Braun *et al.*, 2003). This suggests that relatively critical interactions can be detected within the context of a simplified model sequence. These interactions would normally go unnoticed in the WT or singular mutation due to a manifold of compensating native interactions. It cannot be excluded, however, that there are structural modifications in the model sequence context which further enhance the stabilising effects of α Ser -4.

Residue α Ser -4 was first proposed to partake in H-bonding to BChl-B850, based on the Raman data and its close proximity to the isocyclic ring of BChl-B850 (Sturgis *et al.*, 1995). Recently, this has been evidenced by site-directed mutagenesis and

resonance Raman spectroscopy studies (for details see Braun *et al.*, 2003). The Raman signals for the BChl of WT LH2 complex from *Rb sphaeroides* have been described and assigned previously (Robert & Lutz, 1985). In brief, the signals between 1620 and 1700 cm^{-1} arise from the stretching modes of either the acetyl or keto carbonyl substituents of the BChl macrocycles. The band at 1651 cm^{-1} is shifted relative to the Raman band of keto carbonyl groups which are free from strong interaction with the surrounding environment. Exchange of α Ser -4 by alanine (α WT_{-4A}/ β WT), results in a shift of the 1651 cm^{-1} band to higher wavenumbers. This shift of the 1651 cm^{-1} band indicates that the H-bond to the C13¹ keto carbonyl of one of the BChl-B850 has been disrupted or significantly weakened in α WT_{-4A}/ β WT (Braun *et al.*, 2003) (figure 3-9). Computer modelling suggests that the hydroxyl group of the α Ser -4 and the keto carbonyl group of the β BChl-B850 C13¹ partake in H-bonding (Braun *et al.*, 2003).

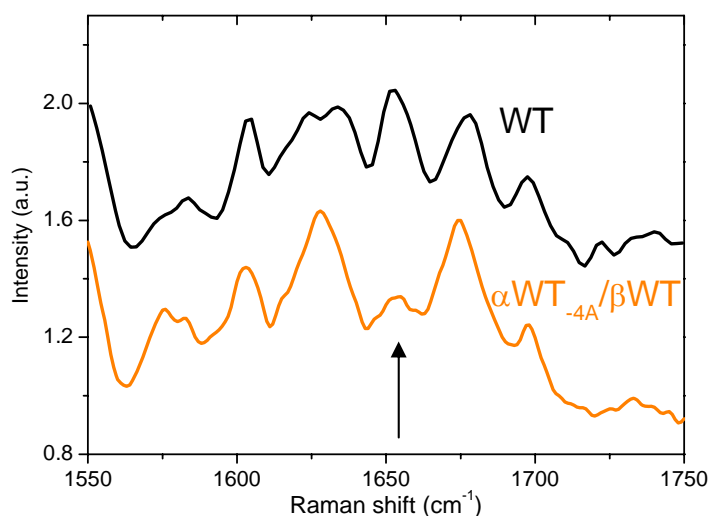


Figure 3-9: Resonance Raman spectra of LH2 WT (black) and α WT_{-4A}/ β WT (orange) membranes from *Rb sphaeroides* DD13 strain in the 1550-1750 cm^{-1} carbonyl stretching region (Braun *et al.*, 2003). The Raman band at 1651 cm^{-1} is indicated by arrow.

Taken together, the side chain hydroxyl group of the serine residue participates in H-bonding with β BChl-B850 C13¹ keto carbonyl group of β BChl-B850. This H-bond increases the thermal stability of the model complex in the native membrane.

The importance of α Ser -4 and thus the H-bond at the BChl-B850-protein interface is further evidenced by use of LH2 model complex, α AL/ β AL with Ala-Leu sequences replacing both the native BChl-B850 binding sites in the α - and β -subunits. Use of both, α AL and β AL simultaneously, has resulted in a complete loss of assembled LH2 from the membrane. The assembly of this doubly modified complex can be restored by the re-introduction of serine at position -4 of the α -subunit, α AL_{-4S}/ β AL (figure 3-10A).

LH2 α AL_{-4S}/ β AL shows similar spectral properties as LH2 WT. In the optical spectrum of α AL_{-4S}/ β AL (figure 3-10A), a number of minor changes are observed. The red-most absorption band is red-shifted from 848 nm in LH2 WT to 853 nm in α AL_{-4S}/ β AL. The BChl-B800/B850 absorption ratio is reduced which indicates either a minor structural rearrangements of the BChl-B800 molecules and/or a partial loss of BChl-B800. The T_m of LH2 α AL_{-4S}/ β AL is at \sim 40 °C as compared to the T_m of LH2 WT which is at \sim 74 °C (figure 3-10B). Remarkably, this model complex which is constituted by subunits with a total of 12 mutations is more stable than α AL/ β WT ($T_m = 34$ °C, figure 3-8) which contains 8 mutations. This further supports the notion that the H-bond formed by α Ser -4 is particularly crucial for the structural stability of this complex. Taken together, the H-bond of serine -4 residue increases the thermal stability and thus is crucial for the expression of LH2-like complex.

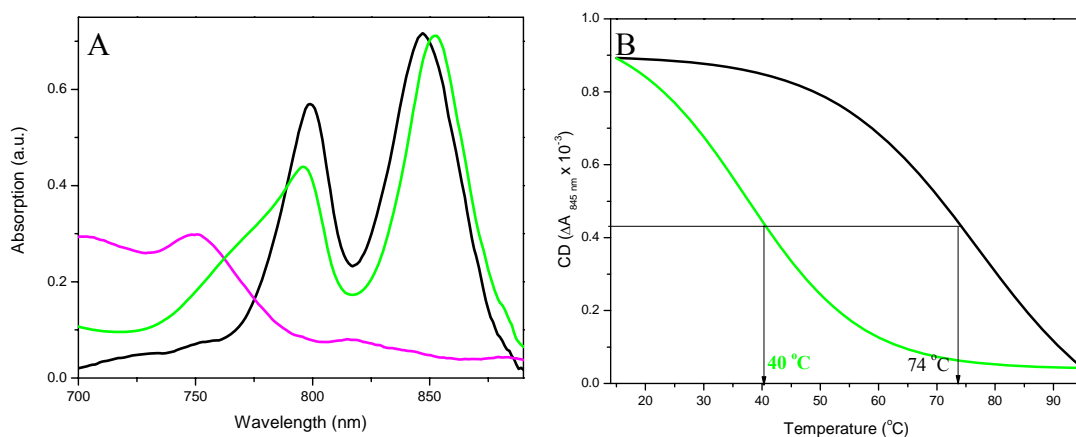


Figure 3-10: Critical role of residue α Ser -4 in the assembly and stability of model LH2. (A) NIR absorption spectra of LH2 WT (black line), α AL/ β AL (magenta line) and α AL_{4S}/ β AL (green line). (B) Thermal stability of LH2 WT (black line) and α AL_{4S}/ β AL (green line). Changes of the CD signal at 845 nm during constant heating of LH2 membrane. The T_m values are indicated by arrows. The heating rate is 2 °C per min.

H-bond donor residue at position -4 of β -subunit

In most light-harvesting bacteria, the residue at position -4 of the α - and β -subunits is highly conserved (Zuber & Brunisholz, 1991; Olsen *et al.*, 1997; Braun *et al.*, 2002). This position is occupied by alanine or serine (found in *Rb sphaeroides* and *Rb sulfidophilus* only) in the α -subunit and exclusively alanine in the β -subunit (figure 3-11), which indicates the importance of the residue at position -4.

Hydrogen-bonds are recognised to play an important role in the stabilisation and function of proteins in general (Jiang & Lai, 2002; Braun *et al.*, 2003; Sarkhel & Desiraju, 2004). A H-bond has about 5-10 % of the strength of a covalent bond but in the membrane interior, this interaction is proposed to be stronger due to the low dielectric lipid environment (Ippolito *et al.*, 1990; Derewenda *et al.*, 1995). Moreover, it has been shown that H-bonding interactions may drive the association of transmembrane α -helical bundles in native and model proteins (e.g. Ippolito *et al.*, 1990; Senes *et al.*, 2001; Adamian & Liang, 2001; Sarkhel & Desiraju, 2004).

TMH region of β -subunit sequences:

		-10	-5	0	+5
RHOSH	LH2 [P0C0Y2]	LTVAEAE	EVHKQL	LILGTRV	FGGMALIAHFLAAAATPWLG
RHOAC	LH2 [P26790]	LTAEQSEEL	HKYVIDG	TRVFLGL	<u>ALVAH</u> FLAFSATPWLH
RHOSU	LH2 [P95654]	LTAEAE	EVHKQL	LIDGTRV	FGAI <u>ALFAH</u> FLAAIATPWLG
RHOCA	LH2 [P07368]	LSLKEAE	EIHSYL	IDGTRV	FGAM <u>ALVAH</u> ILSAIATPWLG
RHOPA	LH2 [P35107]	LTIAEAE	EELKHV	IDGTRIF	GAI <u>AIVAH</u> FLAYVYSPWLH
RHOGE	LH2 [P72281]	LTAEAE	EELQKGL	VLDGTRV	FGV <u>AVLAH</u> ILAYAYTPWLH
RHOVI	LH2 [P04124]	LTEEAKE	EFHGIF	VTSVLY	LATA <u>AVIVH</u> YLVWTARPWIA
RHOTE	LH2 [P80587]	LTVAEAE	EELHTY	VTNGFR	VFVGI <u>AVVAH</u> VLVFAAHPWGR
RHOMO	LH1 [Q9R4K4]	LSESEAE	QEFHGIF	VTSFIS	FIVV <u>AIVAH</u> FLAWKWRPWL
RHOCA	LH1 [P02950]	LTDEQA	QELHAV	YMSGLS	AFIAV <u>AVLAH</u> LAVMIWRPWF
RHOSH	LH1 [Q0C0YE]	LTDEQA	QELHSV	YMSGLW	PFSAV <u>AIVAH</u> LAVYIWRPWF
RHOPA	LH1 [Q6N9L5]	LSEAEAK	EFHSIF	VTSFFL	FIVV <u>AVVAH</u> ILAWMWRPWL
RHOGE	LH1 [P51757]	LTDEQA	QEFHKF	WVQGF	VGTAV <u>AVVAH</u> FLVWVWRPWL
RHORU	LH1 [P04125]	ITEGEAK	EFHKIF	TSSILV	FFGV <u>AFAH</u> LLVWIWRPWP
RHOSU	LH1 [Q9WXD9]	LTDEQA	QEIHAV	YMSGLW	LFSAV <u>AVLAH</u> LAVYIWRPWL
RHOAC	LH1 [P35099]	VSDAEAK	EFHALF	VSSFTA	FIVIA <u>AVLAH</u> VLAWAWRPWIP
RHOSH	LH1 [P0C0Y1]	LTDEQA	QELHSV	YMSGLW	PFSAV <u>AIVAH</u> LALVYIWRPWF
RHOMA	LH1 [P80260]	LTEGEAR	EFHGVF	MFSFMV	FAV <u>AIVAH</u> ILAWMWRPWI

RHOSH: *Rhodobacter sphaeroides*; RHOAC: *Rhodospseudomonas acidophila*; RHOMO: *Rhodospirillum molischianum*; RHOTE: *Rhodocyclus tenuis*; RHOMA: *Rhodospseudomonas marina*; CHRVI: *Chromatium vinosum*; RHOSU: *Rhodobacter sulfidophilus*; RHOCA: *Rhodobacter capsulatus*; RHOPA: *Rhodospseudomonas palustris*; RHOGE: *Rhodobacter gelatinus*; RHOVI: *Rhodobacter viridis*.

Figure 3-11: Amino acid alignment of TMH of β -subunits of LH2 and LH1 of photosynthetic bacteria. The His 0 is shown in bold and the -4 residues are shown in bold and underlined. Exspasy sequence code numbers are shown in brackets [www.exspasy.org].

The hydroxyl group of serine is able to act as a proton donor for the H-bond with the C13¹ keto carbonyl group of BCHls (Braun *et al.*, 2002). This residue contributes substantially to the stability of the novel LH2 complex as shown previously (Braun *et al.*, 2003; Kwa *et al.*, 2004). On the other hand, alanine is usually regarded as a non-potential participant in H-bonding as it has only the H of the methyl group. Nevertheless, it has been suggested that the CH could act as a H-bond donor in some recent studies (Desiraju, 2002; Braun *et al.*, 2003) and CH...O contacts are now being increasingly accepted as genuine H-bonds (Jiang & Lai, 2002; Sarkhel & Desiraju, 2004).

The free energy of H-bonds can be estimated by structural studies (Sarkhel & Desiraju, 2004). Accordingly, the energy of H-bonding to methyl hydrogen (CH...O) has been estimated to be ~2 kJ/mol (Scheiner *et al.*, 2001; Jiang & Lai, 2002), while

the H-bond to hydroxyl groups of serine ($\text{OH}\cdots\text{O}$) is estimated to be ~ 10 kJ/mol (Zadorozhnyi & Ishchenko, 1965). Due to the intrinsic nature of macromolecular systems, there is a compromise between several interactions of varying strengths that may interfere with each another significantly (Jiang & Lai, 2002). Therefore, the weak H-bonds of $\text{CH}\cdots\text{O}$ are less readily identified compared to the stronger H-bonds of $\text{OH}\cdots\text{O}$.

The structure of the LH2 of *Rb sphaeroides* has not yet been determined by crystallography; but only by cryo-electron microscopy (Walz *et al.*, 1998). It is however generally regarded to resemble the structure of the *Rps acidophila*. To model putative H-bond between residues at -4 of the α - and β -subunits and the C13¹ keto carbonyl group of BChl-B850s, the high-resolution structure of LH2 (McDermott *et al.*, 1995) has been used to substitute the respective residues of *Rb sphaeroides* with the ones from *Rps acidophila*. The angles and distances between the residues at -4 of the α - and β -subunits and the C13¹ keto carbonyl group of BChl-B850s are found to be highly similar (figure 3-12). Both the distance and angle, between the -4 residues' hydroxyl group of serine residue to C13¹ keto carbonyl group of BChl-B850, favours a H-bond formation (Ippolito *et al.*, 1990; Derewenda *et al.*, 1995).

As discussed above, further simplification of the model LH2 α WT/ β AL leads to the loss of the LH2 assembly. Thus, an improvement in the structural stability of this model complex has been attempted by introducing a serine residue at position -4 of the β -subunit. Our rationale has been that this may establish a H-bond between the C13¹ keto group of the α BChl-B850 and the β -polypeptide, analogous to the H-bond in the α -polypeptide and thereby enhance the stability of α WT/ β AL.

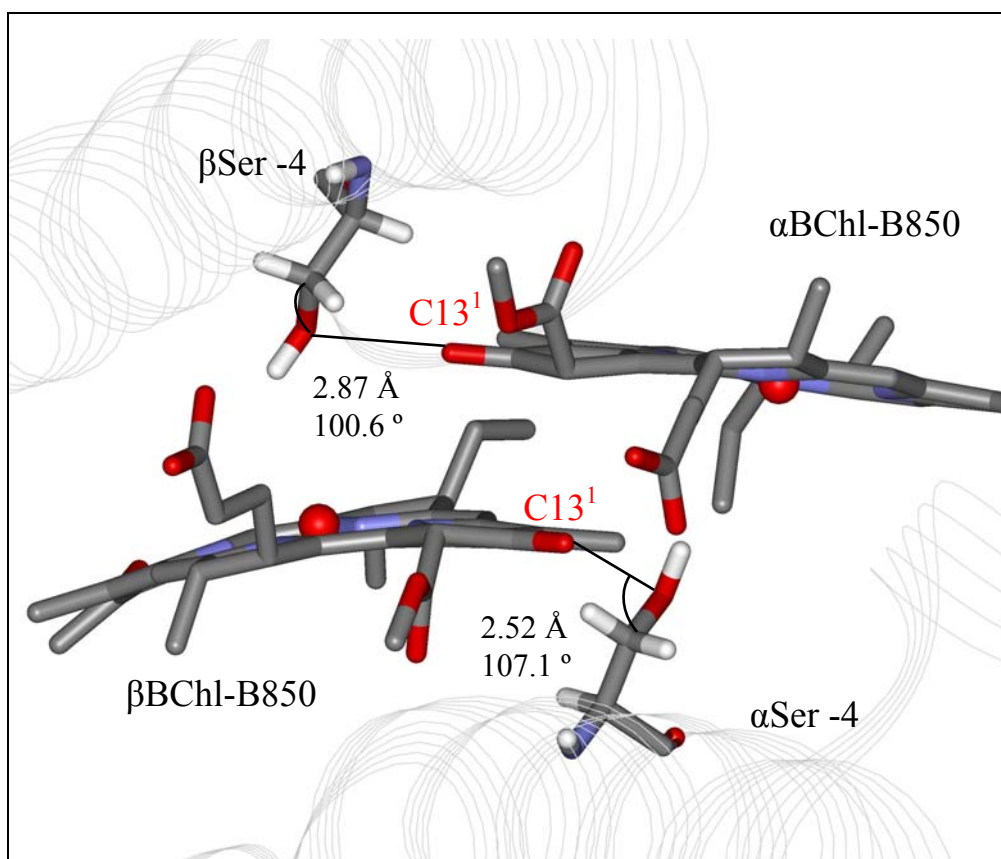
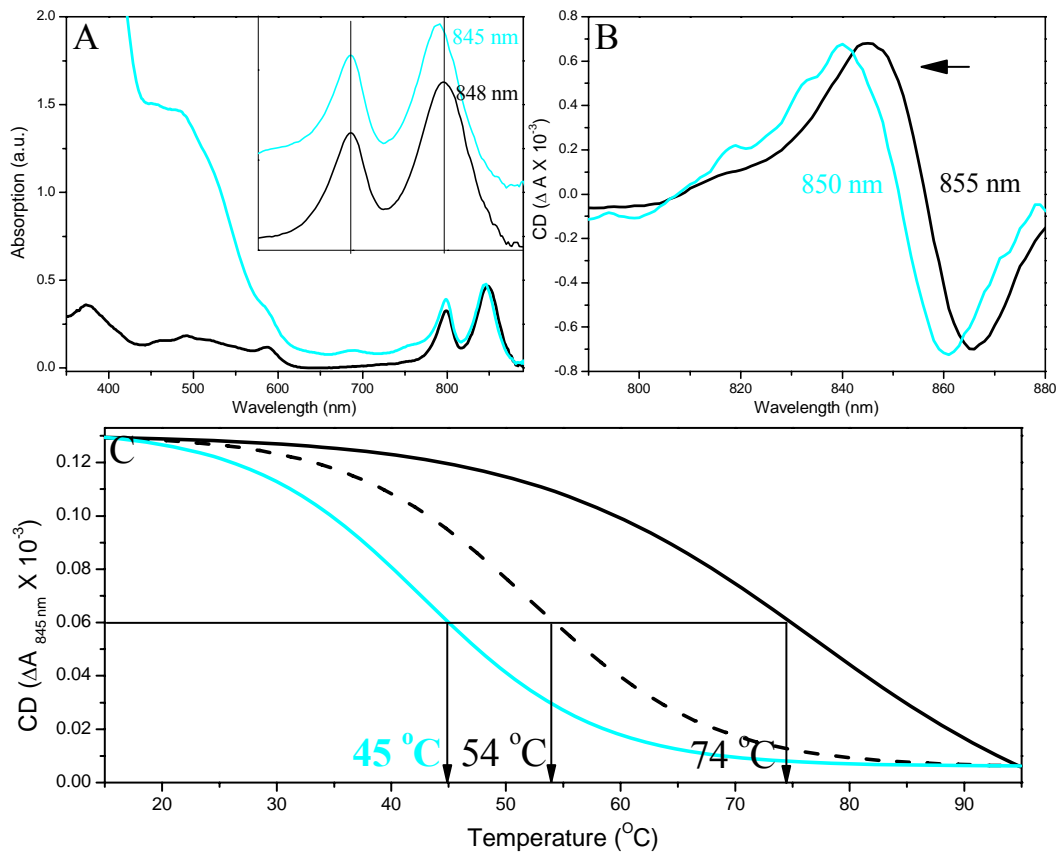


Figure 3-12: Putative H-bonding between α - and β -serine at position -4 and the keto carbonyl group of BChl-B850. Both the Ala -4 residues of α - and β -polypeptide in the native LH2 structure from *Rps acidophila* (McDermott *et al.*, 1995) have been replaced by serine in the modelled structure. Depicted is the H-bonding between the serine residues at position -4 in the α - and β -subunits and the C13¹ keto carbonyl groups of the α - and β -BChl-B850. The distance and angle between α Ser -4 and β BChl-B850 C13¹ keto carbonyl group is remarkably similar to the distance and angle between β Ser -4 and α BChl-B850 C13¹ keto carbonyl group.

Despite the structural similarities between the H-bonds formed by the serine in the α - and β -subunits shown in figure 3-12, the insertion of serine at the position -4 of β -subunit neither improves the expression level nor the stability of LH2 α WT/ β AL complex. On the contrary, the insertion of this serine resulted in the further reduction of assembled LH2 complex in the membrane, as judged by the increase in scattering effects (figure 3-13A). The absorption maximum of the red-most transition of the BChl-B850 is blue-shifted by ~ 3 nm. Similarly, this blue-shift is also observed in its CD signal. The zero crossing at 855 nm in WT is blue-shifted to 850 nm (figure 3-13B). Importantly, LH2 α WT/ β AL_{-4S} is destabilised in comparison to α WT/ β AL; its

T_m value dropped by further ~ 9 °C (figure 3-13C), resulting in a complex even less stable than the α WT/ β AL.



β WT: AEAEVHKQLILGTRVFGGMALIAHFLAAAAT
 α WT/ β AL_{4S}: AEAEVHKQLILGTRVFL**LLISLLAHL**LAAAAT

Figure 3-13: LH2 assembly and stability of LH2 WT (solid black line) and α WT/ β AL_{4S} (cyan line). The amino acid sequence of the β -subunit of WT and α WT/ β AL_{4S} are shown underneath the graph. (A) Absorption spectra of purified membranes of *Rb sphaeroides* DD13 strain of LH2 WT and α WT/ β AL_{4S}. Spectra are normalised at 850 nm. Inset shows the NIR absorption spectra. Absorption spectra are vertically displayed for clarity. Note ~ 3 nm blue-shifts of the BChl-B850 of α WT/ β AL_{4S}. (B) Circular dichroism spectra of LH2 WT and α WT/ β AL_{4S} in NIR region. (C) Thermal denaturation of LH2 WT, α WT/ β AL (dash line, shown previously in figure 3-6) and α WT/ β AL_{4S}. Changes of the CD signal at 845 nm during constant heating of LH2 membranes. The T_m values are indicated by arrows and the heating rate is 2 °C per min.

Substitution of alanine by serine at position -4 of the β -subunit does not enhance the stability of model LH2 complex and thus cannot be used as a basis for further modifications. The underlying reason for this additional destabilisation is not known yet. It appears that either the H-bond is not formed between the hydroxyl group of β Ser and the C13¹ carbonyl group of α BChl-B850 and/or that the BChl-packing with the BChl-B850 may not be suited to accommodate the bulkier side-chain of serine without loss of stabilising interactions. Possibly β Ala forms a weak H-bond with the C13¹ carbonyl group of α BChl-B850 and perfectly fits in with the surrounding molecules and does not permit any further modification without loss of structural stability. Clearly, the conserved residue β Ala -4 is important for proper LH2 complex assembly and stability. Even the replacement of alanine with the very similar serine already results in considerable further destabilisation of the model complex.

3.3 CONCLUSIONS

In this chapter, the peripheral interactions between BChls' macrocycle and polypeptides are investigated. Despite their proximity to the BChl-B850 macrocycles, the residues at the BChl-B850/protein interface have little effects on the specification of the BChl-B850 array and light-harvesting activity in LH2. Instead, they clearly contribute to the complex thermal stability.

The use of simplified model complexes can be employed to detect individual interactions which usually go unnoticed in WT due to the multitude of interactions. The critical contribution of the H-bond between α Ser -4 and C13¹ keto carbonyl group of β BChl-B850 has been identified in this manner. This residue has shown to be crucial for both the stability and assembly of the model complexes.

The LH2 complex is shown to be more susceptible to alteration of the β -subunit as compared to the α -subunit. This is further investigated in the following chapter. Despite the structural similarities of the protein environment around the C13 groups of the BChl-B850, substitution of serine at position -4 in the simplified β -subunit does not confer additional stability to the LH2 complex, unlike the improvement observed upon the substitution of alanine by serine in the simplified α -subunit. This suggests that either the strong H-bond between β Ser -4 and the keto carbonyl group of α BChl-B850 is not establish or disadvantageous for the stable assembly of the model LH2 complex. Moreover, the slightly larger volume of the serine residue may results in unfavourable packing with the BChl.

In conclusion, H-bonding at the BChl-protein interface is shown to drive the assembly of model LH2 complex and highly sensitive to the exact structural context. Thus, H-bonding may be a key structural motif in BChl-protein assembly.

Model LH2	Modified sequences		T _m value of LH2 membrane (°C)
	α-subunit	β-subunit	
WT	TVGVPLFLSAAVIASVVIHAAVLTTT	AEEVHKQLILGTRVFGGMALIAHFLAAAA	74
αWT _{-4A} /βWT	TVGVPLFLSAAVIAAVVIHAAVLTTT	AEEVHKQLILGTRVFGGMALIAHFLAAAA	71
αWT/βAL	TVGVPLFLSAAVIASVVIHAAVLTTT	AEEVHKQLILGTRVFLLI IAL LAHLLAAAA	54
αWT/βAL _{-4S}	TVGVPLFLSAAVIASVVIHAAVLTTT	AEEVHKQLILGTRVFLLI ISL LAHLLAAAA	45
αWT/βAL _{-7A}	TVGVPLFLSAAVIASVVIHAAVLTTT	AEEVHKQLILGTRV FAL LI AL LAHLLAAAA	No complex
αWT/βAL _{-9A}	TVGVPLFLSAAVIASVVIHAAVLTTT	AEEVHKQLILGTRV FLLI LI AL LAHLLAAAA	No complex
αWT/βAL _{+5LL}	TVGVPLFLSAAVIASVVIHAAVLTTT	AEEVHKQLILGTRVFLLI IAL LAHLL ALL	No complex
αAL/βWT	TVGVPLFLSAALLA ALL IHAALLAAT	AEEVHKQLILGTRVFGGMALIAHFLAAAA	34
αAL _{-4S} /βWT	TVGVPLFLSAALLAS LL IHAALLAAT	AEEVHKQLILGTRVFGGMALIAHFLAAAA	57
αAL _{-4S} /βAL	TVGVPLFLSAALLAS LL IHAALLAAT	AEEVHKQLILGTRVFLLI IAL LAHLLAAAA	40
αAL/βAL	TVGVPLFLSAALLA ALL IHAALLAAT	AEEVHKQLILGTRVFLLI IAL LAHLLAAAA	No complex

Table 3-1: Amino acid sequences of model LH2 complexes used in this chapter.

CHAPTER 4

Bacteriochlorophylls' phytol chain-protein interactions underlying LH2 assembly and function

4.1 INTRODUCTION

(B)Chls are lipophilic compounds due to the presence of a long esterifying alcohol chain. This long alcohol component is attached during the final step of (B)Chl biosynthesis, which involves the esterification of the C17³-carboxyl group at ring D of the BChl's macrocycle (Rüdiger & Schoch, 1991; Bollivar *et al.* 1994; Addelee & Hunter, 1999). In nature, the alcohol components of (B)Chls vary. Phytol (C₂₀H₃₉OH) is the most common esterified alcohol of Chl *a* in plants and BChl *a* in photosynthetic bacteria (Rüdiger & Schoch, 1991). Other esterifying alcohols such as geranylgeraniol (GG) in BChl *a*, e.g. in *Rsp rubrum* (Katz *et al.*, 1972) and farnesol in BChl *c*, e.g. in *Chlorobium* (Caple *et al.*, 1978) may also be esterified to (B)Chls (figure 4-1). One third of the (B)Chl carbon atoms are contributed by this long-chain alcoholic moiety (Scheer, 1991; Rüdiger & Schoch, 1991). However, little is known about the importance and role of this esterified alcohol moiety of (B)Chl.

The biosyntheses of the phytol and tetrapyrrole moieties of (B)Chl proceed by entirely different pathways (Goodwin, 1967). The two components are combined by the initial esterification of (B)Chlide *a* with geranylgeranyl pyrophosphate. The syntheses of phytol and Mg-pyrrole portions are found to be strictly regulated; no accumulations of phytol moieties were detected in mutant strains when their BChl synthesis was blocked at several stages (Brown & Lascelles, 1972; Akhtar *et al.*, 1984).

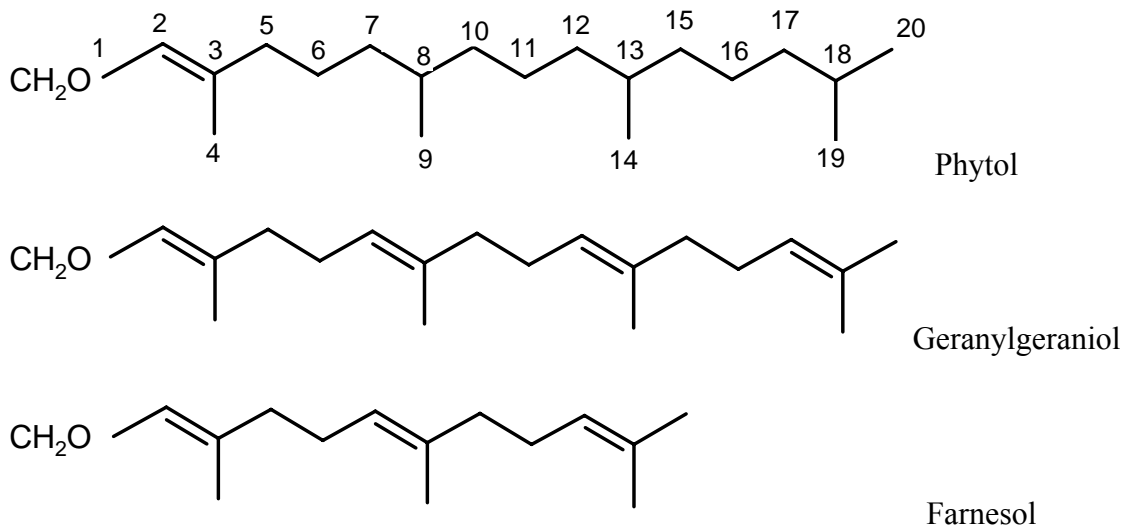


Figure 4-1: Isoprenoid esterifying alcohols of (B)Chls. From top to bottom phytol (found in BChls *a* and *b*), geranylgeraniol (found in BChls *a*) and farnesol (found in BChls *c*, *d*, *e*, *g*) (Scheer, 1991; Rüdiger & Schoch, 1991). The numbering shown is according to IUPAC system.

Removal of the long alcohol chain by chlorophyllase is regarded as the initial step of (B)Chl biodegradation (Fang *et al.*, 1998; Hörtensteiner, 1999). Chlorophyllase catalyses the hydrolysis of the C17³ ester bond of tetrapyrrole to yield (B)Chlorophyllide ((B)Chlide) and phytol (Weast & Mackinney, 1940; Fang *et al.*, 1998; Tsuchiya *et al.*, 2003) (figure 4-2), which undergo further biodegradation (Hörtensteiner, 1999; Tsuchiya *et al.*, 2003).

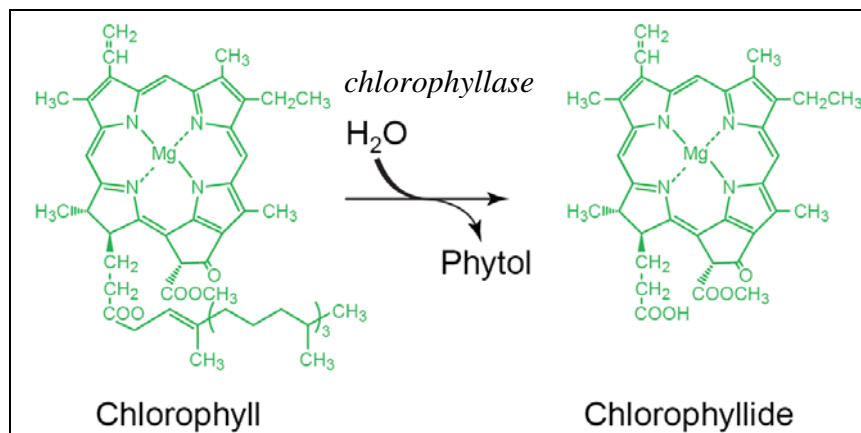


Figure 4-2: The initial step of chlorophyll degradation. Chlorophyll is dephytylated to chlorophyllide by the action of chlorophyllase.

Chlorophyllase (chlorophyll-chlorophyllido hydrolase, Chlase) was one of the very first plant enzymes to be studied (Willstätter & Stoll, 1913). A great variation in the Chlase activity is found depending on internal and external factors such as temperature, pH, plant varieties and plant growing seasons (e.g. Holden, 1961; Terpstra & Lambers, 1983; Drazkiewicz, 1994). In general, after extraction from chloroplast membranes, Chlase is only activated in the presence of either detergents such as Triton X-100 (Matile *et al.*, 1997) or high concentrations of organic solvents such as acetone (40-70 %, w/v), methanol (70-80 %, w/v) or ethanol (Weast & Mackinney, 1940; Tanaka *et al.*, 1983; Hörtensteiner, 1999). Among these reagents, acetone was found to be the most effective for Chlase activity (Holden, 1961; Tanaka *et al.*, 1982, 1983). In previous works, the optimal range of acetone spans from 30 to 60 % with essentially equal rates of hydrolysis (Weast & Mackinney, 1940). The optimal pH range spans from 6.0 to 8.5 and the temperature range from 20 to 50 °C (Weast & Mackinney, 1940; Holden, 1961). The Chlase studies have been mostly conducted *in vitro* on (B)Chl extracted from the binding proteins and solubilised in organic solvent or detergent. Huge variations in the optimal conditions for Chlase activity have been observed, largely due to the wide reaction conditions. The optimal *in vivo* conditions for Chlase activity are still largely unknown.

The isoprenoid esterifying alcohol moiety has been proposed to be important for the function and assembly of photosynthetic pigment-protein complexes (Rüdiger & Schoch, 1991; Bollivar *et al.*, 1994). Brown *et al.* (1972) have demonstrated that the formation of intracytoplasmic membrane (ICM) in *Rb sphaeroides* depends on the synthesis of BCHls. Mutants that are defective in the completion of BChl synthesis at the final phytolation step, have not been able to form normal vesicles (Brown *et al.*, 1972). They therefore proposed that the intact BChl molecules are required for proper ICM formation (Brown *et al.*, 1972). The assembly of the BChl-protein complexes has not been examined, and it is therefore impossible to conclude that the phytol chains are vital for ICM formation. The organisation of Chls is also found to be influenced by the various phytol moieties (Agostiano *et al.*, 2000). By the insertion of various modified Chl pigments into artificial membranes, Agostiano and co-workers (2000) showed that the alcohol chain favours the formation of lamellar bilayer as well as driving the anchoring of the Chl derivatives to the membrane.

Without the alcohol moiety, the cyclic tetrapyrrole is not anchored properly in bilayer, especially for the newly synthesised Chl derivatives. Little is known on the assembly of pigment-protein complexes *in vivo* and the exact involvement of the phytol chains in the assembled complexes.

The phytol moieties do not (or only very little) (Fiedor *et al.*, 2003) contribute to the spectroscopic properties of (B)Chls (Rüdiger & Schoch, 1991). Bollivar and co-workers (1994) studied the role of the phytol in mutants by replacing the usual phytylated BChls by GG-esterified BChl. The modified alcohol moiety in the BChl resulted in severe reduction in the mutants' photosynthetic growth capacities and the stability of bacterial photosystem. The energy transfer efficiency between LH1 antennae to RC, however, was not found to be affected. The energy transfer from LH2 to LH1 and RC could not be determined due to experimental limitations. As pointed out further in the study of Addlesee & Hunter (2002), LH2 complex assembly appears to be highly susceptible to changes in phytol moiety. In LH2 complex, the phytol tails may favour a tight packing of the pigments and proteins (Loach & Parkes-Loach, 1995; Law *et al.*, 2004). Taken together, these observations have shown that the isoprenoid esterifying alcohol of the BChl has potentially crucial roles in assembly of LH complexes, ICM formation, photosynthetic growth capability and complex stability.

In the high resolution structure of LH2 from *Rsp acidophila* (Papiz *et al.*, 2003), the phytol of both the α - and β -BChls-B850 are found to have extensive contacts with the peptide residues (Law *et al.*, 2004). Another important feature of the BChls phytol tails within LH2 complex is that the phytol tails of BChl-B800, -B850 and the carotenoids are closely intertwined and highly packed within the $\alpha\beta$ -polypeptides. It has been proposed that the phytols control the orientation of the transition dipoles of the BChl molecules and subsequently have an important role in functional assembly of these complexes (Loach & Parkes-Loach, 1995; Addlesee & Hunter, 1999; Agostiano *et al.*, 2000; Law *et al.*, 2004). Yet, the exact contribution of the phytol moiety to the LH2 assembly has not yet been explored experimentally.

The objective of this chapter is to explore the role of the BChls phytol tails in the assembly and function of the LH2 complex. Phytol-amino acid interactions and their

contribution to LH2 assembly and stability are examined by structural, mutagenetic, enzymatic and statistical analyses.

4.2 RESULTS AND DISCUSSION

STUDY OF THE ROLE OF BCHLS PHYTOL BY MUTATING PROTEIN BINDING RESIDUES

In the mutagenesis study of the BChl-binding site (chapter 3), it has been observed that further simplification of the residues at positions -7 and -9 of the model sequence of the LH2 β AL towards the N-terminus, results in the complete absence of assembled LH2 in the membrane. As shown in figure 4-3, model LH2 α WT/ β AL with either additional mutation at -7 or -9, have major absorption band at \sim 760 nm, but lack of the ‘typical’ LH2 absorption bands at \sim 800 and \sim 850 nm. Interestingly, there is a minor absorption at \sim 820 nm. This band however, is only observed in the whole cells and not in purified membranes, and thus has not been examined further in this study.

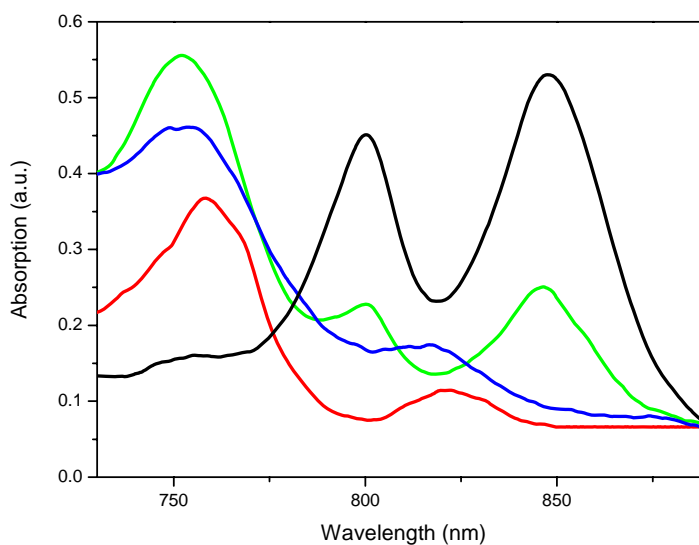


Figure 4-3: NIR absorption spectra of LH2 WT (black line), model sequences α WT/ β AL (green line), α WT/ β AL_{-7A} (red line) and α WT/ β AL_{-9A} (blue line). Absorption spectra are of whole cell single colony of *Rb sphaeroides* DD13 using reflection spectroscopy. Note the loss of BChls-B800 and -B850 absorption bands in cells expressing α WT/ β AL_{-7A} and α WT/ β AL_{-9A}.

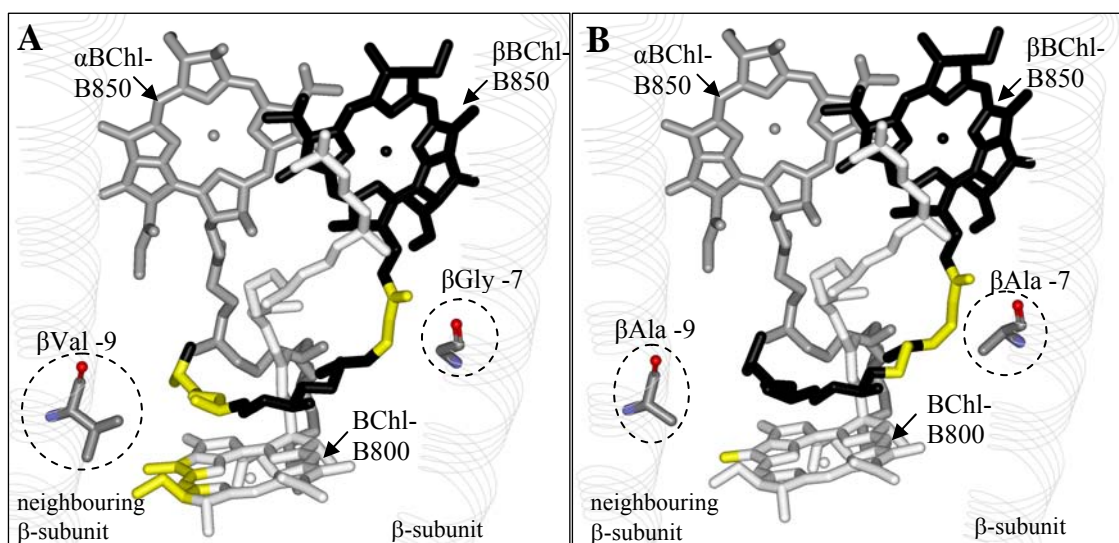


Figure 4-4: Contacts between the BChls' phytol chains and the amino acid residues at positions -7 and -9 of the β -subunits in the LH2 complex (McDermott *et al.*, 1995). α BChl-B850 is displayed in grey, β BChl-B850 is displayed in black and BChl-B800 is displayed in white. Note the residue shown at position -9 belongs to the β -subunit of the neighbouring $\alpha\beta$ -subunit complex.

(A) LH2 WT: The contacts between glycine at positions -7 and valine at -9 with the BChls within a radius of ≤ 5 Å are shown in yellow. The residue β Gly -7 is modified from the original leucine residue found in *Rps acidophila* sequence.

(B) Mutant LH2: The contacts between alanine at positions -7 and -9 with the BChls within a radius of ≤ 5 Å are shown in yellow. Both the residues have been modified by Weblab viewer (see chapter 2). Note the loss of contacts between β BChl-B850's phytol tail upon mutating β Val -9 \rightarrow Ala and gain of contacts upon mutating β Gly -7 \rightarrow Ala.

Based on the high-resolution structure of LH2 (McDermott *et al.*, 1995), the close vicinities of the residues at positions -7 and -9 of the LH2 β -subunit are analysed; in particular, for the interactions with the BChls pigment molecules. Figure 4-4 shows the contacts between these residues and BChls molecules within a radius of 5 Å. Both β Ala -9 and β Ala -7 appear to have close contacts with the BChls pigments of the $\alpha\beta$ -elementary subunit; in particular, with atoms of β BChl-B850's phytol chain and with atoms of the BChl-B800's macrocycle. Figure 4-4A shows the interactions of β Gly -7 and β Val -9. The glycine at -7 interacts with the C17³ propionate ester bond of β B850's ring D and the C1 atom of the phytol tail. While the residue valine at -9 of a neighbouring $\alpha\beta$ -subunit interacts with the β BChl-B850's phytol tail; in particular, with the atoms C13 to C18 and C20 as well as with part of the rings B and C of BChl-B800 macrocycle. Upon mutating β Gly -7 to Ala, the interactions with BChl molecules appear to change insignificantly. Additional close contacts at

the atoms C2 to C4 of the β BChl-B850's phytyl tails are observed. On the other hand, when β Val -9 is mutated to Ala, the interactions with the neighbouring β BChl-B850's phytyl tail are lost completely and the only remaining contact is with the C12 methyl group of the BChl-B800's macrocycle.

Alignment of the β -subunit of *Rb sphaeroides* with other photosynthetic bacteria shows that neither the residues at positions -7 nor -9 are strictly conserved (table 4-1); no alanine residue is found at these positions among the various photosynthetic bacteria. It is worth to note that the neighbouring residues β Arg -10 and β Phe -8 have previously been suggested to be important for the assembly of monomeric BChl-B800 (McDermott *et al.*, 1995; Gall *et al.*, 1997) and both the residues are relatively conserved (exception in *Rb viridis*). This suggests that this section of the helix may of structural importance and that these residues may play an important role in peptide-pigment interactions.

Photosynthetic bacteria		Amino acid sequence of β -polypeptides
RHOSH	LH2 [P0C0Y2]	EAEEVHKQLILGTRVFGMALIAHFLAAAAT
RHOAC	LH2 [P26790]	QSEELHKYVIDGTR V FLGLALVAHFLAFSAT
RHOSU	LH2 [P95654]	EAE E VHKQLIDGTR V FGAIALFAHFLAAIAT
RHOCA	LH2 [P07368]	EAE E IHSYLIDGTR V FGAMALVAHILSAIAT
RHOPA	LH2 [P35107]	ESEELHKHVIDGTR I FGAIAIVA H FLAYVYS
RHOGE	LH2 [P72281]	EAEELQKGLVDGTR V FGVIAVLA H ILAYAYT
RHOVI	LH2 [P04124]	EAKEFHGIFVTSTV L YLATAVIV H YLVWTAR
RHOTE	LH2 [P80587]	EAEELHTYVTNGFR V FVGIAVVA H VLVFAAH
BRAD	LH2 [Q35160]	ESEELHKHVIDGAR V FBVIACVA H LLAYIYS
JANSC	[Q28S14]	EAE E VHSYLIDGTR V FGGIALVA H FLVAVST

RHOSH: *Rhodobacter sphaeroides*; RHOAC: *Rhodopseudomonas acidophila*; RHOSU: *Rhodobacter sulfidophilus*; RHOCA: *Rhodobacter capsulatus*; RHOPA: *Rhodospseudomonas palustris*; RHOGE: *Rhodocyclus gelatinus*; RHOVI: *Rhodobacter viridis*; RHOTE: *Rhodocyclus tenuis*, BRAD: Bradyrhizobium sp. BTAi1.; JANSC: Jannaschia sp. (strain CCS1).

Table 4-1: Alignment of amino acid sequence of β -polypeptides of purple bacteria. Residues at the positions -7 and -9 are displayed in blue and red respectively. Exspasy sequence search codes are shown in brackets [www.exspasy.org].

To investigate the role of residues -7 and -9, the amino acid glycine at position -7 and/or valine at position -9 of the WT LH2 sequence were replaced with alanine. Figure 4-5 shows the optical absorption spectra of WT and mutants LH2 (upper panel). The absorption spectra are largely similar for LH2 WT, α WT/ β WT_{-7-9A} and α WT/ β WT_{-9A}. A noticeable reduction in the BChls-B800 absorption band is observed, especially in α WT/ β WT_{-7-9A} (blue line). This is also obvious in the fluorescence excitation spectra (figure 4-5, lower panel). The energy transfer from BChl-B800 to -B850 in the α WT/ β WT_{-7-9A} is clearly reduced by more than half the intensity in comparison to WT. In contrast, the single mutant α WT/ β WT_{-9A} (red line), shows only a slight reduction in energy transfers from BChl-B800 to -B850. Furthermore, some reduction in the energy transfer from carotenoid to BChls is observed in the double-point mutant α WT/ β WT_{-7-9A}.

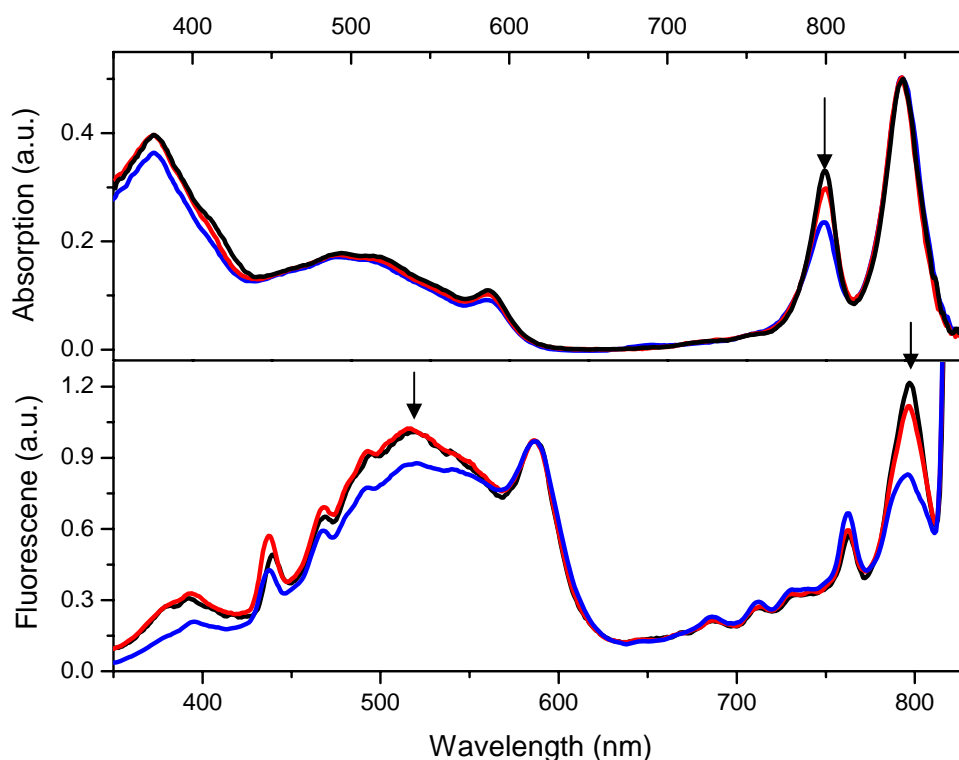


Figure 4-5: Absorption (upper panel) and fluorescence excitation (lower panel) spectra of the WT LH2 (black line), mutants α WT/ β WT_{-9A} (red line) and α WT/ β WT_{-7-9A} (blue line). Absorption spectra are normalised at 850 nm. The fluorescence is detected at $\lambda_{em} = 880$ nm. The excitation spectra are normalised to the BChl Q_x band (~590 nm) to provide an indication for the relative efficiencies of the energy transfer process.

The CD spectra of intact membranes containing mutants and WT are compared in figure 4-6. No significant differences are observed between the mutants and WT in their BChls arrangement in the complex (figure 4-6A). Both α WT/ β WT_{9A} (red line) and α WT/ β WT_{7-9A} (blue line) produce a similar S-shape CD signal and zero-crossing values as found in WT complex. Despite the reduction in BChl-B800 absorption and the energy transfer bands; no reduction in the CD signal at ~800 nm is observed. This may be due to the already relative weak CD signal in this range and the contributions from the upper exciton component of BChl-B850 (Koolhaas, *et al.*, 1998).

The structural stability of the LH2 complexes was examined by thermal denaturation (figure 4-6B). A clear reduction of the midpoint of denaturation (~11 °C) is observed in the double-point mutant α WT/ β WT_{7-9A} (blue line) in comparison to WT (black line). Considering that only two residues have been altered in the WT β -sequence, this reduction is considered significant; indicating that both the residues at position -7 and -9 of the β -polypeptide contribute to the thermal stability of LH2. On the other hand, the thermal stability of the single point mutant α WT/ β WT_{9A} (red line) is closely similar to the WT LH2 stability in membrane, the mid-point of denaturation is reduced by ~4 °C.

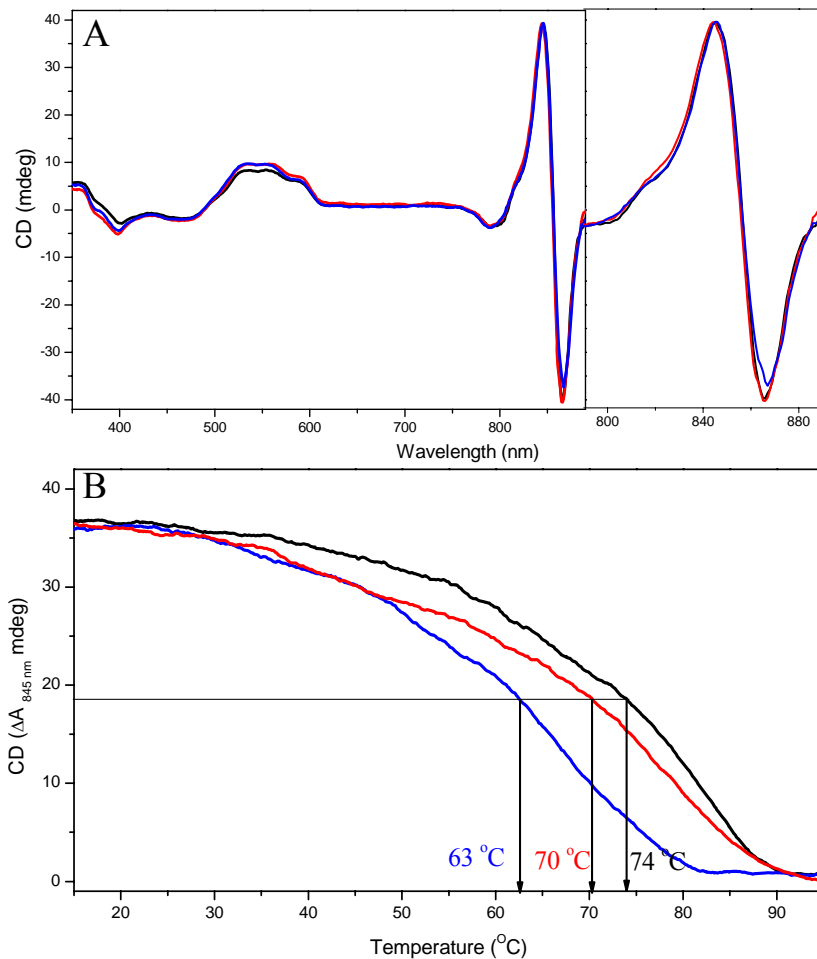


Figure 4-6: CD and thermal denaturation spectra of WT LH2 (black line), mutants α WT/ β WT_{.9A} (red line) and α WT/ β WT_{.7-9A} (blue line) chromatophores.

(A) CD spectra. Left panel: the spectra range from 350 to 900 nm. Right panel: the magnification of BChl-B850 signals. CD are measured at 15 °C with a scan rate of 1 nm per sec.

(B) Thermal denaturation. The thermal denaturation spectra are monitored by loss of the CD signal at 845 nm. T_m values are indicated by the arrows. Signals are normalised at the starting point at 15 °C. Heating rate is 2 °C per min.

The stability of LH2 WT and mutants are also explored devoid of the contributions of membrane lipids. In figure 4-7A, the CD spectra of purified LH2 complex α WT/ β WT_{.9A} and α WT/ β WT_{.7-9A} relative to the WT LH2 are shown. A minor blue-shift of ~3 nm is observed in the BChl-B850 signal extrema in purified mutant complexes in comparison to WT.

In figure 4-7B, the thermal stabilities of purified mutant complexes' are compared to purified WT complexes. The T_m value of isolated WT LH2 in β OG is increased by

~7 °C (black line). This observation of increase in thermal stability of WT LH2 in β OG micelles may be due to several possibilities, such as stabilising ionic interactions between detergent-protein molecules or because of a diminished curvature tension in micelles (for further details see chapter 5). An opposite trend is detected in the mutants; instead of an increase in the thermal stability, a drop in stability is observed in α WT/ β WT_{-9A} and α WT/ β WT_{-7-9A} (figure 4-7B). The T_m value of α WT/ β WT_{-9A} (red line) is decreased from ~70 °C in membranous environment to ~64 °C in micelles. In comparison to WT, the T_m of α WT/ β WT_{-9A} is decreased significantly by ~17 °C. Similarly, the T_m value of the purified α WT/ β WT_{-7-9A} (blue line) is decreased from ~63 °C in the membranous environment to ~51 °C in detergent, which results in a total shift of T_m by ~30 °C in comparison to WT LH2. This drastic reduction in the thermal stability of purified mutant complexes relative to WT suggests that the replacement of residues -7 and -9, which closely interact with LH2 BChl-B850 phytol as well as BChl-800, alters the pigment-protein interactions and possibly the packing of the LH2 mutant complexes. Clearly, the LH2 become more vulnerable to environmental changes. The appearance of a blue-shift in the CD spectra of the purified α WT/ β WT_{-9A} and α WT/ β WT_{-7-9A} suggests that there are some changes in the relative configuration of BChls.

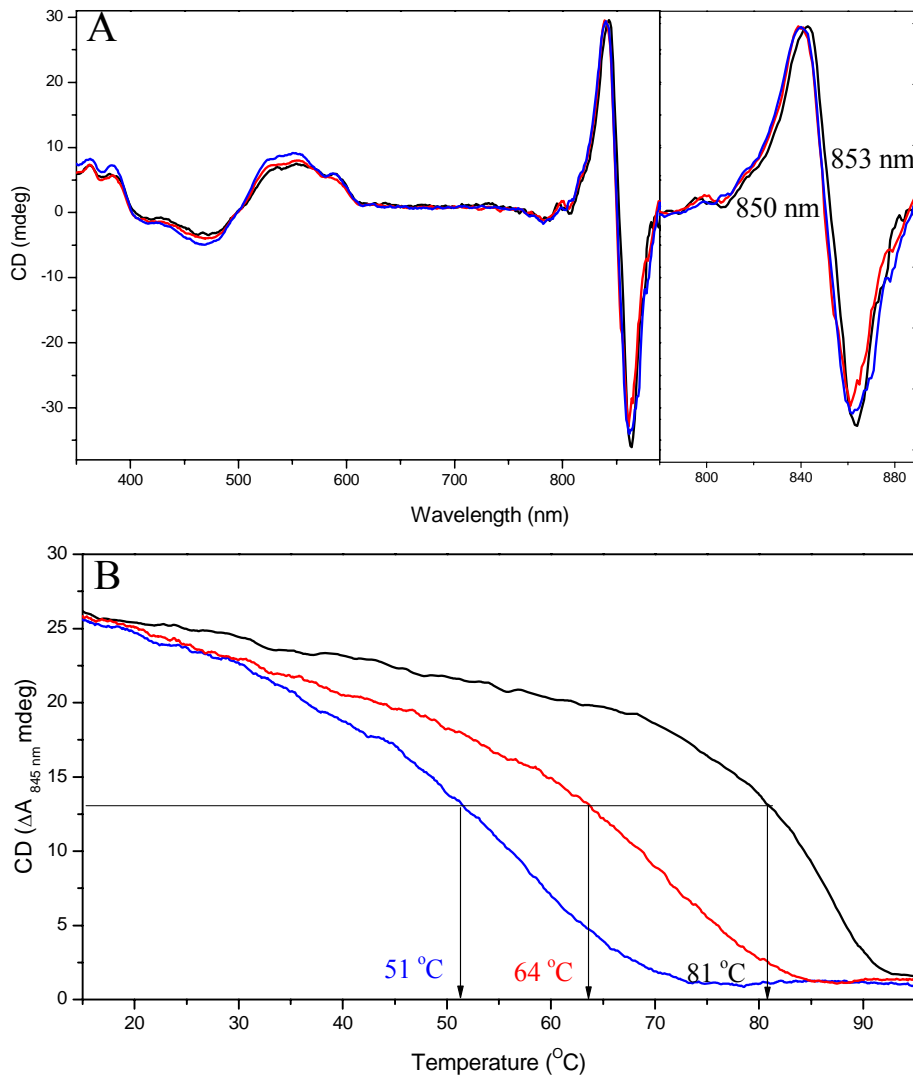


Figure 4-7: CD and thermal denaturation spectra of isolated WT LH2 (black line), mutants α WT/ β WT_{9A} (red line) and α WT/ β WT_{7-9A} (blue line).

(A) CD spectra. Left panel: the spectra range from 350 to 900 nm. Right panel: the magnification of BChl-B850 signals. CD are measured at 15 °C with scan rate of 1 nm per sec.

(B) Thermal denaturation. The thermal denaturation spectra are monitored by loss of the CD signal at 845 nm. T_m values are indicated by the arrows. Signals are normalised at the starting point at 15 °C. Heating rate is 2 °C per min.

In summary, the functional binding of BChl-B800 in both the single- and the double-point mutants is reduced, which affects the energy transfer and thermal stabilities of the complexes in the membranous environment. The CD spectra reveal no perturbations of BChls-B850 arrangements suggest that the dipole-dipole interactions of the BChl pigments have not been significantly altered. The complex destabilisation of both the mutations at -7 and -9 is particularly obvious when the

complexes are purified from the membrane. In addition, a ~3 nm blue-shift of their zero-crossing point is observed. Taken together, the data suggest that the residues at positions -7 and -9 contribute significantly to BChl-B800 bindings which affect the LH2 complex energy transfer and thermal stability, especially when the membrane lipids are removed.

Based on the structural modelling of the LH2 from *Rb sphaeroides*, both the residues -7 and -9 are found to have close contacts with the β BChl-B850 phytol chains and/or the BChl-B800 macrocycle. The β Val -9 has many contacts with the BChls-B800 macrocycle; however, the loss of these interactions by the replacement of alanine at -9, neither induced significant alteration of complex assembly nor complex destabilisation. Only by the combined mutations of both residues at -7 and -9, will the reduction in BChls-B800 absorption band and LH2 stability be significant. The construction of LH2 α WT/ β WT_{-7A} mutant has not been possible despite many attempts. Several difficulties have been encountered in the production of β Gly -7 mutant for reasons which are not understood. Therefore, LH2 α WT/ β WT_{-7A} has not been analysed in this work.

Based on the amino acid sequence alignment of the β -subunits, this stretch of the helices is found to be relatively conserved especially the residues β Phe -8 and β Arg -10. These residues have been suggested previously to have a crucial role for the binding of pigments in LH2 (McDermott *et al.*, 1995; Hunter, 1995; Gall *et al.*, 1997). Furthermore, BChl-B800 is known to be relatively sensitive to its surroundings (Clayton & Clayton, 1981; Hunter, 1995). The findings presented here indicate that binding of the BChl-B800 is sensitive to the proper packing of the complexes BChl phytol tails. Phytol tails in LH2 complex are packed tightly between the helices of the $\alpha\beta$ -polypeptides (McDermott *et al.*, 1995; Papiz *et al.*, 2003). Both the residues -7 and -9 appear to determine the optimal conformation of the phytols for the packing interactions. By the replacement of the native residues with alanines at these positions, the arrangement of the pigments is disturbed and considerable loss of BChl-B800 binding is observed. In order to further examine the interactions between phytol chains and its surrounding pigment and protein

environment, their contacts patterns are analysed in the available high-resolution structure (table 4-2).

			Phytol chain					
			β BChl-B850		α BChl-B850		BChl-B800	
			Contacts ^a	%	Contacts ^a	%	Contacts ^a	%
BChl	Macrocycle	Own ^b	4	4.55	5	6.8	5	6.9
		Other ^c	38	43.2	10	13.5	28	38.9
	Phytol	Other ^c	12	13.6	4	5.4	10	13.9
Carotenoid	-	-	7	8.0	4	5.4	10	13.9
Polypeptide	Binding helix^d	Polar ^f	5	5.7	5	6.8	0	0
		Non polar ^g	11	12.5	16	21.6	0	0
	TMH^e	Polar ^f	0	0	2	2.7	0	0
		Non polar ^g	11	12.5	20	27.0	10	13.9
		Basic ^h	0	0	0	0	6	8.3
	Loop/parallel helix	Polar ^f	0	0	0	0	1	1.4
Non polar ^g		0	0	8	10.8	2	2.8	
Total			88	100	74	100	72	100

Table 4-2: Contacts of the BChls' phytol within the LH2 complex (McDermott *et al.*, 1995).

^a Contacts are defined as the number of atoms within a radius of ≤ 5 Å.

^b Own is defined as contacts with atoms of the identical BChl pigment.

^c Other is defined as contacts with atoms of non-identical BChl pigment.

^d Binding helix is defined as the helix which provides the amino acid ligand to the central Mg atom.

^e TMH is defined as transmembrane helix.

^f Polar is defined as polar residues (Asn, Gln, Ser, Thr and Tyr).

^g Non polar is defined as non-polar residues (Ala, Cys, Gly, Ile, Leu, Met, Phe, Pro, Trp and Val).

^h Basic is defined as basic residues (Arg, His and Lys).

Note that no contacts with acidic residues (Asp and Glu) are found.

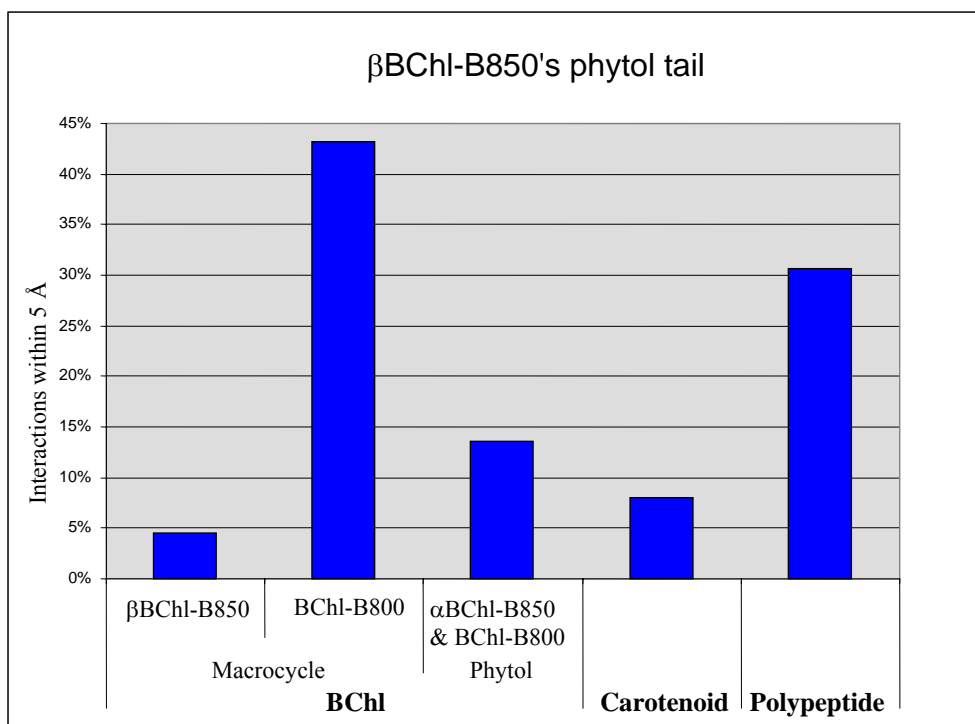


Figure 4-8: Contacts between the phytol of βBChl-B850 and its surrounding molecules. The majority of interactions of the phytol of βBChl-B850 are to the other pigment molecules, predominantly to the macrocycle of the BChl-B800 (43.18 %) and to the polypeptide (30.68 %).

Table 4-2 summarises the contacts of BChl’s phytol chains with its surrounding molecules in the LH2 complex by the structural analysis of the high-resolution LH2 structure (McDermott *et al.*, 1995). As shown in the table 4-2, the phytyl chains of the BChls interact with the BChls’ macrocycles, phytol tails of ‘other’ BChls, carotenoid molecules and extensively with the surrounding polypeptides. A noticeable difference is observed between the contacts of phytyl chains of βBChl-B850 and αBChl-B850. The phytyl of the βBChl-B850 molecules interact extensively with the macrocycles of ‘other’ pigments (~43 %) while there are little of such interactions (~14 %) found in the interactions of αBChl-B850. The αBChl-B850 is observed to have relatively more contacts with the polypeptide residues (~69 %).

The contacts of the phytyl of βBChl-B850 are summarised in figure 4-8. Most of the contacts are with the ‘other’ BChls’ macrocycles; in particular, with the macrocycles of BChl-B800 (>40 %). This supports the experimental results; where BChl-B800 is

susceptible to the alterations of β BChl-B850 phytol chains as induced by the replacement of alanine at positions -7 and -9 in LH2 β -subunit.

In conclusion, (1) residues -7 and -9 interact with β BChl-B850's phytyl tail, (2) the residues -7 and -9 are important for the proper binding of BChl-B800 and (3) the binding of BChl-B800 is highly susceptible to its immediate surroundings, especially the phytol chains.

Point mutation yields structural information of the residue to the complex assembly by its interactions with the surrounding components. Even though no significant alterations are observed in the contacts of the immediate residues when -7 and -9 are replaced by alanine (modelling results not shown), we cannot exclude the possibility that the binding of β Phe -8 and β Arg -10 maybe altered and contributed to the observations. Moreover, in the detergent experiment, the thermal destabilisation of double-point mutant is more significant than membranous environment, which suggests the involvement of membrane lipids in LH2 structural stability (see chapter 5).

REMOVAL OF THE BCHL PHYTOL TAILS IN ASSEMBLED LH2 BY ENZYMATIC DIGESTION

Point mutations on polypeptides allow us to gain the structural information of potential interactions between pigment-protein; however, replacement of amino acids may have multiple effects on its surrounding environment. In order to further elucidate the contribution of BChl's phytol chains to the assembly of LH2 structure; the phytol chains are removed by an enzymatic approach.

Chlorophyllase degrades (B)Chl by hydrolysis the C17 ester linkage between the esterifying alcohol and porphyrin moieties of (B)Chls pigments, subsequently this will yield (B)Chlide and phytol (Fang *et al.*, 1998; Tsuchiya *et al.*, 2003). Here, Chlase is applied to the assembled LH2 complex in β OG. The conversion of BChl to BChlide is verified by thin layer chromatography (TLC), and the LH2 is examined for its structural and functional integrity by spectroscopic and denaturation experiments.

The approach of enzymatic dephytylation by Chlase of BChls of intact LH2 complexes in β OG has been explored for the first time in the thesis. It is known that the Chlase activity is not influenced by β OG at or below 1 mM (Terpstra & Lambers, 1983). Moreover, (B)Chls embedded in artificial or natural membranes are found to be little or not hydrolysed in the presence of added Chlase if no acetone is added (Tanaka *et al.*, 1983; Terpstra & Lambers, 1983). Chlase action on bound BChls in chromatophores and spheroplasts of *Rsp rubrum* has been reported previously (Tanaka *et al.*, 1983). Chlase could hydrolysed the C17 ester bond of BChls buried well within the bilayer and packed at the interface of α - and β -subunits when the acetone concentration has been higher than 15 %. Nevertheless, *Rsp rubrum* contains geranylgeraniol instead of phytol as esterifying alcohol and lacks of LH2 complex, which appear to be much more dependent on the phytol moiety in comparison to LH1 and RC (Addlesee & Hunter, 2002).

The optimal concentration of acetone for the hydrolysis activity of Chlase in the presence of LH2 complex from *Rb sphaeroides* in β OG has been determined (figure 4-9). To that end, the concentrations of acetone in samples of isolated WT LH2 are

increased gradually from 0 to 50 %. The absorption intensity of BCHls decreases according to the relative dilution factors of acetone in the concentration range from 0 to 40 %. Remarkably, the maximum absorption of the BCHls-B800 does not shift at concentrations below 45 % acetone; whereas, the BCHls-B850's peak red-shifted from ~843 to ~847 nm with increasing concentrations of acetone (figure 4-9). An abrupt drop of the BCHls absorption is observed when the acetone concentration is raised to 45 % or higher. The drop in absorption was irreversible (data not shown), indicating that when the acetone concentration reaches 45 % or higher, the BCHls bound to the LH2 complex partly disassociate by acetone treatment. The purpose of adding acetone is to activate the Chlase; yet, excessive acetone concentrations obviously cause the disassociation of the BChl from the LH2 assemblies. In the case of isolated LH2, it is found that a concentration of 40 % acetone allows for efficient Chlase activity without excessive loss of BChl. For the incubation procedure, such as temperature or pH, Holden (1961) and Chiba *et al.* (1967) were followed.

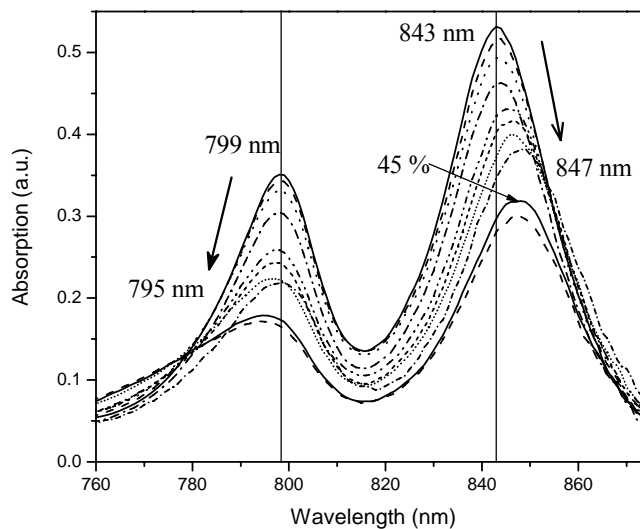


Figure 4-9: NIR absorption spectra of WT LH2 in β OG treated with increasing concentrations of acetone (0 %, 5 %, 10 %, 15 %, 25 %, 30 %, 35 %, 40 %, 45 %, and 50 %). Each sample was incubated at 34 °C in dark for ~10 min.

In the following, the effect of the removal of the phytol chain by Chlase on assembled isolated LH2 WT is studied. All the following data are derived from the sequential experiments from identical set of samples which included the absorption, hydrolysis conversion and structural stability examinations. Figure 4-10 shows the absorption spectra of isolated WT LH2 with and without Chlase treatment. The optical density of BChls is reduced in the enzyme treated sample especially the one of BChl-B800. In the absence of the enzyme (black line), the optical density of the BChl hardly changed whereas in the presence of Chlase (red line), the absorption bands of both BChl-B800 and -B850 are reduced by ~35 % and ~13 % respectively during the 2 hours incubation in the presence of 40 % acetone.

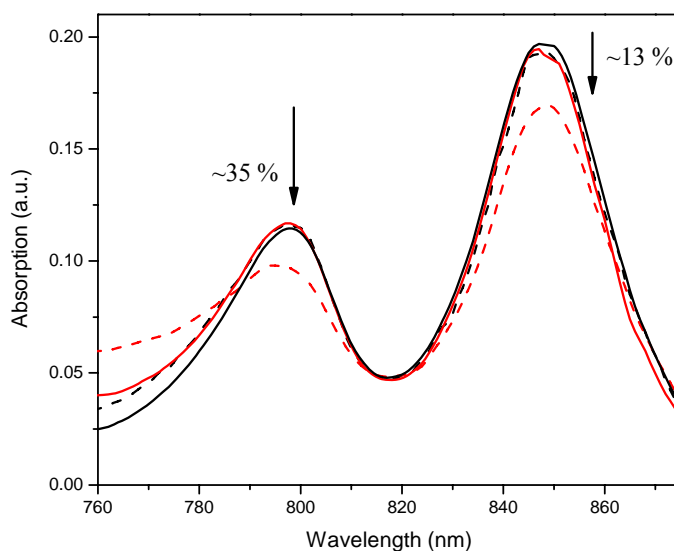


Figure 4-10: NIR absorption spectra of isolated WT LH2 complex, treated with (red line) and without (black line) Chlase enzyme. Samples are incubated in the presence of 40 % acetone (solid line) and after 2 hours incubation (dash line). Samples are incubated at 34 °C in dark (for experiment procedure, see chapter 2).

As shown in figure 4-11, in samples which are treated with Chlase, irreversible loss of the BChl-B800 and -B850 absorption bands is observed (red line). In contrast, in the control sample (black line), no loss occurred as obvious from the entire recovery of BChl-B800 and -B850 absorption upon the removal of acetone. It is interesting to note that the loss in the BChls absorption intensities is mainly observed during the

first 35 min, possibly reflecting loss of enzyme activity thereafter. To the best of our knowledge, we cannot find any literature that addresses this issue, especially in isolated LH2 environment.

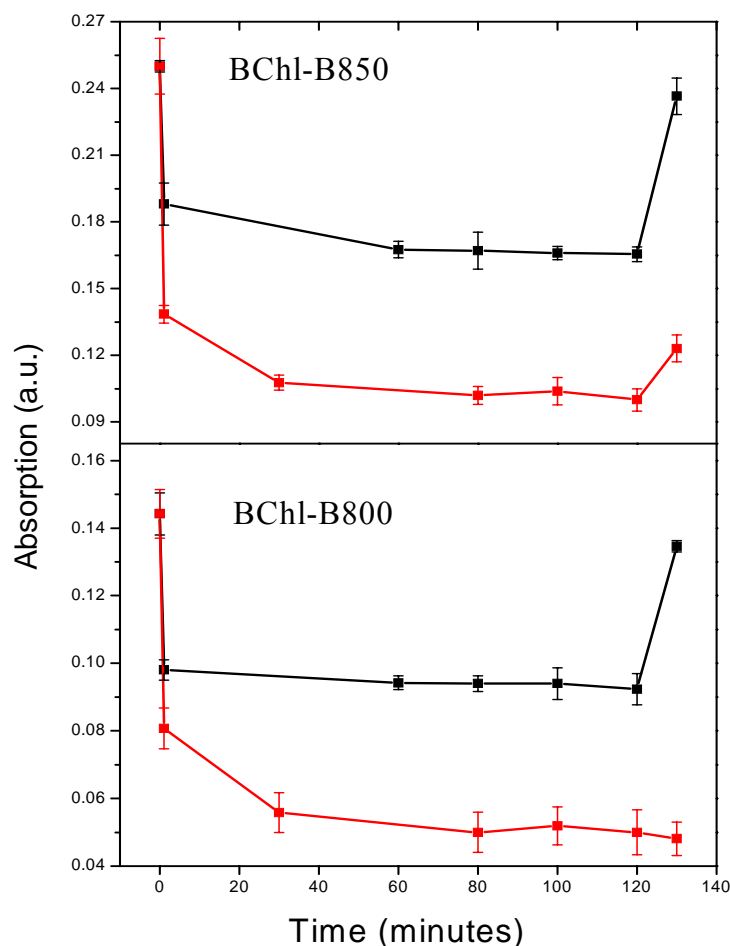


Figure 4-11: The optical densities of BChls-B850 (upper panel) and -B800 (lower panel) during the 120 minutes of incubation. Control sample (black line), was incubated with 40 % acetone only. Chlase treated sample (red line) was incubated with Chlase and 40 % acetone. Standard deviations are derived from three individual experiments. The initial ODs of the samples were identical. A further drop at the initial time in Chlase treated sample was due to the dilution factor contributed by Chlase. The last point of each line represents the OD taken after the removal of acetone.

To determine whether enzymatic hydrolysis occurred, the pigments were extracted from treated and non-treated samples and separated by TLC (figure 4-12). Figure 4-12A shows the TLC of control (without Chlase) and treated sample (with Chlase).

Approximately $88.7\% \pm 5.6\%$ (background correction) of the BCHls are found to be converted to BChlides (figure 4-12A, lane 2; determined by AIDA densitometry, see chapter 2). The absorption spectra taken directly from these spots on TLC plate are shown in figure 4-12B. Both dominant spots migrating on the plates as BCHls (lane 1) and BChlides (lane 2) give rise to absorption spectra with the maxima at ~ 776 nm and ~ 590 nm (black lines). In addition, there is a clear shoulder at ~ 695 nm in both the spectra, indicative of some oxidation of BCHls (Pröll, 2005). The contribution of this is even more pronounced in the spectrum of the pale spot (figure 4-12B lower panel, red line) corresponding to the residual BCHls of LH2 samples incubated with Chlase for two hours. Extended exposure of ‘free’ BCHls/BChlides leads to degradation by oxidation. Taken together, these data suggest that Chlase hydrolysed the bound BCHls of the assembled LH2 complex.

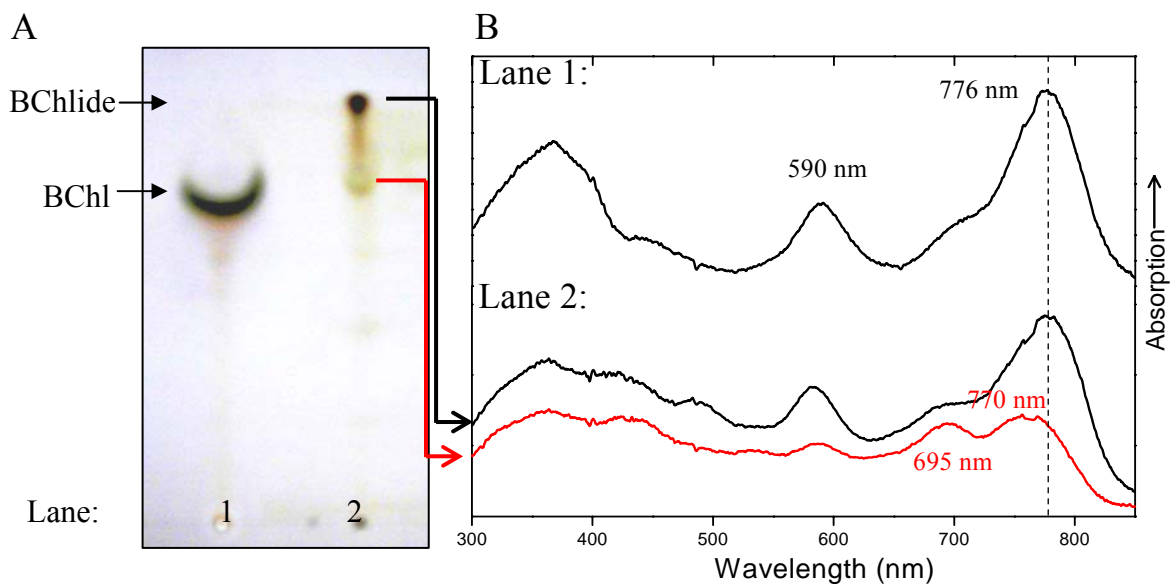


Figure 4-12: Thin layer chromatography of LH2 pigment extract after Chlase treatment.

(A) Thin layer chromatography. Lane 1: isolated WT LH2 without Chlase treatment. Lane 2: as sample 1 with Chlase treatment. Running buffer for TLC is methanol: acetone: water (30:20:2). For details see chapter 2.

(B) Reflectance spectra of TLC-separated pigments. The spectra are taken directly on the spots. Upper panel: absorption spectrum of the spot in the lane 1 and lower panel: absorption spectra of the two visible spots in the lane 2.

The CD signal of Chlase treated LH2 sample is altered. The signal of the BChl-B800 is clearly diminished and of the BChl-B850 is slightly red-shifted. The BChl-B850 signals' extrema and the zero crossing point are shifted by ~ 4 nm in comparison to untreated LH2 (figure 4-13A). This may either result from the loss of BChl-B800 in the LH2 complex (Bandilla *et al.*, 1998) and/or the loss of phytol tails from the BChls pigment. The appearance of a shift in the zero crossing point is also observed in the previous section (see figure 4-7A) in the purified LH2 of α WT/ β WT_{.9A} and α WT/ β WT_{.7-9A} which have significantly reduced BChl-B800 as well.

The thermal stability of Chlase treated WT LH2 complex was examined by monitoring the CD signal of the BChl-B850 during heat denaturation (figure 4-13B). The T_m value of Chlase treated sample shows a ~ 15 °C reduction as compared to LH2 WT. It is important to note that the acetone treated control sample has a similar T_m value as WT (see figure 4-6). Thus destabilisation of Chlase treated sample is solely due to the effect of the Chlase treatment on the LH2 pigment-protein.

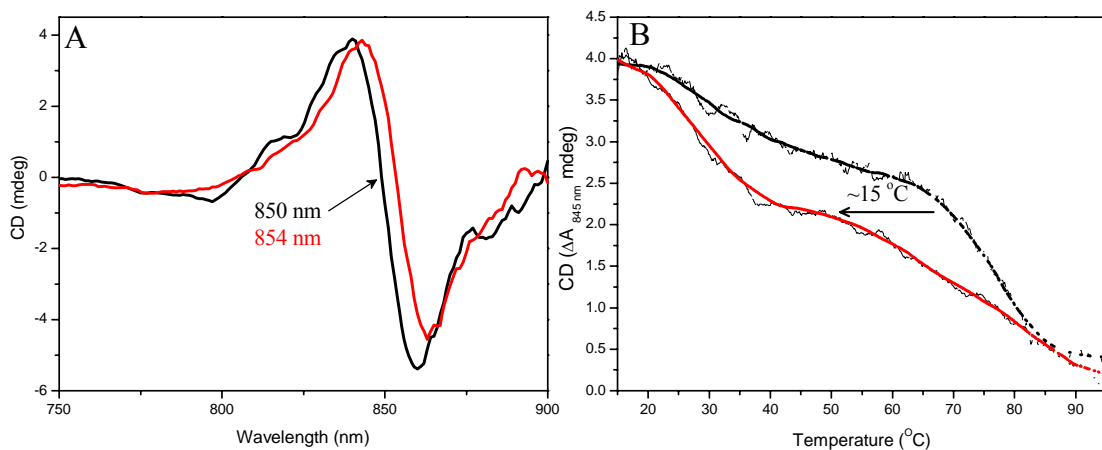


Figure 4-13: Comparison of Chlase treated (red line) and non-treated (black line) isolated WT LH2 samples.

(A) NIR CD spectra. CD is measured at 15 °C with 1 nm per 1 sec scan rate.

(B) Thermal denaturation. Changes of the CD signal at 845 nm. Signals are normalised at the starting point at 15 °C with a constant 2 °C per min heating rate.

In summary, Chlase treatment on the assembled LH2 complex in β OG results in hydrolysis of the ester bonds of the BCHls attached to LH2 yielding BChlide and phytol. According to the quantification of the pigments on TLC plates, up to ~89 % of BChl have been converted. Thus the enzyme was capable of hydrolysis of pigments tightly bound in the assembled LH2 complex. The removal of phytol tails results in diminished the BChl content in the LH2 complex, especially of the BChl-B800 and in a reduction of the thermal stability of LH2. It should be noted that loss of BChl-B800 has also affected the complex stability and thus the observed reduction is likely due to the combined effects. Possibly there is some residual BChl bound to the Chlase treated samples, which may marks the reduction in stability upon dephytylation.

Taken together, these findings implicate the critical role of the phytol chains for assembled LH2 antenna. To the best of our knowledge, for the first time, BChl attached to assembled LH2 are shown to be converted to BChlide in the presence of Chlase and acetone. Moreover, the stabilising role of phytol chains in assembled LH2 complex is demonstrated experimentally. Previously, it has been shown that the complex assembly is severely impaired upon modification of the phytol moiety during biosynthesis (Bollivar *et al.*, 1994; Addlesee & Hunter, 2002). Here, it is demonstrated that the phytol moiety is critical not only for the assembly process but also for the structural stability of assembled LH2 complex. It appears that upon hydrolysis of the BCHls to BChlide and phytol, the LH2 antenna undergoes destabilisation and partly disassembles. The BChlide and/or phytol tails still appear to be partly present in the assembled complex; it is conceivably that they are held in place by respective peptide interactions. In conclusion, this study shows the importance of phytol chains for the assembly of LH2, especially of BChl-B800.

STATISTICAL ANALYSES OF α - AND β -LIGATED (B)CHLS

The phytol chain of (B)Chl is a C₂₀ isoprenoid alcohol. It has been proposed to contribute to the localisation and the arrangement of the (B)Chl macrocycle (e.g. Loach & Parkes-Loach, 1995; Agostiano *et al.*, 2000); this is critical for their photosynthetic function (e.g. Rüdiger & Schoch, 1991; Addelee & Hunter, 1999). In this chapter, it has been shown that by (1) mutating the polypeptide residues in the close vicinity of the β BChl-B850 phytol tails and (2) by the removal of the phytol tails, the LH2 complexes' composition, spectral properties and stability are altered. These results point towards a critical role of BCHls' phytol chains in the maintenance of the assembly and structural stability of LH2.

Phytyl chains are very hydrophobic and usually reside within the hydrophobic transmembrane region of the membrane protein complexes. Little is known, however, on how the hydrophobic phytol chains are recognised and specifically bound by the polypeptides. It may require particular interaction motifs, i.e. the combination of particular residues which may exist across different (B)Chl containing proteins. In parallel to the experimental approaches, analysing phytyl-protein interactions in the structures of different photosystems may provide further insights into the mechanism underlying the binding of phytol tails by polypeptides and their contributions to the make up of the photosynthetic system.

Potential phytol-protein interactions motifs may be identified by statistical analysis of (B)Chl binding pockets of high-resolution structures of different photosystem. The following analyses were performed on the latest LH2 crystal structures of *Rsp acidophila* (Papiz *et al.*, 2003), which has been generally regarded as a model structure for *Rb sphaeroides* (Walz *et al.*, 1998) and on the crystal structure of photosystem I (PSI) from thermophilic cyanobacterium *Thermosynechococcus elongatus* (Jordan *et al.*, 2001). This complex binds almost 100 Chls and thus provides a substantial data base for statistical pigment-protein studies (e.g. Oba & Tamiaki, 2002; Loll *et al.*, 2003; Garcia-Martin *et al.*, 2006a). BChl and Chl are comparable as they are structurally similar with only two differences found in their macrocycle (see chapter 1, figure 1-6). Therefore, it is likely that potential Chl and BChl phytol binding motifs would be highly similar if not identical.

PSI is a large photosynthetic complex composed as a homotrimer. Each monomer is comprised of 12 protein subunits. The largest subunits PsaA and PsaB share 42 % sequence identity and are structurally similar (Jordan *et al.*, 2001; Loll *et al.*, 2003). Each of them have 11 TMHs, and forms the core region of PSI. The remaining smaller subunits surrounds this core region. In total 96 Chls *a* and 22 carotenoids are present in PSI, 40 Chls in subunit PsaA (subunit A) and 39 Chls in subunit PsaB (subunit B) (Jordan *et al.*, 2001). The large number of Chls in the TMHs offers a large data base for studying phytol-protein interactions. The majority of the C20 phytol atoms of the 96 Chls in PSI have been resolved; however, 19 and 21 Chls' phytol tails are not completely resolved in subunit A and B respectively. In addition, 8 phytols in the surrounding subunits are not completely resolved. This results in a total of 48 Chls out of the total of 96 with incomplete resolved phytol tails. The remaining 48 Chls with fully resolved phytol tails are used for the analysis of phytol-amino acid interactions.

Phytol interactions with the surrounding polypeptides are analysed for two stereochemically distinct ligation forms of (B)Chls which have been suggested to have distinct roles in photosystem (Balaban *et al.*, 2002; Oba & Tamiaki, 2002; Garcia-Martin *et al.*, 2006a). When the 17-propionic acid phytol ester is positioned opposite the ligand to the central Mg^{2+} atom of the macrocycle, it is known as α - or anti-ligation; and when positioned on the same side, it is known as β - or syn-ligation (figure 4-14).

Within PSI, the two types of configurations are present and distributed unevenly. Only 14 Chl molecules in PSI are found to be ligated in the β -conformation whereas 82 are in the α -conformation. β -ligated Chls appear specifically in the inner core of the antenna system only (Balaban *et al.*, 2002). It has been proposed that the arrangement of these Chls is highly regulated and its red-most absorption is further red-shifted compared to α -ligated (B)Chls (Balaban, 2003). (B)Chl ligated in α -position differ in several aspects from (B)Chl ligated in the β -position. For example, the energy states of these conformations differ by ~ 4.3 kJ/mol; that is binding of α -ligated (B)Chl is energetically more favourable than binding of β -ligated (B)Chl (Balaban *et al.*, 2002). Secondly, the hydrogen-bonding patterns for α - and β -ligated

Chls, in particular, of their C13¹ oxo groups are found to be significantly different. H-bonding for the α -ligated Chls occurs with loop structure or the binding helix itself while H-bonding to adjacent helices is very common for the β -ligated Chls (Garcia-Martin *et al.*, 2006a).

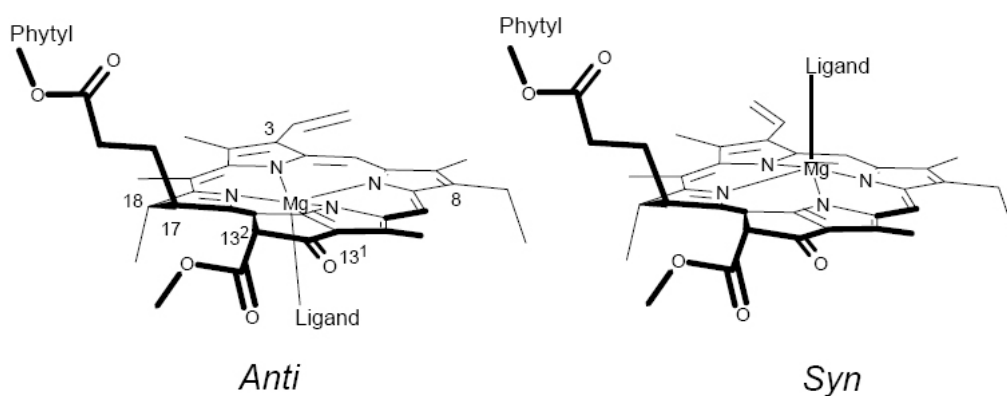


Figure 4-14: Anti- (α -) and syn- (β -) diastereoisomers of (bacterio)chlorophylls.

Analysis of phytol-protein interactions in PSI

As shown in table 4-2, the major difference between α - (BChl-B800) and β - (BChl-B850) ligated BChls of the LH2 complex is the extent of phytol interaction with their own binding helices. In LH2, there is no interaction between α -ligated BChl-B800 phytol tail and its own binding helix. On the contrary, more than 18 % of the total contacts of the β -ligated BChl are with the own binding helices. Figure 4-15 compares the contacts between the (B)Chls' phytol tails and the surrounding environment at a radius of ≤ 5 Å in the LH2 complex and in the A subunit of PSI. The contacts are listed for own binding helix, TMH, Chls, loop or parallel helix, carotenoid and others such as lipids (found in PSI only). Only the result of subunit A is presented here (figure 4-15) because the pigments binding pockets in both subunits A and B are highly homologous (Jordan *et al.*, 2001).

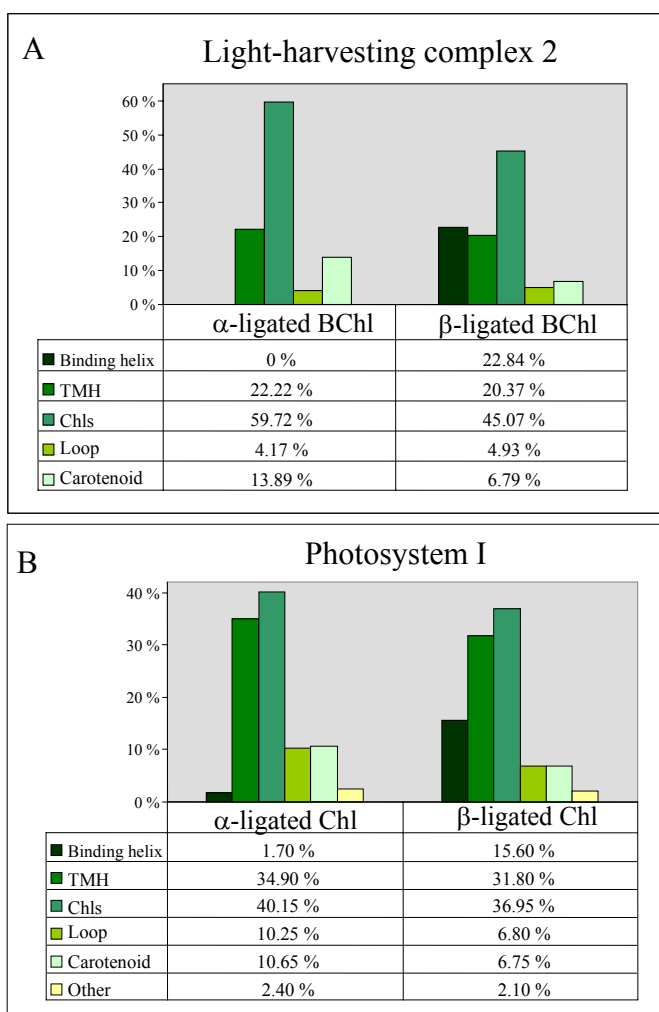


Figure 4-15: Analysis of contacts of the α - and β -ligated (B)Chl's phytol chains and protein environment.

(A) LH2 complex
 (B) Subunit A of PSI
 Contacts have been divided into five or six categories:
 (1) Binding helix: Binding helix that provides the ligand to the central Mg^{2+} atom of BChls;
 (2) TMH: Transmembrane helices except the binding helix;
 (3) Chls: Chls and BChls;
 (4) Loop: Loop structures including helices parallel to the membrane;
 (5) Carotenoid and
 (6) Other: Lipids include 1, 2 dipalmitoyl-phosphatidylglycerole, 1, 2 distearoyl-monogalactosyl-diglyceride and phylloquinone (found in PSI only).

In both LH2 and PSI complex, phytyl tails have most of their contacts with TMH (other than the binding helices) and (B)Chls; these constitute approximately 80 % of the total interactions that occur for the phytols. A distinct differences is observed in the contact patterns of α - and β -ligated (B)Chls; there is no or very little interaction observed between α -ligated phytyl and the own binding helix. Whereas, the remaining contacts which are contributed by TMH, loop and carotenoids, are basically similar in α - and β -ligated (B)Chls.

In summary, these data show that (1) the phytyl chains have extensive contacts with both the TMHs and the (B)Chls, (2) the general contacts of the phytyl chains are similar in the LH2 and PSI complexes, (3) the contact patterns for α - and β -ligated (B)Chls differ in one respect, namely, the contact between the phytol and the BChl's binding helices are exclusively occurring for β -ligated (B)Chls and (4) the phytol tails of (B)Chl ligated in α -position tend to interact primarily with structural elements other than their adjacent binding helices.

Analysis of phytyl-amino acid contacts

A major difference between the contact patterns of α - and β -ligated (B)Chl is observed in the frequency of contacts to their binding helices. To examine whether the amino acid environment around the phytols is distinct, the amino acid distribution in the close vicinity of the phytols is analysed. In the present PSI high-resolution structure at 2.5 Å (Jordan *et al.*, 2001), only 48 out of 96 Chls' phytol tails have been resolved completely. Out of these, 37 are of the α - and 11 of β -ligated Chls. The contacts of these phytyl chains have been analysed for their amino acid distributions. Figure 4-16 shows the amino acid distribution around the Chls' phytol tails with the α - and β -configuration in PSI. It is found that the phytyl chains interact primarily with hydrophobic residues, which account for approximately 80 % of the total contacts. The most extensive contacts are between Leu residue and the Chl ligated in α -position and between Trp residue and the Chl ligated in β -position. Conspicuously, there are clearly more interactions between the polar and basic residues Thr, Ser and His and the phytol of β -ligated Chls as compared to α -ligated Chls.

A similar observation is found in the analysis of BChl-protein contacts in LH2 (data not shown). Both the α - and β -positioned phytyl chains interact most frequently with hydrophobic residues and make up more than 65 % of the total interactions. In addition, in β -ligated BChl, the phytyl interacts more with polar residues (~20 %) while relatively little such interactions are found in the α -position phytyl. No interaction with acidic residues is found in both the α - and β -conformations.

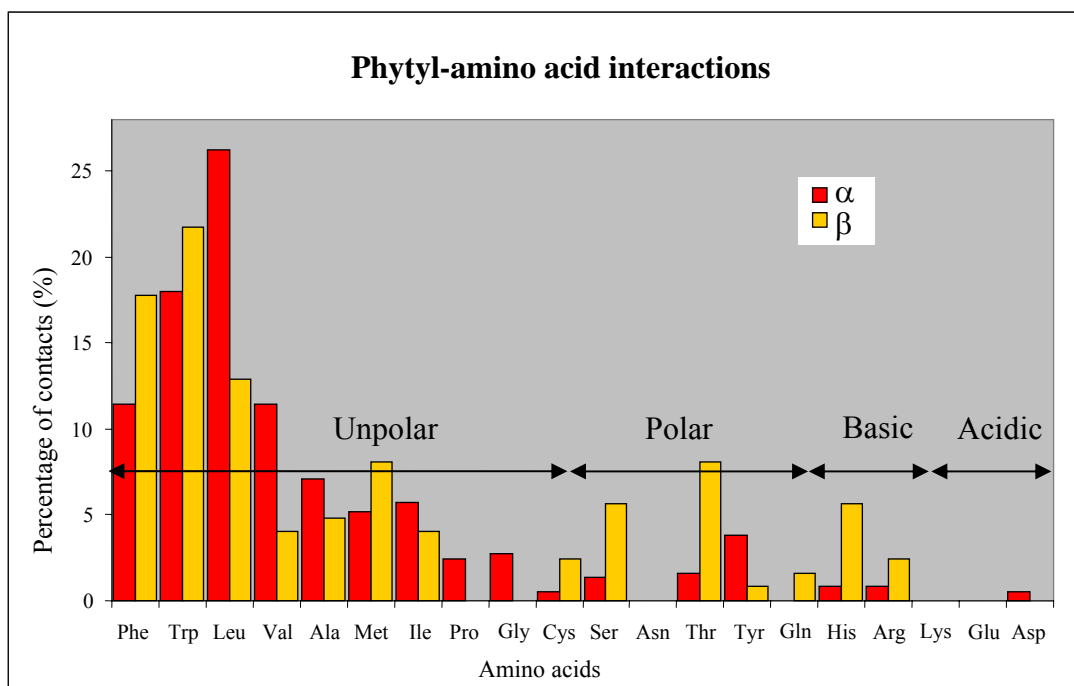


Figure 4-16: Distribution of amino acids residues around the Chl's phytyl chains in PSI. The values of phytyl chains contacts to amino acids were performed with Chi-square test using Microsoft Office Excel (2003). In all cases, significance was assumed if $P < 0.005$ (for detail see chapter 2).

The interactions between the phytyl chains and amino acids were further analysed by looking at the interactions between individual atoms of the phytyl chain, from C1 to C20 and the amino acid atoms. Figures 4-17 (table 4-3) and 4-18 (table 4-4) show the contacts between the amino acids and the phytyl carbon atoms of α - and β -ligated Chls respectively within a radius of ≤ 5 Å.

Phytol atom	Interactions between α -ligated chlorophylls and amino acids within a radius of 5 Å in PSI																				Total	%
	Phe	Trp	Leu	Val	Ala	Met	Ile	Pro	Gly	Cys	Ser	Asn	Thr	Tyr	Gln	His	Arg	Lys	Glu	Asp		
C1	14	15	11	3	3	0	7	0	0	0	0	0	0	2	0	1	0	0	0	0	56	15.30
C2	7	2	7	2	2	0	0	2	2	0	0	0	0	0	0	0	0	0	0	1	25	6.83
C3	2	1	5	1	1	0	0	1	0	0	1	0	0	0	0	0	0	0	0	0	11	3.01
C4	8	7	13	2	5	3	6	2	4	0	1	0	0	4	0	2	0	0	0	1	58	15.85
C5	0	2	7	1	1	1	1	1	0	0	0	0	0	0	0	0	0	0	0	0	14	3.83
C6	4	1	6	0	0	1	0	0	1	0	0	0	0	0	0	0	1	0	0	0	14	3.83
C7	1	2	5	1	0	0	0	0	0	0	0	0	0	0	0	0	0	0	0	0	9	2.46
C8	0	0	0	0	0	2	0	0	0	0	0	0	0	0	0	0	0	0	0	0	2	0.55
C9	3	3	12	1	1	1	1	0	0	0	0	0	0	0	0	0	0	0	0	0	22	6.01
C10	0	1	0	0	0	0	0	0	0	0	0	0	0	0	0	0	0	0	0	0	1	0.27
C11	1	2	0	0	0	1	0	0	0	0	0	0	0	0	0	0	2	0	0	0	6	1.64
C12	0	6	2	3	0	0	0	0	0	0	1	0	0	0	0	0	0	0	0	0	12	3.28
C13	0	1	2	0	0	0	0	0	0	0	0	0	0	0	0	0	0	0	0	0	3	0.82
C14	0	8	8	9	3	0	0	0	0	1	0	0	0	3	0	0	0	0	0	0	32	8.74
C15	0	5	3	1	0	1	1	0	0	1	2	0	0	0	0	0	0	0	0	0	14	3.83
C16	0	2	3	4	1	1	2	0	0	0	0	0	0	0	0	0	0	0	0	0	13	3.55
C17	0	4	1	1	1	3	1	0	1	0	0	0	0	0	0	0	0	0	0	0	12	3.28
C18	0	2	0	2	0	0	1	0	0	0	0	0	1	2	0	0	0	0	0	0	8	2.19
C19	1	2	4	4	7	2	0	0	0	0	0	0	4	2	0	0	0	0	0	0	26	7.10
C20	1	0	7	7	1	3	1	3	2	0	1	0	1	1	0	0	0	0	0	0	28	7.65
Total	42	66	96	42	26	19	21	9	10	2	5	0	6	14	0	3	3	0	0	2	366	
%	11.48	18.03	26.23	11.48	7.10	5.19	5.74	2.46	2.73	0.55	1.37	0.00	1.64	3.83	0.00	0.82	0.82	0.00	0.00	0.55		100.00

Table 4-3: List of residues within a radius of ≤ 5 Å in PSI of the α -ligated Chl phytol tail.

Interactions between β -ligated chlorophylls and amino acids within a radius of 5 Å in PSI																						
Phytol atom	Phe	Trp	Leu	Val	Ala	Met	Ile	Pro	Gly	Cys	Ser	Asn	Thr	Tyr	Gln	His	Arg	Lys	Glu	Asp	Total	%
C1	0	0	3	0	0	0	1	0	0	0	1	0	0	0	0	0	0	0	0	0	5	4.03
C2	1	0	0	0	0	1	0	0	0	0	0	0	0	0	0	0	0	0	0	0	2	1.61
C3	0	0	0	1	0	1	0	0	0	0	0	0	0	0	0	0	0	0	0	0	2	1.61
C4	0	0	5	1	1	1	2	0	0	1	3	0	0	0	0	0	0	0	0	0	14	11.29
C5	1	2	0	1	0	0	0	0	0	0	0	0	0	0	0	2	0	0	0	0	6	4.84
C6	2	1	0	0	0	1	0	0	0	1	0	0	0	0	0	1	0	0	0	0	6	4.84
C7	0	0	0	1	3	0	1	0	0	1	0	0	0	0	0	0	0	0	0	0	6	4.84
C8	0	0	0	1	2	0	0	0	0	0	0	0	0	0	0	0	0	0	0	0	3	2.42
C9	8	4	1	0	0	0	0	0	0	0	0	0	0	0	0	1	0	0	0	0	14	11.29
C10	0	0	0	0	0	0	0	0	0	0	0	0	0	0	0	0	0	0	0	0	0	0.00
C11	6	2	1	0	0	1	0	0	0	0	0	0	0	0	0	0	0	0	0	0	10	8.06
C12	2	0	1	0	0	0	0	0	0	0	0	0	0	0	1	0	0	0	0	0	4	3.23
C13	0	0	0	0	0	0	0	0	0	0	0	0	0	0	0	0	0	0	0	0	0	0.00
C14	2	0	1	0	0	4	0	0	0	0	0	0	3	0	0	2	1	0	0	0	13	10.48
C15	0	0	0	0	0	0	0	0	0	0	0	0	0	0	1	0	0	0	0	0	1	0.81
C16	0	0	1	0	0	0	0	0	0	0	0	0	2	0	0	1	0	0	0	0	4	3.23
C17	0	0	0	0	0	0	0	0	0	0	0	0	2	0	0	0	0	0	0	0	2	1.61
C18	0	6	0	0	0	0	0	0	0	0	0	0	0	0	0	0	0	0	0	0	6	4.84
C19	0	4	3	0	0	0	0	0	0	0	1	0	0	1	0	0	2	0	0	0	11	8.87
C20	0	8	0	0	0	1	1	0	0	0	2	0	3	0	0	0	0	0	0	0	15	12.10
Total	22	27	16	5	6	10	5	0	0	3	7	0	10	1	2	7	3	0	0	0	124	
%	17.74	21.77	12.90	4.03	4.84	8.06	4.03	0.00	0.00	2.42	5.65	0.00	8.06	0.81	1.61	5.65	2.42	0.00	0.00	0.00		100.00

Table 4-4: List of residues within a radius of ≤ 5 Å in PSI of the β -ligated Chl phytol tail.

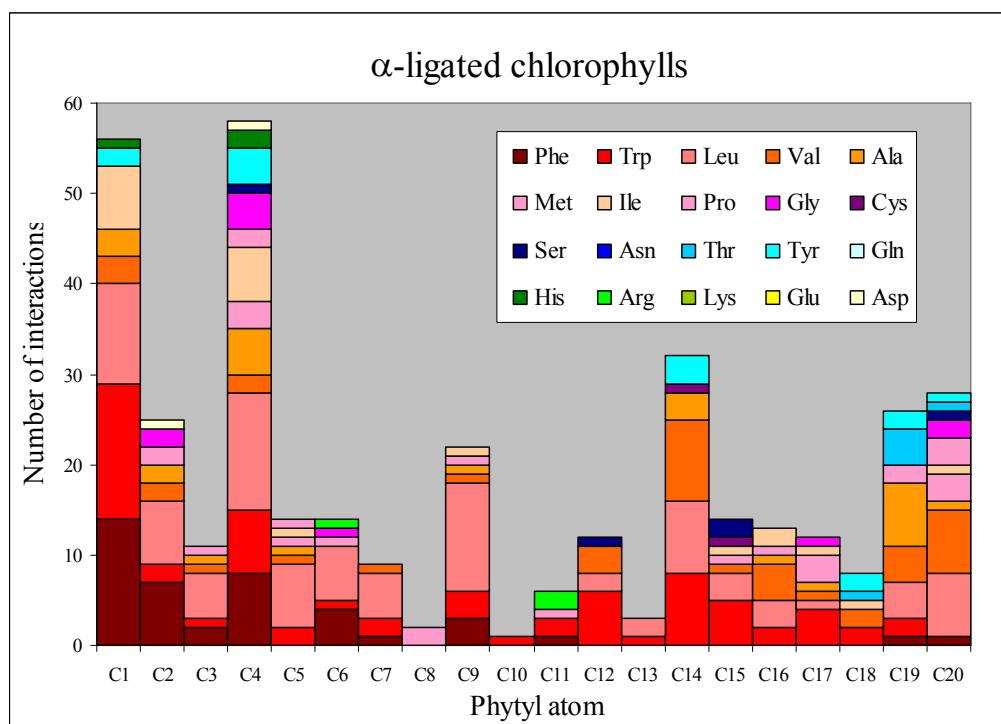


Figure 4-17: The contacts between α -ligated Chls' phytol moieties and amino acid residues within a radius of $\leq 5 \text{ \AA}$ in PSI. Unpolar residues are displayed in red, polar residues in blue, basic residues in green and acidic residues in yellow. Graph illustration of table 4-3.

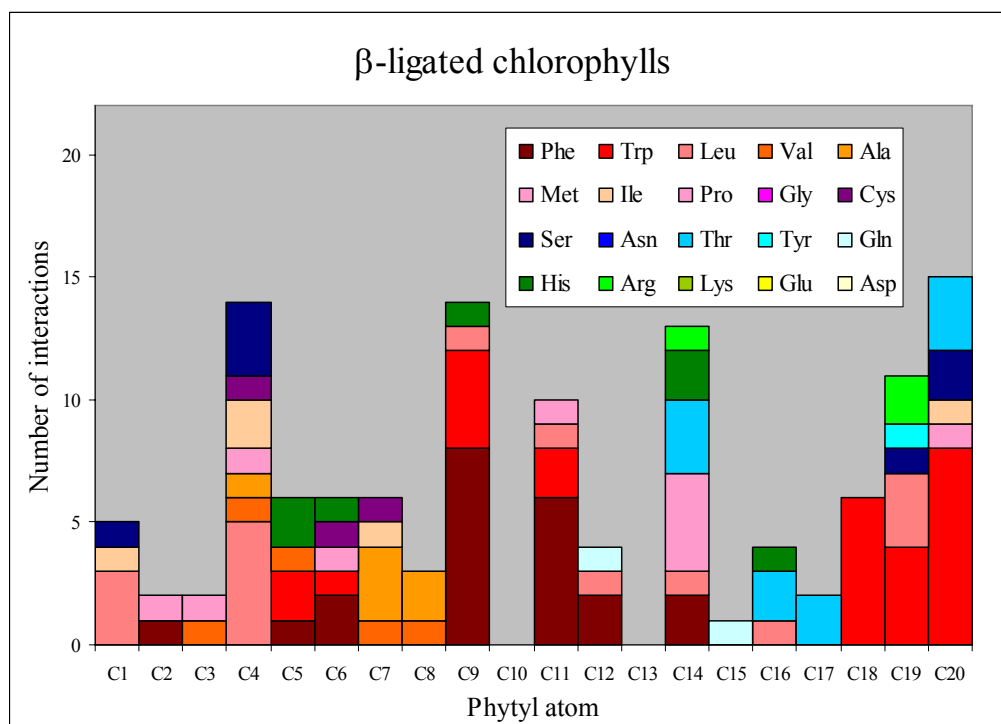


Figure 4-18: The contacts between β -ligated Chls' phytol moieties and amino acid residues within a radius of $\leq 5 \text{ \AA}$ in PSI. Unpolar residues are displayed in red, polar residues in blue, basic residues in green and acidic residues in yellow. Graph illustration of table 4-4.

In α -ligated Chls (figure 4-17) the carbons with the most contacts are C1 and C4 atoms, which have ~60 contacts each. The least interactive atoms are C8, C10 and C13 atoms in the phytol chain; they have less than 5 contacts each. The remaining atoms have between 10 to 30 contacts. As expected, most of the interactions are found with unpolar residues, such as Phe, Trp and Leu. Interestingly, Phe residue is observed mainly in the close vicinity of the C1-C7 of the phytol chain; whereas Trp and Leu residues interact more or less throughout the phytol chain. Residues like tryptophan and lysine are commonly observed at the interface between the membrane and the water phase and at the lipid headgroup region. In general, there are few contacts found with polar residues and even less with basic and acidic residues.

Figure 4-18 shows the β -ligated Chls phytol interactions with amino acids in PSI. Naturally for β -ligated Chl, the number of contact is significantly lower as compared to the number of contacts for the α -ligated Chls (figure 4-17) (11 compared to 37 are analysed). Most frequent contacts to polypeptide involve atoms C4, C9, C11, C14, C19 and C20 of the phytol. There are (nearly) no contacts observed for C10, C13 and C15 atoms. A mixture of interactions with unpolar, polar and basic residues along the phytol chain is observed in β -ligated Chls. No contacts with acidic residues are found. Phe residue interactions are mainly concentrated in the middle part of the phytol chain, C9-C14. Furthermore, more interactions with Trp residue are found at the end of the phytol chain, C18-C20.

In summary, the statistical analyses of the amino acid distribution around the phytols show that (1) the pattern of amino acid-phytyl interactions in α - and β -ligated Chls are significantly different ($P < 0.005$). Generally, contacts with the β -ligated phytols are distributed evenly throughout the entire chain, and are particularly high for the methyl side groups; whereas contacts with the α -ligated Chls' phytol are particularly high for the C1 and C4 methyl atoms. (2) In both, however, C4 of the phytol chain seems to be most interactive and C10 and C13 of the phytol chain seem to be the least interactive. (3) Generally, unpolar residues, in particular, Phe, Trp, Leu and Val are distributed most frequently around the phytol chain of α -ligated Chl. (4) In β -ligated Chl, the aromatic residues (Phe, Trp) are clearly over represented. At C9 and

C11, Phe and Trp make up more than 80 % of the residues observed and at C18 it is exclusively Trp. In addition, polar and charged residues make up a considerable part at these contact points.

In conclusion, the analysis of the phytol interactions with their surrounding environment shows that the pattern of contacts between α - and β -ligated (B)Chls are significantly different. H-bonding of β -ligated Chl appears to contribute to tertiary interaction among the helices (Garcia-Martin *et al.*, 2006a). Possibly, phytol moieties further contribute to the tertiary assembly of BChl/TMH units by frequent and specific interactions with the surrounding protein. This will reinforce the link between the BChl/TMH units. This analysis provides the basic information on the patterns of contacts between pigment and protein. It aids in deciding which residues to address by mutagenesis for the further study of phytol-protein interactions. Moreover, it may help to guide the design of BChl-binding pockets in model studies. To date, many artificial synthetic polypeptides in (B)Chls-protein studies have been performed with the use of (B)Chlide molecules instead of (B)Chl (e.g. Dewa *et al.*, 2005; Nango, 2006) due to the difficulties in handling the very hydrophobic phytol chain moieties and/or the lack of knowledge of the phytol-protein interactions.

Model LH2	Modified sequences		T _m value of LH2 membrane (°C)
	α -subunit	β -subunit	
WT	TVGVPLFLSAAVIASVVIHAAVLTTT	AEEVHKQLILGTRVFGGMALIAHFLAAAA	74
α WT/ β AL	TVGVPLFLSAAVIASVVIHAAVLTTT	AEEVHKQLILGTRVFLLIALLAHLLAAAA	54
α WT/ β AL _{.7A}	TVGVPLFLSAAVIASVVIHAAVLTTT	AEEVHKQLILGTRVFLLIALLAHLLAAAA	No complex
α WT/ β AL _{.9A}	TVGVPLFLSAAVIASVVIHAAVLTTT	AEEVHKQLILGTRAFLLIALLAHLLAAAA	No complex
α WT/ β WT _{.9A}	TVGVPLFLSAAVIASVVIHAAVLTTT	AEEVHKQLILGTRAFGGMALIAHFLAAAA	70
α WT/ β WT _{.7A}	TVGVPLFLSAAVIASVVIHAAVLTTT	AEEVHKQLILGTRVFA GMALIAHFLAAAA	ND
α WT/ β WT _{.7-9A}	TVGVPLFLSAAVIASVVIHAAVLTTT	AEEVHKQLILGTRAFAGMALIAHFLAAAA	63

Table 4-5: Amino acid sequences of model LH2 used in this chapter. ND = not detected.

RESULTS

PART II:

Protein-lipid and pigment-lipid interactions in model and native light-harvesting complex 2

CHAPTER 5

Study of the relationship between *Rb sphaeroides* LH2 protein-phospholipids interactions and ICM morphology

5.1 INTRODUCTION

All biological membranes contain a diversity of lipids and proteins. They are bilipid layers and are composed primarily of phospholipids, to a lesser extent glycolipids (except for chloroplast thylakoids membrane), sulfolipids and sterols (except for prokaryotic organism, which do not synthesise sterols) (Rohmer *et al.*, 1979; Quinn & Chapman, 1980). The lipid membrane harbours a vast variety of membrane proteins which perform most of the membrane functions, such as cell-cell signalling, transports of inorganic and organic compounds or ATP synthesis.

Membrane lipids spontaneously self-organise into bilipid layers as a result of their chemical properties, most importantly their amphipathic structure (Lee, 2003). Amphipathic molecules consist of both a polar, hydrophilic part and a non-polar, hydrophobic part (figure 5-1). In aqueous solvents, amphipathic molecules orientate themselves to ensure that the polar groups associate with water molecules, whereas the hydrophobic chains interact with each another. In this way, a maximal number of water molecules are excluded from the hydrophobic phase (Lee, 2003, 2004). If the lipid is roughly cylindrical in dimension, biplanar leaflets will be the most thermodynamically stable configuration (Dowhan, 1997; van den Brink-van der Laan *et al.*, 2004b). Some lipids have a cone shape such as cholesterol and some phosphatidylethanolamines; the polar headgroup of these lipids occupies a smaller area than the hydrophobic region. In addition, there are inverted cone-shaped lipid molecules, such as sphingolipids and phosphatidic acid; the polar headgroup of these lipids is larger than the hydrophobic region (figure 5-1) (van den Brink-van der Laan

et al., 2004b). The latter two forms of lipids tend to destabilise the planar bilayer configuration.

The fluid membrane bilayers do not only make up the vital permeability barriers of cells and organelles but also provide a fluid matrix for the membrane proteins. There is now ample evidence accumulated that, as opposed to the long-standing dogma of the lipid bilayer being an inert matrix, the interplay of lipids and membrane proteins is vital for maintaining and optimising the function of membranes (for recent reviews see e.g. Dowhan, 1997; Lee, 2004; McMahon & Gallop, 2005).

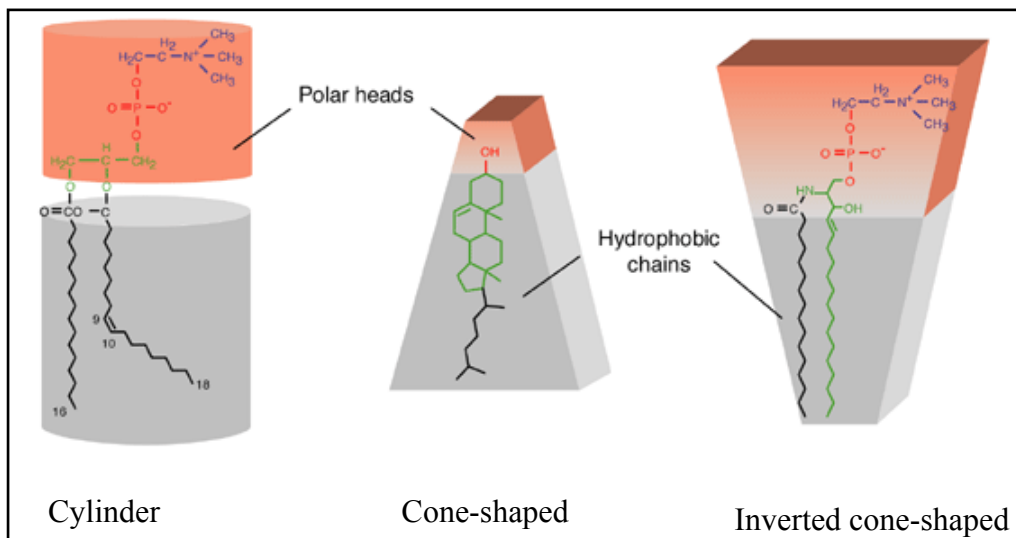


Figure 5-1: General depiction of three types of amphipathic phospholipid molecules, each consists of a polar headgroup (red) and non polar, hydrophobic chains (grey).

In energy converting membranes, the protein to lipid ratio is usually very high (~5:1) (Kaplan *et al.*, 1983); and a large fraction of the lipids are in close contacts with the proteins (Lee, 2003, 2004, 2005). There are three types of lipids found in biological membranes: (1) Boundary lipids (also known as annular lipids) are a population of lipids which interact directly with the membrane protein. (2) Bulk lipids which are not at all in contact with the membrane proteins. (3) Structural lipids (or non-annular lipids) which are structural co-factors for membrane proteins (Lee, 2004, 2005) (figure 5-2). Several high-resolution structures, such as the plant photosystems (Jordan *et al.*, 2001, Yang *et al.*, 2005) and LHC (Nussberger *et al.*,

1993; Dekker & Boekema, 2005; Gonen *et al.*, 2005) as well as reaction centres in photosynthetic purple bacteria (McAuley *et al.*, 1999; Camara-Artigas *et al.*, 2002; Páli *et al.*, 2003; Fyfe *et al.*, 2004), have revealed binding sites for a number of lipids. Most of the lipid molecules resolved in high-resolution structures of membrane proteins are likely to be structural lipids as these lipids are strongly embedded in the protein interior (Lee, 2003, 2004). On the other hand, boundary lipids will usually be too disordered to appear in high-resolution structures as during the procedures of purification, these lipids attached to the protein surface will largely distort (Lee, 2004). However, in bacteriorhodopsin trimer, many fatty acyl chains of the boundary lipids have been resolved (Belrhali *et al.*, 1999; Luecke *et al.*, 1999).

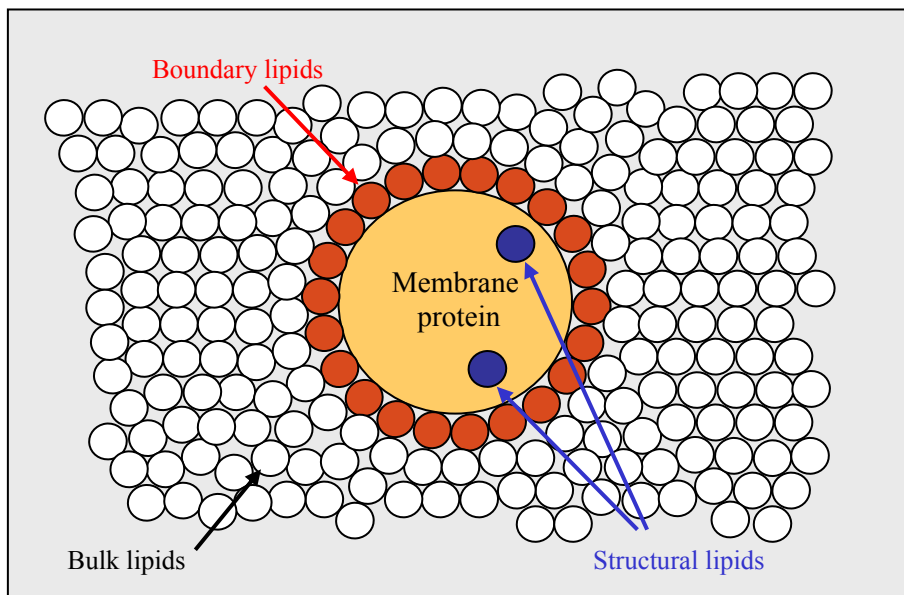


Figure 5-2: Illustration of the spatial relationship between lipids and integral membrane proteins. The integral membrane protein is surrounded by a shell of lipids (boundary lipids shown in red) which interact directly with the hydrophobic surface of the protein (this shell may consist of several lipid layers which exchange with the bulk lipids). The bulk lipids which are not in contact with membrane proteins are shown in white. The structural lipids embedded in the protein interior are shown in blue.

The lipids bound at the lipid-protein interface appear to be important for the proper packing of the transmembrane protein within the membrane (Gruner, 1985; Marsh & Horvath, 1998; Lee, 2005). It is well documented that both the lipid chains and lipid

headgroups interact with proteins and affect the overall conformation, oligomeric state, function and stability of membrane proteins (e.g. Marsh & Horvath, 1998; Fyfe *et al.*, 2001; Lee, 2003, 2004; Hunte, 2005; McMahon & Gallop, 2005; Marsh & Páli, 2006). Some of these effects arise from general physiochemical properties of the lipid environments (such as lipid composition, lipid bilayer fluidity and lipid bilayer curvature), while others may be induced by protein-lipid selectivity (Gruner, 1985; Lee, 2003, 2004).

The specificity of lipid-protein interactions depends on the lipid structure and whether it is closely associated with the protein. Both, the lipid headgroup and acyl chain provides the structural basis for selective accumulation around proteins (Marsh & Horvath, 1998; Lee, 2005; Hunte, 2005; Marsh & Páli, 2006). The binding of lipid headgroups to membrane protein involves a combination of ionic or electrostatic interactions (Tocanne & Teissié, 1990; Dumas *et al.*, 1999; Mukherjee & Maxfield, 2004). Depending on the charge of the headgroup, it may modulate the activity of membrane proteins through interfacial electrostatic phenomena (Tocanne & Teissié, 1990). On the other hand, the interactions between lipid acyl chains and membrane protein are less understood. Van der Waals forces are likely to be involved in the interactions between lipid tails and electroneutral intramembrane surfaces of the protein (McAuley *et al.*, 1999; Dumas *et al.*, 1999; Marsh & Páli, 2006).

The phospholipid biosynthesis pathway in bacteria branches from phosphatidic acids (PA) with one branch producing phosphatidylglycerol (PG) and cardiolipin (CL) and the other phosphatidylethanolamine (PE) and phosphatidylcholine (PC) (figure 5-3) (Dowhan, 1997). In response to the growth condition and protein composition(s), bacteria regulate the phospholipid biosynthesis pathway, particularly their PC/PE levels (Dowhan, 1997; Russell *et al.*, 2002). PC and PE are zwitterionic phospholipids; together they comprise the majority of the membrane phospholipids of gram-negative bacteria, many gram-positive bacteria and eukaryotic cells (Dowhan, 1997). PG and CL are anionic lipids; in most membranes, they comprise less than 30 % of the membrane phospholipids (Dowhan, 1997). The unsaturated PE and CL tend to form nonbilayer phases, whereas PG and PC form bilayer

(lamellar) phases (Harlos & Eibl, 1981; Dowhan, 1997; van den Brink-van der Laan *et al.*, 2004b). The ratio of bilayer/nonbilayer-forming phospholipids influence the biophysical properties of the membrane, it affects the lipid phase behaviour, charge distribution, membrane curvature and subsequently influence the protein-lipid interactions (Dowhan, 1997; Lee, 2004).

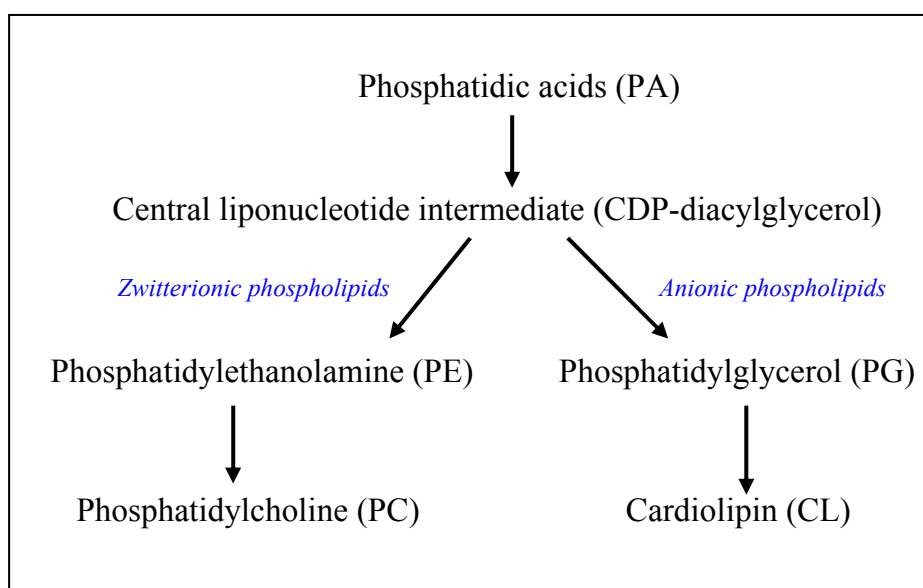


Figure 5-3: Phospholipid biosynthetic pathway in bacteria. The pathway begins with PA being converted to the central liponucleotide intermediate CDP-diacylglycerol. Of which is the precursor to the major zwitterionic phospholipids (PE and PC), and the major anionic phospholipids (PG and CL), found in almost all bacteria. This pathway is adapted from *E. coli* synthesis, modified from Dowhan (1997).

PE appears to be the major phospholipid in many organisms (Cronan, 2003; van den Brink-van der Laan *et al.*, 2004a, 2004b; Lee, 2004; Liu F *et al.*, 2004). For example, the inner membrane of *E. coli* contains about 75 % PE (Cronan, 2003). It has been suggested that bacteria control the lipid compositions of their membranes to maintain a constant proportion of lipids favouring the non-planar, hexagonal H_{II} phase (Dowhan, 1997; Cronan, 2003). The presence of membrane proteins and/or bilayer-forming lipids will counteract this tension and force the nonbilayer lipids into bilayer formation (Cullis & de Kruijff, 1979). Proper assembly and function of membrane proteins are known to require these interactions with nonbilayer lipids

(Liu F *et al.*, 2004; van den Brink-van der Laan *et al.*, 2004a, 2004b); for example, correct folding of integral membrane proteins, as in the case of lactose permease (Bogdanov & Dowhan, 1998; Zhang *et al.*, 2003) and proper protein function, as in rhodopsin (Brown, 1997; van den Brink-van der Laan *et al.*, 2004a, 2004b). It is also important to note that the nonbilayer lipids, such as PE play an important role in membrane curvature (van den Brink-van der Laan *et al.*, 2004b; Lee, 2004). In contrast, PC and PG are bilayer forming phospholipids and do not generally form hexagonal H_{II} phases.

The ammonium headgroup of PE is fully protonated and positively charged under relevant physiological conditions (Liu F *et al.*, 2004; Murzyn *et al.*, 2005). These characteristics of PE result in both a net attractive electrostatic interaction with negatively charged groups and potential for H-bonding interactions with H-bonding acceptor groups (Boggs, 1980, 1987; Liu F *et al.*, 2004). Potential acceptor groups are the phosphate and carbonyl oxygen atoms of adjacent PE or PG molecules or the negatively charged amino acids side chains at the N- and C-termini of membrane proteins (Boggs, 1987; Gil *et al.*, 1998; Liu F *et al.*, 2004; Murzyn *et al.*, 2005). These intermolecular forces underlie and strengthen the interlipid and lipid-protein contacts and thus, the stability of the protein (Liu F *et al.*, 2004; van den Brink-van der Laan *et al.*, 2004a; Murzyn *et al.*, 2005). Even though the phosphodiester group of PG has a potential to form H-bonding and/or ionic interactions with basic amino acids (Páli *et al.*, 2003; Liu Z *et al.*, 2004), no stabilising effect on the protein were found in the presence of PG (van den Brink-van der Laan *et al.*, 2004a). Furthermore, PC does not have the H-bonding donor groups on its headgroup. As a result it does not participate in H-bonding interactions or form electrostatic attractions in the immediate environment (Dowhan, 1997; Liu F *et al.*, 2004).

Facultative photoheterotrophic bacterium *Rb sphaeroides* has been used for the study of protein-lipid interactions and its impact on membrane morphology. In response to low oxygen tension and light illumination levels, *Rb sphaeroides* produces a specialised intracytoplasmic membrane comprised of interconnected vesicles-like invaginations which harbour light-harvesting complexes and reaction centres (figure 5-4) (Brown *et al.*, 1972; Fraley *et al.*, 1979; Drews & Oelze, 1981). The

macromolecular arrangement of these pigment-protein complexes in ICM is optimised to allow for the highly efficient photosynthetic processes.

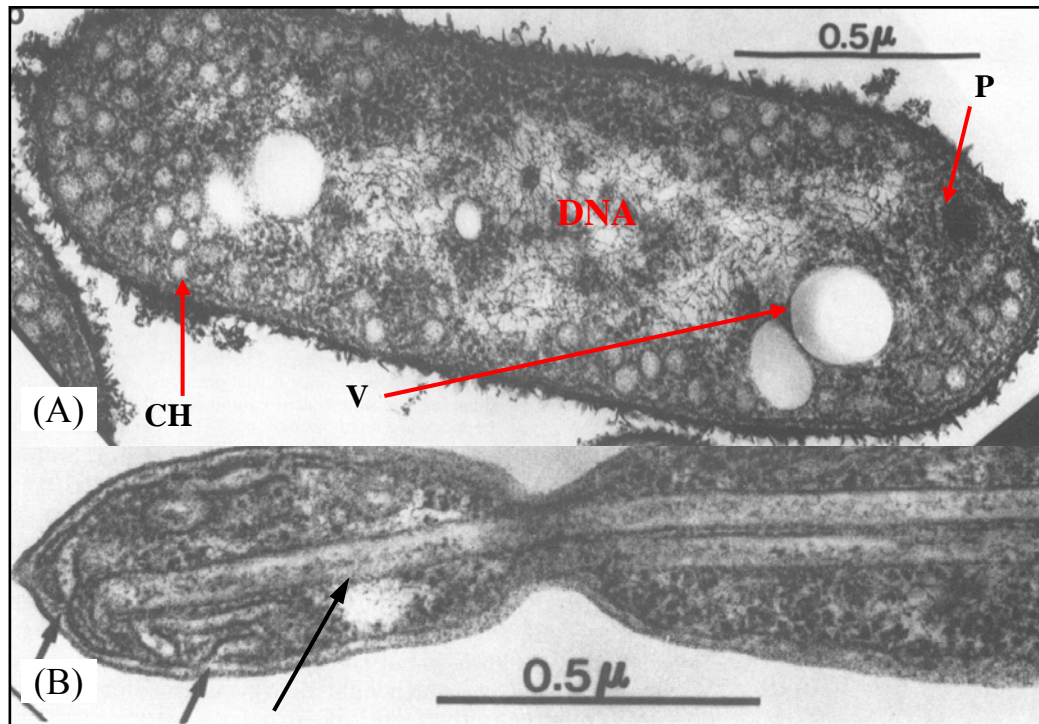


Figure 5-4: Intracytoplasmic membrane of *Rb sphaeroides* harbouring the bacterial photosystems. Ultrastructure of (A) wild type RS2 strain ($LH2^+ LH1^+ RC^+$) and (B) carotenoidless mutant RS104 ($LH2^- Car^- LH1^+ RC^+$) strains of photosynthetically grown *Rb sphaeroides* cells (Figure is taken from Kiley *et al.*, 1988). CH corresponds to chromatophores; V corresponds to fat vacuoles or the large non-staining poly- β -hydroxybutyric acid granules and P corresponds to polyphosphate granules. DNA appears in the central region of the cell as a high density. Black arrows in panel B indicate the irregular shaped of ICM in RS104 strain.

The structure, function and biogenesis of ICM in *Rb sphaeroides* have been extensively studied (e.g. Clayton & Haselkorn, 1972; Fraker & Kaplan, 1972; Huang & Kaplan, 1973; Takemoto & Lascelles, 1973; Fraley *et al.*, 1978, 1979; Al-Bayatti & Takemoto, 1981; Marinetti & Cattieu, 1981; Kiley & Kaplan, 1988). Many of these studies involved either the induction of ICM biogenesis following a switch from chemoheterotrophic to photoheterotrophic growth or depression of ICM synthesis following a shift in light intensity. The development of the ICM, i.e. membrane invaginations and surface enlargement, has been found to be correlated with the emergence of the fully pigmented light harvesting proteins. The most

abundant ICM protein complexes are BChls and carotenoids containing light-harvesting complexes (Fraley *et al.*, 1979). The amount of vesicles per cell and the whole-cell BChl *a* content increase proportionally as a result of decreasing the growth incident light intensities (Kiley & Kaplan, 1988; Sturgis & Niederman, 1996).

For the complete maturation of vesicularised ICM in *Rb sphaeroides*, properly assembled peripheral LH2 complexes and the presence of carotenoid are required; whereas, complete maturation is independent of the presence of RC or LH1 complexes (figure 5-4B) (Kiley *et al.*, 1988; Hunter *et al.*, 1988). Mutants with disruptions in their carotenoid biosynthetic process have gross alterations in ICM morphology (Lommen & Takemoto, 1978; Lang & Hunter, 1994). These changes may result from a failure to assemble the LH2 complex in the absence of the carotenoid. In essence, both the LH2 complex and carotenoid are required for the proper development of vesicular ICM formation in *Rb sphaeroides* and determines the size of the resulting vesicular invaginations (Hunter *et al.*, 1988; Sturgis & Niederman, 1996). However, the molecular factors and forces involved in this process are still unknown.

Early investigations of membrane phospholipid composition of *Rb sphaeroides* 2.4.1 (LH2⁺ LH1⁺ RC⁺, grown photosynthetically, e.g. Takemoto & Lascelles, 1973; Birrell *et al.*, 1978; Russell & Harwood, 1979; Al-Bayatti & Takemoto, 1981; Cain *et al.*, 1981), had suggested that the major phospholipids are PE, PG and PC (figure 5-5A) and the minor lipids are CL and PA. The major phospholipids are characteristically rich in 11-cis-vaccenic acid (C18:1 Δ 11) (Kenyon 1978; Russell & Harwood, 1979), stearic acid (C18:0), palmitoleic acid (C16:1 Δ 9) and palmitic acid (C16:0) (Wood *et al.*, 1965; Russell & Harwood, 1979; Onishi & Niederman, 1982) (figure 5-5B). The relative proportions of these phospholipids quoted in these works fluctuated significantly. For example, Al-Bayatti & Takemoto (1981) failed to find PC, whereas ~11 % was reported by Russell & Harwood, (1979) and 23 % by Birrell *et al.* (1978). This divergence may be explained, by the variations in culture conditions and methods of lipid analysis.

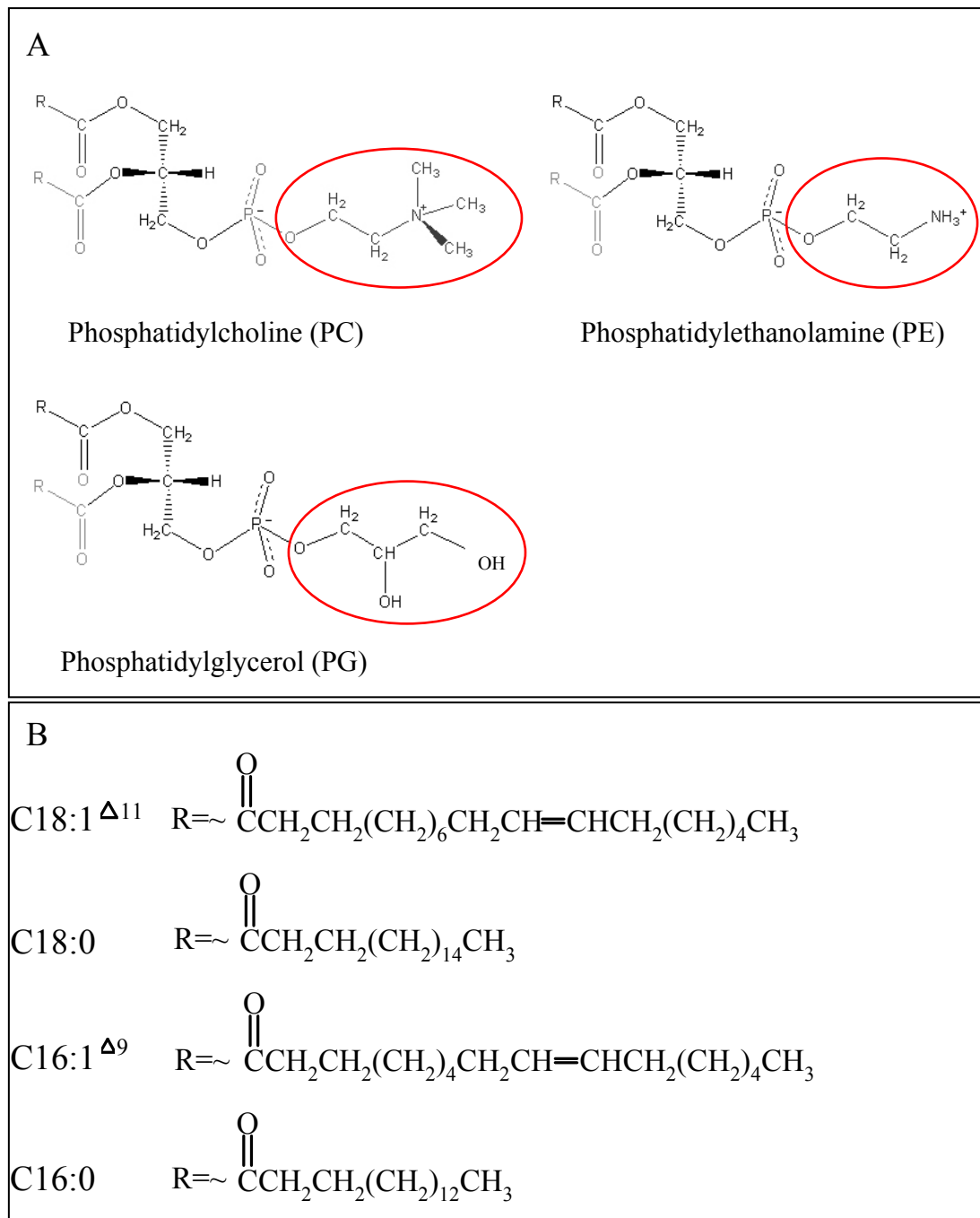


Figure 5-5: Major phospholipids of *Rb sphaeroides*.

(A) Chemical structures of zwitterionic phosphatidylcholine (PC), phosphatidylethanolamine (PE) and negatively charged phosphatidylglycerol (PG). The functional groups derived from the esterified alcohol are circled in red. These phospholipids contain many combinations of fatty-acyl groups (R).

(B) The most common fatty-acyl chains (R) found in photosynthetically grown *Rb sphaeroides*.

Studies on the distribution of phospholipids and their biosynthetic enzymes in different membrane fractions of *Rb sphaeroides* have been performed by several groups (e.g. Cain *et al.*, 1981; Knacker *et al.*, 1985; Sturgis & Niederman, 1996). However, there is no specific information about the lipid compositions in the immediate vicinity of LH2 complexes. In the context of the present study, we are interested in LH2 proteins and its interactions with phospholipids. In general, the approach of modifying phospholipids by genetic alteration of its biosynthesis is indirect and has multiple unpredictable pleiotropic effects. In other words, mutations cannot be made directly in a phospholipid but rather to its biosynthetic pathway; this however will compromise not only singular cell integrity but whole cell functions. The elimination or drastic alteration of certain phospholipid will affect several cellular processes simultaneously and therefore may complicate the interpretation of results. Genetically modified *Rb sphaeroides* are available which permit site-directed mutations of the LH proteins and selective expression of individual photosynthetic complexes (Hunter, 1995). This system thus provides an unique opportunity to study specific protein-lipid interactions and their effects on the morphogenesis of the photosynthetic membrane.

The high-resolution crystal structure of LH2 (McDermott *et al.*, 1995; Papiz *et al.*, 2003) permits visualisation of LH2 protein on a molecular level. The N-termini of α - and β -polypeptides are of functional significance and have been suggested to be involved in membrane targeting, protein insertion, formation of the $\alpha\beta$ -heterodimer and complex assembly (Richter & Drews, 1991; Meadows *et al.*, 1995; McDermott *et al.*, 1995; Drews, 1996). The net concentration of negatively charged amino acids at the N-terminus of the β -polypeptides of LH2 has been suggested to interfere with the negatively charged phospholipid headgroups (Stamouli *et al.*, 2003). The negatively charged amino acids may form H-bonds or electrostatic interaction with the ammonium group of PE.

The aim of this chapter is to further the understanding of the specific interactions between LH2 protein and membrane phospholipids and the contributions of these interactions to the development of the photosynthetic membrane. The immediate goals are: (1) to elucidate the interdependence of intracytoplasmic lipid

compositions, morphology and LH2 expression levels, (2) to explore the role of specific lipid-LH-protein interactions in the modulation of the lipid composition and membrane morphology and (3) to shed a light on the molecular basis for lipid-LH2 protein interactions.

5.2 RESULTS AND DISCUSSION

STUDY OF THE RELATIONSHIP BETWEEN LH2 AND ICM MORPHOLOGY

The size and morphology of ICM chromatophores are affected by both the light intensity and LH2 concentrations in the membrane (Sturgis & Niederman, 1990, 1996). ICM diameter decreases with the increasing concentrations of LH2 and decreasing light intensity (Hunter *et al.*, 1988; Sturgis & Niederman, 1996). In addition, it has been shown previously that in the absence of LH2 complexes, the formation of fully vesicularised ICM and subsequent maturation cannot be completed even though LH1 and RC core particles are present (Hunter *et al.*, 1988; Kiley *et al.*, 1988; Verméglio & Joliot, 1999) (figure 5-3). However, in these systems, interpretations are complicated due to the presence of additional BChl-binding complexes (LH1 and RC). Here in the chapter, the relationship between ICM membrane formation and LH2 assembly is examined in deletion strains of DD13 (LH2⁻ LH1⁻ RC⁻, spheroidenone) or DG2 (LH2⁻ LH1⁻ RC⁻, neurosporene), expressing normal, reduced or altered LH2 complexes. Changes in ICM development may thus be directly correlated with changes in LH2 expression and assembly.

Model LH2 protein, α AL_{4S}/ β AL (see chapter 3), has been used to study the assembly of LH2 complexes, in particular the BChl-binding and assembly in the native membrane. Although, α AL_{4S}/ β AL assembles to LH2-like complexes, the energy transfer efficiency among the photoactive pigments, the structural stability and the level of assembled LH2 α AL_{4S}/ β AL in the membrane are significantly reduced (figure 5-6). The total protein concentration in the membrane of α AL_{4S}/ β AL mutant (~700 μ g/ml) is approximately seven times higher in comparison to DD13 WTⁱ (~120 μ g/ml) (see chapter 2, materials and methods and appendix 2), possibly indicating the accumulation of disassembled LH2 proteins.

ⁱ DD13 WT refers to *Rb. sphaeroides* mutant strain DD13 (LH2⁻ LH1⁻ RC⁻) expressing the wild type LH2 complex (LH2 WT⁺ LH1⁻ RC⁻).

Isolated chromatophores containing $\alpha\text{AL}_{4\text{S}}/\beta\text{AL}$ are highly viscous and rapidly precipitate compared to DD13 WT chromatophores. Figure 5-7 shows the ultrastructure of ICM in *Rb sphaeroides* cells not expressing LH2 (DD13), expressing LH2 WT (DD13 WT) and expressing mutant LH2 ($\alpha\text{AL}_{4\text{S}}/\beta\text{AL}$) complexes. In the absence of LH2 complex, no ICMs invaginations are observed (figure 5-7A), while in the presence of LH2 proper ICM develop with vesicle-like invaginations ranging from 35 nm to 55 nm in diameter (figure 5-7B). The ultrastructure of the ICM of $\alpha\text{AL}_{4\text{S}}/\beta\text{AL}$ mutant is distinctively different from the ultrastructure of DD13 WT. The distribution in size and shape of the invaginated ICM in WT is similar to those reported previously for *Rb sphaeroides* 2.4.1 strain (i.e. photosynthetically grown $\text{LH2}^+ \text{LH1}^+ \text{RC}^+$) (Gibson, 1965; Fraker & Kaplan, 1972; Kiley & Kaplan, 1988; Feniouk *et al.*, 2002). In contrast, the ICM of $\alpha\text{AL}_{4\text{S}}/\beta\text{AL}$ mutant are more enlarged relative to the ICM vesicles of WT and are changed from normal vesicular to an abnormal tubular shape.

By using this system, it has been shown that in DD13 strain, no ICM are formed but once the LH2 is expressed (DD13 WT), mature vesicularised ICM are found. Furthermore, as obvious from the altered membrane morphology of $\alpha\text{AL}_{4\text{S}}/\beta\text{AL}$, LH2 structural stability and abundance is correlated with altered ICM size and morphology in the DD13 strain. Previously, it has been shown that *Rb sphaeroides* strain without LH2 and carotenoid but in the presence of LH1 and RC will result in the formation of tubular ICM (Kiley *et al.*, 1988). However, formation of tubular shapes has to the best of our knowledge not been observed before in the presence of LH2.

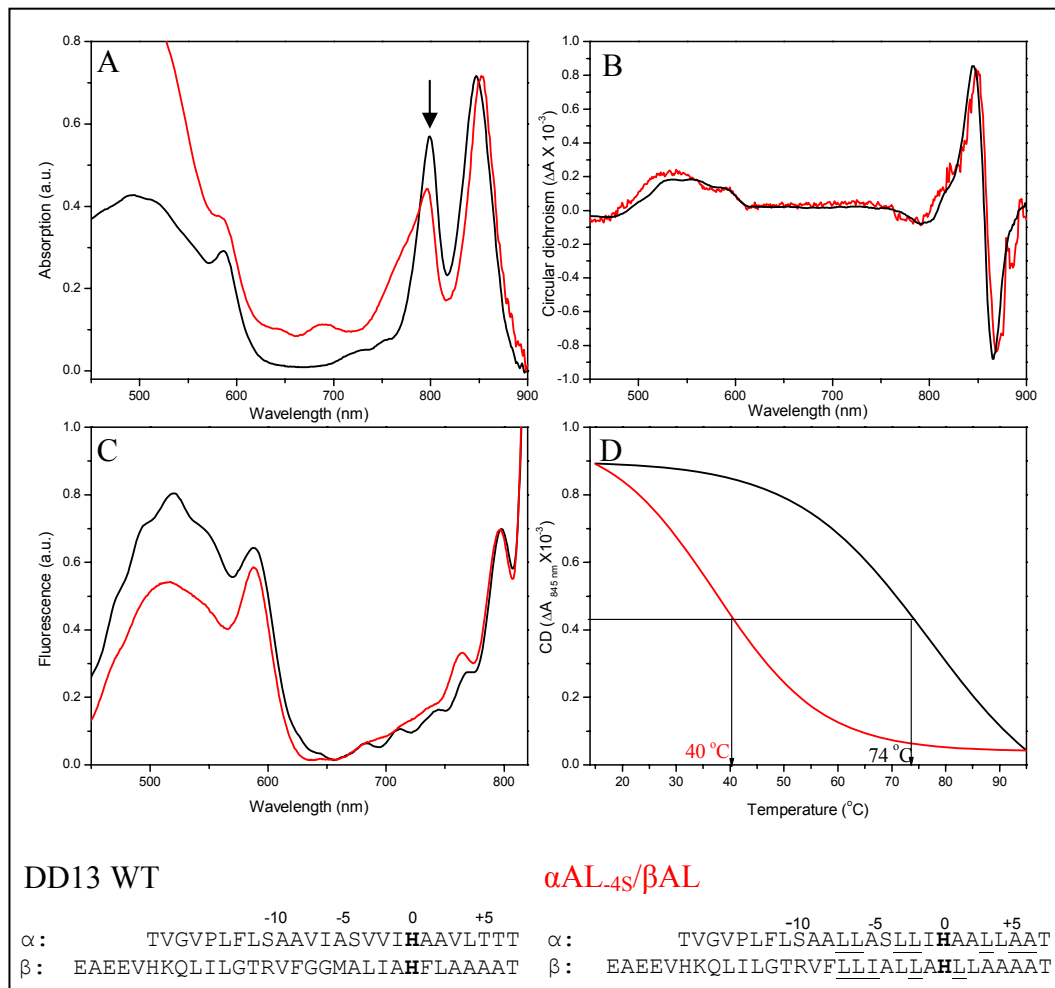


Figure 5-6: Functional assembly of DD13 WT (black line) and α AL_{4S}/ β AL (red line). A section of amino acid sequences from $\alpha\beta$ -polypeptides are shown with the altered residues underlined.

- (A) Absorption spectra. Spectra are normalised at 850 nm. Note, the retention of the BChl-B850 and -B800 absorption bands in α AL_{4S}/ β AL.
- (B) Circular dichroism spectra. Note the retention of the S-shaped signal of the red-most transition in α AL_{4S}/ β AL.
- (C) Fluorescence excitation spectra. The excitation bands at ~450 nm to ~550 nm arise from carotenoid, the band at ~595 nm arise from the Q_x transition of the BChl and the band at 800 nm arise from BChl-B800 ($\lambda_{em} = 870$ nm).
- (D) Thermal denaturation. Changes of the CD signal at 845 nm during heating of suspended LH2 membranes. The T_m values are indicated by arrows.

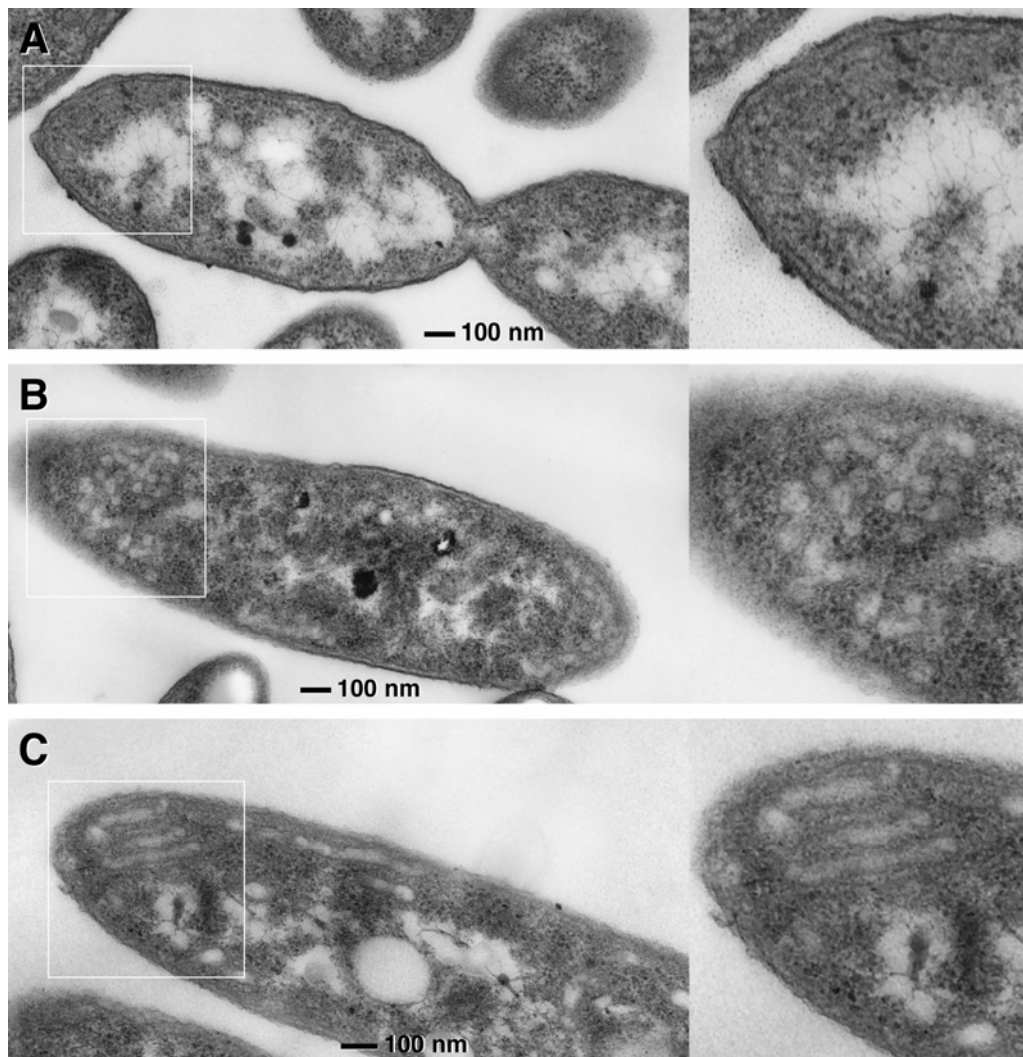


Figure 5-7: Comparison of the ultrastructure of *Rb sphaeroides* cells. (A) DD13 strain (LH2⁻ LH1⁻ RC⁻), (B) DD13 WT (LH2 WT⁺ LH1⁻ RC⁻) and (C) α AL_{4S}/ β AL mutant (LH2 mutant⁺ LH1⁻ RC⁻). Details for the comparison of chromatophores are shown at higher magnifications marked in framed.

PHOSPHOLIPID COMPOSITION OF RB SPHAEROIDES EXPRESSING LH2 WT AND MODEL LH2 α AL_{4S}/ β AL

The interplay between LH2 complex assembly and ICM morphology has been further addressed by studying the phospholipid composition in mutant and wild type membranes. The phospholipid compositions of WT and mutant were determined by thin layer chromatography (TLC). However, the TLC results did not allow efficient identification and quantification of the phospholipids (see appendix 3). Therefore, the electrospray ionisation mass spectrometry (ESI-MS) was used in collaboration with Drs. D. Wegmann and B. Brügger (University of Heidelberg, Germany) for the determination and quantification of phospholipid. At present, ESI-MS is one of the most applied techniques for quantitative studies of non-volatile lipids at low concentrations (Brügger *et al.*, 2000, 2004; Koivusalo *et al.*, 2001). The phospholipid composition of cellular (intact cells), isolated membrane (chromatophores) and isolated LH2 in β OG samples were determined and quantified by ESI-MS as described in Brügger *et al.*, 2000 (see chapter 2 for details, for all the raw data of ESI-MS measurements, see Appendix 4). In general, no major differences were observed between cellular and isolated membrane (data shown in appendix 4); a finding which is similar to those reported for *Rb sphaeroides* 2.4.1 (Russell & Harwood, 1979; Onishi & Niederman, 1982).

Phospholipid headgroup compositions

Table 5-1 shows the relative amounts of the three major phospholipids, PE, PC and PG, observed in *Rb sphaeroides* DD13, DD13 WT and α AL_{4S}/ β AL cells. PE is the most dominant phospholipids in all three samples. In DD13 and DD13 WT, PE contributes ~58 % and ~60 % of the total phospholipids respectively, whereas, it is reduced to ~53 % in DD13 α AL_{4S}/ β AL. The relative amount of PC is ~27 % in DD13 and is reduced to ~23 % in DD13 WT and rose to ~30 % in DD13 α AL_{4S}/ β AL. PG makes up less than 20 % in all three cases; ~15 % in DD13, ~16 % in DD13 WT and ~18 % in DD13 α AL_{4S}/ β AL.

Samples ^a	Percentage of phospholipid ^b			PC+PG/PE
	PC	PE	PG	
DD13 ^c	27.22	58.21	14.57	0.72
DD13 WT ^d	23.44	60.68	15.88	0.65
α AL _{4S} / β AL ^d	29.43	52.50	18.07	0.90

Table 5-1: Percentage of the major phospholipids (PC, PE and PG) in *Rb sphaeroides* DD13, DD13 WT and α AL_{4S}/ β AL.

- ^a The *Rb sphaeroides* are grown semi-aerobically in the dark at 28 °C. Cultures were harvested in their mid-logarithm phase when the absorbance at 650 nm reached 1.2 to 1.5. (DD13-24 hour; DD13 WT-28 hour; α AL_{4S}/ β AL-39 hour).
- ^b The 3 major phospholipids, PC, PE and PG of *Rb sphaeroides* cells are determined by ESI-MS, expressed here as percentage of their combined total (PC+PE+PG). Other minor phospholipids are below reliable detection levels by ESI-MS analysis.
- ^c The average values are derived from at least 2 measurements from 2 samples.
- ^d The average values are derived from at least 4 measurements from 3 samples.

Changes in the phospholipid compositions due to ICM development (as obvious from the composition of *Rb sphaeroides* cells expressing LH2 (DD13 WT) or lacking LH2 (DD13)) are that the relative amounts of major phospholipids PC dropped by ~14 % while PE and PG rose by ~4.2 % and ~9.0 % respectively. This results in a reduction of the bilayer to nonbilayer forming phospholipids ratio (PC+PG/PE) from 0.72 in DD13 to 0.65 in DD13 WT. The phospholipid composition of α AL_{4S}/ β AL mutant as compared to the composition of DD13 WT is dramatically changed. The relative amount of PE dropped by ~13.5 % while PC and PG rose by ~25.6 % and ~13.8 % respectively. The PC+PG/PE ratio is increased from 0.65 in DD13 WT to 0.90.

As mentioned in the introduction, PE tends to assume the H_{II} hexagonal phase and therefore supports local nonbilayer phase formation. Both membrane proteins (van den Brink-van der Laan *et al.*, 2004b) and bilayer forming phospholipid (Cullis & de Kruijff, 1979; Goldfine, 1984) are known to counter the nonbilayer tendency of PE. During ICM formation in DD13 WT, the PC+PG/PE ratio declined as LH2 is expressed. This may suggest that the requirement for bilayer phospholipids is reduced upon expression and assembly of LH2 during biogenesis of the ICM.

Possibly, the presence of the LH2 balances the rise in PE and thus maintains the fluidity of a nascent ICM invagination.

The change in the PC+PG/PE ratio in α AL_{-4S}/ β AL mutant is difficult to interpret as multiple events are taking place. The expression level of LH2-like complex and its structural stability are significantly reduced and is accompanied by a high level of membrane proteins and change of ICM shape. Perhaps, the abnormal LH2 α AL_{-4S}/ β AL is not able to counter the nonbilayer forming effects of PE; subsequently resulting in the higher bilayer phospholipid concentrations.

Phospholipid hydrocarbon chain compositions

In order to gain further information about the marked changes in lipid compositions, the phospholipid fatty-acyl in *Rb sphaeroides* expressing LH2 WT or α AL_{-4S}/ β AL are analysed for chain length and degree of saturation. In table 5-2, the relative amounts of different fatty-acyl chains of PE are presented. In all the three samples, the major fatty-acyl chain composition is 36:2 (> 60 %). As reported before, the relative amounts of unsaturated fatty-acid are usually high in bacterial cells (Kenyon, 1978). 36:2 likely represents two fatty-acids with C18 and two double bonds; these bonds are either in each chain (18:1, 18:1) or in one chain (18:0, 18:2) or any other combinations. Due to the constraint in the determination method, we are unable to resolve this further at this stage.

The relative amount of the PE phospholipid with acyl chain composition 36:2 is ~76 % in DD13 and ~79 % in DD13 WT. In general, the acyl-chains of the membrane lipids in *Rb sphaeroides* show only minor variations; neither the amount nor the degree of saturation varied significantly. Similarly, PC acyl-chains also consist primarily of 36:2 and are not altered upon expression of LH2 (data not shown here, see appendix 4). The PG fatty-acyl chains could not be detected with sufficient accuracy and can not be resolved further at this stage.

PE Fatty-acyl chain ^c	Percentage (%) ^b		
	DD13 ^d	DD13 WT ^e	α AL _{4S} / β AL ^e
29:0	-	-	1.41
30:0	0.42	-	3.20
31:0	-	-	1.91
32:1	0.19	0.12	1.17
32:0	0.25	0.36	1.74
33:1	0.20	-	3.07
34:2	2.61	2.40	1.88
34:1	7.10	5.45	8.14
34:0	0.61	0.46	1.23
35:1	0.42	0.27	0.67
36:2	76.44	79.15	60.50
36:1	10.25	9.79	12.32
37:2	0.64	0.78	1.04
Others	0.87	1.22	1.72

Table 5-2: PE fatty-acyl chain length composition in *Rb sphaeroides* DD13, DD13 WT and α AL_{4S}/ β AL^a. Data are derived from m/z spectra (mass to elementary charge ratio) measured by ESI-MS (see chapter 2 for details). The most abundant (36:2) is shown in bold.

^a The *Rb sphaeroides* are grown semi-aerobically in the dark at 28 °C (see table 5-1).

^b Values are percentage of total fatty-acyl chains of PE.

^c The number of carbon atoms (X) and the number of double bonds between carbons (Y) of the fatty-acyl chains is termed (X: Y).

^d The average values are derived from 4 measurements from 2 samples.

^e The average values are derived from 6 measurements from 3 samples.

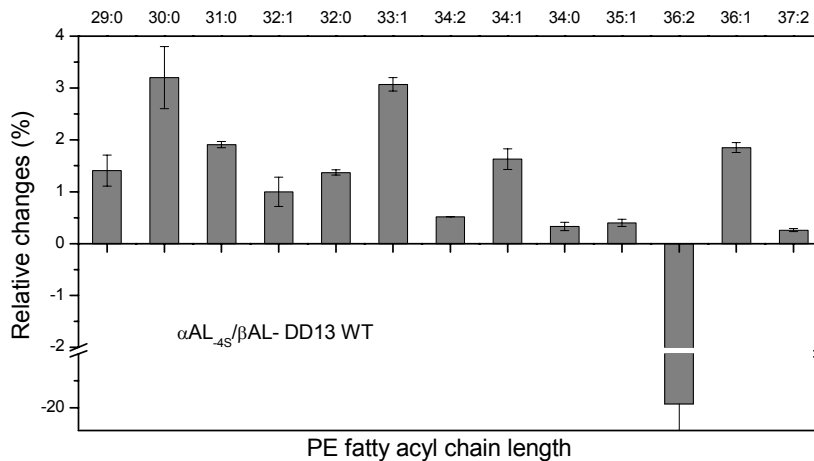


Figure 5-8: Relative changes in percentage of fatty acids in PE of α AL/ β AL_{4S} and DD13 WT. The differences between fatty acids (% PE α AL/ β AL_{4S} – % PE DD13 WT) are shown. Note, the significant decrease (≥ 20 %) in 36:2 and increase in shorter, more saturated phospholipids.

On the other hand, the hydrocarbon composition of the membrane lipids in α AL_{4S}/ β AL changes significantly in comparison to DD13 WT. The major PE acyl-chain 36:2 is reduced from ~79 % in DD13 WT to ~61 %. Concurrently, shorter fatty-acid chains such as 29:0, 30:0, 31:0, 32:1, 32:0 and 33:1 are increased. In both DD13 and DD13 WT, these shorter acyl-chain compositions were either untraceable and/or present in only scarce amounts (table 5-2). The differences in phospholipid content of DD13 WT and DD13 α AL_{4S}/ β AL is shown in figure 5-9. Interestingly, the hydrocarbon composition of PC in DD13 WT and DD13 α AL_{4S}/ β AL show only minor variations (result is discussed with table 5-9).

These results show that the changes in morphology of the ICM are accompanied by the changes in the phospholipid compositions. The relative content of bilayer lipids is increased as well as the content of shorter fatty-acyl chain length in these lipids. This concurs with the more planar morphology of the ICM in α AL_{4S}/ β AL. Both the ratio of bilayer/nonbilayer lipid and fatty-acid chain length have been implied to partake in the regulation of membrane curvature energy (e.g. Wieslander *et al.*, 1980; van den Brink-van der Laan *et al.*, 2004b).

The results so far can be summarised as follow: (1) LH2 protein governs ICM invagination and maturation independent of LH1 and RC complexes. (2) Alteration in LH2 structural stability and expression level in α AL_{4S}/ β AL mutant are reflected in the observed changes in ICM morphology. (3) The ICM of *Rb sphaeroides* contain as major lipids, in descending order; PE, PC and PG. (4) The unsaturated hydrocarbon 36:2 is the most abundant form of acyl-chain present in all samples. (5) Upon the expression of LH2, and ICMs formation, the bilayer to nonbilayer-lipid ratio (PC+PG/PE) is reduced. (6) Mutant α AL_{4S}/ β AL expression results in a rise in PC+PG/PE ratio, and is accompanied by tubular ICM formation. (7) No changes in PC and PE hydrocarbon compositions were observed during normal ICM formation. (8) The PE hydrocarbon chain volume in mutant α AL_{4S}/ β AL ICM is reduced (shorter chains and more saturation) while the PC hydrocarbon chains are unchanged.

The significance of these results will be discussed in chapter 6. In essence, the results suggest a close inter-relationship between LH2 protein, membrane

composition and membrane morphology. In the following, specific interactions between the LH2 proteins and the membrane lipids are examined.

PHOSPHOLIPID COMPOSITION OF RB SPHAEROIDES LH2 WT DEPENDING ON TEMPERATURE

Phospholipid headgroup compositions

Membrane lipid composition is known to change in response to temperature changes (Goldfine, 1984; Lee, 2003). To know how the lipid composition is modulated in *Rb sphaeroides* DD13 by temperature variation, the correlation between phospholipid composition and growth temperature were examined. The temperature range used here corresponds to the growth temperature used in this chapter. In this experiment, WT *Rb sphaeroides* cells were grown at four different temperatures; 28 °C, 30 °C, 32 °C and 34 °C. The cells were harvested during their mid-logarithm phase when the $A_{650\text{ nm}}$ reached between 1.2 and 1.5. The phospholipid composition is compared across the range of temperatures (for raw data, see appendix 4). Figure 5-9 shows the percentage of major phospholipids in DD13 WT cells, grown at 28 °C and 34 °C. Interestingly, the relative content of the three major phospholipids; PE, PC and PG are nearly identical within these temperatures range. The differences between the compositions at different temperatures are negligible and comparable to the deviation observed between different batches grown at a particular temperature.

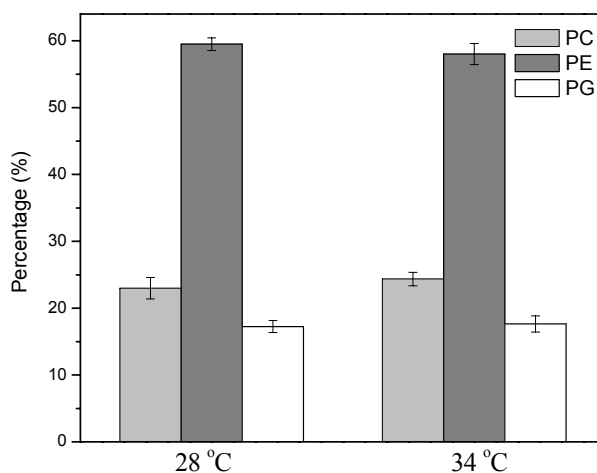


Figure 5-9: Comparison of phospholipid composition in *Rb sphaeroides* cells containing LH2 WT at different growth temperature. All data represent the average of two measurements from one sample. The percentage of individual phospholipids is derived from the total percentage of phospholipids (PC+PE+PG).

Phospholipid hydrocarbon chain compositions

The hydrocarbon chain compositions at different temperatures are shown in figure 5-10. The figure shows the fatty-acyl chain lengths of PC and PE at four different growth temperatures. PG values are below reliable detection level. The major fatty-acid chain of both PC and PE is 36:2 (see appendix 4), this acyl-chain accounts for more than 70 % of the total acyl-chains. This 36:2 phospholipid in PC and PE falls by ~6 % and ~10 % respectively when the temperature is increased. Concurrently, the concentration of other unsaturated acyl-chains (i.e. 34:2 and 37:2) changes marginally. On the other hand, monounsaturated phospholipids 34:1 and 36:1 of PE and PC increase significantly with increasing temperature. In summary, the proportion of PE, PC and PG does not alter within the temperature range, 28-34 °C; however, the chain length and degree of saturation of these phospholipids are systematically altered. It appears that the membrane fluidity is maintained by adjusting the chain length and degree of saturation of phospholipids even within this small temperature range.

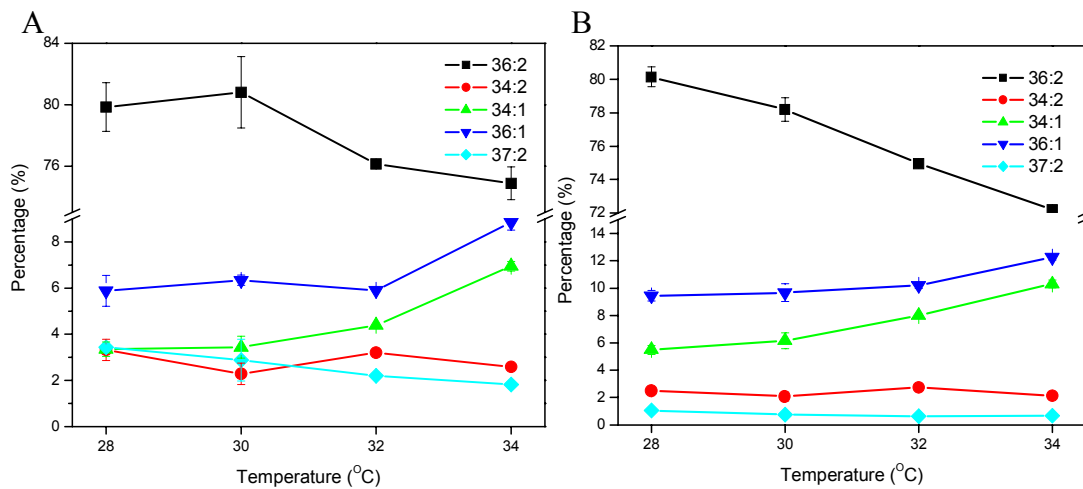


Figure 5-10: Changes in fatty-acyl compositions of (A) PC and (B) PE in WT *Rb sphaeroides* as a function of temperature. Bacteria are cultivated at 28 °C, 30 °C, 32 °C and 34 °C. The fatty-acid chain length and saturation are shown in different colours. 36:2 black lines, 34:2 red lines, 34:1 green lines, 36:1 blue lines and 37:2 light blue lines.

Previous works (e.g. Kaplan *et al.*, 1983; Goldfine, 1984), suggested that the phospholipid composition in *Rb sphaeroides* changes only when the temperature fluctuates by more than 15 °C. Here, the relative amounts of PE, PC and PG fluctuate very little within the temperatures range used in the experiments (28 to 34 °C). However, changes were observed in their acyl-chain lengths and degree of saturations; these changes were detected when temperature fluctuates by more than 2 °C. Therefore, we used the temperature range between 28 to 30 °C as growth temperature throughout this chapter for meaningful comparison.

*PHOSPHOLIPID COMPOSITION OF ISOLATED LH2 COMPLEX**Phospholipid headgroup compositions*

PE, PC and PG are the three major phospholipids present in *Rb sphaeroides* cells. In order to examine the population of lipids interacting closely with the LH2 complex, WT LH2 is purified from the membrane and the lipids which remain associated with this purified LH2 are analysed by ESI-MS. This idea has been used previously to explore the boundary layer of lipids surrounding membrane proteins (Russell *et al.*, 2002; Lee, 2003, 2004; Dekker & Boekema, 2005).

Table 5-3 shows the relative content of the major phospholipids of *Rb sphaeroides* DD13 containing LH2 WT in intact cells and in detergent. In isolated LH2, both PE and PC are found to be associated with the LH2 protein after detergent treatment. Obviously, the relative amount of phospholipids detected in the isolated LH2 complex is much lower than of cell samples, as most of the lipids have been removed during the isolation procedure. Nearly 88 % of the lipids identified in the isolated LH2 are PE molecules. Only ~12 % are PC whereas PG is not detected in isolated LH2.

Samples ^a	Phospholipid composition ^b		
	PC	PE	PG
DD13 WT ^c	23.44	60.68	15.88
Isolated LH2 ^{c,d}	12.28	87.72	n.d.

Table 5-3: Phospholipid composition of *Rb sphaeroides* isolated LH2 WT and of DD13 WT cells.

^a The *Rb sphaeroides* samples are grown semi-aerobically in the dark. The cultures were harvested in the mid-logarithm phase when the absorbance at 650 nm reached 1.2 to 1.5. (WT-28 °C 28 hour; isolated LH2-30 °C 43 hour).

^b The 3 major phospholipids, PC, PE and PG of *Rb sphaeroides* cells are determined by ESI-MS, presented here as percentage of their combined total (PC+PE+PG). Other minor phospholipids are below reliable detection level of the MS analysis.

^c The average values are derived from 6 measurements from 3 samples.

^d Isolated LH2 are purified by β OG as described in Walz *et al.*, (1998). PG values are below reliable detection level (n.d. = not detected).

In a recent work by Russell *et al.* (2002), no PG phospholipid but predominantly PE (43.3 ± 2.8 %) and PC (42.3 ± 5.6 %) were found in purified LH2 from *Rps acidophila* grown anaerobically in high light intensity. This is consistent with our results that no PG is found in close association with LH2 protein. However, the relative amount of the PE and PC lipids identified in isolated LH2 are different, and may reflect the distinct differences in the LH2-protein-lipid interactions in these two species. Interestingly, the ICM in *Rps acidophila* have flattened membrane sacks and hence distinct from the vesicularised ICM in *Rb sphaeroides* (Sturgis & Niederman, 1996). It should also be kept in mind that there are significant differences in the conditions of cultivation and purification methods. Comparison of the two systems should thus be treated with some caution. In addition, the high selectivity of PE may not be so pronounced in the *Rb sphaeroides* 2.4.1 strain with LH2, LH1 and RC. The PC/PE ratio in *Rb sphaeroides* 2.4.1 cells grown photoheterotrophically is close to 1; thus the relative PE content is somehow reduced as compared to the content in the LH2 only strains. Nevertheless, the relatively high amount of PE identified in isolated LH2 suggests that PE is preferably accumulated around LH2 complex and that PE is enriched at the LH2-protein-lipid interface in *Rb sphaeroides* DD13 strains.

Phospholipid hydrocarbon chain compositions

In order to determine whether a particular acyl-chain is favoured in the boundary lipids of LH2, the hydrocarbon compositions of isolated LH2 are analysed (table 5-4 and table 5-5). Table 5-4 shows the fatty-acyl chain length and saturation of PE present in DD13 WT cellular membranes and in isolated LH2 WT. The predominant PE fatty-acyl chain, 36:2, is reduced from ~79 % in DD13 WT cells to ~59 % in the boundary lipids. On the other hand, acyl-chains 34:1, 34:0, 36:1 and 37:2 are increased. In figure 5-11, the differences are shown between phospholipids in membrane and purified LH2. Curiously, the hydrocarbon composition of PC in isolated LH2 is different from those of intact cells. Similarly, the major hydrocarbon composition of PE, 36:2 is reduced from 80 % to 62.5 %. Thus, there is a reduction in the relative content of the major phospholipids' acyl chain, 36:2, from ~80 % in

cells to ~59 % in the isolated LH2. Previous study has shown that the acyl chain 18:1 is the predominant one (59.1 %) in isolated LH2 of *Rps acidophila* (Russell *et al.*, 2002).

PE Fatty-acyl chain	Percentage (%) ^b	
	DD13 WT ^c	Isolated LH2 ^c
32:1	0.12	-
32:0	0.36	1.89
34:2	2.40	1.83
34:1	5.45	7.79
34:0	0.46	3.41
35:1	0.27	1.34
36:0	0.42	2.14
36:2	79.15	59.03
36:1	9.79	12.69
37:2	0.78	3.72
38:1	0.05	1.33
Others	0.75	4.82

Table 5-4: PE fatty-acyl chain length composition of *Rb sphaeroides* DD13 WT in bacterial cells and in isolated LH2^a.

^a Samples were cultivated as described in Table 5-3.

^b Values are percentage of total fatty-acyl chains of PE in bacterial cells and isolated LH2. The fatty-acyl chains are presented as described previously.

^c The average values are derived from at least 4 measurements from 3 samples.

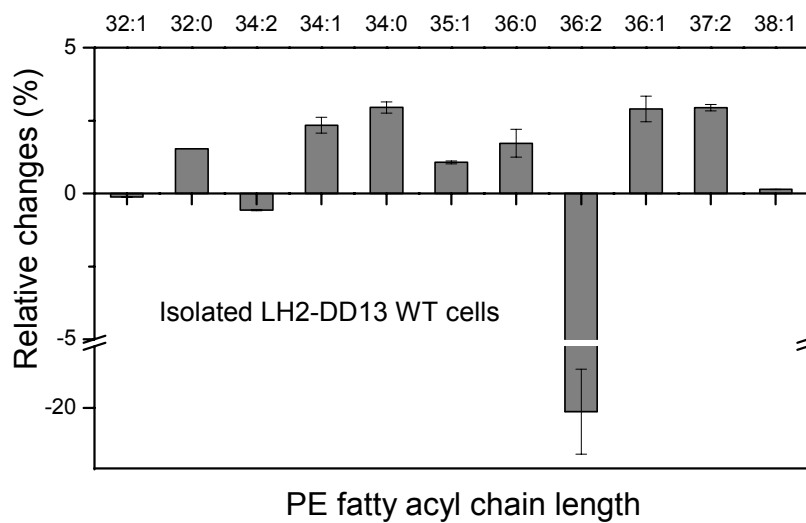


Figure 5-11: Relative changes in percentage of fatty acids in PE of isolated LH2 and DD13 WT cells. The differences between fatty acids (% PE isolated LH2 – % PE DD13 WT cells) are shown. Note, the significant decrease ($\geq 20\%$) in 36:2 fatty-acyl-chain.

PC Fatty-acyl chain	Percentage (%) ^b	
	DD13 WT ^c	Isolated LH2 ^d
34:2	2.78	5.00
34:1	3.91	6.36
35:1	0.25	2.90
36:1	6.37	11.63
36:2	80.05	62.49
36:0	0.28	1.52
37:2	2.82	6.60
37:1	2.30	1.21
38:2	0.43	1.09
Others	0.81	1.20

Table 5-5: PC fatty-acyl chain length composition of *Rb sphaeroides* DD13 WT in bacterial cells and isolated LH2^a.

^a Samples were cultivated as described in Table 5-3.

^b Values are percentage of total fatty-acyl chains of PC in bacterial cells and isolated LH2. The fatty-acyl chains are presented as described previously.

^c The average values are derived from at least 5 measurements from 3 samples.

^d The average values are derived from at least 3 measurements from 3 samples.

Taken together, these results suggest that (1) PE and PC are closely associated with LH2 proteins whereas no PG is detected and (2) the relative PE and PC proportions and the hydrocarbon compositions of the LH2 boundary lipids are different from the bulk lipids. This preferential accumulation of phospholipids, predominantly PE around LH2 protein suggests that LH2 protein selectively accumulate distinct lipids at the protein/lipid interface. In the following sections, the molecular factors for accumulation of PE in the close vicinity of LH2 are examined.

STUDY OF THE MOLECULAR INTERACTIONS BETWEEN LH2 COMPLEX AND PE

In α AL_{-4S}/ β AL, the mutant LH2 complex is structurally impaired and is present at reduced levels in the membrane (figure 5-6). Concurrently, the relative PE content in the membranes is reduced and the membrane morphology is severely altered (figure 5-7). These findings suggest the possibility of altered protein-lipid interactions. In order to further understand these interactions at a molecular level, the LH-protein-lipid interactions are examined in detail by site-directed mutagenesis of residues located at potential protein-lipid interfaces. The aim here is to alter putative LH2 protein-lipid interaction sites without significantly impairing the assembly and function of LH2.

In LH2 α - and β -polypeptides, relatively few residues are found to be highly conserved (Zuber, 1985; Braun *et al.*, 2002). Only the residue histidine at position 0 and residues at position -4 are noted to be strictly conserved. Conspicuously, the residue glutamate (Glu) at position -20 at the N-terminal domain of the β -subunit is also found to be strictly conserved even when the β -sequences are aligned for LH1 and LH2 complexes. Furthermore, Glu -20 is found even in the β -subunits from relatively remote genii, such as *Erythrobacter* and *Chromatium* (figure 5-12), pointing possibly towards a critical role of this residue.

Wild type β -sequences:

		-20	-10	-5	0	+5	
RHOSH	LH2 [P0C0Y2]	<u>LTVAEAEAE</u>	<u>EV</u>	<u>HKQL</u>	<u>ILGTRV</u>	<u>FGGMALIAHFLAAAA</u>	<u>TPWLG</u>
RHOAC	LH2 [P26790]	LTAEQSE	<u>EL</u>	LHKYVIDG	TRVFLGLALVAH	FLAFS	SATPWLH
RHOSU	LH2 [P95654]	LTAEAE	<u>EV</u>	HKQLIDG	TRVFGAIALFAH	FLAAI	AATPWLG
RHOCA	LH2 [P07368]	LSLKEAE	<u>EI</u>	HSYLIDG	TRVFGAMALVAH	ILSAI	AATPWLG
RHOPA	LH2 [P35107]	LTIAESE	<u>EL</u>	LHKHVIDG	TRIFGAIAIVA	HFLAY	VVSPWLH
RHOGE	LH2 [P72281]	LTAEAE	<u>EL</u>	QKGLVDG	TRVFGVIAVLAH	ILAYAY	TPWLH
RHOVI	LH2 [P04124]	LTEEEAK	<u>EF</u>	HGIFVT	STVLYLATAVIV	HYL	VWTARPWIA
RHOTE	LH2 [P80587]	LTVAEAE	<u>EL</u>	LHTYVTNG	FRVFGI	AVVAH	VLVFAAHPWGR
RHOMO	LH1 [Q9R4K4]	LSESEAQ	<u>EF</u>	HGIFVTS	SFISFIVVAIVA	HFLAW	KWRPWL
RHOCA	LH1 [P02950]	LTDEQAQ	<u>EL</u>	HAVYMSGL	SAFI	AVAVLAH	LAVMIWRPWF
RHOSH	LH1 [Q0C0YE]	LTDEQAQ	<u>EL</u>	HSVYMSGL	WPFSAVAIVA	H	LAVYIWRPWF
RHOPA	LH1 [Q6N9L5]	LSEAEAK	<u>EF</u>	HSIFVTS	SFFLFIVVAVVA	HILAW	MWRPWL
RHOGE	LH1 [P51757]	LTDEQAQ	<u>EF</u>	HKFWVQGF	VGFTAVAVVA	HFLV	VVWRPWL
RHORU	LH1 [P04125]	ITEGEAK	<u>EF</u>	HKI	FTSSILVFFG	VAAFAH	LLVWIWRPWP
RHOSU	LH1 [Q9WXD9]	LTDEQAQ	<u>EI</u>	HAVYMSGL	WLFSAVAVLAH	LAVYI	WRPWL
RHOAC	LH1 [P35099]	VSDAEAK	<u>EF</u>	HALFVSS	FIAFIVIAVLAH	VLA	WAWRPWI
RHOSH	LH1 [P0C0Y1]	LTDEQAQ	<u>EL</u>	HSVYMSGL	WPFSAVAIVA	H	LALVYIWRPWF
RHOMA	LH1 [P80260]	LTEGEAR	<u>EF</u>	HGVFMTS	SFMVFI	AVAVVAH	ILAWMWRPWI
CHRVI	LH1 [O82948]	LTEDEAR	<u>EF</u>	HGIFVSS	FVVFTGIVVVA	HILV	WLWRPWL
ERYLO	LH1 [Q9KWI6]	LTDEEAK	<u>EI</u>	HGAFMGT	FGLYVGI	AVVAH	ILLVWNKRWLP
RHOAC	LH3 [P35095]	LTADQAE	<u>EL</u>	LHKYVIDG	ARAFVAIAAFAH	FLAYS	LTPWLH

RHOSH: *Rhodobacter sphaeroides*; RHOAC: *Rhodopseudomonas acidophila*; RHOMO: *Rhodospirillum molischianum*; RHOTE: *Rhodocyclus tenuis*; RHOMA: *Rhodopseudomonas marina*; CHRVI: *Chromatium vinosum*; RHOSU: *Rhodobacter sulfidophilus*; RHOCA: *Rhodobacter capsulatus*; RHOPA: *Rhodopseudomonas palustris*; RHOGE: *Rhodobacter gelatinus*; RHOVI: *Rhodobacter viridis*; ERYLO: *Erythrobacter longus*.

Figure 5-12: Alignment of β -subunits of LH1, LH2 and LH3. The central histidine (H) which is ligated to the Mg^{2+} atom is positioned at 0 and shown in bold. The glutamate -20 are shown in bold and underlined. Expsy sequence search codes are shown in square brackets. [www.expsy.org]

The high-resolution structure of LH2 from *Rps acidophila* (McDermott *et al.*, 1985; Papiz *et al.*, 2003) shows that β Glu -20 is neither in close contact with BChls pigments nor residues from neighbouring subunits. It is facing outwards from the pigment binding pocket and is likely to be in close contact with surrounding lipid membrane. LH2 complex is a transmembrane hollow cylinder of ~ 7 nm in diameter and ~ 4 nm in height (McDermott *et al.*, 1995, chapter 1 figure 1-4). The height of LH2 is similar to the bilayer thickness (~ 3 nm); in reconstituted PC liposome, the LH2 complex appears to have an asymmetrical arrangement (Stamouli *et al.*, 2003). Based on atomic force microscopy, it suggests that the LH2 complex extends by 1.0 nm from the lipid bilayer on the cytoplasmic side and 0.2 nm from the periplasmic side (Stamouli *et al.*, 2003). β Glu -20 is located at the second turn of the β -helices at

the cytoplasmic end. Each turn of the helix rises by 1.5 Å, thus $\beta\text{Glu -20}$ can potentially interact with the surrounding lipid headgroups on the cytoplasmic side as it has a fairly long side chain (~ 6.8 Å) (figure 5-13). Finally, the cytoplasmic side of the LH2 complex has a net negative charge (Stamouli *et al.*, 2003). The negative charged and the H-bonding potential of its carboxyl side chain might contribute to the selective interactions of $\beta\text{Glu -20}$ with the polar headgroups of phospholipids like PE.

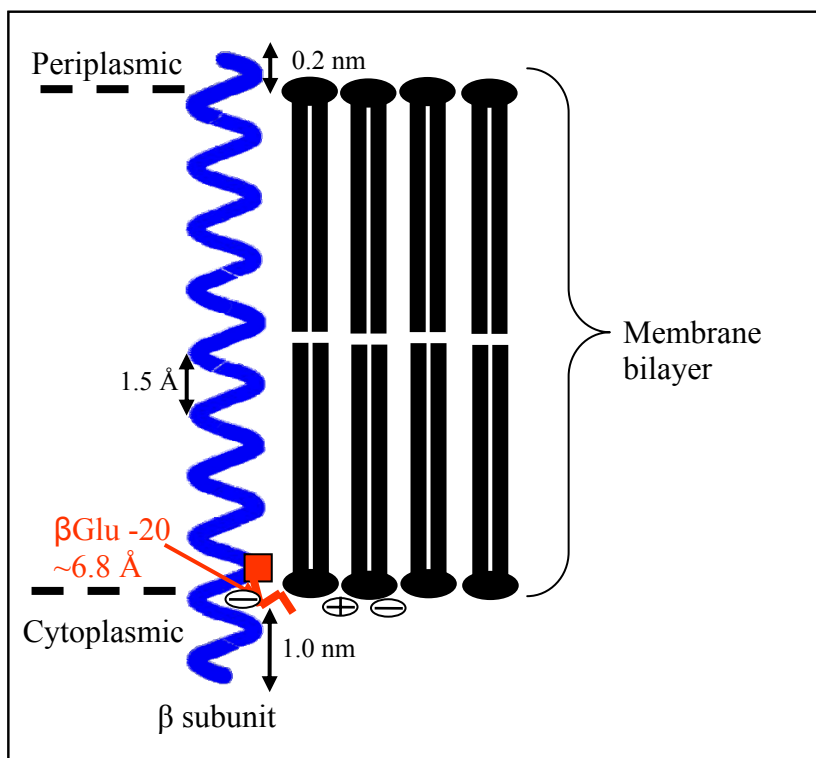


Figure 5-13: Schematic illustration of the location of the residue glutamate at position -20 of β -subunit and its surrounding lipid environment. The $\beta\text{Glu -20}$ at the cytoplasmic membrane is shown in red. Its side chain is approximately 6.8 Å and may interact with the surrounding lipid headgroup. For details, see the text.

There are three individual findings supporting the involvement of PE in this putative protein-lipid interface. Firstly, PE was suggested by Cain *et al.*, (1981) and Marinetti & Cattieu (1981) to be selectively accumulated on the cytoplasmic face of the ICM. The fully protonated ammonium group of PE is ideally suited to interact with the negatively charged cytoplasmic terminus of LH2. Secondly, PE headgroup has the capability of forming electrostatic- or hydrogen-bonds with the side chains of amino

acid residues, a property not shared with PC. Finally, from our previous findings, PE is the most abundant phospholipid found in close proximity with LH2 protein. This selective enrichment suggests that specific interactions take place between LH2 protein and PE. The residue β Glu -20 may be a good candidate for the study of this interaction.

Modelling of a potential PE binding site in close proximity of β Glu -20 is based on the high resolution structure of *Rps acidophila* (McDermott *et al.*, 1995). Figure 5-13 shows a potential LH2-protein-lipid interface. As obvious from this model, the carotenoid (spheroidenone) moiety, in particular its polar group may be in close proximity of this site. Therefore, these two moieties (β Glu -20 and carotenoid) may form a putative lipid-binding cleft (figure 5-14). In order to investigate this further, three approaches have been taken. Firstly, the residue β Glu -20 is mutated; in particular, the charge, volume and hydrophobicity of its side chain are altered. Secondly, LH2 complex is expressed in the DG2 strain with neurosporene as the dominant carotenoid which lacks of any polar groups (see chapter 1). Finally, both the residue β Glu -20 and carotenoid will be altered in combination.

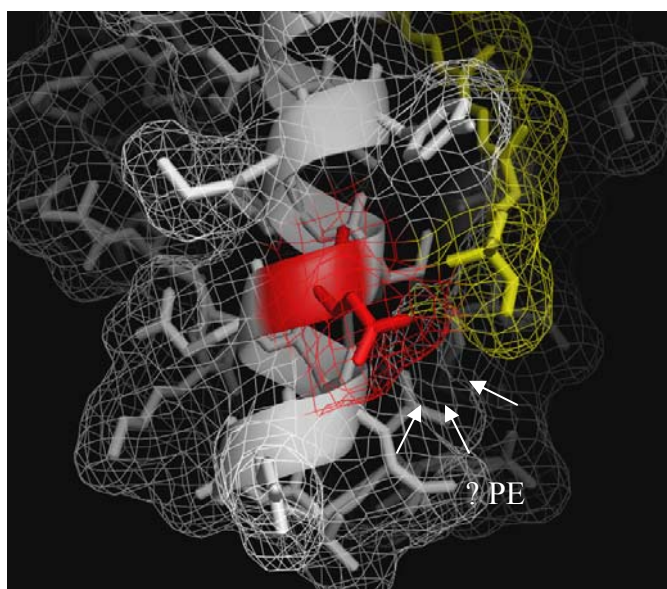


Figure 5-14: Illustration of LH2 protein-lipid interface. The residue -20 glutamate (red) and carotenoid, spheroidenone (yellow) are located at the lipid-protein boundary. A cleft is present (indicated by arrows), where a potential boundary lipid-protein interaction can occur. The figure is modelled in PyMol Viewer version 0.98 (DeLano Scientific LLC, South San Francisco, California, USA).

Point mutation of β Glu -20: Effects on LH2 protein

In order to alter any putative interactions with surrounding lipids, the side chain of β Glu -20 was changed; β Glu -20 was replaced with glutamine (Gln), alanine (Ala) and lysine (Lys). Thereby, the charged carboxyl group is replaced either by the polar amino and carbonyl groups of Gln or by the imino (NH) group of Lys, both which are capable of hydrogen-bonding. Naturally, Lys is positively charged while Ala has neither a charged nor a polar group.

The spectral properties of LH2 mutants, α WT/ β WT-_{20Q}, α WT/ β WT-_{20A} and α WT/ β WT-_{20K} are shown in figure 5-15. No significant changes are observed in these spectra (except for the increased absorbance in the blue region of α WT/ β WT-_{20K}, which indicates a high scattering, see chapter 3), indicating that the fully assembled LH2 complex is not affected by the replacement of β Glu -20 with Gln, Ala or Lys.

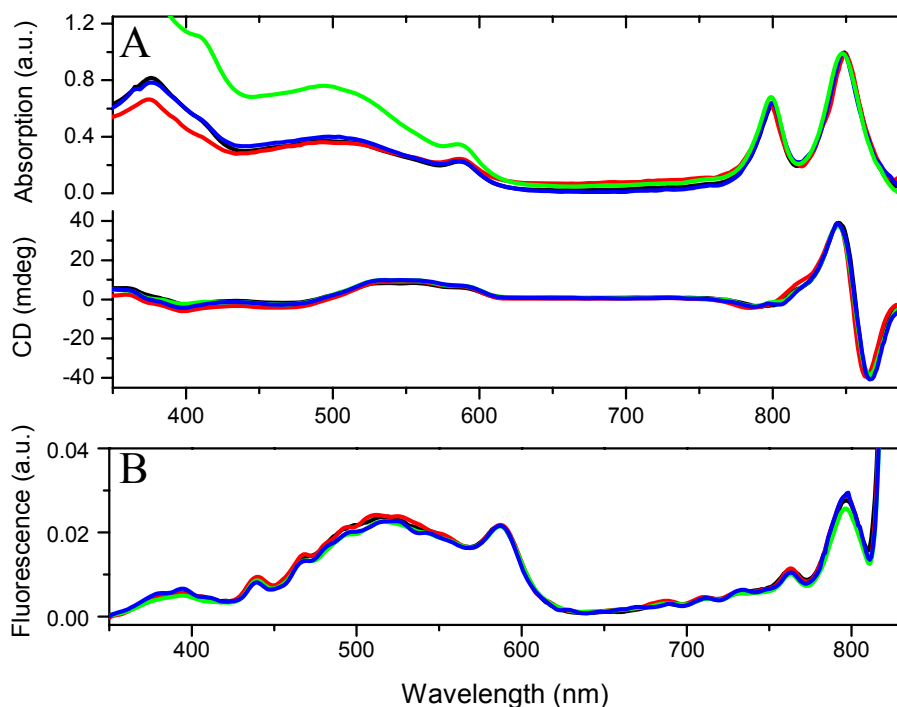


Figure 5-15: Absorption, CD and fluorescence excitation spectra of LH2 WT (black line), α WT/ β WT-_{20Q} (red line), α WT/ β WT-_{20K} (green line) and α WT/ β WT-_{20A} (blue line).

- (A) Upper panel: absorption spectra. Spectra are normalised at 850 nm. Lower panel: circular dichroism spectra. Spectra are normalised at the (+) maxima at ~843 nm.
 (B) Fluorescence excitation spectra. Spectra are normalised at ~590 nm.

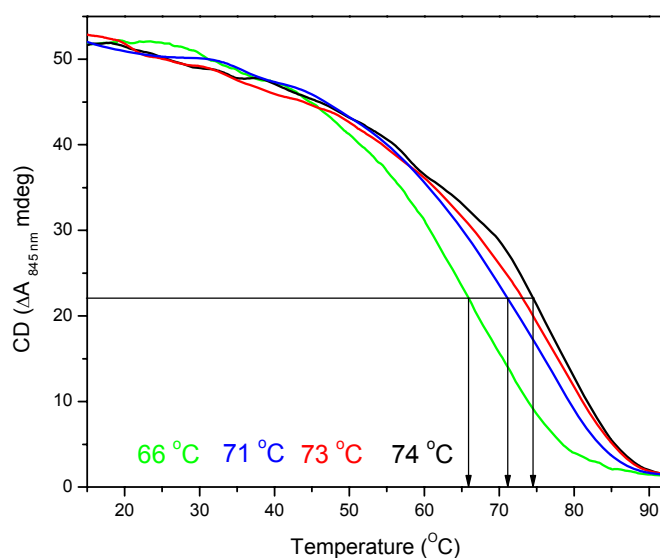


Figure 5-16: Thermal denaturation of LH2 WT (black line), α WT/ β WT_{-20Q} (red line), α WT/ β WT_{-20K} (green line) and α WT/ β WT_{-20A} (blue line). The changes are monitored using the CD signal at 845 nm during the constant heating of LH2 membranes in DD13 strains. The T_m values are indicated by arrows and their values are shown in the corresponding colours. The heating rate is 2 °C per min. Signals are normalised at the starting temperature of 15 °C.

The thermal stability of LH2 mutant α WT/ β WT_{-20Q}, α WT/ β WT_{-20A} and α WT/ β WT_{-20K} is assessed by heat denaturation (figure 5-16). As shown in figure 5-16, the T_m values of WT and α WT/ β WT_{-20Q} are nearly identical and the reduction in the T_m of α WT/ β WT_{-20A} is relatively minor (~3 °C). Thermal destabilisation is found in α WT/ β WT_{-20K} mutant (T_m shift ~8 °C). These findings suggest that in spite of the strict conservation of β Glu -20 residue among many different species (figure 5-12), the particular side chain of glutamate appears not to be critical for either the structural or functional assembly of LH2 protein.

Modification of carotenoid's polar group and/or β Glu -20: Effects on LH2 protein

Based on the high-resolution structure of *Rps acidophila* (McDermott *et al.*, 1995), it is apparent that β Glu -20 has many close contacts (≤ 5 Å distance) with the carotenoid molecule, rhodopin glucoside, particularly the polar headgroup of the glucoside moiety (figure 5-17A). In figure 5-17B, the carotenoid rhodopin glucoside has been modified to spheroidenone (which is the carotenoid present in *Rb sphaeroides* grown semi-aerobically) (Fraker & Kaplan, 1972; Kaplan *et al.*, 1983) by molecular modelling (see chapter 2). Both rhodopin glucoside and spheroidenone are structurally very similar, except for their headgroup moieties. The polyene backbone is identical except for an additional double bond. The headgroup in spheroidenone is the methoxy group and keto group, while in rhodopin glucoside it is a glucoside moiety (figure 5-18).

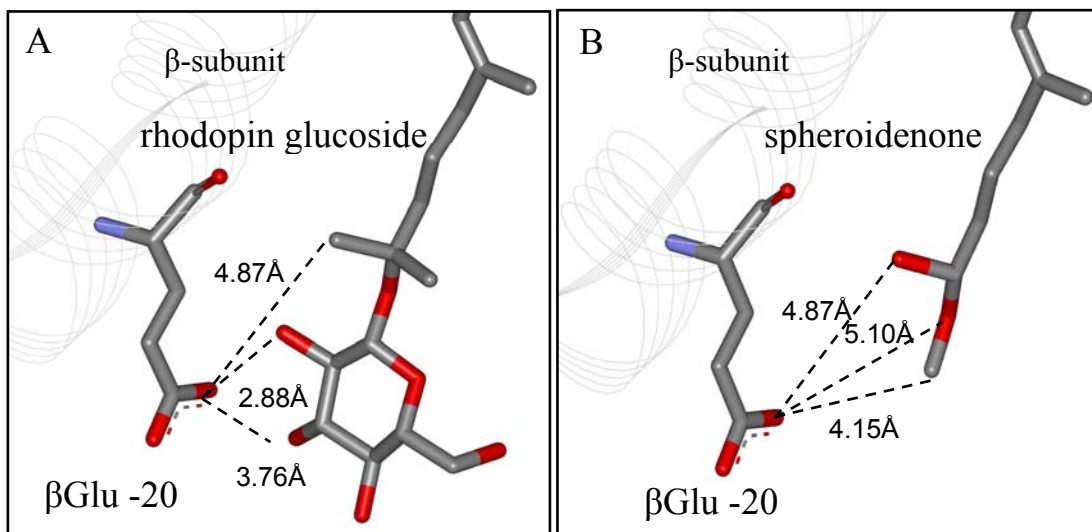


Figure 5-17: Modelling of the interactions of β Glu -20 with carotenoid in LH2 complex. (A) Rhodopin glucoside in *Rps acidophila*. (B) Spheroidenone in *Rb sphaeroides*. Note that β Glu -20 has multiple interactions with the carotenoid, in particular to the glucoside moiety.

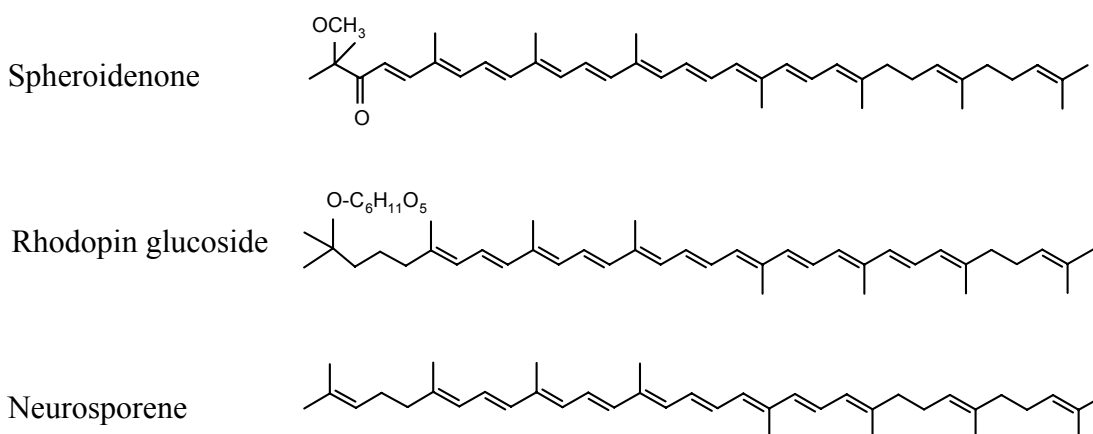


Figure 5-18: Chemical structures of carotenoids used in the study.

The *Rb sphaeroides* mutant strain, DG2 (see chapter 1) is defective in carotenoid biosynthesis and has as major carotenoid the biosynthetic precursor neurosporene (figure 5-18, figure 1-7). It is formed by a mutation in the *crtC* gene in the carotenoid synthesis pathway. The removal of this gene prevents the bacteria from completing the synthesis of the normal end product, spheroidenone, and neurosporene accumulates (Hunter *et al.*, 1997). Neurosporene lacks any polar group and thus DG2 *Rb sphaeroides* strain may be used to study the contribution of this group to the putative LH2 lipid-binding site. Subsequently, we studied the effects of altering both the carotenoid and β Glu -20 moieties on the functional assembly of LH2 by expressing the -20 mutants in DG2 strains which contain neurosporene carotenoid. In spite of this additional change, no significant alterations are observed in functional assembly of the mutant complexes (figure 5-19). Some minor modifications are observed in the energy transfer in comparison to DG2 WT characteristics. The energy transfer from carotenoid to BChls is slightly reduced, particularly, in DG2 α WT/ β WT_{.20K} and there are slight alterations in the shape of the excitation spectra, observed in carotenoid, which currently we have no explanation for (figure 5-19B). It may be due to interference from scattering as seen in the absorption spectra (figure 5-19A upper panel).

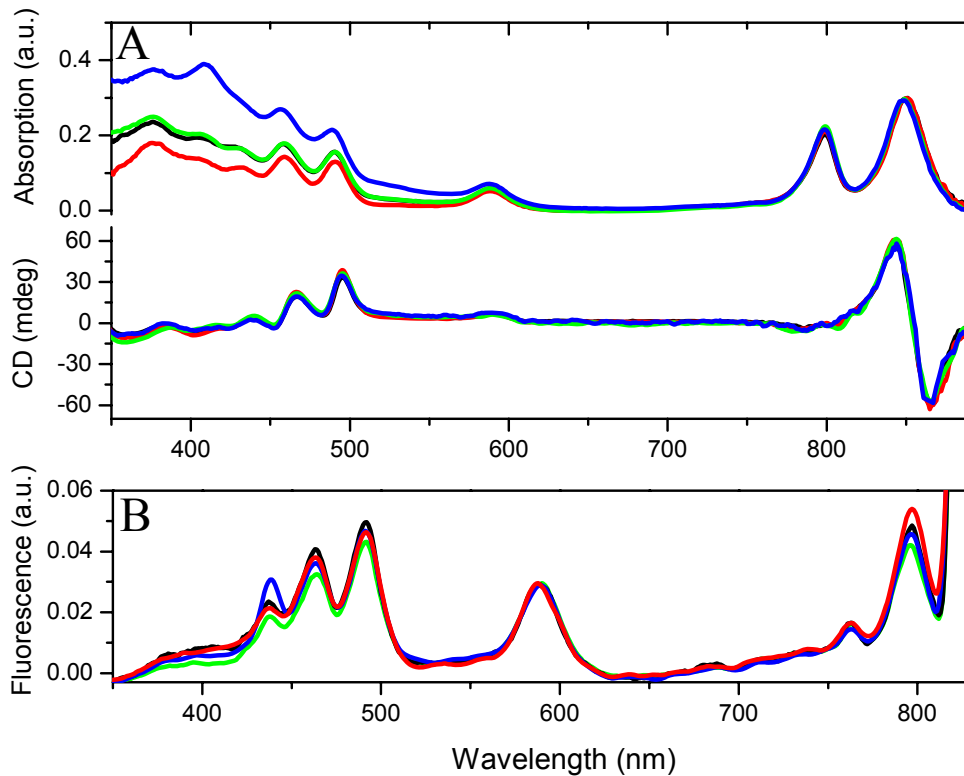


Figure 5-19: Absorption, CD and fluorescence spectra of LH2 WT (black line), α WT/ β WT-20Q (red line), α WT/ β WT-20K (green line) and α WT/ β WT-20A (blue line) in DG2 strains.
 (A) Upper panel: absorption spectra. Spectra are normalised at 850 nm. Lower panel: circular dichroism spectra. Spectra are normalised at the (+) maxima at ~843 nm.
 (B) Fluorescence excitation spectra. Spectra are normalised at ~590 nm.

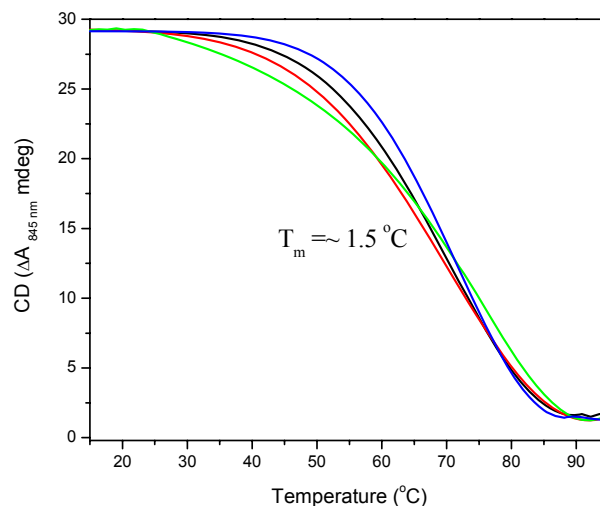


Figure 5-20: Thermal denaturation of LH2 WT (black line), α WT/ β WT-20Q (red line), α WT/ β WT-20K (green line) and α WT/ β WT-20A (blue line) in DG2 strains. The changes are using the CD signal at 845 nm during constant heating of LH2 membranes. The heating rate is 2 $^{\circ}\text{C}$ per min. Signals are normalised at the starting temperature of 15 $^{\circ}\text{C}$.

The thermal stability of the mutant LH2 α WT/ β WT_{-20Q}, α WT/ β WT_{-20K} and α WT/ β WT_{-20A} in the membranous environment is similar to the thermal stability of DG2 WT, with insignificant reductions (figure 5-20). This suggests that neither β Glu -20 nor the polar group of the carotenoid spheroidenone contribute noticeably to the structural stability or functional assembly of LH2 in the native membrane.

Effect of delipidation on LH2 WT and β Glu -20 complexes

The purified LH2 complexes of mutants α WT/ β WT_{-20Q}, α WT/ β WT_{-20A} and α WT/ β WT_{-20K} (both in DD13 and DG2 strains) in β OG detergent, are thermally destabilised in comparison to the corresponding LH2 WT, independent of the carotenoid present. Figure 5-21 shows the thermal denaturation of isolated LH2 WT and LH2 α WT/ β WT_{-20A} in β OG detergent which have been expressed in either *Rb sphaeroides* DD13 (spheroidenone) or DG2 (neurosporene) strains. The thermal stabilities of isolated LH2 complexes are increased for DD13 WT and DD13 α WT/ β WT_{-20A} as compared to their membranous stability in the native membrane (similar phenomenon has been described previously in Kwa *et al.*, (2004); Garcia-Martin *et al.*, (2006b)). In contrast, there is a significant reduction in thermal stability for DG2 WT and DG2 α WT/ β WT_{-20A} in β OG detergent. The T_m value drops from ~ 81 °C in DD13 WT to ~ 72 °C in DG2 WT. This destabilisation is even more pronounced in α WT/ β WT_{-20A} mutation. The T_m value drops from ~ 77 °C in DD13 α WT/ β WT_{-20A} to ~ 64 °C in DG2 α WT/ β WT_{-20A}.

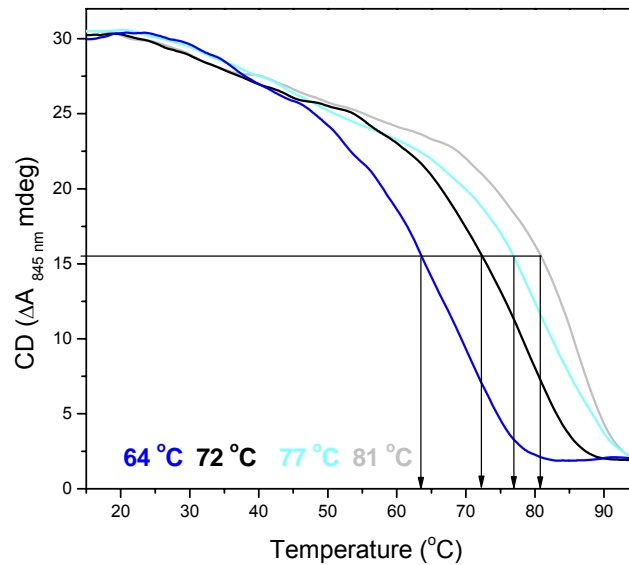


Figure 5-21: Thermal denaturation of LH2 DD13 WT (grey line), DD13 α WT/ β WT_{-20A} (cyan line); DG2 WT (black line) and DG2 α WT/ β WT_{-20A} (blue line) in β OG detergent. The changes are monitored using the CD signal at 845 nm during constant heating of LH2 membranes. The T_m values are indicated by arrows and their values are shown in the corresponding colours. The heating rate is 2 °C per min and signals are normalised at the starting temperature of 15 °C.

The exchange of spheroidenone with neurosporene in WT results in destabilisation of LH2 complex (T_m shift by ~ 9 °C). Mutating β Glu -20 also results in a minor destabilisation of LH2 complex (T_m shift by ~ 4 °C). An enhancement of this destabilisation occurs with the alterations of both the carotenoid and β Glu -20 (T_m shift by ~ 17 °C), indicating that the β Glu -20 and carotenoid polar moiety synergistically contribute to LH2 stability. However, this becomes obvious only in detergent, when most of the lipids are removed from the complex. Obviously, the surrounding lipids contribute to the mutant LH2 stability.

It is tempting to speculate that in the WT (β Glu -20 and spheroidenone) binding cleft, lipids are held on tightly and are not removed by the detergent treatment; the thermal stability of LH2 WT is maintained. Conversely, when the carotenoids' polar moiety and the negative charge of glutamate are removed, the binding cleft is unable to withhold its surrounding lipids during detergent treatment. Exposure of the protein-lipid interface to detergent or water molecules results in destabilisation of LH2. In this model, the residue β Glu -20 and the polar group of carotenoid

synergistically bind lipid molecule(s) and thus make up a lipid/protein interactions site.

MEMBRANE PROTEIN CONTENTS

In α AL_{4S}/ β AL mutant, when the LH2-expression level is reduced significantly (figure 5-6), the protein content in the mutant relative to LH2 WT is unusually high which potentially contributes to its abnormal membrane morphology (figure 5-7C). In WT, the protein concentration is ~117 μ g/ml in DD13 and ~125 μ g/ml in DG2 strains. Seven times more proteins are found in DD13 α AL_{4S}/ β AL mutant (~680 μ g/ml) in comparison to DD13 WT. On the other hand, in α WT/ β WT_{-20A} DD13 and DG2 strains, the total protein concentrations is marginally increased in comparison to WT (table 5-6).

Strains	Protein Concentration (μ g/ml)	
	DD13	DG2
WT	117	125
α AL _{4S} / β AL	680	-
α WT/ β WT _{-20A}	150	190

Table 5-6: Comparison of total protein concentrations of WT and mutants. Comparison of WT and mutants proteins content of membranes with OD_{850 nm} = 1. (For details, see Chapter 2 materials and methods; appendix 2).

The protein concentrations in α WT/ β WT_{-20A} DD13 and DG2 strains are increased by a factor of 1.3 and 1.5 respectively in comparison to the WT comparing their structural stabilities in membrane, no notable differences between the mutant LH2 complexes and WT were observed. Despite the possibility of determination errors for protein concentration (see appendix 2), the increases in the total protein concentration relative to LH2 WT points towards a slight reduction in assembled LH2, especially in the absence of both the native carotenoid and β Glu -20 in the

membrane. The reduction in the assembled LH2 $\alpha\text{AL}_{4\text{S}}/\beta\text{AL}$ is clearly much more pronounced.

PHOSPHOLIPID COMPOSITION OF RB SPHAEROIDES EXPRESSING LH2 WT OR LH2 $\alpha\text{WT}/\beta\text{WT}_{-20\text{A}}$ IN DD13 AND DG2 STRAINS

Phospholipid headgroup compositions

So far, it has been shown that the structural stability of LH2 $\alpha\text{WT}/\beta\text{WT}_{-20\text{A}}$ in the presence of neurosporene in detergent βOG is reduced. One possibility for the observed destabilisation may be an alteration at the LH2-protein-lipid interface. In order to gain further insights into potential LH2 lipids interactions, the phospholipid compositions were analysed in DD13 $\alpha\text{WT}/\beta\text{WT}_{-20\text{A}}$ and DG2 $\alpha\text{WT}/\beta\text{WT}_{-20\text{A}}$. Mutant $\alpha\text{WT}/\beta\text{WT}_{-20\text{A}}$ was chosen over $\alpha\text{WT}/\beta\text{WT}_{-20\text{K}}$ and $\alpha\text{WT}/\beta\text{WT}_{-20\text{Q}}$, because it shows the greatest change in thermal stability between native membrane and detergent; and the least change in LH2 structure and functions. Table 5-7 shows the relative amounts of PC, PE and PG in WT and $\alpha\text{WT}/\beta\text{WT}_{-20\text{A}}$ of *Rb sphaeroides* DD13 and DG2 strains. All the samples are highly similar in their relative amounts of PC, PE and PG; consequently, there is no significant alteration in their bilayer and nonbilayer forming phospholipids (PC+PG/PE) ratios.

Carotenoid	Samples ^a	Phospholipid composition ^b			PC+PG/PE
		PC	PE	PG	
Spheroidenone	DD13 WT ^c	23.44	60.68	15.88	0.65
	DD13 α WT/ β WT _{-20A} ^d	23.94	61.90	14.16	0.62
Neurosporene	DG2 WT ^e	25.36	59.62	15.01	0.68
	DG2 α WT/ β WT _{-20A} ^e	24.94	60.46	14.60	0.65

Table 5-7: Percentage of the major phospholipids (PC, PE and PG) in *Rb sphaeroides* WT and α WT/ β WT_{-20A} in DD13 strains (spheroidenone) and DG2 strains (neurosporene).

^a The *Rb sphaeroides* are grown semi-aerobically in the dark at 28 °C. Cultures were harvested in the mid-logarithm phase when the absorbance at 650 nm reached 1.2 to 1.5. (DD13 WT- 28 hour; DD13 α WT/ β WT_{-20A}- 25 hour; DG2 WT- 26 hour; DG2 α WT/ β WT_{-20A}- 30 hour).

^b The 3 major phospholipids, PC, PE, PG of *Rb sphaeroides* cells are determined by ESI-MS, presented here as percentage of total phospholipids (PC+PE+PG). Other minor phospholipids are below reliable detection level of the ESI-MS analysis.

^c The average values are derived from 6 measurements from 3 samples.

^d The average values are derived from 10 measurements from 5 samples.

^e The average values are derived from 4 measurements from 2 samples.

Phospholipid hydrocarbon chain compositions

The hydrocarbon compositions of PE and PC of LH2 WT and α WT/ β WT_{-20A} mutants in DD13 and DG2 strains are shown in tables 5-8 and 5-9 respectively.

PE Fatty-acyl chain ^b	Percentage (%)			
	Spheroidenone		Neurosporene	
	DD13 WT ^c	DD13 α WT/ β WT _{-20A} ^d	DG2 WT ^e	DG2 α WT/ β WT _{-20A} ^f
32:0	0.36	0.26	0.43	0.17
34:2	2.40	2.03	2.14	2.06
34:1	5.45	5.17	6.80	6.71
34:0	0.46	0.35	0.52	1.26
35:1	0.27	0.22	0.45	10.95
36:2	79.15	79.69	78.75	63.01
36:1	9.79	9.48	8.39	7.31
36:0	0.42	0.43	0.44	0.60
37:2	0.78	0.95	1.14	2.79
37:1	0.10	0.11	0.09	0.64
38:1	0.05	0.07	-	0.08
Others	0.89	1.24	0.85	4.42

Table 5-8: PE fatty-acyl chain length composition of *Rb sphaeroides* LH2 WT and α WT/ β WT_{-20A} in DD13 strains (spheroidenone) and DG2 strains (neurosporene)^a.

^a Samples were cultivated as described in Table 5-7.

^b Values are percentage of total fatty-acyl chains of PE in WT and α WT/ β WT_{-20A}. The fatty-acyl chains are presented as described previously.

^c The average values are derived from at least 5 measurements from 3 samples.

^d The average values are derived from at least 6 measurements from 5 samples.

^e The average values are derived from at least 2 measurements from 2 samples.

^f The average values are derived from 4 measurements from 2 samples.

Table 5-8 shows the PE hydrocarbon compositions of *Rb sphaeroides* cells expressing LH2 WT and α WT/ β WT_{-20A} in DD13 and DG2 strains. No significant differences of PE chain lengths or degree of saturation is observed in DD13 α WT/ β WT_{-20A} in comparison to DD13 WT. Similarly, no differences are observed in hydrocarbon chain composition, when DD13 WT is compared to DG2 WT. In contrast, in DG2 α WT/ β WT_{-20A}, the main PE 36:2 is reduced by ~15 % compared to WT, whereas, the relative amounts of PE with other hydrocarbon chains 34:0, 35:1, 37:2 and 37:1 are increased.

PC Fatty-acyl chain ^b	Percentage (%)				
	DD13 WT ^c	Spheroidenone		Neurosporene	
		DD13 α WT/ β WT _{-20A} ^d	DD13 α AL _{-4S} / β AL ^e	DG2 WT ^f	DG2 α WT/ β WT _{-20A} ^g
32:0	0.10	0.08	0.16	0.12	0.07
34:2	2.78	2.94	2.22	2.50	2.85
34:1	3.91	3.64	6.53	5.23	4.35
34:0	0.14	0.13	0.38	0.21	0.57
35:2	0.11	0.11	0.20	0.27	3.19
35:1	0.25	0.23	0.55	0.48	6.71
36:2	80.05	78.97	73.00	77.40	61.00
36:1	6.37	5.72	8.68	6.48	6.34
37:3	0.42	0.37	0.16	0.51	0.74
37:2	2.82	3.27	4.16	3.10	7.28
37:1	0.30	0.42	0.60	0.36	1.25
38:4	0.44	0.37	0.11	0.66	1.14
39:2	0.26	0.20	0.22	0.47	0.82
Others	2.05	3.55	3.03	2.21	3.69

Table 5-9: PC fatty-acyl chain length composition of *Rb sphaeroides* LH2 WT, α WT/ β WT_{-20A} and α AL_{-4S}/ β AL in DD13 strains (spheroidenone) and LH2 WT and α WT/ β WT_{-20A} in DG2 strains (neurosporene)^a.

^a Samples were cultivated as described in Table 5-1 and 5-7.

^b Values are percentage of total fatty-acyl chains of PC in WT, α WT/ β WT_{-20A} and α AL_{-4S}/ β AL. The fatty-acyl chains are presented as described previously.

^c The average values are derived from at least 4 measurements from 3 samples.

^d The average values are derived from at least 7 measurements from 5 samples.

^e The average values are derived from at least 3 measurements from 3 samples.

^f The average values are derived from at least 3 measurements from 2 samples.

^g The average values are derived from 4 measurements from 2 samples.

The PC hydrocarbon compositions of WT, α WT/ β WT_{-20A} and α AL_{-4S}/ β AL in DD13 strain are compared to the composition of WT and α WT/ β WT_{-20A} in DG2 strain (table 5-9). Clearly, there were no significant alterations found in the hydrocarbons of PC in DD13 WT, DD13 α WT/ β WT_{-20A} and DG2 WT. This is similar to the earlier mutant DD13 α AL_{-4S}/ β AL; as discussed at the beginning of this chapter, α AL_{-4S}/ β AL compensates most of the loss of LH2 by altering its PE acyl-chain and its bilayer/nonbilayer ratio. Considering that PC is present in relatively smaller amounts, their changes in fatty-acyl chain lengths are minor relative to the more pronounced differences observed in PE (table 5-2). On the other hand, significant changes are observed in PC of DG2 α WT/ β WT_{-20A}, the predominant PC, 36:2 is

reduced by ~16 % as compared to DG2 WT and ~19 % as compared to DD13 WT; whereas, other hydrocarbons such as 35:2, 35:1, 37:2 and 37:1 are increased. The acyl-chain lengths and degree of saturation of PC and PE are similar for DD13 WT, DG2 WT and DD13 α WT/ β WT_{-20A}, but clearly distinct for DG2 α WT/ β WT_{-20A}. This suggests that the alterations in hydrocarbon chains of DG2 α WT/ β WT_{-20A} cells are a result of modification of both the β Glu -20 residue and carotenoid. Modification of carotenoid or β Glu -20 alone will not induce the modification in the PE acyl-chain composition of these membranes.

PHOSPHOLIPID COMPOSITION OF ISOLATED DD13 α WT/ β WT_{-20A}

LH2 α WT/ β WT_{-20A} was isolated from the membrane by detergent β OG to investigate the boundary lipids of this mutant. Despite several attempts, isolation of α WT/ β WT_{-20A} in DG2 strain did not produce sufficient amount of LH2 for ESI-MS analysis (see chapter 2, materials and methods; chapter 6 for discussion). On the other hand, LH2 α WT/ β WT_{-20A} in DD13 strain is readily isolated in β OG at sufficient amounts for ESI-MS measurements. The results are presented in the tables 5-10 and 5-11.

Isolated samples ^a	Phospholipid composition ^b		
	PC	PE	PG
LH2 WT ^c	12.28	87.72	n.d.
LH2 α WT/ β WT _{-20A} ^d	27.34	72.67	n.d.

Table 5-10: Percentage of the major phospholipids (PC, PE and PG) in *Rb sphaeroides* DD13 strain isolated of LH2 WT and α WT/ β WT_{-20A} in β OG. (n.d. = not detected)

^a The isolated LH2 WT and LH2 α WT/ β WT₋₂₀ in DD13 are purified as described in Walz *et al.*, 1998.

^b The 3 major phospholipids, PC, PE and PG are determined by ESI-MS, presented here as percentage of total phospholipids (PC+PE). Other minor phospholipids are below reliable detection level of the ESI-MS analysis.

^c The average values are derived from 6 measurements from 3 samples.

^d The average values are derived from 4 measurements from 2 samples.

PE Fatty-acyl chain ^a	Percentage (%)	
	LH2 WT ^b	LH2 α WT/ β WT _{-20A} ^c
32:0	1.89	-
34:2	1.83	0.66
34:1	7.79	4.73
34:0	3.41	-
35:1	1.34	0.58
36:2	59.03	71.25
36:1	12.69	16.00
37:2	3.72	2.15
38:1	1.33	-
Others	6.97	1.07

Table 5-11: PE fatty-acyl chain composition in *Rb sphaeroides* DD13 strain isolated of LH2 WT and α WT/ β WT_{-20A} in β OG.

^a Values are percentage of total fatty-acyl chains of PE. The fatty-acyl chains are presented as described previously.

^b The average values are derived from at least 4 measurements from 3 samples.

^c The average values are derived from at least 2 measurements from 2 samples.

From both the tables 5-10 and 5-11, the following observations are found: PE and PC are the phospholipids attached to the isolated LH2 complex in both the DD13 WT and DD13 α WT/ β WT_{-20A}, while no PG was detected. PE remained the dominant phospholipids; however, the relative amount of PE is reduced by ~17 % in DD13 α WT/ β WT_{-20A} in comparison to DD13 WT. The hydrocarbon chains 36:2 remain as the predominant acyl-chains of PE but in isolated LH2 α WT/ β WT_{-20A}; the 36:2 and 36:1 chains are increased relative to WT and the remaining fatty-acyl chains are reduced. These findings indicate that mutation of the residue glutamate -20 to alanine results in changes of the phospholipid compositions closely associated with the LH2 complex. In contrast, the bulk lipid composition is not significantly affected by the substitution of glutamate with alanine. Analysis of lipid composition of *Rps acidophila* has previously shown that the cell lipid composition and LH2 boundary lipids may be distinctively different (Russell *et al.*, 2002).

In summary, when β Glu -20 was substituted by alanine, the structure and function appears to be unchanged. In addition, its thermal stability in the membrane is closely similar to the stability of WT LH2. There were no significant changes observed in

bulk phospholipid compositions, neither the phospholipid headgroups nor the hydrocarbon acyl chains. However, the thermal stability of LH2 α WT/ β WT_{-20A} isolated from the membrane is reduced. In addition, the selectivity of phospholipid headgroup and fatty acyl chain are altered in LH2 α WT/ β WT_{-20A} compared to isolated LH2 DD13 WT. These findings support the idea that the residue β Glu -20 and the spheroidenone's polar group are involved in protein-lipid interaction; particularly with PE. The unsuccessful isolation of LH2 DG2 α WT/ β WT_{-20A} in β OG also hints at the function of these LH2 moieties and their putative significance in lipid-protein interactions. It is quite remarkable that the combined alteration is so resistant to delipidation as compared to the ease of delipidation of DG2 WT and DD13 α WT/ β WT_{-20A}. It would appear that the double mutation resulted in a particularly unstable complex upon removal of the lipids, which is also consistent with the diminished value of T_m of DG2 α WT/ β WT_{-20A} in detergent. If sufficient mutant complex could be purified for MS analysis, the boundary lipids of DG2 α WT/ β WT_{-20A} could be examined. It appears quite likely that they have been undergone some modifications since the bulk PC and PE hydrocarbon compositions have shown alterations even in membranous environment. All these findings would suggest a significant change in the protein-lipid interactions, as a result of altering putative lipid binding site contributed by the carboxyl side chain of glutamate and the polar headgroups of spheroidene.

MODIFICATIONS OF ICM MORPHOLOGY IN MUTANTS DD13 α AL_{-4S}/ β AL and α WT/ β WT_{-20A}

The ICM morphology of *Rb sphaeroides* is known to be related to LH2 assembly. It has been speculated that LH2 protein specifically interacts with phospholipids which contribute to the ICM formation in as yet not well understood manner (Russell *et al.*, 2002). As shown in figure 5-7, tubular formation of ICM is observed in DD13 α AL_{-4S}/ β AL when the LH2 proteins are significantly mutated. Here, the morphologies of the ICM containing LH2 WT, α AL_{-4S}/ β AL and α WT/ β WT_{-20A} are compared (figure 5-22 and table 5-12).

In DD13 and DG2 strains expressing LH2 WT, all of the ICM vesicles are of oval shape with sizes ranging from 35 nm to 55 nm. The ICM containing LH2 α WT/ β WT_{-20A} in DD13 have a closely similar morphology as the ICM containing LH2 WT, indicating that the changes at the LH2-protein-lipid interface upon alteration of β Glu -20 does not result in the alteration of membrane morphology. On the contrary, the ICM of LH2 α WT/ β WT_{-20A} in the DG2 strain have membrane invaginations of the normal oval shape vesicles, but there are also a substantial number of 'abnormal' cytoplasmic invaginations and of enlarged vesicular structures ranging from 35 nm to as large as 90 nm in diameter (figure 5-22D). Interestingly, the morphology of enlarged vesicular ICM invaginations was observed in the carotenoidless *Rb sphaeroides* R26.1 strain (figure 5-22B). Loss of carotenoids from LH2 or the reduction in LH2 expression level results in the 'abnormal' changes in ICM morphology. At present, it is not possible to clearly relate the changes in membrane morphology with a single factor. The LH2 α WT/ β WT_{-20A} containing neurosporene has impaired structural stability and possibly results in multiple effects. If sufficient mutant complex could have been purified for MS analysis, the boundary lipids of DG2 α WT/ β WT_{-20A} could be analysed. Perhaps, these would be further modified (as compared to DD13 α WT/ β WT_{-20A}) since their bulk PC and PE hydrocarbon compositions have shown alterations even in membranous environment. Nevertheless, these findings point at a close coordination between LH protein, carotenoid, phospholipids and membrane morphology.

Samples	Normal vesicles		Abnormal vesicles		ICM morphology
	Number	%	Number	%	
DD13 WT	205	98.6	3	1.40	Vesicles size: 35-55 nm
DD13 α AL _{4S} / β AL	257	72.2	99	27.8	Abnormal vesicles: Tubular formation
DD13 α WT/ β WT _{-20A}	188	98.9	2	1.10	Normal vesicles as WT
DG2 α WT/ β WT _{-20A}	157	57.7	115	42.3	Abnormal vesicles: 55- 90 nm; abnormal cell membrane formation

Table 5-12: Summary of LH2 vesicles ultrastructure in WT and mutants. More than 200 vesicles are counted and compared.

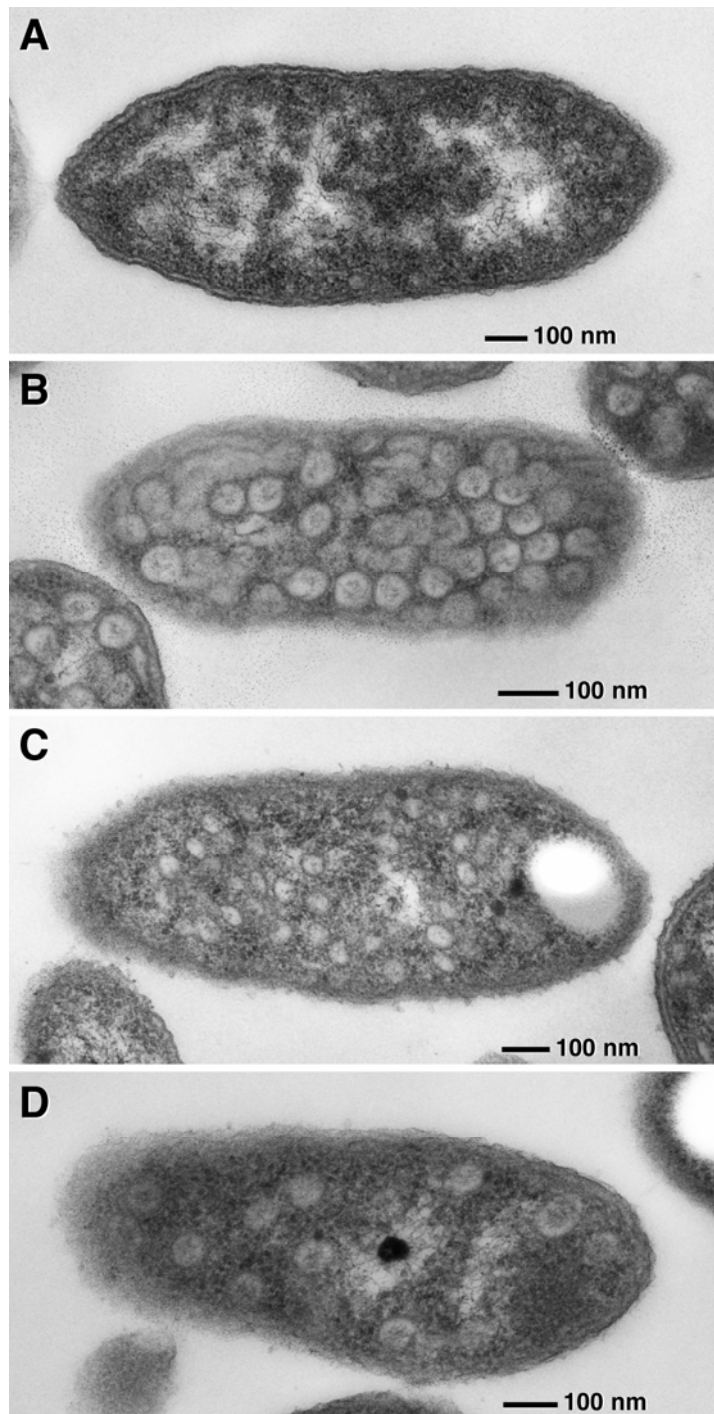


Figure 5-22: Ultrastructure of bacterial cells of (A) DG2 WT, (B) *Rb sphaeroides* R26.1 strain (C) DD13 α WT/ β WT_{-20A} and (D) DG2 α WT/ β WT_{-20A}.

5.3 CONCLUSIONS

In summary, these studies represent the first determination of phospholipid compositions by ESI-MS measurement of LH2 only membranes from *Rb sphaeroides* strains. In addition, the membrane lipids closely associated with the LH2 complex from *Rb sphaeroides* have been determined. It provides evidence that the nonbilayer phospholipid, PE, is preferentially accumulated in the close vicinity of the complex in LH2 only membranes. The amino acid residue Glu -20 at the N-terminus of the transmembrane β -helices plays an important role in the specific accumulation of PE at the LH2 protein-lipid interface. Importantly, it is shown that the β Glu -20 residue and the close by carotenoid synergistically contribute to the LH2 stability, possibly due to altered LH2-lipid interactions. The specific local interactions between LH2 protein and lipids not only contribute to the LH2 protein stability but also appears to be involved in ICM morphology.

This is the first work demonstrating local LH2-lipid specificity *in vivo*. This approach yield important clues about the functions of boundary lipids and their inter-relationship with membrane protein. However, the relationship between LH2 assembly and interactions with its surrounding lipids and the modulation of membrane shape would require further investigations.

Model LH2	Modified sequences		T _m value of LH2 membrane (°C)
	α-subunit	β-subunit	
DD13 WT	TVGVPLFLSAAVIASVVIHAAVLTTT	AEVHKQLILGTRVFGGMALIAHFLAAAA	74
αAL _{-4S} /βAL	TVGVPLFLSAA LL AS LL I H AA L LAAT	AEVHKQLILGTRV LLI AL L A H LLAAAA	40
DD13 αWT/βWT _{-20Q}	TVGVPLFLSAAVIASVVIHAAVLTTT	AE Q VHKQLILGTRVFGGMALIAHFLAAAA	73
DD13 αWT/βWT _{-20A}	TVGVPLFLSAAVIASVVIHAAVLTTT	AE A VHKQLILGTRVFGGMALIAHFLAAAA	71
DD13 αWT/βWT _{-20K}	TVGVPLFLSAAVIASVVIHAAVLTTT	AE K VHKQLILGTRVFGGMALIAHFLAAAA	66

Table 5-13: Amino acid sequences of model LH2 used in this chapter.

CHAPTER 6

DISCUSSION

The current understanding of photosynthesis arises from a multitude of studies. Light-harvesting complex 2 is a membrane embedded protein-pigment complex that has been structurally and functionally well characterised. However, there are still questions regarding protein-pigments interactions underlying the functional assembly of the complex. Moreover, comparatively little is known about the interactions between protein and lipid and their functional roles. The focus of my work has been to further the understanding of these specific protein-pigment and protein-lipids interactions. The findings are discussed as follows.

Part I: Protein-bacteriochlorophyll interactions in model and native light-harvesting complex 2

Chapter 3: Bacteriochlorophylls' macrocycle-protein interactions underlying LH2 assembly and function

Pigment-protein interactions in bacterial LH complexes have been extensively studied. Apart from the well defined ligation between the central Mg²⁺ atom of the BChls' macrocycle and amino acid residue from the polypeptides (Coleman & Youvan, 1990; Olsen *et al.*, 1997), interactions between the peripheral substituents of the BChl macrocycle and the polypeptides are still little known. In Chapter 3 of the thesis, the peripheral interactions between the BChls' macrocycle and polypeptides are addressed by the use of model LH proteins which are comprised of BChl binding sites of largely simplified Ala-Leu model sequences. In this way,

subtle structural binding motifs and the interactions that fine tune the electronic properties of the photopigments were identified.

Simplification of the BChl-B850 binding site: model sequences in the TMH of the β -subunit

Modified residues (-7, -6, -5, -2 and +1) of β AL in the close vicinity of BChl-B850 macrocycles were found to have little contribution to the red-most absorption maxima of BChl-B850 transitions and its energy transfer properties. Yet, the thermal stability of α WT/ β AL complex was significantly reduced. These findings suggest that these residues at the BChl-B850/protein interface are of little importance for the pigments spectral properties (thus their function) but are of importance for the pigment-protein complexes' stability. Possibly, the 'minimal' requirements for BChl-B850 binding is already fulfilled by the central Mg^{2+} -His ligand, together with a few key residues such as the aromatic residues anchored in the bilayer interface (Fowler *et al.*, 1992). Indeed, residues from the positions -9 to +10 (except His 0 and β Ala -4) further away from the BChl-B850 toward the N- and C-terminus are noticeably less conserved (Zuber, 1985; Zuber & Cogdell, 1995; Braun *et al.*, 2002) which supports the idea that they have little importance for the function and fine tuning of the BChl-B850 binding (Garcia-Martin *et al.*, 2006b). Therefore it is not surprise that neither α WT/ β AL nor α AL/ β WT significantly impaired the functional assembly of BChl-B850. However, the instability of the model complexes indicates the importance of these residues for structural stability. Model synthesis studies (Noy *et al.*, 2006) on the minimal BChl-binding protein designs has found that the smallest peptide is still capable of BChls assembly and has the formation of BChl-B820 analogs consists of at least 24 native residues. Shorter peptides were postulated to be unable to span the typical BChl molecules and were expected to be unable to support assembly into native-like complexes (Noy *et al.*, 2006). In view of that, a few residues appear to be crucial for the binding and functional tuning of the pigments but the majority of residues appear to be important for the overall BChl organisation and complex stability.

In the simplified α -subunit, α AL/ β WT, eight residues out of the stretch of 14 have been modified without severely disturbing the BChl-protein array and function (Braun *et al.*, 2003; Kwa *et al.*, 2004; Garcia-Martin *et al.*, 2006b). In the β -subunit, only up to 5 residues are modified and any further simplification towards the N- or C-terminus of β AL result in the complete loss of LH2 assembly. This indicates a lower tolerance of β -subunit to the changes in the transmembrane stretch compared to the α -subunit. In the model LH2 structure (McDermott *et al.*, 1995), the β -polypeptides make up the outer ring of the LH2 complex. Based on this, it has been proposed previously that the β -polypeptides have a less constrained environment, permitting greater flexibility in the length and orientation of the BChl ligand than α -polypeptides (Olsen *et al.*, 1997). As shown by this study, this appears not to be the case, which provides a new insight on the β -subunit/BChl binding characteristics. The β -polypeptides appear more stringent than the α -polypeptides in their interactions with the surroundings.

The α AL/ β AL in which the simplified Ala-Leu sequences with a total of 13 mutations on both the α - and β -polypeptides does not assemble to LH2-like complex. The ‘minimal’ requirement for pigment to be assembled within the protein was fulfilled by the re-introduction of a serine residue at the position -4 of α -subunit, α AL_{-4S}/ β AL. This hydroxyl group of the residue α Ser -4, has been shown to make a H-bond with the C13¹ keto carbonyl group of the β BChl-B850 (Braun *et al.*, 2003). This ‘rescues’ the LH2-like assembly and has shown to significantly improve the thermal stability of α AL/ β WT (the T_m shifts by ~ 23 °C). Here, it demonstrated that up to 12 of the native residues at the BChl-B850/protein interface can be replaced with Ala or Leu without significantly upsetting the pigment-protein assembly and function, as long as the crucial residues are still present. Statistical analyses of (B)Chl-binding proteins (Braun *et al.*, 2002; Garcia-Martin *et al.*, 2006b) show that the BChl macrocycle substituents interact mainly with the residues at the positions -4, +3, -1 and ± 7 of the apoprotein. Especially, the interaction between the C13² oxo groups of BChl and the residue -4 of the binding helix (Braun *et al.*, 2002; Garcia-Martin *et al.*, 2006b). This data supports the ability of our approach to identify subtle but crucial interactions; in particular, the identified α Ser -4 H-bond is critical for the assembly of the model LH2.

Putative H-bonding between β Ser -4 and α BChl-B850

In the attempt of further simplify β AL, we first tried to improve the thermal stability of α WT/ β AL complex by replacing β Ala -4 to a serine. The idea is derived from the earlier observation (Braun *et al.*, 2003) that α Ser -4 exerts a stabilising effect on the simplified α -subunit, α AL/ β WT by its H-bond interactions with BChl-B850. The residue at -4 position of both the α - and β -subunit is highly conserved (Zuber, 1985; Zuber & Cogdell, 1995; Braun *et al.*, 2002; Kwa *et al.*, 2004). Alanine is exclusively found in the β -subunit, which hints at its potential role. Using the model LH2 structure, both the distance and angle between residue at -4 position of α - and β -subunit and the C13¹ keto carbonyl groups of BChls-B850 are found to be highly similar. Their spatial positioning is ideal for H-bond formation. Despite the similarities, the introduction of a serine at position -4 of β -subunit in the α WT/ β AL mutant did not improve the model complex assembly and stability. On the contrary, further reduction in its mid-point thermal transition is observed. The OH \cdots O H-bond is either not established between the β Ser -4 and α BChl-B850 as found in the α -polypeptide or its establishment had somehow destabilised the complex. Serine has a bulkier side-chain than alanine, which may not favour the tight packing required within this compact environment. In addition, the distance between the hydroxyl group of β Ser -4 and the C13¹ carbonyl oxygen of α BChl-B850 may be slightly too far (2.87 Å), and thus less favourable for the H-bond formation. The next nearest C=O groups (such as C17³ or C13³) are located more than 4 Å from the hydroxyl group, which is too far for an H-bond formation. For β -subunit, alanine is clearly more favourable for the complex assembly/stability than serine. The examination of a possible H-bond by Raman spectroscopy has not been achieved successfully. Due to the complexity of Raman signals in the membrane, only spectra of mutants with expression levels similar to WT may be reliably measured. Neither α WT/ β AL nor α WT/ β AL_{4S} resonance Raman data could be obtained as their level of expression were too low.

The BChl-B850 Q_y absorption maximum of α WT/ β AL_{4S} is slightly but noticeably blue-shifted by ~3 nm (figure 6-1). A shift in the absorption peaks of the BChl-B850 has previously been correlated with the breakage of H-bond to the C3 acetyl group

(Fowler *et al.*, 1994) but not with the one to the C13¹ keto carbonyl group (Braun *et al.*, 2003). Shifts of the absorption peaks of the BChl-B850 to the red region were previously observed in the simplified α -subunit, α AL/ β WT, α AL_{-4S}/ β WT and α AL_{-4S}/ β AL (Braun *et al.*, 2002). These likely reflects the structural rearrangement of the BChl-B850 dimer due to the modifications of the BChl-B850 protein interface in α AL (Kwa *et al.*, 2004) including the loss of OH \cdots H H-bond between serine and the BChl's C13¹ keto carbonyl group. On the other hand, simplified β -subunit, α WT/ β AL, does not give rise to any shifts at the 850 nm, only by the additional mutation at position -4 to serine, α WT/ β AL_{-4S}, would this result in a 3 nm shift (albeit in the opposite direction, blue shifted, figure 6-1). This therefore reflects a different structural arrangement at the interface of the BChl-B850 dimer with the α - and β -subunit. Whether alanine is involved in a weaker H-bonding with the C13¹ keto carbonyl could not be determined. The breakage of the alanine-BChl CH \cdots O H-bonds could be the direct cause of this blue-shift at the 850 nm peak. On the one hand, disruption of H-bonding to C13¹ has not been shown to result in spectral shifting (Braun *et al.*, 2003). On the other hand, some studies have suggested that alanine has the potential to form a H-bond albeit a weak one (Desiraju, 2002; Jiang & Lai, 2002; Sarkhel & Desiraju, 2004).

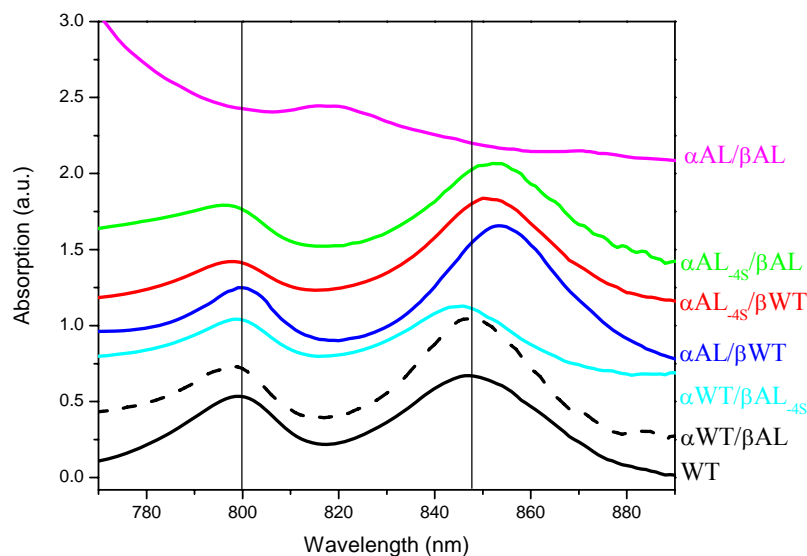


Figure 6-1: Near infrared absorbance spectra of membranes of LH2 WT and LH2 complexes containing simplified model sequences. Spectra are displayed vertically for clarity. Note, the shifts in absorption maximum of BChl-B850.

The residue alanine at position -4 is exclusively conserved, particularly, in the β -polypeptides of LH2 across numerous proteobacterial species. Yet, mutation to serine is tolerated in the model LH2, despite its already poor complex assembly/stability. Serine has a packing value closely similar to alanine, which may partially compensate for alanine in its role to sequestrate the polar keto carbonyl group from the hydrophobic lipid core, surrounding TMH, and pigments and thereby to prevent incorrect folding. The polar NH group of His 0 is also close (less than 4 Å) to the BChl-B850 keto group (figure 6-2); it might contribute to a strong NH \cdots O H-bond to C13¹ and hold the pigment in place.

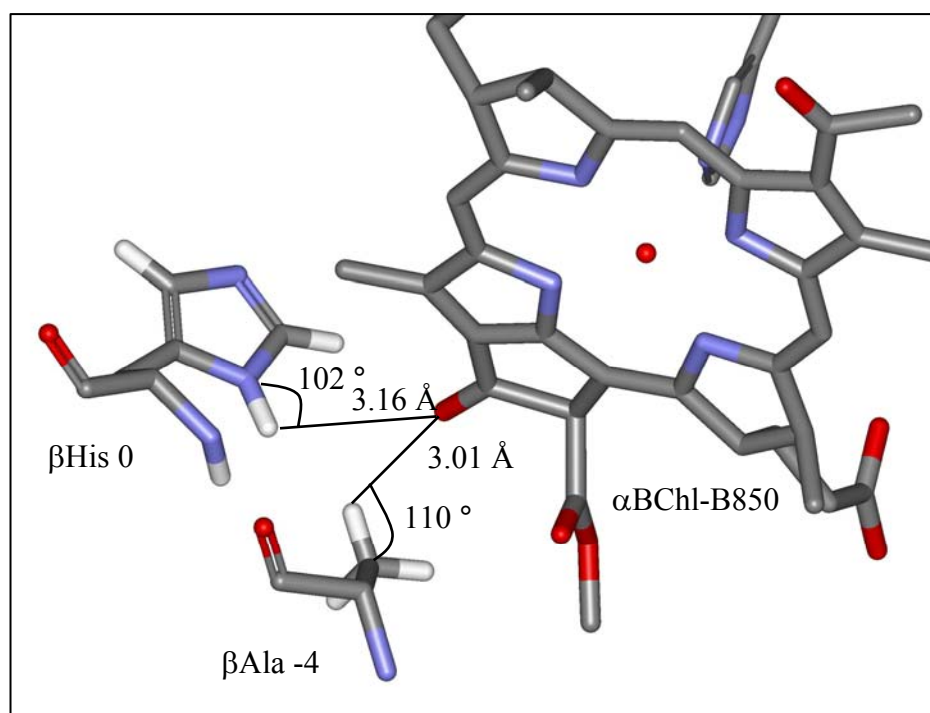


Figure 6-2: Modelling of putative H-bonding between α BChl-B850 C13¹ keto carbonyl group and β His 0 and β Ala -4. The α BChl-B850 C13¹ keto carbonyl group is in close vicinity to the β His 0 which may form a strong H-bond (NH \cdots O) as well as to the β Ala -4 to form a weak CH \cdots O H-bond.

Taken together, we may conclude: (1) The α - and β -polypeptides have different roles in their interactions with the BChl pigments, in spite of the highly similar polypeptides environment. (2) Despite the very high degree of conservation at -4 position of the β -polypeptide, alanine can be altered to serine in the model complex

and maintain LH2-like assembly. (3) The blue-shift in the BChl-B850 absorption maximum in α WT/ β AL_{-4S} may be due to the structural rearrangement of existing interactions between residue β Ala -4 and α BChl-B850.

By use of the model system, noticeable differences are demonstrated in the binding and interactions of BChl molecules by the α - and β -polypeptides. Crucial residues such as α Ser -4, have been identified and their contribution to the stability and assembly of the model complex, α AL/ β AL were determined. Through the process of simplifying the polypeptides, it was shown that the H-bonding at the BChl-polypeptide interface is a key interaction motif in model proteins. The identified H-bond clearly enhances the structural stability in a context-dependent manner.

Biological interactions are subtle, small structural changes alone often does not lead to large functional differences due to multiple supporting interactions. Weaker C-H \cdots O H-bonds is not as readily identified as stronger H-bonds, such as N-H \cdots O or O-H \cdots O. The latter stronger interactions contribute enthalpically, but the weaker interactions, due to their inherent flexibility, make only modest entropic contributions to the system (Jiang & Lai, 2002; Sarkhel & Desiraju, 2004). In addition, the weak interactions are usually unnoticed in WT. In the context of the model sequence, such subtle protein-pigment interactions and their effects on pigment binding and tuning can be examined systematically.

This chapter highlights the importance of the H-bond interactions between pigment molecules and residues. It extends our understanding of the flexibility/stringency of specific residues surrounding His 0 in the BChl binding site in natural membrane proteins. The importances of subtle differences in side-chains properties of residues as similar as α Ser -4 or β Ala -4 are demonstrated. The minor changes in side chain volume of serine versus alanine, clearly deteriorates complex stability. Due to the inherently instable model sequence context, such effects are amplified which emphasise the power of this model system to study the impact of particular residue at the BChl/protein interface. Additional interactions at the BChls' macrocycles in the protein binding site exist which require systematic investigation. For example, it is still not fully ascertain the exact relationship between different residues and Q_y

absorption maxima. Site-directed mutations in the model LH2 complex should help to clarify this further.

Chapter 4: Bacteriochlorophylls' phytol chain-protein interactions underlying LH2 assembly and function

Phytol tail has been suggested to contribute to the assembly and stability of LH2 (Davis *et al.*, 1996; Addelesee & Hunter, 2002). Although it contributes more than one third of all the carbon atoms of (B)Chl, our understanding of the role of phytol tails is much less than that of (B)Chl tetrapyrrole. The phytol chain is not part of the conjugated electron system of tetrapyrrole and therefore alterations in the phytol tail conformation are not reflected in spectral properties of the (B)Chl (e.g. Rüdiger & Schoch, 1991; Fiedor *et al.*, 2003). Studies of BChl-protein interaction in artificial synthetic polypeptides have usually been performed with (B)Chlide molecules instead of (B)Chl (e.g. Dewa *et al.*, 2005; Nango, 2006). As shown in my thesis, mutating residues in the model LH2 complex, which are closely interacting with the phytol chains of the β BChl-B850 abolishes the structural assembly of the complex. In chapter 4, the contribution of the phytol tails to the pigment-protein function and structural assembly have been examined by mutagenesis, enzymatic digestion as well as the statistical analyses on available high-resolution structures.

Study of the role of BChls phytol by mutating protein binding residues

Mutating residues at positions -7 and/or -9 of the β WT to alanine will lead to the destabilisation of LH2 protein by up to 12 °C in membranous environment and 30 °C in β OG. Both the residues are in a close vicinity to the β BChl-B850 phytol tails. This suggests that the peptide-phytol interactions influence the LH2 stability significantly particularly prominent in purified complexes. The protein stability is greatly reduced in both mutants (α WT/ β WT_{-9A} and α WT/ β WT_{-7-9A}) in β OG indicating that the replacement of the lipids by detergent molecules enhances the thermal destabilisation. This is possibly due to a loose packing environment in the

LH2-like complexes and/or defective pigment-protein interactions. The BChls binding sites appear vulnerable to surrounding environmental changes when β Gly -7 and/or β Val -9 are altered. Usually replacement of membrane lipids by β OG results in an increase of LH2 thermal stability; this is observed in wild type as well as mutant α WT/ β WT_{-20A} (see chapter 5, figure 5-21). Curiously, it is not the case for α WT/ β WT_{-9A} and α WT/ β WT_{-7-9A}, perhaps indicating that residues -7 and -9 of the β -subunit participate in proper packing within the hydrophobic transmembrane region. Native membrane lipid may ‘protect’ the impaired hydrophobic packing surfaces which become exposed upon lipid removal.

Mutating the residues at positions -7 and -9 of β WT may disturb the proper position of phytol tails within the protein; in particular, the assembly of BChl-B800. It has been shown in the LH2 high-resolution structure that the macrocycle of BChl-B800 has in many contacts with the β BChl-B850 phytol tail (figure 6-3). The BChl-B800 binding is therefore susceptible to the modification of the phytol tail. The experimental data shows that the BChl-B800 absorbance and energy transfer are reduced in both the α WT/ β WT_{-9A} and α WT/ β WT_{-7-9A} mutants, indicating the loss of BChl-B800 upon mutating the residues in the vicinity of the BChl-B850 phytol tail. Due to the complexity of the system, it is not possible to distinguish whether the thermal destabilisation of LH2 is due to the loss of bound BChl-B800, improper position of β BChl-B850 phytol tail, improper interaction with membrane lipids or a combination of these possibilities.

Surprisingly, mutating β Val -9 to alanine does not lead to a strong destabilisation of LH2 complex and/or significant changes of complex assembly. From structural modelling, significant losses of protein-phytol interactions were observed when valine -9 is mutated to alanine. β Val -9 may not be that crucial for the structural assembly of LH2. A large destabilising effect is observed in the double-point mutant (α WT/ β WT_{-7-9A}). Unfortunately, examination of α WT/ β WT_{-7A} mutant has not been achieved despite many attempts. The difficulties encountered during the β Gly -7 mutation to alanine and the expression of the mutant α WT/ β WT_{-7A} are rather surprising, it is important to investigate this further in order to gain insight on the relative roles of residues -7 and -9.

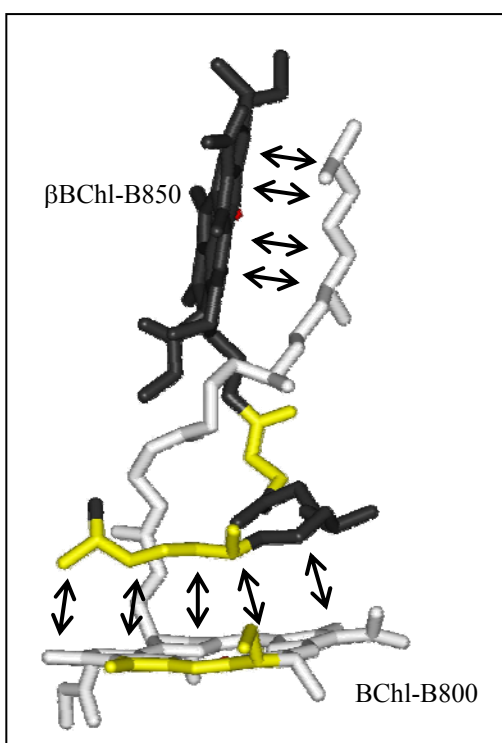


Figure 6-3: Illustration of interactions between the pigments β BChl-B850 and BChl-B800 based on the high-resolution structure of *Rsp acidophila* (McDermott *et al.*, 1995). β BChl-B850 is displayed in black and BChl-B800 is displayed in white (α BChl-B850 is not displayed here for clarity). Contacts made by glycine at positions -7 and valine at -9 of β -subunit within a radius of ≤ 5 Å are displayed in yellow (both the residues are not displayed for clarity). Arrows indicate the close interactions between the phytyl chain and macrocycle.

Removal of BChl phytyl tails in assembled LH2 by enzymatic digestion

The aim of this section is to study the role of phytyl tails to the assembled LH2 by an enzymatic approach. By mutating residues in the close vicinity of the phytyl of β BChl-B850, it has been shown to eliminate proper LH2 assembly. However, clear conclusions from these experiments could not be drawn due to the multitude of possibilities. By Chlase digestion, we aimed at removing the attachment of phytyl tails to the BChl in the assembled complex and study the consequences on the functional and structural properties of LH2.

Upon Chlase treatment, the BChl-B850 CD signal is red-shifted and LH2 complex is thermally destabilised. Mainly BChlide *a* (~89 %) but little BChl *a* is detected in the isolated pigments after Chlase treatment. This suggests that the removal of phytyl by Chlase in the isolated LH2 destabilised the LH2 complex and this further supports the notion that the phytyl tails has functional role in LH2 protein stability.

In the enzymatic experiment, the application of Chlase in the presence of acetone hydrolysed the C17³ ester bond. BChls' macrocycles appears to be still in place after the incubation, as most of the red-most BChls absorbance remained in the sample. This suggests that the BChl's macrocycles are more or less held in position by interactions with the surrounding polypeptide and/or pigments. Moreover, the removal of the phytol tails does not disturbed the interactions between BChl-B850's macrocycle and polypeptides, in the assembled LH2 complex. However, the separation of BChl's macrocycles and phytol tails leads to the destabilisation of LH2, due to either improper LH2 packing and/or loss of pigments (in particular BChl-B800).

To the best of our knowledge, no *in vivo* Chlase experiment has been conducted on the assembled LH2 complexes. The only similar investigation has been in Tanaka *et al.*, (1983) who reported on Chlase treatment of BChls-proteins of *Rsp rubrum* membranes. However, the results are not comparable, as *Rsp rubrum* lacks LH2 complex and the BChls consist of geranylgeraniol rather than phytol. In addition, the complex stability and assembly were not monitored in this investigation. LH2 complexes have been suggested to be more susceptible to the changes in the phytol tails than LH1 complexes (Bollivar *et al.*, 1994; Loach & Parkes-Loach, 1995; Addelee & Hunter, 1999). Yet, the basis for this is still not understood. Possibly, the phytol tails contribute more to tight pigment packing in the hydrophobic environment of LH2 complex.

This study presents the first experimental evidence that the removal of phytyl tails in the assembled LH2 complex results in destabilisation of LH2 structure. This implicates a critical role of the phytol chains for the structural stability of LH2 antenna, as previously proposed by various studies (e.g. Bollivar *et al.*, 1994; Addelee & Hunter, 2002). BChlide and/or phytol tails may still be present in the assembled complex due to its interactions with the polypeptides. However, the pigment arrangement has been affected and there is a reduction in T_m value, a shift in the BChls' CD signal and destabilisation of LH2 complex. Nevertheless, we cannot exclude the possibility that the destabilisation of LH2 complex might be largely the result of loss of bound BChl-B800 in the treated sample. At this stage,

we are unable to clearly attribute the observed effect on the structural stability to the loss of phytol tails alone.

The hydrolysis product of the bound BChls by Chlase has been found to be primarily BChlide. Nearly 89 % of BChls were found to be hydrolysed. The conversion of BChl is solely measured by TLC. Loss of the phytol chains *per se* does not involve a significant change in the BChl absorption spectra (Rüdiger & Schoch, 1991; Fiedor *et al.*, 2003). At the present time, it is not certain whether the Chlase activity is wearing off after the initial 35 min of incubation or whether the remaining esterifying alcohol moiety is well buried in the membrane and are not expose to the enzyme.

Statistical analyses of α - and β -ligated (B)Chls

The statistic study is aimed at increasing the understanding of the phytol/protein interactions by analysing a large BChl-binding data set. In a recent study, the importance of the stereochemical ligation of the Chls' macrocycles in Chl-proteins has been recognised (Balaban *et al.*, 2002). There appear to be non-random distribution patterns of these two distinctly ligated (B)Chls molecules (Balaban *et al.*, 2002). It was found that the Chl molecules preferentially bind to the protein from one side (α type) and much less from the other side (β type). The α - to β -ligated Chls ratio is 82:14 in PSI reaction centre (Jordan *et al.*, 2001) and 5:2 in the Fenna-Matthews-Olson (FMO) antenna complex (Camara-Artigas *et al.*, 2003). The role of the diastereotopic distinctly ligated (B)Chls is still under dispute (Balaban *et al.*, 2002; Garcia-Martin *et al.*, 2006a). PSI provides a large pigment database with nearly 100 Chl molecules and thus an in depth analysis of the phytol-protein interactions may provide further insights to the role of the diastereotopic distinctly ligated (B)Chls, in particular the phytol moiety.

From the preliminary analysis, the binding characteristics of phytol tails of these two ligated-Chls are found to be different. In particular, the β -ligated (B)Chls binds to their own binding helix while little or no such interactions are found in the α -ligated (B)Chls (in both PSI and LH2). Apart from the suggestions that absorption

maximum of β -ligated (B)Chls more red-shifted (Balaban, 2003) and the C13¹ oxo groups more involve in H-bonding to adjacent helices (Garcia-Martin *et al.*, 2006a); β -ligated (B)Chls may also play a role in protein assembly and are likely to govern specific interactions with the protein (Garcia-Martin *et al.*, 2006a).

In α - and β -ligated Chls, the residues Phe, Trp and Leu are the three most interactive amino acids. It is interesting to note that both Phe and Trp are aromatic compounds. It has been suggested that aromatic amino acid residues in integral membrane proteins and peptides are not uniformly distributed (Ippolito *et al.*, 1990). Furthermore, these residues tend to be localised toward the membrane interface and are involved in H-bonding. The data derived from this analysis provides a useful system for future study of the role of these aromatic amino acid residues in pigment-protein structure and function by substitution or deletion.

The carbon atoms of α - and β -ligated Chls' phytol tails have a different contact pattern with the surrounding amino acids. C1 and C4 carbon atoms of α -ligated Chls have the clearly the highest interaction frequency with amino acids; whereas C4, C9, C11, C14, C19 and C20 have nearly equal number of interactions with amino acids in β -ligated Chls. Moreover, contacts with residue Phe are mostly concentrated in the beginning of the phytol chain in α -ligated Chls, while in β -ligated Chls, high number of contacts are found between Phe residues and the middle section of the phytol chain. It is fascinating to reveal the diverse pattern of interactions in these two diastereotopic ligated Chls. Future work may lead to further insights into the role of phytol tails in the assembly of the pigment-binding proteins.

Part II: Protein-lipid and pigment-lipid interactions in model and native light-harvesting complex 2

Chapter 5: Study of the relationship between Rb sphaeroides LH2 protein-lipid interactions and ICM morphology

The importance of membrane lipids to protein function and assembly has generally been recognised; however, little is known about the molecular basis of protein-lipid interactions and their physiological significance. Transmembrane protein complexes interact with lipid bilayers in complex and multifaceted ways. Previous works have shown that LH2 complex is essential for the formation of fully vesicularised ICM in purple bacterium *Rb sphaeroides* (e.g. Kiley *et al.*, 1988; Hunter *et al.*, 1988; Verméglio & Joliot, 1999). These studies suggest that the complete maturation of ICM requires the presence of the fully assembled B800-850 complex and a functional *pucC* gene is necessary for the expression of its apoprotein (Lang & Hunter, 1994). The molecular factors underlying this interdependence are still not understood. Here, LH2-lipid interactions and their influences on ICM morphology were investigated without the interference of other pigment-protein complexes in the native membranes of modified *Rb sphaeroides*.

At first, the occurrence of ICM in response to LH2 expression has been confirmed in *Rb sphaeroides* DD13 strain. Typical vesicular invaginations of ICM appeared upon the expression of LH2 WT complex (WT DD13) and suggest that LH2 can trigger ICM invagination and its effect on the membrane is independent of RC and LH1. Concurrently, when LH2 assembly is significantly impaired (as in $\alpha\text{AL}_{-4\text{S}}/\beta\text{AL}$), morphogenesis of the ICM becomes arrested at a tubular stage. Hitherto, tubular ICM morphology has only been reported for LH2 null mutants that express only LH1 and RC (Kiley *et al.*, 1988). These findings show that LH2 expression and assembly are closely linked to membrane biogenesis and morphology in *Rb sphaeroides* DD13 strain. The incorporation of LH2 coordinates the formation of ICM, moreover, the ‘fitness’ of the proteins to assemble into stable LH2 influences ICM morphology.

The second observation is that ICM invagination is accompanied by changes in phospholipid compositions of the cells membranes in *Rb sphaeroides* DD13 strain. In all samples, PC, PE and PG are the predominant phospholipids with major acyl-chains of 36:2. The nonbilayer-forming PE is the most abundant phospholipid and accounts for approximately two and four times the amount of PC and PG respectively. The relative proportions of these phospholipids in *Rb sphaeroides* cells determined in earlier works fluctuated significantly. For example, Al-Bayatti & Takemoto (1981) failed to find PC, whereas ~11 % was reported by Russell & Harwood, (1979) and ~23 % by Birrell *et al.* (1978). This divergence may be explained by the variations in culture conditions and methods of lipid analysis. Nevertheless, in these early studies, and in the unmodified *Rb sphaeroides* 2.4.1 strain grown photosynthetically, PE is found to be most abundant.

The ratio of bilayer/nonbilayer-forming phospholipids (PC+PG/PE) in the cellular membranes of DD13 and DD13 expressing LH2 WT is different: the PC+PG/PE ratio is decreased in DD13 WT and a fall is thus associated with LH2 expression and ICM formation. In contrast, in tubular ICM of α AL_{4S}/ β AL, the PC+PG/PE ratio is increased. In addition, fatty-acyl chains of PC and PE are found to be similar in DD13 and DD13 WT, whilst changes in PE fatty-acyl chain composition but not in PC were found in α AL_{4S}/ β AL. In cells with tubular ICM and LH2 α AL_{4S}/ β AL, a reduction in nonbilayer lipid content is observed while the content of shorter saturated acyl-chains (such as 29:0; 30:0; 31:0 and 33:1) were increased. Both alterations support the stabilisation of a more bilayer type of lipid arrangement as there present in the tubular membranes of α AL_{4S}/ β AL (Weislander *et al.*, 1980).

Taken together, these findings suggest that PE appears to be particularly important during the biogenesis of photosynthetic membrane of *Rb sphaeroides*. The abundances of PE in the vesicularised ICM and its modulation in abnormal ICM support its importance. One may speculate that LH2 directly affects the level of nonbilayer-forming phospholipid, PE, which in turn alters membrane properties such as curvature and shape. However, further issues must be taken into account while attempting to draw a conclusion from such observations. The changes in ICM morphology observed in cells expressing the model LH2 is likely due to a manifold

of factors, such as abnormal LH2 levels, alteration in nonbilayer to bilayer phospholipids ratio and changes in acyl chain. Changes in membrane compositions therefore cannot be attributed to the changes in mutant protein alone. Bacteria are capable of regulating their phospholipid biosynthesis to maintain membrane bilayer stability (Wieslander *et al.*, 1980; Goldfine *et al.*, 1987). Nonbilayer phospholipids like PE destabilises bilayer formation (Goldfine, 1984; van den Brink-van der Laan *et al.*, 2004a, 2004b; Lee, 2004); it is likely that its synthesis is under strict regulation. However, this issue is not within the scope of my thesis. Rather, the focus is on the correlation of LH2 expression level and PE biosynthesis. For this reason, we consider the possibility that the morphological and compositional changes observed could be directly or indirectly related to LH2 protein.

The tendency of a membrane to appear as nonbilayer forms is essential to a variety of cellular events (Goldfine, 1984; Dowhan, 1997; Mukherjee & Maxfield, 2004; Lee, 2004; McMahon & Gallop, 2005). This tendency is tightly regulated by varying the ratio of bilayer (PC or PG) to nonbilayer-forming lipids (PE) in the membrane (Dowhan, 1997). In most photosynthetic bacteria, this corresponds to the PC+PG/PE ratio (Lee, 2003, 2004). Both membrane proteins (van den Brink-van der Laan *et al.*, 2004b) and bilayer-forming phospholipids (Cullis & de Kruijff, 1979; Goldfine, 1984) are known to counter the nonbilayer-forming tendency of PE. During ICM formation in DD13 WT, PC+PG/PE ratio declined as LH2 is expressed. This suggests that the demands for bilayer-forming phospholipids are reduced since the presence of additional membrane proteins is adequate to 'stabilise' the presence of PE. In addition, the highly curved ICM invaginations are stabilised by PE and the right mixture of PC, PG, PE and membrane protein is required for producing ideal membrane curvature and surface to harbour the light-harvesting apparatus.

On the other hand, PC+PG/PE ratio is increased in the α AL_{-4S}/βAL mutant. It is possible that the mutant LH2 complex is unable to counter the nonbilayer-forming effects of PE, because its assembly is impaired, and thereby the LH2 level in the membrane is significantly reduced. As a response, the bacteria may alter its lipid contents in order to maintain membrane stability. This may explain the higher PC,

PG concentrations observed and the decreased in PE fatty-acyl chain volume (i.e. shorter chain length and higher saturation). It is important to emphasise, however, that nonbilayer lipids (such as PE) play an important role in membrane curvature (Dowhan, 1997; van den Brink-van der Laan *et al.*, 2004b; Lee, 2004) and their relative amounts are usually very high in biological membranes (Brown, 1997; Cronan, 2003; Liu Y *et al.*, 2004; Lee, 2004). Its unique characteristics are not shared or exchangeable with neither PC nor PG lipids. The low concentration of PE, the modification of its acyl-chain composition and the abnormal LH2 complex, α AL_{-4S}/ β AL, all concur with the tubular ICM morphology. This shows again that PE, ICM morphology and LH2 are tightly linked to one another.

The third observation is based on the analysis of LH2 boundary phospholipid compositions. Here, we assume that lipids found attached to LH2 complex are representative of the boundary lipids (Russell *et al.*, 2002; Lee, 2004; and chapter 5 introduction). Relatively few lipids are still attached to isolated LH2 protein (data shown in appendix 4). Approximately seven times more PE than PC molecules were found in isolated LH2 and no PG was detected. This suggests that PE is preferentially accumulated in the LH2 boundary lipids and is closely associated with LH2. In addition to the altered phospholipid composition, the percentage of the major fatty-acyl chains of PE attached to LH2 was significantly different from those in the bulk lipids. In the bulk lipids, ~80 % were of the 36:2 acyl-chains and in the boundary lipids merely ~60 % were of the 36:2 acyl-chains, in agreement with the earlier MS analysis of the boundary lipids of LH2 from *Rsp acidophila* (Russell *et al.*, 2002). This indicates that specific PE accumulates around LH2, and that these boundary lipids form a distinct shell. Previously, it has been shown that the acyl moiety of lipids remaining bound to isolated LH2 is distinctively different from the acyl moiety of the bulk lipids (Russell *et al.*, 2002). While it is not known yet which role these lipids play, it suggests that selective protein-lipid interactions take place at the LH2-lipid interface.

Taken together, the three findings suggest that (1) LH2 assembly and levels in the membrane affect the ICM biogenesis and morphology. (2) LH2 complex levels in the membrane are linked to the phospholipid composition, particularly the

nonbilayer-forming phospholipid, PE. (3) LH2 complex primarily accumulates PE in its close vicinity. In essence, it is shown that expression of LH2 results in membrane invaginations, possibly related to increased levels of PE which are selectively accumulated around LH2.

PG is generally regarded to be important too, as it is the only common phospholipids found in photosynthetic membrane of both bacteria and higher plants (Webb & Green, 1991; Yang *et al.*, 2005). Some studies suggest that PG plays a structural role in pigment-protein complexes, such as partaking in dimerisation of PSII (Kruse *et al.*, 2000), molecular organisation of PSI (Yang *et al.*, 2005) and stability of LHCII trimer (Liu Z *et al.*, 2004). The phosphodiester and hydroxyl groups of PG are also capable of forming hydrogen-bonds and ionic interaction with the side chains of positively charged amino acids (Liu Z *et al.*, 2004). However, PE is more favourable in forming these bonds than PG particularly with negatively charged residues. In addition, our results show that PG is not present in detectable amount in isolated LH2. This is in keeping with the recent finding in *Rsp acidophila* by Russell *et al.*, (2002).

The ESI-MS data suggests that PE is closely association with LH2 and thus PE is addressed further in my studies of lipid-protein interactions. As mentioned earlier, conclusions can be difficult to make in view of possible compensatory bacterial responses to the largely destabilised model LH2 complex and severely altered ICM. The following series of investigations is aimed at minimising the structural and stability defects in LH2. Site-directed and limited changes are thus made and addressed specifically towards putative protein-lipid interaction sites.

The fourth observation revolves around the putative sites of LH2-lipid interactions (figure 6-4). Based on a number of independent indications (see chapter 5 for details), the amino acid glutamate at position -20 of the β -subunit was proposed as a good candidate for interactions with the surrounding boundary lipids.

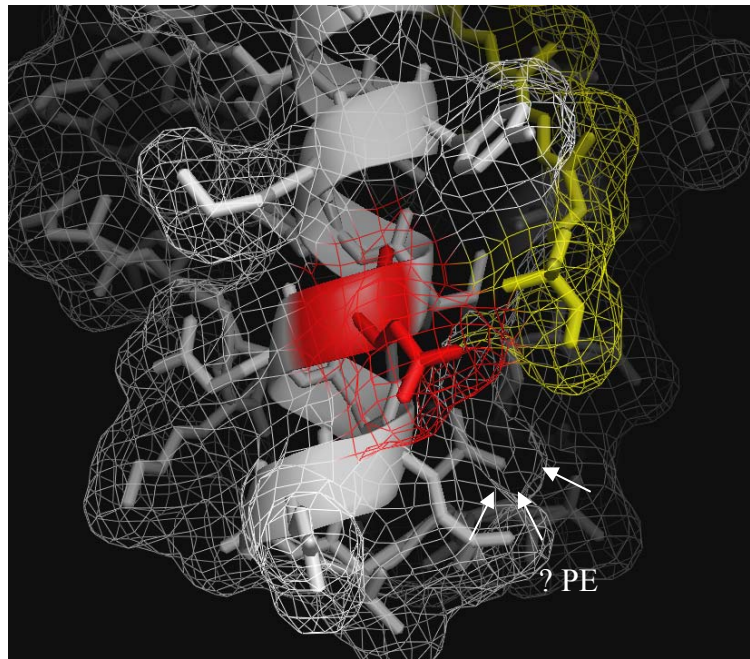


Figure 6-4: Illustration of LH2 protein-lipid interface. The residue -20 glutamate (red) and carotenoid, spheroidenone (yellow) are located at the lipid-protein boundary. A cleft is present (indicated by arrows), where a potential boundary lipid-protein interaction can occur. The figure is modelled in PyMol Viewer version 0.98 (DeLano Scientific LLC, South San Francisco, California, USA).

The replacement of glutamate with alanine (DD13 α WT/ β WT_{-20A}) did neither affect LH2 assembly, LH2 function nor ICM morphology. Notably, the phospholipids composition in close vicinity of LH2 but not in the bulk membrane was altered as compared to the compositions of LH2 WT in *Rb sphaeroides* DD13 strain. In isolated LH2, the bilayer/nonbilayer-forming phospholipids ratio increased and alterations of the PE acyl-chain composition was observed. The results suggest that upon mutating β Glu -20, the selectivity for PE as surrounding boundary lipids has been somehow impaired.

The fifth observation revolved around the role of the carotenoid for the LH2 protein-lipid interactions. The polar methoxy and keto carbonyl groups of spheroidenone (DD13 strain) which are negatively charged and may also potentially form strong interactions with the positively charged PE amine group are absent in the case of neurosporene (DG2 strain). The modification of carotenoid at the putative lipid-protein interaction site (DG2 WT) affects neither the LH2 assembly nor function.

The ICM morphology and lipid composition of the membranes remain unchanged. In the membrane, the protein-pigment complex thermal stabilities were nearly identical for DD13 WT and DG2 WT. However, the thermal stability of isolated WT containing neurosporene as carotenoid was reduced (Table 6-1). This suggests that in the presence of the WT carotenoid the membrane asserts a stabilising effect on LH2 assembly compared to detergent; perhaps by close interactions between the lipids and the carotenoid polar end group, thus shielding it from surrounding water molecules in the lipid headgroup region.

Samples	Thermal stability, T_m (°C)		Presence or absence of changes in intact cells relative to DD13 WT	
	Membrane	Micelles	PC+PG/PE ratio	PE acyl-chain
DD13 α WT/ β WT _{-20A}	71	77	✗	✗
DD13 WT	74	81	-	-
DG2 WT	74	72	✗	✗
DG2 α WT/ β WT _{-20A}	74	64	✗	✓

Table 6-1: Summary of LH2 and α WT/ β WT_{-20A} thermal stabilities and phospholipid compositions. Ticks indicate that changes were observed and crosses indicate that no changes were observed in comparison to DD13 WT. Significant changes are shown in red.

The final observation is based on the changes observed in LH2 by alteration of both the amino acid residue and carotenoid at the putative site of protein-lipid interactions (DG2 α WT/ β WT_{-20A}). Upon alteration: (1) LH2 α WT/ β WT_{-20A} containing neurosporene, assembly and function are nearly identical to LH2 WT containing spheroidenone, indicating that the complex assembly has not been significantly disturbed. (2) The thermal stability of isolated complex (64 °C) was however, severely reduced compared to LH2 WT, LH2 α WT/ β WT_{-20A} containing spheroidenone or LH2 WT containing neurosporene (table 6-1). Interestingly, no such thermal destabilisation was observed prior to purification from the membrane, indicating that membrane lipids assert a stabilising effect. (3) The hydrocarbon

compositions of the bulk membrane lipids were altered while the headgroup composition and thus the PC+PG/PE ratio remained unchanged. It is important to note that no changes in lipid compositions were found upon exchange of carotenoids or mutation of β Glu -20 alone. Curiously, in the lipid membrane of the doubly modified LH2, the content of the major 36:2 acyl-chain was significantly reduced, and longer acyl-chains were increased. Possibly, alterations in LH2 affect the fatty-acyl chain biosynthesis. However, in the boundary lipids of isolated LH2 WT, the amount of these longer acyl-chains in PE was also increased as compared to the relative amount in bulk lipids. This may indicate that LH2 has some elevated affinity for longer acyl-chains. This affinity may be compromised in α WT/ β WT_{-20A} containing neurosporene but needs further investigations. (4) The ICM morphology of DG2 α WT/ β WT_{-20A} is affected, beside the normal sized vesicles (≤ 55 nm), large vesicles (≥ 55 nm) are found in these cells. The impaired stability of DG2 α WT/ β WT_{-20A} may result in reduced assembled LH2 in the membrane. The total protein content relative to LH2 WT content is slightly increased (1.5x), indicating a minor reduction of the LH2 level in these membranes. In a previous work, it has been shown that decreasing the LH2 content results in enlargement of *Rb sphaeroides* chromatophores (Sturgis & Niederman, 1996). However, in this study, it has been shown that doubling the LH2 content resulted in a decrease of a few nanometres in the chromatophores diameter (from 37 to 41 nm). In my study, the significant enlargement in diameter (up to 90 nm) observed for the vesicular invaginations of DG2 α WT/ β WT_{-20A} is unlikely to be due to the slight reduction in LH2 level in the membrane, rather it appears to be either directly related to the altered protein-lipid interface or related to the alterations of fatty-acyl chain compositions in the membrane lipids.

These data supports the idea of a specific LH2 protein-lipid inter-relationship. We propose that the amino acid residue at the position -20 of β -subunit together with the polar group of the carotenoid form a binding site for the headgroup of membrane lipids, in particular PE. This protein-lipid interaction is thus specific and determines the composition of boundary lipids that interact closely with LH2. Possibly, the lipid also interacts with the hydrocarbons of the carotenoid, which need further examination.

Modifications of the proposed lipid binding site (DG2 α WT/ β WT_{-20A}) (figure 6-4) did not significantly affect the structure or function of LH2. In particular, while in the native lipids environment, the thermal stability of the mutant remained similar to DD13 WT. However, the PC and PE acyl chains (chain length and saturation) have been found altered in the membranes of DG2 α WT/ β WT_{-20A}. When DD13 WT and DG2 α WT/ β WT_{-20A} mutant were isolated from the membrane, the thermal stability of the latter dropped significantly by 17 °C. The severe reduction of the T_m value is rather unusual, considering the absence of significant changes in LH2 assembly. Our interpretation to this is that the membrane lipids contribute to the structural stability of LH2. Upon modification of the putative lipid binding site, the contribution of membrane lipid to the complex stability maybe modified, likely due to a weakened interaction between the PE and the LH2 complex.

Removal of the carboxyl group of the glutamate and the methoxy and keto groups of spheroidenone may abolish the potential hydrogen-binding or electrostatic-interactions with the amine group of PE. Consequently, binding of the lipids at the cleft boundary may be weakened and easily washed away during delipidation. This may account for the pronounced difference in T_m . A good candidate for the protein-lipid interaction is PE. Its headgroup but not that of PC may participate in H-bonding interactions with suitable groups of the polypeptide. In addition, phospholipid headgroup were shown to influence integral membrane protein stabilisation by ~18 °C (Maneri & Low, 1988), a value similar to our finding. As mentioned previously, other reasons to consider the involvement of headgroups are: (1) β Glu -20 is potentially located at the level of the membrane surface, adjacent to the lipid headgroup. (2) The cleft region has a net negative charge, which in theory can form hydrogen- or electrostatic-interactions to the PE amine headgroup. Taken together, these findings indicate that the PE headgroup interacts specifically with the region, which is made up by the edge of the β -transmembrane helix, in particular, the β Glu -20 and the end groups of the spheroidenone. However, we cannot conclude that the LH2 stability altered is solely due to the lipid, because of the complexity of supporting interactions.

We know from isolated DD13 WT that LH2 complex selectively accumulates boundary lipids. Concurrently, we observe that the cleft region too has selectivity towards the PE headgroup. Therefore, examination of the boundary lipids is useful for understanding its selectivity. In DD13 α WT/ β WT_{-20A}, significant modifications of its boundary lipids were observed despite the absence of alterations in its bulk lipids. It would be interesting to examine the boundary lipids in LH2 DG2 α WT/ β WT_{-20A}. However, we have been unsuccessful despite many attempts. Based on all the current evidences, the boundary lipids of these mutants are likely to be altered as well.

Another interesting finding in DG2 α WT/ β WT_{-20A} is the alteration of its ICM morphology; large vesicular forms were observed. This morphology is similar to the carotenoidless *Rb sphaeroides* R26.1 strain (Drews & Golecki, 1995). Possibly, the binding cleft in this mutant is similarly disrupted and large ICM are formed. The precise association between ICM and photosynthetic protein syntheses is not known. The concentrations of total protein relative to LH2 in α WT/ β WT_{-20A} DD13 and DG2 strains are increased by a factor of 1.3 and 1.5 respectively in comparison to the WT, despite the absence of notable differences in their structural stabilities. Large ICM tubules or sheets are often correlated with a high lipid-to-protein ratio (Chory *et al.*, 1983). We cannot exclude some modifications in α WT/ β WT_{-20A} complex assembly/expression but these appear to be fairly limited. However, how a single binding cleft could alter ICM morphology is uncertain. It has been suggested that biomembranes, especially photosynthetic membranes, are not simply lipid bilayers where proteins are randomly distributed. Instead, these membranes are organised and differentiated into mini-compartments (Karrash *et al.* 1995; Drews, 1996). It was speculated that the insertion of photosynthetic proteins forms mini-membrane compartments, which are vital to the formation of ICM. Our study here supports this notion. LH2 is important for ICM formation in RC and LH1 deficient *Rb sphaeroides*. Specific LH2 sites seem to determine the composition of its surrounding boundary lipids, in essence, forming a mini-compartment. Therefore, if LH2 synthesis (α AL_{-4S}/ β AL) or LH2-lipid interactions (DG2 α WT/ β WT_{-20A}) are altered, proper ICM formation will be affected.

All in all, in this chapter, we show the presence of specific interactions between LH2 and membrane lipids. The boundary lipids of LH2 are enriched in PE. We propose the existence of a specific protein lipid interface site in LH2, which preferentially interacts with PE headgroup. This lipid-protein interaction is involved in determining membrane ICM morphology. This is the first finding demonstrating lipid-LH2 specificity *in vivo*. We hope that this work can be taken further to enhance our understanding of lipid-protein interactions.

Additional notes:

In my thesis, the mosaic $\alpha\beta$ -subunit polypeptides were expressed in *Rb sphaeroides* DD13 or DG2 strains (Burgess *et al.*, 1989; Jones *et al.*, 1992), which are devoid of endogenous BChl binding proteins (LH1⁻, LH2⁻ and RC⁻) but are still capable of BChl synthesis (Jones *et al.*, 1992). In both the strains, the operon *pucBA* is deleted (Burgess *et al.*, 1989), which consists of two structural genes, *pucB* and *pucA*, encoding the β - and α -polypeptides of LH2 complex respectively (Lee *et al.*, 1989). The existence of a second set of LH2 genes (*puc2BA*) has been identified recently in the genome of *Rb sphaeroides* 2.4.1 (Zeng *et al.*, 2003); 16 years after the LH2 genes were first sequenced and expressed (Ashby *et al.*, 1987; Kiley & Kaplan, 1987).

The expression level of *puc2BA* operon is not as high as the *puc1BA* operon, and is dependent upon the *puc1BA* structural genes and the *puc1C* gene. In *puc1BA* mutant, no LH2 complexes were found, despite the presence of the second transcript (Lee *et al.*, 1989; Zeng *et al.*, 2003). In the presence of both the *puc1BA* and *puc2BA* operons, the α -subunits of *puc2A*-encoded polypeptides are not found in the assembled LH2; however, the β -subunits of *puc2B*-encoded polypeptides are known to participate in LH2 formation (Zeng *et al.*, 2003). Relevant to this thesis, the presence of plasmid-borne, severely mutated β -subunits of LH2 complex were observed to abolish any complex formation despite of the presence of genomic β -subunits, *puc2B* (Kwa *et al.* 2004). This indicates that plasmid borne β -subunits instead of genomic β -subunits are principally built into LH2. Expression of mutant

β -subunits was observed by MS analysis of LH2 containing mutated β -subunits (data not shown, analysis performed by colleague). The effect of any modification of β -subunits should therefore be clearly reflected in the assembled LH2.

It is however difficult to determine accurately the amount (if any) of mosaic LH2 consisting of plasmid borne α -subunits and genomic β -subunits. If present, the expression level is expected to be very low. Whether the results of my thesis would be accentuated in the absence of the genomic β -subunits is yet to be determined, and may be decided when *puc2BA* is deleted from the *Rb sphaeroides* genome (experiments are ongoing in the laboratory of Prof. C.N. Hunter, personal communication).

REFERENCES

1. Adamian L., Liang J. (2001) **Helix-helix packing and interfacial pair-wise interactions of residues in membrane proteins.** J. Mol. Biol. 311, 891-907.
2. Adamian L., Liang J. (2002) **Interhelical hydrogen bonds and spatial motifs in membrane proteins: polar clamps and serine zippers.** Proteins 47, 209-218.
3. Addelese H.A., Hunter C.N. (1999) **Physical mapping and functional assignment of the geranylgeranyl-bacteriochlorophyll reductase gene, *bchP*, of *Rhodobacter sphaeroides*.** J. Bacteriol. 181 (23), 7248-7255.
4. Addelese H.A., Hunter C.N. (2002) ***Rhodospirillum rubrum* possesses a variant of the *bchP* gene, encoding geranylgeranyl-bacteriopheophytin reductase.** J. Bacteriol. 184 (6), 1578-1586.
5. Agostiano A., Catucci L., Colafemmina G., Della M., Scheer H. (2000) **Relevance of the chlorophyll phytyl chain on lamellar phase formation and organisation.** Biophys. Chem. 84, 189-194.
6. Akhtar M., Ajaz A.A., Corina D.L. (1984) **The mechanism of the attachment of esterifying alcohol in bacteriochlorophyll *a* biosynthesis.** Biochemistry J. 224, 187-194.
7. Al-Bayatti K.K., Takemoto J.Y. (1981) **Phospholipid topography of the photosynthetic membrane of *Rhodopseudomonas sphaeroides*.** Biochemistry 20, 5489-5495.
8. Allen J.P., Feher G., Yeates T.O., Komya H., Rees D.C. (1987) **Structure of the reaction centre from *Rhodobacter sphaeroides* R-26: the cofactors.** Proc. Natl Acad. Sci. USA 84, 5730-5734.
9. Ashby M.K., Coomber S.A., Hunter C.N. (1987) **Cloning, nucleotide sequence and transfer of genes for the B800-850 light-harvesting complex of *Rhodobacter sphaeroides*.** FEBS Lett. 209, 83-86.
10. Bahatyrova S., Frese R.N., Siebert C.A., Olsen J.D., van der Werf K.O., van Grondelle R., Niederman, R.A., Bullough P.A., Otto C., Hunter C.N. (2004) **The native architecture of a photosynthetic membrane.** Nature 430, 1058-1062.
11. Balaban T.S. (2003) **Are syn-ligated (bacterio)chlorophyll dimers energetic traps in light-harvesting systems?** FEBS Lett. 545, 97-102.
12. Balaban T.S., Fromme P., Holzwarth A.R., Krauss N., Prokhorenko VI. (2002) **Relevance of the diastereotopic ligation of magnesium atoms of chlorophylls in Photosystem I.** Biochim. Biophys. Acta 1556, 197-207.
13. Bandilla M., Ucker B., Ram M., Simonin I. I., Gelhaye E., McDermott G., Cogdell R.J., Scheer H. (1998) **Reconstitution of the B800 bacteriochlorophylls in the**

- peripheral light harvesting complex B800-850 of *Rhodobacter sphaeroides* 2.4.1 with BChl *a* and modified (bacterio)chlorophylls.** *Biochim. Biophys. Acta* 1364, 390-402.
14. Belrhali H., Nollert P., Royant A., Menzel C., Rosenbusch J.P., Landau E.M., Pebay-Peyroula E. (1999) **Protein, lipid and water organisation in bacteriorhodopsin crystals: a molecular view of the purple membrane at 1.9 Å resolution.** *Structure* 7, 909-917.
 15. Birrell G.B., Siström W.R., Griffith O.H. (1978) **Lipid-protein associations in chromatophores from the photosynthetic bacterium *Rhodospseudomonas sphaeroides*.** *Biochemistry* 17, 3768-3773.
 16. Bligh E.G., Dyer W.J. (1959) **A rapid method of total lipid extraction and purification.** *Can. J. Biochem. Physiol.* 37, 911-917.
 17. Bogdanov M., Dowhan W. (1998) **Phospholipid-assisted protein folding: phosphatidylethanolamine is required at a late step of the conformational maturation of the polytopic membrane protein lactose permease.** *EMBO J.* 17, 5255-5264.
 18. Boggs J.M. (1980) **Intermolecular hydrogen bonding between lipids: influence of organisation and function of lipids in membranes.** *Can. J. Biochem.* 58, 755-770.
 19. Boggs J.M. (1987) **Lipid intermolecular hydrogen bonding: influence on structural organisation and membrane function.** *Biochim. Biophys. Acta.* 906, 353-404.
 20. Bollivar D.W., Wang S., Allen J.P., Bauer C.E. (1994) **Molecular genetic analysis of terminal steps in bacteriochlorophyll *a* biosynthesis: characterization of a *Rhodobacter capsulatus* strain that synthesizes geranylgeraniol-esterified bacteriochlorophyll *a*.** *Biochemistry* 33, 12763-12768.
 21. Bramley P.M., Machkenzie A. (1988) **Regulation of carotenoid biosynthesis.** *Curr. Top. Cell. Regul.* 29, 291-343.
 22. Branden C., Tooze J. (1999) **Introduction to protein structure.** 2nd ed., Garland publishing.
 23. Braun P., Olsen J.D., Strohmam B., Hunter C.N., Scheer H. (2002) **Assembly of light-harvesting bacteriochlorophyll in a model transmembrane helix in its natural environment.** *J. Mol. Biol.* 318, 1085-1095.
 24. Braun P., Vegh A.P., von Jan M., Strohmam B., Hunter C.N., Robert B., Scheer H. (2003) **Identification of intramembrane hydrogen bonding between 13(1) keto group of bacteriochlorophyll and serine residue alpha27 in the LH2 light-harvesting complex.** *Biochim. Biophys. Acta* 1607, 19-26.
 25. Braun P., von Heijne G. (1999) **The aromatic residues Trp and Phe have different effects on the positioning of a transmembrane helix in the microsomal membrane.** *Biochemistry* 38, 9778-9782.

26. Brown A.E., Lascelles J (1972) **Phytol and bacteriochlorophyll synthesis in *Rhodopseudomonas sphaeroides***. J Plant Physiol. 50, 747-749.
27. Brown A.E., Eiserling F.A., Lascelles J. (1972) **Bacteriochlorophyll synthesis and the ultrastructure of wild type and mutant strains of *Rhodopseudomonas sphaeroides***. J Plant Physiol. 50, 743-746.
28. Brown M.F. (1997) **Influence of nonlameller-forming lipids on rhodopsin**. Curr. Top. Membr. 44, 285-356.
29. Brügger B., Sandhoff R., Wegehingel S., Gorgas K., Malsam J., Helms J.B., Lehmann W.D., Nickel W., Wieland F.T. (2000) **Evidence for segregation of sphingomyelin and cholesterol during formation of COPI-coated vesicles**. J. Cell Biol. 151, 507-518.
30. Brügger B., Graham C., Leibrech I., Mombelli E., Jen A., Wieland F., Morris R. (2004) **The membrane domains occupied by glycosylphosphatidylinositol-anchored prion protein and Thy-1 differ in lipid composition**. J. Biol. Chem. 279, 7530-7536.
31. Brunisholz R.A., Zuber H. (1988) **Primary structure analysis of bacterial antenna polypeptides: correlation of aromatic amino acids with spectral properties. Structural similarities with reaction centre polypeptides**. In Photosynthetic light-harvesting systems (Scheer H., Schneider S. Eds.), pp, 1103-1114, Berlin, Germany: Walter de Gruyter.
32. Burgess J.G., Ashby M.K., Hunter C.N. (1989) **Chromosomal deletion of genes encoding B800-850 (LH2) polypeptides of *Rhodobacter sphaeroides***. J. General. Microb. 135, 1809-1816.
33. Bylina E.J., Robles S.J., Youvan D.C. (1988) **Directed mutations affecting the putative bacteriochlorophyll-binding sites in light-harvesting I antenna of *Rhodobacter capsulatus***. Isr. J. Chem. 28, 73-78.
34. Cain B.D., Deal C.D., Fraley R.T., Kaplan S. (1981) ***In vivo* intermembrane transfer of phospholipids in the photosynthetic bacterium *Rhodopseudomonas sphaeroides***. J. Bacteriol. 145, 1154-1166.
35. Camara-Artigas A., Brune D., Allen J.P. (2002) **Interactions between lipids and bacterial reaction centres determined by protein crystallography**. Proc. Natl. Acad. Sci. USA 99, 11055-11060.
36. Camara-Artigas A., Blankenship R.E., Allen J.P. (2003) **The structure of the FMO protein from *Chlorobium tepidum* at 2.2 Å resolution**. Photosynth. Res. 75, 49-55.
37. Caple M.B., Chow H.C., Strouse C.E. (1978) **Photosynthetic pigments of green sulphur bacteria. The esterifying alcohols of bacteriochlorophylls *c* from *Chlorobium limicola***. J. Biol. Chem. 253, 6730-3737.
38. Chang C.H., Tiede D., Tang J., Smith U., Norris J., Schiffer M. (1986) **Structure of *Rhodopseudomonas sphaeroides* R-26 reaction centre**. FEBS Lett. 205, 82-86.

REFERENCES

39. Chang M.C., Callahan R.M., Parker-Loach P.S., Cotton T., Loach P.A. (1990) **Spectroscopic characterization of the light-harvesting complex *Rhodospirillum rubrum* and its structural subunit.** *Biochemistry* 29, 421-429.
40. Cherezov V., Clogston J., Papiz M.Z., Caffrey M. (2006) **Room to move: crystallizing membrane proteins in swollen lipidic mesophases.** *J. Mol. Biol.* 357, 1605-1618.
41. Chiba Y., Aiga I., Idemori M., Satoh Y., Matsushita K., Sasa T. (1967) **Studies on chlorophyllase of *Chlorella protothecoides*.** *Plant Cell Physiol.* 8, 23-635.
42. Choma C., Gratkowski H., Lear J. D., DeGrado W. F. (2000) **Asparagine-mediated self-association of a model transmembrane helix.** *Nat. Struct. Biol.* 7, 161-166.
43. Chory J., Donohue T.J., Varga A.R., Staehelin L.A., Kaplan S. (1984) **Induction of the photosynthetic membranes of *Rhodospseudomonas sphaeroides*: Biochemical and morphological studies.** *J. Bacteriol.* 159, 540-554.
44. Clayton R.K., Clayton B.J. (1981) **B850 pigment-protein complex of *Rhodospseudomonas sphaeroides*: extinction coefficient, circular dichroism and the reversible binding of bacteriochlorophyll.** *Proc. Natl. Acad. Sci. USA* 78, 5583-5587.
45. Clayton R.K., Haselkorn R. (1972) **Protein components of bacterial photosynthetic membranes.** *J. Mol. Biol.* 68, 97-105.
46. Cogdell R.J., Durant I., Valentine J., Lindsay J.G., Schmidt K. (1983) **The isolation and partial characterisation of the light-harvesting pigment-protein complexes of *Rhodospseudomonas acidophila*.** *Biochim. Biophys. Acta* 722, 427-435.
47. Cogdell R.J., Hawthornthwaite A.M. (1993) **Preparation, purification and crystallization of purple bacteria antenna complexes.** In *The Photosynthetic Reaction Centre Volume 1.* (Deisenhofer J., Norris J.R. Eds.) pp 23-42, Academic Press, Inc., California.
48. Cogdell R.J., Fyfe P.K., Barrett S.J., Prince S.M, Freer A.A., Isaacs N.W., McGlynn P., Hunter C.N. (1996) **The purple bacterial photosynthetic unit.** *Photosyn. Res.* 48, 55-63.
49. Cogdell R.J., Isaacs N.W., Freer A.A., Howard T.D., Gardiner A.T., Prince S.M., Papiz M.Z. (2003) **The structural basis of light-harvesting in purple bacteria.** *FEBS Lett.* 555, 35-39.
50. Cogdell R.J., Lindsay J.G. (2000) **The structure of photosynthetic complexes in bacteria and plants: an illustration of the importance of protein structure to the future development of plant science.** *New Phytol.* 145, 167-196.
51. Cogdell R.J., Scheer H. (1985) **Circular dichroism of light-harvesting complexes from purple photosynthetic bacteria.** *Photochem. Photobiol.* 42, 669-678.
52. Cohen-Bazire G., Sistrom W.R., Stanier R.Y. (1959) **Kinetic studies of pigment synthesis by non-sulphur purple bacteria.** *J. Cell. Comp. Physiol.* 49, 25-68.

53. Coleman W.J., Youvan D.C. (1990) **Spectroscopic analysis of genetically modified photosynthetic reaction centres.** *Annu. Rev. Biophys. Biophys. Chem.* 19, 333-367.
54. Conn P.R., Schalch W., Truscott T.G. (1991) **The singlet oxygen and carotenoid interaction.** *J. Photochem. Photobiol. Biol.* 11, 41-48.
55. Conroy M.J., Westerhuis W.H.J., Parker-Loach P.S., Loach P.A., Hunter C.N., Williamson M.P. (2000) **The solution structure of *Rhodobacter sphaeroides* LH1 β reveals two helical domains separated by a more flexible region: structural consequences for the LH1 complex.** *J. Mol. Biol.* 298, 83-94.
56. Cronan J.E. (2003) **Bacterial membrane lipids: where do we stand?** *Annu. Rev. Microbiol.* 57, 203-224.
57. Crouse J.B., Feldman R.P., Clayton R.K. (1963) **Accumulation of polyene precursors of neurosporene in mutant strains of *Rhodospseudomonas sphaeroides*.** *Nature (London)* 198, 1227-1228.
58. Cullis P.R., de Kruijff B. (1979) **Lipid polymorphism and the functional roles of lipids in biological membranes.** *Biochim. Biophys. Acta* 559, 399-420.
59. Davis C.M., Parkes-Loach P.S., Cook C.K., Meadows K.A., Bandilla M., Scheer H., Loach P.A. (1996) **Comparison of the structural requirements for bacteriochlorophyll binding in the core light-harvesting complexes of *Rhodospirillum rubrum* and *Rhodobacter sphaeroides* using reconstitution methodology with bacteriochlorophyll analogs.** *Biochemistry* 35, 3072-3084.
60. Deisenhofer J., Epp O., Miki K., Huber R., Michel H. (1985) **X-ray structure analysis at 3 Å resolution of a membrane protein complex: folding of the protein subunits in the photosynthetic reaction centre from *Rhodospseudomonas viridis*.** *Nature* 318, 618-624.
61. Dekker J.P., Boekema E.J. (2005) **Supramolecular organisation of thylakoids membrane proteins in green plants.** *Biochim. Biophys. Acta* 1706, 12-39.
62. Derewenda Z.S., Lee L., Derewenda U. (1995) **The occurrence of C-H...O hydrogen bonds in proteins.** *J. Mol. Biol.* 252, 248-262.
63. Desiraju G.R. (2002) **Hydrogen bridges in crystal engineering: interactions without borders.** *Acc. Chem. Res.* 35, 565-573.
64. Dewa T., Yamada T., Ogawa M., Sugimoto M., Mizuno T., Yoshida K., Nakao Y., Kondo M., Iida K., Yamashita K., Tanaka T., Nango M. (2005) **Design and expression of cysteine-nearing hydrophobic polypeptides and their self-assembling properties with bacteriochlorophyll a derivatives as a mimic of bacterial photosynthetic antenna complexes. Effect of steric confinement and orientation of the polypeptides on the pigment/polypeptide assembly process.** *Biochemistry* 44, 5129-5139.
65. Dowhan W. (1997) **Molecular basis for membrane phospholipid diversity: why are there so many lipids?** *Annu. Rev. Biochem.* 66, 199-232.

REFERENCES

66. Drazkiewicz M. (1994) **Chlorophyllase: occurrence, functions, mechanism of action, effects of external and internal factors.** *Photosynthetica* 30, 321-331.
67. Drews G. (1996) **Forty-five years of developmental biology of photosynthetic bacteria.** *Photosynth. Res.* 48, 325-352.
68. Drews G., Oelze J. (1981) **Organisation and differentiation of membranes of phototrophic bacteria.** *Adv. Microb. Physiol.* 22, 1-92.
69. Drews G., Golecki J.R. (1995) **Structure, molecular organization and biosynthesis of membranes of purple bacteria.** In *Anoxygenic Photosynthetic Bacteria* (Blankenship R.E., Madigan M.T., Bauer C.E., Eds.) pp 231-257, Kluwer Academic Publishers, The Netherlands.
70. Dumas F., Lebrun M.C., Tocanne J.F. (1999) **Is the protein/lipid hydrophobic matching principle relevant to membrane organisation and functions?** *FEBS Lett.* 458, 271-277.
71. Dunker A.K., Jones T.C. (1978) **Proposed knobs-into-holes packing for several membrane proteins.** *Memb. Biochem.* 2, 1-16.
72. Ermler U., Fritsch G., Buchanan S.K., Michel H. (1994) **Structure of the photosynthetic reaction centre from *Rhodobacter sphaeroides* at 2.65 Å resolution: cofactors and protein-cofactor interactions.** *Structure* 2, 925-936.
73. Evans J.R. (1989) **Photosynthesis and nitrogen relationships in leaves of C3 plants.** *Oecologia* 78, 9-19.
74. Fang J., Barcelona M.J., Semrau J.D. (2000) **Characterisation of methanotrophic bacteria on the basis of intact phospholipid profiles.** *FEMS Microbiol. Lett.* 189, 67-72.
75. Fang Z.Y., Bouwkamp J.C., Solomos T. (1998) **Chlorophyllase activities and chlorophyll degradation during leaf senescence in non-yellowing mutant and wild type of *Phaseolus vulgaris* L.** *J. Exptl. Botany* 49, 503-510.
76. Feniouk B.A., Cherepanov D.A., Voskoboynikova N.E., Mulkidjanian A.Y., Junge W. (2002) **Chromatophore vesicles of *Rhodobacter capsulatus* contain on average one F₀F₁-ATP synthase each.** *Biophys. J.* 82, 1115-1122.
77. Fiedor L., Rosenbach-Belkin V., Scherz A. (1992) **The stereospecific interaction between chlorophylls and chlorophyllase. Possible implication for chlorophyll biosynthesis and degradation.** *J. Biol. Chem.* 267, 22043-22047.
78. Fiedor L., Stasiek M., Mysliwa-Kurdizerl B., Strzalka K. (2003) **Phytol as one of the determinants of chlorophyll interactions in solution.** *Photosynth. Res.* 78, 47-57.
79. Fleming G.R., van Grondelle R. (1997) **Femtosecond spectroscopy of photosynthetic light-harvesting systems.** *Curr. Opin. Struct. Biol.* 7, 738-748.
80. Fowler G.J.S., Gardiner A.T., Mackenzie R.C., Barratt S.J., Simmons A.E., Westerhuis W.H.J., Cogdell R.J., Hunter C.N. (1995) **Heterologous expression of**

- genes encoding bacterial light-harvesting complexes in *Rhodobacter sphaeroides*.** J. Biol. Chem. 270, 23875-23882.
81. Fowler G.J.S., Hess S., Pullerits T., Sundstrom V., Hunter C.N. (1997) **The role of β Arg-10 in the B800 bacteriochlorophyll and carotenoid pigment environment within the light harvesting LH2 complex of *Rhodobacter sphaeroides*.** Biochemistry 36, 11282-11291.
 82. Fowler G.J.S., Visschers R.W., Grief G.G., van Grondelle R., Hunter C.N. (1992) **Genetically modified photosynthetic antenna complexes with blue-shifted absorbance bands.** Nature 355, 848-850.
 83. Fraker P.J., Kaplan S. (1972) **Isolation and characterisation of a bacteriochlorophyll-containing protein from *Rhodospseudomonas sphaeroides*.** J. Biol. Chem. 247, 2732-2737.
 84. Fraley R.T., Jameson D.M., Kaplan S. (1978) **The use of the fluorescent probe α -parinaric acid to determine the physical state of the intracytoplasmic membranes of the photosynthetic bacterium, *Rhodospseudomonas sphaeroides*.** Biochim. Biophys. Acta 511, 52-69.
 85. Fraley R.T., Yen G.S.L., Lueking D.R., Kaplan S. (1979) **The physical state of the intracytoplasmic membrane of *Rhodospseudomonas sphaeroides* and its relationship to the cell division cycle.** J. Biol. Chem. 254, 1987-1991.
 86. Francis G.A., Richards W.R. (1980) **Localisation of photosynthetic membrane components in *Rhodospseudomonas sphaeroides* by a radioactive labelling procedure.** Biochemistry 19, 5104-5111.
 87. Frank H.A., Brudvig G. W. (2004) **Redox functions of carotenoids in photosynthesis.** Biochemistry 43, 8607-8615.
 88. Frank H.A., Cogdell R.J. (1993) **Photochemistry and function of carotenoids in photosynthesis.** In Carotenoids in Photosynthesis (Young A., Britton G. Eds.), pp 253-326, Chapman & Hall, London.
 89. Frank H.A., Cogdell R.J. (1997) **Carotenoids in photosynthesis.** Photochem. Photobiol. 63, 257-264.
 90. Freer A.A., Prince S.M., Sauer K., Papiz M.Z., Hawthorthwaite-Lawless A.M., McDermott G. (1996) **Pigment-pigment interactions and energy transfer in the antenna complex of the photosynthetic bacterium *Rhodospseudomonas acidophila*.** Structure 4, 449-462.
 91. Fyfe P.K., Cogdell R.J. (1996) **Purple bacterial antenna complexes.** Cur. Opin. Struct. Biol. 6, 467-472.
 92. Fyfe P.K., Isaacs N.W., Cogdell R.J., Jones M.R. (2004) **Disruption of a specific molecular interaction with a bound lipid affects the thermal stability of the purple bacterial reaction centre.** Biochim. Biophys. Acta 1608, 11-22.

93. Fyfe P.K., McAuley K.E., Roszak A.W., Isaacs N.W., Cogdell R.J., Jones M.R. (2001) **Probing the interface between membrane proteins and membrane lipids by X-ray crystallography.** Trends Biochem. Sci. 26, 106-112.
94. Gall A., Fowler G.J.S., Hunter C.N., Robert B. (1997) **Influence of the protein binding site on the absorption properties of the monomeric bacteriochlorophyll in *Rhodobacter sphaeroides* LH2 complex.** Biochemistry 36, 16282-16287.
95. Gall A., Gardiner A.T., Cogdell R.J., Robert B. (2006) **Carotenoid stoichiometry in the LH2 crystal: no spectral evidence for the presence of the second molecule in the α/β -apoprotein dimer.** FEBS Lett. 580, 3841-3844.
96. Garcia-Martin A., Kwa L.G., Strohmman B., Robert B., Holzwarth A.R., Braun P. (2006a) **Structural role of (bacterio)chlorophyll ligated in the energetically unfavourable β -position.** J. Biol. Chem. 281, 10626-10634.
97. Garcia-Martin A., Kwa L.G., von Jan M., Hunter N.C., Braun P. (2006b) **Assembly of model bacteriochlorophyll proteins in the native lipid environment.** In Chlorophylls and Bacteriochlorophylls: Biochemistry, Biophysics, Functions and Applications, Vol. 25, (Grimm B., Porra R.J., Rüdiger W., Scheer H. Eds.), pp 387-396. Springer, Dordrecht, The Netherlands.
98. Geyer T., Helms V. (2006) **A spatial model of the chromatophores vesicles of *Rhodobacter sphaeroides* and the position of the cytochrome bc_1 complex.** Biophys. J. 91, 921-926.
99. Gibson K.D. (1965) **Electron microscopy of chromatophores of *Rhodopseudomonas sphaeroides*.** J. Bacteriol. 90, 1059-1072.
100. Gil T., Ipsen J.H., Mouritsen O.G., Sabra M.C., Sperotto M.M., Zuckermann M.J. (1998) **Theoretical analysis of protein organization in lipid membranes.** Biochim. Biophys. Acta 1376, 245-266.
101. Gillbro T., Cogdell R.J., Sundström (1988) **Energy transfer from carotenoid to bacteriochlorophyll a in the B800-820 antenna complexes from *Rhodopseudomonas acidophila* strain 7050.** FEBS Lett. 235, 169-172.
102. Glaeser J. (2003) ***In situ* metabolism and biogeography of phototrophic Consortia.** PhD thesis, Biology faculty, Ludwig-Maximilians University München, pp 21.
103. Goldfine H. (1984) **Bacterial membranes and lipid packing theory.** J. Lipid Res. 25, 1501-1507.
104. Goldfine H., Johnston N. C., Mattai J. and Shipley G. G. (1987) **Regulation of bilayer stability in *clostridium-butyrlicum* – studies on the polymorphic phase-behavior of the ether lipids.** Biochemistry 26, 2814–2822.
105. Goldsmith J.O., King B., Boxer S.G. (1996) **Mg-coordination by amino acid side chains is not required for assembly and function of the special pair in bacterial photosynthetic reaction centers.** Biochemistry 35, 2421-2428.

106. Golecki J.R., Tadros M.H., Ventura S., Oelze J. (1989) **Intracytoplasmic membrane vesiculation in light-harvesting mutants of *Rhodobacter sphaeroides* and *Rhodobacter capsulatus***. FEMS Microbiol. Lett. 65, 315-318.
107. Golecki J.R., Ventura S., Oelze J. (1991) **The architecture of unusual membrane tubes in the B800-850 light-harvesting bacteriochlorophyll-deficient mutant 19 of *Rhodobacter sphaeroides***. FEMS Microbiol. Lett. 77, 335-340.
108. Goldman E.R., Youvan D.C. (1992) **An algorithmically optimised combinatorial library screened by digital imaging spectroscopy**. Bio/Technology 10, 1557-1561.
109. Gonen T., Chen Y., Sliz P., Hiroaki Y., Fujiyoshi Y., Harrison S.C., Walz T. (2005) **Lipid-protein interactions in double layered two-dimensional AQP0 crystals**. Nature 438, 633-638.
110. Goodwin T.W. (1967) **Terpenoids and chloroplast development**. In Biochemistry of Chloroplasts. (Goodwin T.W., Ed.) Vol. II, pp 721-733, Academic press, New York.
111. Gruner S.M. (1985) **Intrinsic curvature hypothesis for biomembrane lipid composition: A role for nonbilayer lipids**. Proc. Natl. Acad. Sci. USA 82, 3665-3669.
112. Gudowskanowak E., Newton M.D., Fajer J. (1990) **Conformational and environmental effects on bacteriochlorophyll optical spectra: correlations of calculated spectra with structural results**. J. Phys. Chem. 94, 5795-5801.
113. Harlos K., Eibl H. (1981) **Hexagonal phases in phospholipids with saturated chains: Phosphatidylethanolamines and phosphatidic acids**. Biochemistry 20, 2888-2892.
114. Hawthornthwaite A.M., Cogdell R.J. (1991) **Bacteriochlorophyll-binding proteins**. In Chlorophylls (Scheer H., Ed.) pp 493-528, CRC Press, Boca Raton, Florida.
115. Hess S., Chachisvillis M., Timpmann K., Jones M.R., Fowler G.J.S., Hunter C.N., Sundström V. (1995) **Temporally and spectrally resolved subpicosecond energy transfer within LH2 and from LH2 to LH1 in photosynthetic purple bacteria**. Proc. Natl. Acad. Sci. USA 92, 12333-12337.
116. Hiraishi A. (1997) **Transfer of the bacteriochlorophyll b-containing phototrophic bacteria *Rhodopseudomonas viridis* and *Rhodopseudomonas sulfoviridis* to the genus *Blastochloris* gen. nov.** Int. Syst Bacteriol. 47, 217-219.
117. Holden M. (1961) **The breakdown of chlorophyll by chlorophyllase**. Biochem. J. 78, 359-354.
118. Hörtensteiner S. (1999) **Chlorophyll breakdown in higher plants and algae**. Cell. Mol. Life Sci. 56, 330-347.
119. Hu Q.H., Sturgis J.N., Robert B., Delagrave S., Youvan D.C., Niederman R.A. (1998) **Hydrogen bonding and circular dichroism of bacteriochlorophylls in the *Rhodobacter capsulatus* light-harvesting 2 complex altered by combinatorial mutagenesis**. Biochemistry 37, 10006-10015.

120. Hu X., Ritz T., Damjanović A., Autenrieth F., Schulten K. (2002) **Photosynthetic apparatus of purple bacteria**. Quarterly Rev. Biophys. 35, 1-62.
121. Huang J.W., Kaplan S. (1973) **Membrane proteins from *Rhodopseudomonas sphaeroides*. IV. Characterisation of chromatophores proteins**. Biochim. Biophys. Acta 307, 317-331.
122. Hunte C. (2005) **Specific protein-lipid interactions in membrane proteins**. Biochem. Soc. Transactions 33, 938-942.
123. Hunter C.N. (1995) **Genetic manipulation of the antenna complexes of purple bacteria**. In Anoxygenic Photosynthetic Bacteria (Blankenship R.E., Madigan M.T., Bauer C.E., Eds.) pp 473-501, Kluwer Academic Publishers, The Netherlands.
124. Hunter C.N., Hundle B.S., Hearst J.E., Lang H.P., Gardiner A.T., Takaishi S., Cogdell R.J. (1997) **Introduction of new carotenoids into the bacterial photosynthetic apparatus by combining the carotenoid biosynthetic pathways of *Erwinia herbicola* and *Rhodobacter sphaeroides***. J. Bacteriol. 176, 3692-3697.
125. Hunter C.N., Turner G. (1988) **Transfer of genes coding for apoproteins of reaction centre and light-harvesting LH1 complexes to *Rhodobacter sphaeroides***. J. Gen. Microbiol. 134, 1471-1480.
126. Hunter C.N., Pennoyer J.D., Sturgis J.N., Farrelly D., Niederman R.A. (1988) **Oligomerisation states and associations of light-harvesting pigment protein complexes of *Rhodobacter sphaeroides* as analysed by lithium dodecyl-sulfate polyacrylamide-gel electrophoresis**. Biochemistry 27, 3459-3467.
127. Imhoff J.F. (1995) **Taxonomy and physiology of phototropic purple bacteria and green sulphur bacteria**. In Anoxygenic Photosynthetic Bacteria (Blankenship R.E., Madigan M.T., Bauer C.E., Eds.) pp 1-15, Kluwer Academic Publishers, The Netherlands.
128. Imhoff J.F., Bias-Imhoff U. (1995) **Lipids, quinines and fatty acids of anoxygenic phototropic bacteria**. In Anoxygenic Photosynthetic Bacteria (Blankenship R.E., Madigan M.T., Bauer C.E., Eds.) pp 179-205, Kluwer Academic Publishers, The Netherlands.
129. Imhoff J.F., Petri R., Sueling J. (1998) **Reclassification of species of the spiral-shaped phototrophic purple non-sulphur bacteria of the α -proteobacteria: description of the new genera *Phaeospirillum* gen. nov., *Rhodovibrio* gen. nov., *Rhodotalassium* gen. nov. and *Roseospira* gen. nov. as well as transfer of *Rhodospirillum fulvum* to *Phaeospirillum fulvum* comb. nov., of *Rhodospirillum molischianum* to *Phaeospirillum molischianum* comb. nov., of *Rhodospirillum salinarum* to *Rhodovibrio salinarum* comb. nov., of *Rhodospirillum sodomense* to *Rhodovibrio sodomensis* comb. nov., of *Rhodospirillum salexigens* to *Rhodotalassium salexigens* comb. nov. and of *Rhodospirillum mediosalinum* to *Roseospira mediosalina* comb. nov.** Int. Syst. Bacteriol. 48, 793-398.
130. Imhoff J.F., Truper H.G., Pfennig N. (1984) **Rearrangement of the species and genera of the phototropic "purple non sulphur bacteria"**. Int. J. Syst. Bacteriol. 34, 340-343.

-
131. Ippolito J.A., Alexander R.S., Christianson D.W. (1990) **Hydrogen bond stereochemistry in protein structure and function.** *J. Mol. Biol.* 215, 457-471.
132. Ivancich A., Artz K., Williams J. C., Allen J. P., Mattioli T. A. (1998) **Effects of hydrogen bonds on the redox potential and electronic structure of the bacterial primary electron donor.** *Biochemistry* 37, 11812-11820.
133. Jamieson S.J., Wang P., Qian P., Kirkland J.Y., Conroy M.J., Hunter C.N., Bullough P.A. (2002) **Projection structure of the photosynthetic reaction-antenna complex of *Rhodospirillum rubrum* at 8.5 Å resolution.** *EMBO J.*, 21, 3927-3935.
134. Jensen S.L., Cohen-Bazire G., Nakayama T.O., Stanier R.Y. (1958) **The path of carotenoid synthesis in a photosynthetic bacterium.** *Biochim. Biophys. Acta* 29, 477-498.
135. Jensen S.L., Cohen-Bazire G., Stanier R.Y. (1961) **Biosynthesis of carotenoids in purple bacteria: a re-evaluation based on considerations of chemical structure.** *Nature (London)* 192, 1168-1173.
136. Jiang L., Lai L. (2002) **CH...O hydrogen bonds at protein-protein interfaces.** *J. Biol. Chem.* 277, 37732-37740.
137. Jones M.R., Fowler G.J.S., Gibson L.C.G., Grief G.G., Olsen J.D., Crielaard W., Hunter C.N. (1992) **Construction of mutants of *Rhodobacter sphaeroides* lacking one or more pigment-protein complexes and complementation with reaction centre, LH1 and LH2 genes.** *Mol. Microbiol.* 6, 1173-1184.
138. Jones M.R., Fyfe P.K., Roszak A.W., Isaacs N.W., Cogdell R.J. (2002) **Protein-lipid interactions in the purple bacterial reaction centre.** *Biochim. Biophys. Acta* 1565, 206-214.
139. Jordan P., Fromme P., Witt H.T., Klukas O., Saenger W., Krauß N. (2001) **Three-dimensional structure of cyanobacterial photosystem I at 2.5 Å resolution.** *Nature* 411, 909- 917.
140. Jungas C., Ranck J.L., Rigaud J.L., Joliot P., Vermeglio A. (1999) **Supramolecular organisation of the photosynthetic apparatus of *Rhodobacter sphaeroides*.** *EMBO J.* 18, 534-542.
141. Kaplan S., Cain B.D., Donohue T.J., Shepherd W.D., Yen G.S.L. (1983) **Biosynthesis of photosynthetic membranes of *Rhodospseudomonas sphaeroides*.** *J. Cell. Biochem.* 22, 15-29.
142. Karrasch S., Bullough P.A., Ghosh R. (1995) **The 8.5 Å projection map of the light-harvesting complex I from *Rhodospirillum rubrum* reveals a ring composed of 16 subunits.** *EMBO J.* 14, 631-638.
143. Katz J.J., Shipman L.L., Cotton T.M., Janson T.J. (1978) **Chlorophyll aggregation: coordination interactions in chlorophyll monomers, dimers, and oligomers.** In *The Porphyrins* (Dolphin D., Ed.) pp 401-458, Academic Press, New York.
144. Katz J.J., Strain H.H., Harkness A.L., Studier M.H., Svec W.A., Janson T.R., Cope B.T. (1972) **Esterifying alcohols in the chlorophylls of purple bacteria. A new**

- chlorophyll, bacteriochlorophyll (gg), all-trans-geranylgeraniol bacteriochlorophyllide a.** J. Am. Chem. Soc. 94, 7938-7939.
145. Katz J.J., Strain H.H., Leussing D.L., Dougherty R.C. (1968) **Chlorophyll-ligand interactions from nuclear magnetic resonance studies.** J. Am. Chem. Soc. 90, 784-791.
146. Kennis J.T.M., Streltsov A.M., Aartsma T.J., Nozawa T., Ames J. (1996) **Energy transfer and exciton coupling in isolated B800-850 complexes of the photosynthetic purple sulphur bacterium *Chromatium tepidum*. The effect of structural symmetry on bacteriochlorophyll excited states.** J. Phys. Chem. B, 100, 2438-2442.
147. Kenyon C.N. (1978) **Complex lipids and fatty acids in photosynthetic bacteria.** In the Photosynthetic Bacteria. (Clayton R.K., Sistrom W.R., Eds.) pp 281-313, Plenum Press, New York.
148. Kikuchi J., Asakura T., Loach P.A., Parker-Loach P.S., Shimada K., Hunter C.N. (1999) **A light-harvesting antenna protein retains its folded conformation in the absence of protein-lipid and protein-pigment interactions.** Biopolymers 49, 361-372.
149. Kiley P.J., Kaplan S. (1987) **Cloning, sequence and expression of the *Rhodobacter sphaeroides* light-harvesting B800-850 α and B800-850 β genes.** J. Bacteriol. 169, 3268-3275.
150. Kiley P.J., Kaplan S. (1988) **Molecular genetics of photosynthetic membrane biosynthesis in *Rhodobacter sphaeroides*.** Microbiol. Rev. 52, 50-69.
151. Kiley P.J., Varga A., Kaplan S. (1988) **Physiological and Structural Analysis of Light-Harvesting Mutants of *Rhodobacter sphaeroides*.** J. Bacteriol. 170, 1103-1115.
152. Knacker T., Harwood J.L., Hunter C.N., Russell N.J. (1985) **Lipid biosynthesis in synchronised cultures of the photosynthetic bacterium *Rhodospseudomonas sphaeroides*.** Biochem. J. 229, 701-710.
153. Koepke J., Hu X.C., Muenke C., Schulten K., Michel H. (1996) **The crystal structure of the light-harvesting complex II (B800-850) from *Rhodospirillum molischianum*.** Structure 4, 581-597.
154. Koivusalo M., Haimi P., Heikinheimo L., Kostainen R., Somerharju P. (2001) **Quantitative determination of phospholipid compositions by ESI-MS: effects of acyl chain length, unsaturation and lipid concentration on instrument response.** J. Lipid Res. 42, 663-672.
155. Koolhaas M.H.C., Frese R.N., Fowler G.J.S., Bibby T.S., Georgakopoulou S., van der Zwan G., Hunter C.N., van Grondelle R. (1998) **Identification of the upper exciton component of the B850 bacteriochlorophylls of the LH2 antenna complex, using a B800-free mutant of *Rhodobacter sphaeroides*.** Biochemistry 37, 4693-4698.
156. Koyama Y. (1991) **Structures and functions of carotenoids in photosynthetic systems.** Photochem. Photobiol. 9B, 265-280.

-
157. Kruse O., Hankamer B., Konczak C., Gerle C., Morris E., Radunz A., Schmid G., Barber J. (2000) **Phosphatidylglycerol is involved in the dimerisation of photosystem II.** *J. Biol. Chem.* 275, 6509-6514.
158. Kühlbrandt W., Wang D.N., Fujiyoshi Y. (1994) **Atomic model of plant light-harvesting complex by electron crystallography.** *Nature* 367, 614-621.
159. Kwa L.G., Garcia-Martin A., Vegh A., Strohmann B., Scheer H., Robert B., Braun P. (2004) **Hydrogen bonding in a model bacteriochlorophyll-binding site drives assembly of light harvesting complex.** *J. Biol. Chem.* 279, 15067-15075.
160. Laemmli U.K. (1970) **Cleavage of structural proteins during the assembly of the head of bacteriophage T4.** *Nature* 227, 680-685.
161. Lang H.P., Hunter C.N. (1994) **The relationship between carotenoid biosynthesis and the assembly of light-harvesting LH2 complex in *Rhodobacter sphaeroides*.** *Biochem. J.* 298, 197-205.
162. Lascelles J., Szilagy J.F. (1965) **Phospholipid synthesis in *Rhodospseudomonas sphaeroides* in relation to the formation of photosynthetic pigments.** *J. Gen. Microbiol.* 38, 55-64.
163. Lascelles J. (1968) **The bacterial photosynthetic apparatus.** *Adv. Microbiol. Physiol.* 2, 1-42.
164. Law C.J., Roszak A.W., Southall J., Gardiner A.T., Isaacs N.W., Cogdell R.J. (2004) **The structure and function of bacterial light-harvesting complexes.** *Mol. Memb. Biol.* 21, 183-191.
165. Lechevalier M.P. (1977) **Lipids in bacteria taxonomy- a taxonomist's view.** *Crit. Rev. Microbiol.* 7, 109-210.
166. Lee A.G. (2003) **Lipid-protein interactions in biological membranes: a structural perspective.** *Biochim. Biophys. Acta* 1612, 1-40.
167. Lee A.G. (2004) **How lipids affect the activities of integral membrane proteins.** *Biochim. Biophys. Acta* 1666, 62-87.
168. Lee A.G. (2005) **A greasy grip.** *Nature* 438, 569-570.
169. Lee J.K., Kiley P.J., Kaplan S. (1989) **Posttranscriptional control of *puc* operon expression of B800-850 light-harvesting complex formation in *Rhodobacter sphaeroides*.** *J. Bacteriol.* 171, 3391-3405.
170. Liu F., Lewis R.N.A.H., Hodges R.S., McElhaney R.N. (2004) **Effect of variations in the structure of a polyleucine-based α -helical transmembrane peptide on its interaction with phosphatidylethanolamine bilayers.** *Biophys. J.* 87, 2470-2482.
171. Liu Y., Wu Y., Xu C. (2004) **Elimination of polarity in the carotenoid terminus promotes the exposure of B850-binding sites (Tyr 44, 45) and ANS-mediated energy transfer in LH2 complexes of *Rhodobacter sphaeroides*.** *Biochem. Biophys. Res. Commun.* 325, 600-604.

172. Liu Z., Yan H., Wang K., Kuan T., Zhang J., Gui L., An X., Chang W. (2004) **Crystal structure of spinach major light-harvesting complex at 2.72 Å resolution.** *Nature* 428, 287-292.
173. Loach P.A., Parkes-Loach P.S. (1995) **Structure-function relationships in core light-harvesting complexes (LH1) as determined by characterisation of the structural subunit and by reconstitution experiments.** In *Anoxygenic Photosynthetic Bacteria* (Blankenship R.E., Madigan M.T., Bauer C.E., Eds.) pp 437-471, Kluwer Academic Publishers, The Netherlands.
174. Loll B., Raszewski G., Saenger W., Biesiadka J. (2003) **Functional role of C α -H \cdots O hydrogen bonds between transmembrane α -helices in photosystem I.** *J. Mol. Biol.* 328, 737-747.
175. Lommen M.A.J., Takemoto J. (1978) **Ultrastructure of carotenoid mutant strain R26 of *Rhodospseudomonas sphaeroides*.** *Arch. Microbiol.* 118, 305-308.
176. Luecke H., Schobert B., Richter H.T., Cartailler J.P., Lanyi J.K. (1999) **Structure of bacteriorhodopsin at 1.55 Å resolution.** *J. Mol. Biol.* 291, 899-911.
177. MacPherson A.N., Arellano J.B., Fraser N.J., Cogdell R.J., Gillbro T. (2001) **Efficient energy transfer from the carotenoid S (2) state in a photosynthetic light-harvesting complex.** *Biophys. J.* 80, 923-930.
178. Maneri L.R., Low P.S. (1988) **Structural stability of the erythrocyte anion transporter, band 3, in different lipid environments- a differential scanning calorimetric study.** *J. Biol. Chem.* 263, 16170-16178.
179. Marinetti G.V., Cattieu K. (1981) **Lipid analysis of cells and chromatophores of *Rhodospseudomonas sphaeroides*.** *Chem. Phys. Lipids* 28, 241-251.
180. Marsh D., Horvath L.I. (1998) **Structure, dynamics and composition of the lipid-protein interface. Perspectives from spin-labelling.** *Biochem. Biophys. Acta* 1376, 267-296.
181. Marsh D., Páli T. (2006) **Lipid conformation in crystalline bilayers and in crystals of transmembrane proteins.** *Chem. Phys. Lipids* 141, 48-65.
182. Matile P., Schellenberg M., Vicentini F. (1997) **Localisation of chlorophyllase in the chloroplast envelope.** *Planta* 201, 96-99.
183. Mattioli T. A., Lin X., Allen J. P., Williams J. C. (1995) **Correlation between multiple hydrogen bonding and alteration of the oxidation potential of the bacteriochlorophyll dimer of reaction centers from *Rhodobacter sphaeroides*.** *Biochemistry* 34, 6142-6152.
184. Maxwell K., Johnson G.N. (2000) **Chlorophyll fluorescence-a practical guide.** *J. Exp. Bot.* 51, 659-668.
185. McAuley K.E., Fyfe P.K., Ridge J.P., Isaacs N.W., Cogdell R.J., Jones M.R. (1999) **Structural details of an interaction between cardiolipin and an integral membrane protein.** *Proc. Natl. Acad. Sci. USA* 96, 14706-14711.

-
186. McDermott G., Prince S.M., Freer A.A., Hawthornthwaite-Lawless A.M., Papiz M.Z., Cogdell R.J., Isaacs N.W. (1995) **Crystal structure of an integral membrane light-harvesting complex from photosynthetic bacteria.** *Nature* 374, 517-521.
187. McMahon H.T., Gallop J.L. (2005) **Membrane curvature and mechanisms of dynamic cell membrane remodelling.** *Nature* 438, 590-596.
188. Meadows K.A., Iida K., Tsuda K., Recchina R.A., Heller B.A., Antonio B., Nango M., Loach P.A. (1995) **Enzymatic and chemical cleavage of the core light-harvesting polypeptides of photosynthetic bacteria: determination of the minimal polypeptide size and structure required for subunit and light-harvesting complex formation.** *Biochemistry* 34, 1559-1574.
189. Miller K.R. (1979) **Structure of a bacterial photosynthetic membrane.** *Proc. Natl. Acad. Sci. USA* 76, 6415-6419.
190. Montoya G., Cyrklaff M., Sinning I. (1995) **Two-dimensional crystallisation and preliminary structure analysis of light-harvesting II (B800-850) complex from the purple bacterium *Rhodovulum sulfidophilum*.** *J. Mol. Biol.* 250, 1-10.
191. Mukherjee S., Maxfield F.R. (2004) **Membrane domains.** *Annu. Rev. Cell Dev. Biol.* 20, 839-866.
192. Murzyn K., Róg T., Rasenkiewicz-Gierula M. (2005) **Phosphatidylethanolamine-phosphatidylglycerol bilayer as a model of the inner bacterial membrane.** *Biophys. J.* 88, 1091-1103.
193. Nango M. (2006) **Molecular assembly of bacteriochlorophyll complexes using synthetic light-harvesting model polypeptides.** In *Chlorophylls and Bacteriochlorophylls: Biochemistry, Biophysics, Functions and Applications*, Vol. 25, (Grimm B., Porra R.J., Rüdiger W., Scheer H. Eds.), pp 365-373. Springer, Dordrecht, The Netherlands.
194. Niederman R.A., Mallon D.E., Langan J.J. (1976) **Membranes of *Rhodospseudomonas sphaeroides*. IV. Assembly of chromatophores in low aeration cell suspensions.** *Biochim. Biophys. Acta* 440, 429-447.
195. Noy D., Moser C.C., Dutton P.L. (2006) **Bacteriochlorophyll protein maquettes.** In *Chlorophylls and Bacteriochlorophylls: Biochemistry, Biophysics, Functions and Applications*, Vol. 25, (Grimm B., Porra R.J., Rüdiger W., Scheer H. Eds.), pp 349-363. Springer, Dordrecht, The Netherlands.
196. Nussberger S., Dörr K., Wang D.N., Kühlbrandt W. (1993) **Lipid-protein interactions in crystals of plant light-harvesting complex.** *J. Mol. Biol.* 234, 347-356.
197. Oba T., Tamiaki H. (2002) **Which side of the π -macrocycle plane of (bacterio)chlorophylls is favoured for binding the fifth ligand?** *Photosynth. Res.* 74, 1-10.
198. Ohashi N., KoChi A., Kuki M., Shimamura T., Cogdell R.J., Koyama Y. (1996) **The structures of S-0 spheroidene in the reaction centre of *Rhodobacter sphaeroides* 2.4.1 as revealed by Raman spectroscopy.** *Biospectroscopy* 2, 59-69.

199. Olsen J.D., Hunter C.N. (1994). **Protein structure modelling of the bacterial light-harvesting complex**. Photochem. Photobiol. 60, 521-535.
200. Olsen J.D., Sockalingum G.D., Robert B., Hunter C.N. (1994) **Modification of a hydrogen bond to a bacteriochlorophyll *a* molecule in the light-harvesting 1 antenna of *Rhodobacter sphaeroides***. Proc. Natl. Acad. Sci. USA 91, 7124-7128.
201. Olsen J.D., Sturgis J.N., Westerhuis W.H.J., Fowler G.J.S., Hunter C.N., Robert B. (1997). **Site-directed modification of the ligands to the bacteriochlorophylls of the light-harvesting LH1 and LH2 complexes of *Rhodobacter sphaeroides***. Biochemistry 36, 12625-12632.
202. Onishi J.C., Niederman R.A. (1982) ***Rhodopseudomonas sphaeroides* membranes: Alterations in phospholipid composition in aerobically and phototrophically grown cells**. J. Bacteriol. 149, 831-839.
203. Páli T., Garab G., Horváth L. I., Kóta Z. (2003) **Functional significance of the lipid-protein interface in photosynthetic membranes**. Cell. Mol. Life Sci. 60, 1591-1606.
204. Papiz M.Z., Prince S.M., Howard T.D., Cogdell R.J., Isaacs N.W. (2003) **The structural and thermal motion of the B800-850 LH2 complex from *Rps acidophila* at 2.0 resolution and 100K: new structural features and functionally relevant motions**. J. Mol. Biol. 326, 1523-1538.
205. Penfold R.J., Pemberton J.M (1994) **Sequencing, chromosomal inactivation, and functional expression of ppsR, a gene which represses carotenoid and bacteriochlorophyll synthesis in *Rhodobacter sphaeroides***. J. Bacteriol. 176, 2869-2876.
206. Prince S.M., Howard T.D., Myles D.A.A., Wilkinson C., Papiz M.Z., Freer A.A., Cogdell R.J., Isaacs N.W. (2003) **Detergent structure in crystals of the integral membrane light-harvesting complex LH2 from *Rhodopseudomonas acidophila* strain 10050**. J. Mol. Biol. 326, 307-315.
207. Prince S.M., Papiz M.Z., Freer A.A., McDermott G., Hawthornthwaite-Lawless A.M., Cogdell R.J., Isaacs N.W. (1997) **Apoprotein structure in the LH2 complex from *Rhodopseudomonas acidophila* strain 10050: modular assembly and protein pigment interactions**. J. Mol. Biol. 268, 412-423.
208. Pröll S. (2005) **Chlorophyll-Komplexe mit Apo-Myoglobin und Albumin: Präparation, stabilität und Photochemie**. PhD thesis, Biology faculty, Ludwig-Maximilians University München.
209. Quinn P.J., Chapman D. (1980) **The dynamics of membrane structure**. CRC Crit. Rev. Biochem. 8, 1-117.
210. Ranck J.L., Ruiz T., Pehau-Arnaudet G., Arnoux B., Reiss-Husson F. (2001) **Two-dimensional structure of the native light-harvesting complex LH2 from *Rubrivivax gelatinosus* and of a truncated form**. Biochim. Biophys. Acta 1506, 67-78.

-
211. Rao M., Mayor S. (2005) **Use of Forster's resonance energy transfer microscopy to study lipid rafts.** *Biochim. Biophys. Acta* 1746, 221-233.
212. Richter P., Drews G. (1991) **Incorporation of light-harvesting polypeptides into the intracytoplasmic membrane of *Rb capsulatus*.** *J. Bacteriol.* 173, 5336-5345.
213. Ritz T., Park G., Schulten K. (2001) **Kinetics of excitation migration and trapping in the photosynthetic unit of purple bacteria.** *J. Phys. Chem.* 105, 8259-8267.
214. Robert B. (1996) **Resonance Raman studies in photosynthesis-chlorophyll and carotenoid molecules.** In *Biophysical techniques in photosynthesis* (Amez A., Hoff A. Eds.) pp 161-276, Kluwer Academic Publishers, Amsterdam.
215. Robert B., Lutz M. (1985) **Structures of antenna complexes of several *Rhodospirillales* from their resonance Raman spectra.** *Biochim. Biophys. Acta* 807, 10-23.
216. Rohmer M., Bouvier P, Ourisson G. (1979) **Molecular evolution of membranes: structural equivalents and phylogenetic precursors of sterols.** *Proc. Natl. Acad. Sci. USA* 76, 847-851.
217. Roszak A.W., Howard T.D., Southall J., Gardiner A.T., Law C.J., Isaac N.W., Cogdell R.J. (2003) **Crystal structure of the RC-LH1 core complex from *Rhodopseudomonas palustris*.** *Science* 302, 1969-1972.
218. Rouser G., Fleischer S., Yamamoto A. (1970) **Two dimensional thin layer chromatographic separation of polar lipids and determination of phospholipids by phosphorus analysis of spots.** *Lipids* 5, 494-496.
219. Rüdiger W., Schoch S. (1991) **The last steps of Chlorophyll biosynthesis.** In *Chlorophylls* (Scheer H., Ed.) pp 451-489, CRC Press, Boca Raton, Florida.
220. Russell N.J., Coleman J.K., Howard T.D., Johnston E., Cogdell R.J. (2002) ***Rhodopseudomonas acidophila* strain 10050 contains photosynthetic LH2 antenna complexes that are not enriched with phosphatidylglycerol and the phospholipids have a fatty acyl composition that is unusual for purple non-sulphur bacteria.** *Biochim. Biophys. Acta* 1556, 247-253.
221. Russell N.J., Harwood J.L. (1979) **Changes in the acyl lipid composition of photosynthetic bacteria grown under photosynthetic and non-photosynthetic conditions.** *Biochem. J.* 181, 339-345.
222. Rutkauskas D., Olsen J., Gall A., Cogdell R.J., Hunter C.N., van Grondelle R. (2006) **Comparative study of spectral flexibilities of bacterial light-harvesting complexes: structural implications.** *Biophys. J.* 90, 2463-2474.
223. Sambrook J., Fritsch E.F., Maniatis T. (1989) **Molecular cloning- A laboratory manual.** Second edition. Cold spring harbor laboratory press, New York.
224. Sarkhel S., Desiraju G.R. (2004) **N-H...O, O-H...O and C-H...O hydrogen bonds in protein-ligand complexes: strong and weak interactions in molecular recognition.** *Proteins* 54, 247-259.

-
225. Sato N., Hagio M., Wade H., Tsuzuki M. (2000) **Requirement of phosphatidylglycerol for photosynthetic function in thylakoids membranes.** Proc. Natl. Acad. Sci. USA 97, 10655-10660.
226. Savage H., Cyrklaff M., Montoya G., Kühlbrandt W., Sinning I. (1996) **Two-dimensional structure of light harvesting complex II (LHII) from the purple bacterium *Rhodovulum sulfidophilum* and comparison with LHII from *Rhodospseudomonas acidophila*.** Structure 4, 243-252.
227. Scheer H. (1991) **Structure and occurrence of chlorophylls.** In Chlorophylls (Scheer H., Ed.) pp 3-30, CRC Press, Boca Raton, Florida.
228. Scheer H., Hartwich G. (1995) **Bacterial reaction centres with modified tetrapyrrole chromatophores.** Anoxygenic photosynthetic bacteria, pp. 649-663, Dordrecht, Kluwer Academic Publishers.
229. Scheiner S., Kar T., Gu Y. (2001) **Strength of the CaH...O hydrogen bond of amino acid residues.** J. Biol. Chem. 276, 9832-9837.
230. Scheuring S., Reiss-Husson F., Engel A., Rigaud J.L., Ranck J.L. (2001) **High-resolution AFM topographs of *Rubrivivax gelatinosus* light-harvesting complex LH2.** EMBO J. 20, 3029-3035.
231. Scheuring S., Seguin J., Marco S., Levy D., Breyton C., Robert B., Rigaud J.L. (2003) **AFM characterisation of tilt and intrinsic flexibility of *Rhodobacter sphaeroides* light harvesting complex 2 (LH2).** J. Mol. Biol. 325, 569-580.
232. Scheuring S., Francia F., Busselez J., Melandris B.A., Rigaud J.L., Levy D. (2004a) **Structural role of *PufX* in the dimerisation of the photosynthetic core complex of *Rhodobacter sphaeroides*.** J. Biol. Chem. 279, 3620-3626.
233. Scheuring S., Sturgis J.N., Prima V., Bernadac A., Levy D., Rigaud J.L. (2004b) **Watching the photosynthetic apparatus in native membranes.** Proc. Natl. Acad. Sci. USA 101, 11293-11297.
234. Schubert A., Stenstam A., Beenken W.J.D., Herek J.L., Cogdell R., Pullerits T., Sundström V. (2004) ***In vitro* self-assembly of the light harvesting pigment-protein LH2 revealed by ultrafast spectroscopy and electron microscopy.** Biophys. J. 86, 2363-2373.
235. Senes A., Ubarretxena-Belandia I., Engelman D.M. (2001) **The Ca-H...O hydrogen bond: A determinant of stability and specificity in transmembrane helix interactions.** Proc. Natl. Acad. Sci. USA 98, 9056-9061.
236. Shneour E.A. (1962) **Carotenoid pigment conversion in *Rhodospseudomonas sphaeroides*.** Biochim. Biophys. Acta 440, 429-447.
237. Simon R., Preifer U., Puhler A. (1983) **A broad host range mobilization system for *in vivo* genetic engineering: transposon mutagenesis in Gram negative bacteria.** Biotechnology 1, 1596-1603.
238. Singh R.K., Britton G., Goodwin T.W. (1973) **Carotenoid biosynthesis in *Rhodospseudomonas sphaeroides*.** Biochem. J. 136, 413-419.

-
239. Sistrom W.R. (1978) **Control of antenna pigment components**. In *The Photosynthetic bacteria* (Clayton R.K., Sistrom W.R., Eds.), pp 841-848, Plenum Press, New York.
240. Smith K.M. (1991) **The structure and biosynthesis of bacteriochlorophylls**. In *Biosynthesis of tetrapyrroles* (Jordan P.M., Ed.), *New Comprehensive Biochemistry* (Neuberger A., van Deenen L.L.M., Gen. Eds.), pp 237-255, Elsevier Scientific Publishers, Amsterdam.
241. Sorgen P.L., Cahill S.M., Krueger-Koplin R.D., Krueger-Koplin S.T., Schenck C.C., Girvin M.E. (2002) **Structure of the *Rhodobacter sphaeroides* light-harvesting 1 β subunit in detergent micelles**. *Biochemistry* 41, 31-41.
242. Spurr A.R. (1969) **A low-viscosity epoxy resin embedding medium for electron microscopy**. *J. Ultrastruct. Res.* 26, 31-43.
243. Stamouli A., Kafi S., Klein D.C.G., Oosterkamp T.H., Frenken J.W.M., Cogdell R.J., Aartsma T.J. (2003) **The ring structure and organisation of light harvesting 2 complexes in a reconstituted lipid bilayer, resolved by atomic force microscopy**. *Biophys. J* 84, 2483-2491.
244. Stark W., Kühlbrandt W., Wildhaber I., Wehrli E., Muhlethaler K. (1984) **The structure of the photoreceptor unit of *Rhodospseudomonas viridis***. *EMBO J.* 3, 777-783.
245. Sturgis J.N., Jirsakova V., Reiss-Husson F., Cogdell R.J., Robert B. (1995) **Structure and properties of the bacteriochlorophyll binding site in peripheral light-harvesting complexes of purple bacteria**. *Biochemistry* 34, 517-523.
246. Sturgis J.N., Niederman R.A. (1990) **Role of B800-B850 light-harvesting pigment-protein complex in the morphogenesis of *Rhodobacter sphaeroides* membranes**. In *Current research in photosynthesis* (Baltscheffsky M., Ed), pp 57-60, vol. 2, Kluwer, Dordrecht.
247. Sturgis J.N., Niederman R.A. (1996) **The effect of different levels of the B800-850 light-harvesting complex on intracytoplasmic membrane development in *Rhodobacter sphaeroides***. *Arch. Microbiol* 165, 235-242.
248. Subczynski W.K., Markowska E., Gruszecki W.I., Siewewiesiuk J. (1992) **Effects of polar carotenoids on dimyristoylphosphatidylcholine membranes: a spin-label study**. *Biochim. Biophys. Acta* 1105, 97-108.
249. Subczynski W.K., Markowska E., Siewewiesiuk J. (1993) **Spin-label studies on phosphatidylcholine-polar carotenoid membranes: effects of alkyl-chain length and unsaturation**. *Biochem. Biophys. Acta* 1150, 173-181.
250. Sundström V., Pullerits T., van Grondelle R. (1999) **Photosynthetic light-harvesting: reconciling dynamics and structure of purple bacterial LH2 reveals function of photosynthetic unit**. *J. Phys. Chem. B.* 103, 2327-2346.
251. Takaichi S. (1999) **Carotenoids and carotenogenesis in anoxygenic photosynthetic bacteria**. In *The Photochemistry of Carotenoids*. (Frank H.A., Young A.J., Britton

REFERENCES

- G., Cogdell R.J., Eds.) pp 36-69, Kluwer Academic Publishers, Dordrecht, The Netherlands.
252. Takemoto J., Lascelles J. (1973) **Coupling between bacteriochlorophyll and membrane protein synthesis in *Rhodopseudomonas sphaeroides***. Proc. Nat. Acad. Sci. USA 70, 799-803.
253. Tanaka K., Kakuno T., Yamashita J., Horio J. (1982) **Purification and properties of chlorophyllase from greened rye seedlings**. J. Biochem. 92, 1763-1767.
254. Tanaka K., Kakuno T., Yamashita J. (1983) **Action of chlorophyllase purified from rye seedlings on light-harvesting bacteriochlorophyll of chromatophores and spheroplasts from *Rhodospirillum rubrum***. J. Biochem. 93, 159-167.
255. Terpstra W., Lambers J.W.J. (1983) **Incorporation of chlorophyll and chlorophyllase into artificial membranes**. Photobiochem. Photobiophys. 6, 93-100.
256. Theiler R., Suter F., Zuber H., Cogdell R.J. (1984) **A comparison of the primary structures of the two B800-850 apoproteins from wild type *Rhodopseudomonas sphaeroides* strain 2.4.1 and a carotenoidless mutant strain R26.1**. FEBS Lett. 175, 231-237.
257. Tocanne J.F., Teissié J. (1990) **Ionisation of phospholipids and phospholipid-supported interfacial lateral diffusion of protons in membrane model systems**. Biochim. Biophys. Acta 1031, 111-142.
258. Tsuchiya T., Suzuki T., Yamada T., Shimada H., Masuda T., Ohta H., Takamiya K. (2003) **Chlorophyllase as a serine hydrolase: identification of a putative catalytic triad**. Plant Cell Physiol. 44, 96-101.
259. van den Brink-van der Laan E., Chupin V., Killian J.A., de Kruijff B. (2004a) **Stability of KcsA tetramer depends on membrane lateral pressure**. Biochemistry 43, 4240-4250.
260. van den Brink-van der Laan E., Killian J.A., de Kruijff B. (2004b) **Nonbilayer lipids affect peripheral and integral membrane proteins via changes in the lateral pressure profile**. Biochim. Biophys. Acta 1666, 275-288.
261. van Grondelle R. (1985) **Excitation energy transfer, trapping and annihilation in photosynthetic systems**. Biochim. Biophys. Acta 811, 147-195.
262. van Grondelle R., Decker J.P., Gillbro T., Sundström V. (1994) **Energy transfer and trapping in photosynthesis**. Biochim. Biophys. Acta Bioenerg. 1187, 1-65.
263. Varga A.R., Staehelin L.A. (1983) **Spatial differentiation in photosynthetic and non-photosynthetic membranes of *Rhodopseudomonas palustris***. J. Bacteriol. 154, 1414-1430.
264. Verméglio A., Joliot P. (1999) **The photosynthesis apparatus of *Rhodobacter sphaeroides***. Trends Microbiol. 7, 435-440.
265. von Heijne G. (1999) **Recent advances in the understanding of membrane protein assembly and structure**. Quart. Rev. Biophys. 32, 285-307.

-
266. Wakao N., Yokoi N., Isoyama N., Hiraishi A., Shimada K., Kobayachi M., Kise H., Iwaki M., Itoh S., Takaishi S., Sakurai Y. (1996) **Discovery of natural photosynthesis using Zn-containing bacteriochlorophyll in an aerobic bacterium *Acidiphilium rubrum*.** Plant Cell Physiol. 37, 889–896.
267. Walz T., Jamieson S.J., Bowers C.M., Bullough P.A., Hunter C.N. (1998) **Projection Structures of Three Photosynthetic Complexes from *Rhodobacter sphaeroides*: LH2 at 6 Å, LH1 and RC-LH1 at 25 Å.** J. Mol. Biol. 282, 833-845.
268. Weast C.A., Mackinney G. (1940) **Chlorophyllase.** J. Biol. Chem. 133, 551-558.
269. Webb M.S., Green B.R. (1991) **Biochemical and biophysical properties of thylakoids acyl lipids.** Biochim. Biophys. Acta 1060, 133-158.
270. Wieslander A., Christiansson A., Rilfors L., Lindblom G. (1980) **Lipid bilayer stability in membranes – regulation of lipid-composition in *Acholeplasma – laidlawii* as governed by molecular shape.** Biochemistry 19, 3650–3655.
271. Willstätter R., Stoll A (1913) **Die Wirkungen der Chlorophyllase.** In Untersuchungen über Chlorophyll, pp 172-187, Springer.
272. Wisniewska A., Subczynski W.K. (1998) **Effects of polar carotenoids on the shape of the hydrophobic barrier of phospholipid bilayer.** Biochim. Biophys. Acta 1368, 235-246.
273. Wood B.J.B., Nichols B.W., James A.T. (1965) **The lipid and fatty acid metabolism of photosynthetic bacteria.** Biochim. Biophys. Acta 106, 261-273.
274. Yang Z., Su X., Wu F., Gong Y., Kuang T. (2005) **Effect of phosphatidylglycerol on molecular organisation of photosystem I.** Biophys. Chem. 115, 19-27.
275. Zadorozhnyi B., Ishchenko I. (1965) **Hydrogen bond energies and band shifts of the stretching vibrations of C:O groups.** Opt. Spectrosc. 19, 306-308.
276. Zeng X.H., Choudhary M. Kaplan S. (2003) **A second and unusual *pucBA* operon of *Rhodobacter sphaeroides* 2.4.1: genetics and function of the encoded polypeptides.** J. Bacteriol. 185, 6171-6184.
277. Zhang W., Bogdanov J., Pi J., Pittard A.J., Dowhan W. (2003) **Reversible topological organisation within a polytopic membrane protein is governed by a change in membrane phospholipid composition.** J. Biol. Chem. 278, 50128-50135.
278. Zhou F.X., Merianos H.J., Brunger A.T., Engelman D.M. (2001) **Polar residues drive association of polyleucine transmembrane helices.** Proc. Natl. Acad. Sci. 98, 2250-2255.
279. Zuber H. (1985) **Structure and function of light-harvesting complexes and their polypeptides.** Photochem. Photobiol. 42, 821-844.
280. Zuber H., Brunisholz R.A. (1991) **Structure and function of antenna polypeptides and chlorophyll-protein complexes: principles and variability.** In Chlorophylls (Scheer H., Ed.) pp 627-703, CRC Press, Boca Raton, Florida.

REFERENCES

281. Zuber H., Cogdell R.J. (1995) **Structure and organisation of purple bacterial antenna complexes.** In *Anoxygenic Photosynthetic Bacteria* (Blankenship R.E., Madigan M.T., Bauer C.E. Eds.) pp 315-348, Kluwer Academic Publishers, The Netherlands.

Nucleotide sequence of *pRKCBC1*:

```

+1  |R| |R| |G| |Y| |Q| |L| |G| |D| |D| |T| |V| |T| |D| |D| |L| |N| |K|
    CGTCGAGGGT ACCAGTTGGG AGACCACACA GTGACTGACG ATCTGAACAA 50
    GCAGCTCCA TGGTCAACCC TCTGCTGTGT CACTGACTGC TAGACTTGT
          KpnI
+1  |V| |W| |P| |S| |G| |L| |T| |V| |A| |E| |A| |E| |E| |V| |H| |K| |Q|
    AGTCTGGCCG AGCGGCCTGA CCGTTGCCGA AGCCGAAGAA GTTCATAAGC 100
    TCAGACCGGC TCGCCGGACT GGCAACGGCT TCGGCTTCTT CAAGTATTCG
+1  |L| |I| |L| |G| |T| |R| |V| |F| |G| |G| |M| |A| |L| |I| |A| |H|
    AACTCATCCT CGGCACCCGC GTCTTCGGTG GCATGGCGCT CATCGCGCAC 150
    TTGAGTAGGA GCCGTGGGCG CAGAAGCCAC CGTACCGCGA GTAGCGCGTG
+1  |F| |L| |A| |A| |A| |A| |T| |P| |W| |L| |G| |K| |E| |K| |L| |D|
    TTCCTCGCCG CCGCTGCGAC CCCGTGGCTC GGCTGATAGG AGAAGCTTGA 200
    AAGGAGCGGC GCGGACGCTG GGCACCGAG CCGACTATCC TCTTCCAAC
          HindIII
+1  |M| |T| |N| |G| |K| |W| |L| |V| |V| |K| |P| |T| |V| |G| |V| |P|
    CATGACCAAC GGCAAAATCT GGCTCGTGGT GAAACCGACC GTCGGCGTTC 250
    GTACTGGTTG CCGTTTTAGA CCGAGACCA CTTTGGCTGG CAGCCGCAAG
+1  |L| |F| |L| |S| |A| |A| |V| |I| |A| |S| |V| |V| |I| |H| |A| |A|
    CGCTGTTCCCT CAGCGCTGCC GTCATCGCCT CCGTCGTTAT CCACGCTGCT 300
    GCGACAAGGA GTCGCGACGG CAGTAGCGGA GGCAGCAATA GGTGCGACGA
+1  |V| |L| |T| |T| |T| |T| |W| |L| |P| |A| |Y| |Y| |Q| |G| |S| |A| |A|
    GTGCTGACGA CCACCACCTG GCTGCCCGCC TACTACCAAG GCTCGGCTGC 350
    CACGACTGCT GGTGGTGGAC CGACGGGCGG ATGATGGTTC CGAGCCGACG
+1  |V| |A| |A| |E| |C| |C| |A| |R| |R| |G| |P| |A| |G| |P| |R| |Q|
    GGTCGCGGCC GAGTAATGCT GCGCAAGGCG CGGGCCTGCG GGCCCACGGC 400
    CCAGCGCCGG CTCATTACGA CGCGTCCGC GCCCGGACGC CCGGGTGGCC
+1  |P| |V| |R| |E| |F| |R| |A| |G| |R| |D| |P| |W| |V| |P| |A| |C|
    AGCCAGTCCG TGAGTTCCGA GCAGCCGGG ATCCTTGGGT TCCGGCCTGC 450
    TCGGTCAGGC ACTCAAGGCT CGTCCGGCCC TAGGAACCCA AGGCCGGACG
          BamHI
+1  |S| |S|
    TCGTCACA
    AGCAGTGT
    500

```

Protein concentration determination assays:

Protein concentrations of wild type (WT) and mutant samples were determined and compared by different protein assay kits from Fluka advance protein assay (Seelze, Germany), Roche ESL protein assay (Basel, Switzerland) and Pierce BSA protein assay (Rockford, IL). All the samples were prepared according to the manufacturer's protocol; and repeated more than three times each.

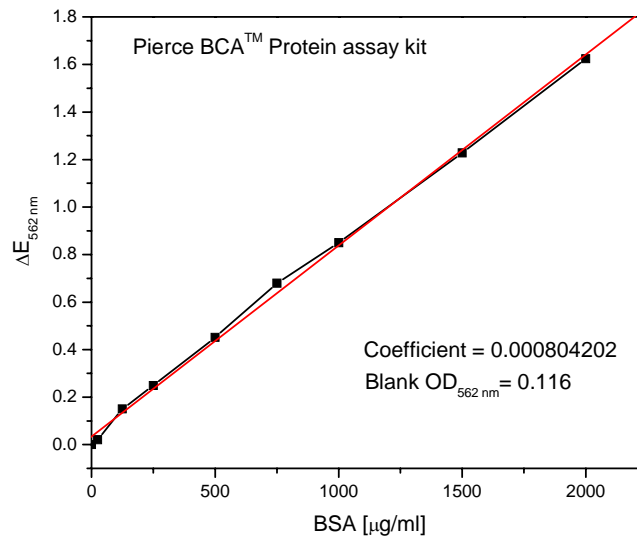


Figure 1: Protein standard obtained from Pierce BCA™ protein assay kit. Linear coefficient is calculated by Origin 7.0.

	Protein Concentration ($\mu\text{g/ml}$):							
	Pierce			Roche		Fluka		OD _{280 nm}
WT	485	280	310	220	172	755	705	117
$\alpha\text{AL}_{\text{S-4}}/\beta\text{AL}$	2500	1600	1720	1750	778	1600	1200	680
$\alpha\text{WT}/\alpha\text{WT}_{-20\text{A}}$	660	430	470	350	450	470	400	150

Table 1: Protein concentrations of *Rb sphaeroides* DD13 strains determined by three different protein determination kits. All the samples were determined in several different dilution factors. Data presented here were calculated from their dilution factors and adjusted to OD_{850 nm} = 1 for comparison.

Protein concentrations of DD13 WT, DD13 $\alpha\text{AL}_{\text{S-4}}/\beta\text{AL}$ and DD13 $\alpha\text{WT}/\alpha\text{WT}_{-20\text{A}}$ were determined by various protein assay kits according to the manufacturers' protocol such as Pierce BCA™ assay kit shown in figure 1. However, variations ($\geq 20\%$) were observed across the measurements and between different assay kits (see table 1). Therefore, the comparison of protein concentration for samples presented in the thesis is not very accurate and should only be considered rough estimation.

Thin layer chromatography for phospholipids determination:

Phospholipids were extracted using the method of Bligh & Dyer (1959). Individual samples were separated by one-dimensional TLC or by two-dimensional TLC using different solvent systems listed below. The running solvents of TLC were prepared in volumes shown in brackets.

Solvent 1: One-dimensional TLC
Chloroform/methanol/water (65/25/4)

Solvent 2: One-dimensional TLC
Chloroform/methanol/acetic acid/ethanol/water (250/80/60/20/5)

Solvent 3: Multiple steps, one-dimensional TLC
1st: Chloroform/methanol/acetic acid (90/10/1);
2nd: Hexane/diethylether/acetone (60/40/5);
3rd: Hexane/diethylether (97/3);
4th: Hexane (100).

Solvent 4: Multiple steps, one-dimensional TLC
1st: Acetone/benzene/water (45/15/4);
2nd: Chloroform/methanol/water (65/25/4);
3rd: Chloroform/acetone/methanol/acetate/water (10/4/2/2/1).

Solvent 5: Two-dimensional TLC
1st: Chloroform/methanol/water (30/10/0.5);
2nd: Chloroform/methanol/33 % ammonia (15/5/1).

For the multiple step methods, the TLC plates were dried completely at room temperature before running each solvent.

Staining reagent:

2 g of FeSO₄ in 120 ml water and 180 mg of KMnO₄ in 80 ml water together with 6 ml of H₂SO₄.

TLC plates (HPTLC silica gel 60, Merck) were heated to ~150 °C after the staining, for ~10 min.

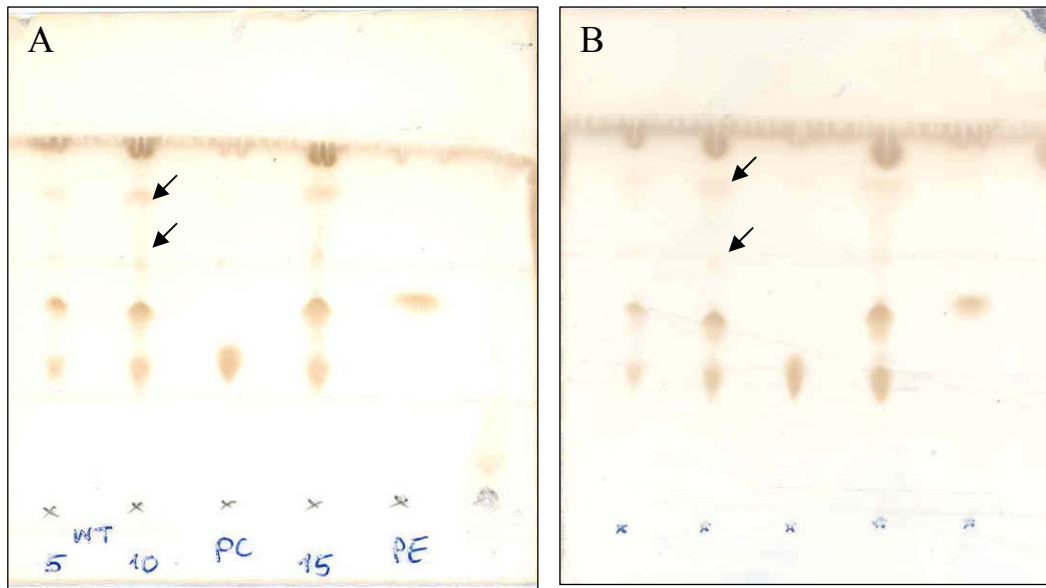


Figure 2: TLC example of samples (A) DD13 WT and (B) α ALS-4/ β AL. The running solvent 1 was used here. Samples applied on the plates are 5 μ g/ml sample, 10 μ g/ml sample, phosphatidylcholine, 15 μ g/ml sample and phosphatidylethanolamine (from left to right).

The identification and quantification of the different phospholipids present in DD13 WT and mutants were carried out by TLC. However, the sensitivity of the method is limited; it is difficult to quantify the relative amounts of phospholipids. Furthermore, additional spots (indicated by arrows) are particularly hard to identify and quantify (figure 2).

Raw data of phospholipids in *Rb sphaeroides* LH2 determined by ESI-MS measurements:

The percentages of phospholipid were derived from the mean values of the phospholipid divided by the total amount of phospholipids (PC+PE+PG) and are presented in percentage.

* The calculation of the percentage of phospholipid was derived from data with the presence of all three phospholipids (PC, PE and PG).

Data shown in italic were not included in the calculation of mean; these results are aberrant and therefore not included.

It is important to note that there are huge variations on the acyl-chain data and the results have to be interpreted with some caution. Further investigations will be required to support these preliminary findings.

Abbreviation used in appendix 4:

Avg	Average
C	Cells
Ch	Chromatophores
n.a.	Not available
n.d.	Not detectable
LD	Represents the internal file names

<i>Rb sphaeroides</i> strains with spheroidenone carotenoid (DD13):																		
Sample	Description	File PC	File PE	File PG	[pmol]			[pmol/ μ l]			PC/PE	Avg [pmol/ μ l]			Total [pmol/ μ l]	Percentage*		
					PC	PE	PG	PC	PE	PG		PC	PE	PG		PC	PE	PG
DD13 WT	C, 28 °C	LD0682	LD0681	n.a.	132.96	358.80	n.a.	13.30	35.88	n.a.								
DD13 WT	C, 28 °C	LD0684	LD0683	n.a.	253.41	676.59	n.a.	12.67	33.83	n.a.								
DD13 WT	C, 28 °C	LD1733	LD1734	LD1864	94.73	253.27	94.96	23.68	63.32	11.87								
DD13 WT	C, 28 °C	LD1736	LD1737	LD1865	177.20	450.93	231.10	22.15	56.37	14.44								
DD13 WT	C, 28 °C	LD2973	LD2974	LD2975	24.70	65.28	18.30	24.70	65.28	18.30								
DD13 WT	C, 28 °C	LD2976	LD2977	LD2978	57.16	143.31	45.07	28.58	71.65	22.54	0.39	24.78	64.16	16.79	105.73	23.44	60.68	15.88
DD13 WT	Ch, 28 °C	LD0678	LD0677	n.a.	87.89	311.94	n.a.	5.86	20.80	n.a.								
DD13 WT	Ch, 28 °C	LD0680	LD0679	n.a.	174.76	676.54	n.a.	5.83	22.55	n.a.								
DD13 WT	Ch, 28 °C	LD1739	LD1740	LD1866	102.14	254.57	83.79	25.54	63.64	10.47								
DD13 WT	Ch, 28 °C	LD1742	LD1743	LD1867	181.17	516.83	178.67	22.65	64.60	11.17								
DD13 WT	Ch, 28 °C	LD2677	LD2678	LD2679	27.39	73.92	28.68	27.39	73.92	28.68								
DD13 WT	Ch, 28 °C	LD2680	LD2681	LD2682	51.15	120.94	46.17	25.58	60.47	23.08	0.39	25.29	65.66	18.35	109.30	23.14	60.07	16.79
α AL _{S-4} / β AL	C, 28 °C	LD1745	LD1746	n.a.	76.88	108.74	n.a.	19.22	27.18	n.a.								
α AL _{S-4} / β AL	C, 28 °C	LD1748	LD1749	n.a.	155.62	174.01	n.a.	19.45	21.75	n.a.								
α AL _{S-4} / β AL	C, 28 °C	LD4342	LD4343	LD3644	32.70	51.72	21.38	32.70	51.72	21.38								
α AL _{S-4} / β AL	C, 28 °C	LD4345	LD4346	LD3647	56.45	84.13	36.47	28.23	42.07	18.24								
α AL _{S-4} / β AL	C, 28 °C	LD4330	LD4331	LD3608	34.51	70.06	20.19	34.51	70.06	20.19								
α AL _{S-4} / β AL	C, 28 °C	LD4333	LD4334	LD3611	53.72	108.66	30.54	26.86	54.33	15.27	0.56	30.57	54.55	18.77	103.89	29.43	52.50	18.07
α AL _{S-4} / β AL	Ch, 28 °C	LD1751	LD1752	n.a.	126.21	310.23	n.a.	31.55	77.56	n.a.								
α AL _{S-4} / β AL	Ch, 28 °C	LD1754	LD1755	n.a.	199.52	510.32	n.a.	24.94	63.79	n.a.								
α AL _{S-4} / β AL	Ch, 28 °C	LD4348	LD4349	LD3546	35.00	62.32	11.92	35.00	62.32	11.92								
α AL _{S-4} / β AL	Ch, 28 °C	LD4351	LD4352	LD3549	75.44	117.19	20.61	37.72	58.59	10.31								
α AL _{S-4} / β AL	Ch, 28 °C	LD4111	LD4112	LD3510	35.38	63.63	13.63	35.38	63.63	13.63								
α AL _{S-4} / β AL	Ch, 28 °C	LD4114	LD4115	LD3513	61.31	112.61	26.34	30.65	56.30	13.17	0.57	34.69	60.22	12.26	107.17	32.37	56.19	11.44

<i>Rb sphaeroides</i> strains with spheroidenone carotenoid (DD13): (continue)																		
Sample	Description	File PC	File PE	File PG	[pmol]			[pmol/ μ l]			PC/PE	Avg [pmol/ μ l]			Total [pmol/ μ l]	Percentage		
					PC	PE	PG	PC	PE	PG		PC	PE	PG		PC	PE	PG
DD13	C, 28 °C	LD0690	LD0689	n.a.	152.61	292.26	n.a.	30.52	58.45	n.a.								
DD13	C, 28 °C	LD0692	LD0691	n.a.	257.60	470.41	n.a.	25.76	47.04	n.a.								
DD13	C, 28 °C	LD1721	LD1859	LD1857	71.92	147.04	76.57	17.98	36.76	9.57								
DD13	C, 28 °C	LD1724	LD1861	LD1858	133.22	298.33	143.41	16.65	37.29	8.96	0.47	17.32	37.03	9.27	63.62	27.22	58.20	14.57
DD13	Ch, 28 °C	LD0686	LD0685	n.a.	142.39	281.07	n.a.	7.12	14.05	n.a.								
DD13	Ch, 28 °C	LD0688	LD0687	n.a.	165.07	370.20	n.a.	4.13	9.26	n.a.								
DD13	Ch, 28 °C	LD1727	LD1728	LD1862	108.51	231.25	93.56	27.13	57.81	11.69								
DD13	Ch, 28 °C	LD1730	LD1731	LD1863	209.77	433.16	189.83	26.22	54.14	11.86	0.48	26.67	55.98	11.78	94.43	28.25	59.28	12.47
LH2 WT	Micelles	LD2133	LD2134	n.d.	10.71	76.59	-	1.07	7.66	-								
LH2 WT	Micelles	LD2135	LD2136	n.d.	22.14	99.05	-	1.11	4.95	-								
LH2 WT	Micelles	LD3991	LD3992	n.d.	7.75	55.84	-	0.78	5.58	-								
LH2 WT	Micelles	LD3994	LD3995	n.d.	14.30	110.08	-	0.72	5.50	-								
LH2 WT	Micelles	LD3997	LD3998	n.d.	8.27	72.65	-	0.83	7.27	-								
LH2 WT	Micelles	LD4000	LD4001	n.d.	21.61	177.54	-	1.08	8.88	-	0.14	0.93	6.64	-	7.57	12.28	87.72	0.00
α WT/ β WT _{-20A}	C, 28 °C	LD2221	LD2222	LD2088	22.56	63.51	92.20	22.56	63.51	9.22								
α WT/ β WT _{-20A}	C, 28 °C	LD2223	LD2224	LD2077	45.67	134.47	124.73	22.84	67.23	6.24								
α WT/ β WT _{-20A}	C, 28 °C	LD2175	LD2176	LD2188	24.86	62.10	110.00	24.86	62.10	11.00								
α WT/ β WT _{-20A}	C, 28 °C	LD2177	LD2178	LD2190	47.56	138.05	187.40	23.78	69.03	9.37								
α WT/ β WT _{-20A}	C, 28 °C	LD3015	LD3016	LD3017	22.53	68.13	23.21	22.53	68.13	23.21								
α WT/ β WT _{-20A}	C, 28 °C	LD3018	LD3019	LD3020	50.83	141.49	51.24	25.41	70.74	25.62								
α WT/ β WT _{-20A}	C, 28 °C	LD2985	LD2986	LD2987	26.02	76.78	21.32	26.02	76.78	21.32								
α WT/ β WT _{-20A}	C, 28 °C	LD2988	LD2989	LD2990	52.82	136.82	35.40	26.41	68.41	17.70								
α WT/ β WT _{-20A}	C, 28 °C	LD4336	LD4337	LD3516	32.32	60.48	14.22	32.32	60.48	14.22								
α WT/ β WT _{-20A}	C, 28 °C	LD4339	LD4340	LD3519	63.51	124.11	30.15	31.75	62.05	15.08	0.39	25.85	66.85	15.30	108.00	23.94	61.90	14.16

<i>Rb sphaeroides</i> strains with spheroidenone carotenoid (DD13): (continue)																		
Sample	Description	File PC	File PE	File PG	[pmol]			[pmol/ μ l]			PC/PE	Avg [pmol/ μ l]			Total [pmol/ μ l]	Percentage		
					PC	PE	PG	PC	PE	PG		PC	PE	PG		PC	PE	PG
α WT/ β WT _{-20A}	Ch, 28 °C	LD3027	LD3028	LD3029	31.41	59.27	18.45	31.41	59.27	18.45								
α WT/ β WT _{-20A}	Ch, 28 °C	LD3030	LD3031	LD3032	59.21	110.66	33.40	29.61	55.33	16.70								
α WT/ β WT _{-20A}	Ch, 28 °C	LD4027	LD4028	LD4029	30.13	66.84	21.68	30.13	66.84	21.68								
α WT/ β WT _{-20A}	Ch, 28 °C	LD4012	LD4013	LD4014	61.59	133.94	36.76	30.80	66.97	18.38								
α WT/ β WT _{-20A}	Ch, 28 °C	LD2991	LD2992	LD2993	26.49	73.38	21.38	26.49	73.38	21.38								
α WT/ β WT _{-20A}	Ch, 28 °C	LD2994	LD2995	LD2996	53.60	143.20	50.46	26.80	71.60	25.23								
α WT/ β WT _{-20A}	Ch, 28 °C	LD4144	LD4145	LD3626	34.06	66.03	19.47	34.06	66.03	19.47								
α WT/ β WT _{-20A}	Ch, 28 °C	LD4147	LD4148	LD3629	55.90	108.94	28.78	27.95	54.47	14.39								
α WT/ β WT _{-20A}	Ch, 28 °C	LD2225	LD2226	LD2079	29.68	50.86	92.97	29.68	50.86	9.30								
α WT/ β WT _{-20A}	Ch, 28 °C	LD2227	LD2228	LD2080	52.64	96.82	164.81	26.32	48.41	8.24								
α WT/ β WT _{-20A}	Ch, 28 °C	LD2179	LD2180	LD2192	20.08	43.65	90.48	20.08	43.65	9.05								
α WT/ β WT _{-20A}	Ch, 28 °C	LD2181	LD2182	LD2194	54.19	97.48	145.34	27.09	48.74	7.27								
α WT/ β WT _{-20A}	Ch, 28 °C	LD2229	LD2230	LD2084	22.68	44.19	56.06	22.68	44.19	5.61								
α WT/ β WT _{-20A}	Ch, 28 °C	LD2231	LD2232	LD2087	43.83	90.22	132.14	21.92	45.11	6.61								
α WT/ β WT _{-20A}	Ch, 28 °C	LD2183	LD2184	LD2195	21.16	39.51	87.73	21.16	39.51	8.77								
α WT/ β WT _{-20A}	Ch, 28 °C	LD2185	LD2186	LD2196	40.42	79.28	104.81	20.21	39.64	5.24	0.47	26.65	54.62	13.49	94.76	28.12	57.64	14.23
α WT/ β WT _{-20A}	Micelles	LD3121	LD3122	n.d.	47.24	105.85	-	4.72	10.58	-								
α WT/ β WT _{-20A}	Micelles	LD3130	LD3131	n.d.	93.28	262.11	-	4.66	13.11	-								
α WT/ β WT _{-20A}	Micelles	LD2886	LD2887	n.d.	12.05	38.61	-	1.21	3.86	-								
α WT/ β WT _{-20A}	Micelles	LD2889	LD2890	n.d.	21.21	68.55	-	1.06	3.43	-	0.38	2.91	7.75	-	10.66	27.34	72.67	0.00

Rb sphaeroides strains with neurosporene carotenoid (DG2):

Sample	Description	File PC	File PE	File PG	[pmol]			[pmol/μl]			PC/PE	Avg [pmol/μl]			Total [pmol/μl]	Percentage		
					PC	PE	PG	PC	PE	PG		PC	PE	PG		PC	PE	PG
DG2 WT	C, 28 °C	LD2242	LD2243	LD2260	19.11	42.16	115.97	19.11	42.16	11.60								
DG2 WT	C, 28 °C	LD2244	LD2245	LD2261	35.62	89.25	205.16	17.81	44.62	10.26	0.42	18.46	43.39	10.93	72.78	25.36	59.62	15.01
DG2 WT	C, 28 °C	LD2704	LD2705	LD2706	32.08	85.62	35.39	32.08	85.62	35.39								
DG2 WT	C, 28 °C	LD2707	LD2708	LD2709	55.13	152.87	60.11	27.57	76.44	30.05								
DG2 WT	Ch, 28 °C	LD2246	LD2247	LD2262	22.55	61.34	104.46	22.55	61.34	10.45								
DG2 WT	Ch, 28 °C	LD2248	LD2249	LD2263	39.09	119.88	223.07	19.55	59.94	11.15								
DG2 WT	Ch, 28 °C	LD2710	LD2711	LD2712	27.30	72.30	24.18	27.30	72.30	24.18								
DG2 WT	Ch, 28 °C	LD2713	LD2714	LD2715	51.03	141.30	48.85	25.51	70.65	24.42	0.36	23.73	66.06	17.55	107.34	22.11	61.54	16.35
αWT/βWT _{-20A}	C, 28 °C	LD2233	LD2234	LD2256	16.04	41.47	132.20	16.04	41.47	13.22								
αWT/βWT _{-20A}	C, 28 °C	LD2236	LD2237	LD2257	33.86	83.15	247.50	16.93	41.57	12.37								
αWT/βWT _{-20A}	C, 28 °C	LD4186	LD4187	LD3668	24.57	56.16	10.57	24.57	56.16	10.57								
αWT/βWT _{-20A}	C, 28 °C	LD4189	LD4190	LD3671	45.08	109.83	21.44	22.54	54.92	10.72	0.41	20.02	48.53	11.73	80.28	24.94	60.46	14.60
αWT/βWT _{-20A}	Ch, 28 °C	LD2265	LD2266	LD2258	24.47	42.63	91.28	24.47	42.63	9.13								
αWT/βWT _{-20A}	Ch, 28 °C	LD2267	LD2268	LD2259	45.14	77.39	188.36	22.57	38.70	9.42								
αWT/βWT _{-20A}	Ch, 28 °C	LD3033	LD3034	LD3035	22.76	72.09	21.83	22.76	72.09	21.83								
αWT/βWT _{-20A}	Ch, 28 °C	LD3036	LD3037	LD3038	44.47	143.04	39.38	22.23	71.52	19.69								
αWT/βWT _{-20A}	Ch, 28 °C	LD4015	LD4016	LD4017	24.97	60.77	15.04	24.97	60.77	15.04								
αWT/βWT _{-20A}	Ch, 28 °C	LD4024	LD4025	LD4026	47.39	120.71	32.02	23.69	60.36	16.01								
αWT/βWT _{-20A}	Ch, 28 °C	LD4192	LD4193	LD3674	21.83	52.59	13.68	21.83	52.59	13.68								
αWT/βWT _{-20A}	Ch, 28 °C	LD4195	LD4196	LD3677	47.25	107.03	23.51	23.62	53.51	11.76	0.43	23.27	56.52	14.57	94.36	24.66	59.90	15.44

DD13 WT: PC acyl chain lengths															
M/Z	PC	Cells, 28 °C							Chromatophores, 28 °C						
		LD000682	LD000684	LD001733	LD001736	LD002973	LD002976	Mean	LD000678	LD000680	LD001739	LD001742	LD002677	LD002680	Mean
678	28:1	1.146	0.644	0.187		0.200	0.104	0.456	0.673	0.372	0.190	0.100	0.242		0.315
688	29:2	0.078			0.023	0.053		0.051	1.651	0.275	0.057		0.109	0.061	0.431
690	29:1	0.147	0.058	0.278	0.140	0.594	0.128	0.224	0.196	0.066	0.259	0.145	0.319	0.241	0.204
692	29:0	0.057	0.061	0.009	0.019		0.005	0.030	0.118	0.078			0.005		0.067
704	30:1	0.214	0.088	0.061	0.045	0.110	0.093	0.102	0.253	0.131		0.042	0.166	0.077	0.134
706	30:0	0.136	0.063	0.035	0.028	0.024		0.057	0.072	0.067	0.038	0.033	0.009		0.044
718	31:1	0.081	0.099	0.027	0.018			0.056	0.228	0.137	0.005				0.123
720	31:0	0.141	0.099	0.031	0.015	0.013		0.060	0.220	0.158	0.002	0.006			0.097
730	32:2	0.214	0.132	0.148	0.143	0.020	0.090	0.125	0.373	0.173	0.149	0.123	0.088	0.156	0.177
732	32:1	0.156	0.221	0.193	0.190	0.301	0.135	0.199	0.336	0.409	0.222	0.138	0.235	0.201	0.257
734	32:0	0.109	0.140	0.096	0.088	0.092		0.105	0.371	0.194	0.083	0.090		0.006	0.149
744	33:2	0.059	0.002	0.012	0.012			0.021	0.220	0.069					0.145
746	33:1	0.058	0.099	0.024	0.030			0.053	0.710	1.188		0.015	0.020		0.483
748	33:0	0.102	0.144	0.021	0.007			0.069	0.269	0.031					0.150
756	34:3			0.035	0.027		0.021	0.028			0.005	0.007			0.006
758	34:2	2.288	2.286	2.694	2.767	4.113	2.539	2.781	3.349	3.056	2.690	2.663	2.473	2.345	2.763
760	34:1	3.395	3.488	5.032	4.844	3.720	2.990	3.911	4.686	4.105	5.018	5.000	2.502	3.009	4.053
762	34:0	0.119		0.213	0.174	0.109	0.095	0.142		0.259	0.201	0.199	0.173		0.208
772	35:2	0.131	0.115	0.112	0.115	0.086	0.127	0.114	0.431	0.387	0.095	0.091	0.678	0.334	0.336
774	35:1	0.238	0.356	0.215	0.222	0.279	0.177	0.248	0.399	0.454	0.197	0.185	0.186	0.159	0.263
784	36:3					0.255	0.069	0.162			0.093	0.052	0.006	0.035	0.047
786	36:2	80.505	81.117	79.722	80.579	76.041	82.340	80.051	74.905	77.381	79.448	80.026	82.635	82.061	79.409
788	36:1	6.878	5.794	6.756	6.516	6.508	5.755	6.368	6.388	5.417	6.698	6.314	4.287	5.323	5.738
790	36:0	0.118	0.546	0.384	0.271	0.162	0.205	0.281	0.387	0.344	0.302	0.227	0.217	0.255	0.288
798	37:3	0.377	0.480	0.433	0.513	0.353	0.345	0.417			0.279	0.257	0.342	0.462	0.335
800	37:2	2.742	3.007	2.079	2.196	3.530	3.351	2.818	4.938	4.444	2.222	2.300	3.504	3.576	3.497
802	37:1		0.402	0.247	0.253	0.351	0.238	0.298	0.570	0.562	0.345	0.327	0.333	0.228	0.394
810	38:4			0.342	0.349	0.767	0.310	0.442			0.175	0.210	0.467	0.507	0.340
812	38:3			0.106	0.099	0.151	0.111	0.117			0.220	0.257	0.066	0.154	0.174
814	38:2	0.545	0.504	0.356	0.369	0.406	0.398	0.429	0.811	0.257	0.316	0.375	0.464	0.372	0.433
816	38:1			0.056	0.046	0.111	0.030	0.061			0.065	0.050	0.026	0.013	0.038
818	38:0			0.056	0.058		0.003	0.039			0.037	0.056		0.028	0.040
826	39:3			0.071	0.088		0.069	0.076			0.050	0.081		0.022	0.051
828	39:2			0.215	0.312	0.253	0.267	0.262			0.509	0.614	0.449	0.353	0.481
830	39:1				0.042	0.057		0.049			0.052			0.022	0.037
832	39:0			0.013	0.013		0.002	0.009				0.009			0.009

DD13 WT: PE acyl chain lengths

M/Z	PE	Cells, 28 °C							Chromatophores, 28 °C						
		LD000681	LD000683	LD001734	LD001737	LD002974	LD002977	Mean	LD000677	LD000679	LD001740	LD001743	LD002678	LD002681	Mean
648	29:1								0.053		0.016			0.011	0.013
660	30:2											0.017			0.017
662	30:1								1.318	0.883	0.021	0.028			0.024
688	32:2	0.071	0.165	0.148	0.246	0.010	0.150	0.132	0.906	0.537	0.215	0.154	0.063	0.257	0.172
690	32:1	0.080	0.082	0.054	0.251	0.201	0.054	0.120	5.597	6.267	0.253	0.268	0.028		0.183
692	32:0	0.493	0.720	0.411	0.373	0.069	0.076	0.357	1.763	2.271	0.407	0.428	0.447	0.072	0.339
704	33:1								5.101	5.975	0.017				0.017
706	33:0								0.682	0.605		0.003			0.003
714	34:3	0.072	0.056		0.010			0.046	0.566	0.241		0.009			0.009
716	34:2	2.110	1.877	2.510	2.949	2.703	2.254	2.400	2.723	2.580	2.590	2.507	2.449	2.060	2.401
718	34:1	5.258	5.465	5.696	5.319	5.572	5.412	5.454	4.985	4.918	8.129	8.248	5.123	4.598	6.524
720	34:0	0.320	0.390	0.873	0.721	0.124	0.355	0.464	0.146	0.307	0.583	0.661	0.392	0.321	0.489
730	35:2	0.069	0.019	0.064	0.078			0.057	1.163	0.874	0.080	0.082	0.070	0.026	0.064
732	35:1	0.338	0.377	0.164	0.240	0.246	0.241	0.268	0.715	0.640	0.219	0.199	0.024	0.200	0.160
734	35:0			0.009	0.001			0.005			0.006	0.007			0.006
744	36:2	78.837	79.696	77.966	78.089	80.253	80.046	79.148	37.405	36.355	75.130	74.930	80.106	82.596	78.190
746	36:1	10.306	9.033	10.419	10.099	9.101	9.778	9.790	3.012	4.144	10.673	10.848	9.192	8.210	9.731
748	36:0	0.404	0.326	0.509	0.515	0.493	0.265	0.419			0.432	0.395	0.439	0.219	0.371
756	37:3	0.037		0.102	0.085		0.019	0.061			0.052	0.045		0.065	0.054
758	37:2	0.668	0.709	0.664	0.573	1.038	1.043	0.783	0.783	0.683	0.677	0.723	1.145	1.041	0.896
760	37:1	0.066	0.166	0.089	0.088		0.113	0.104	0.002	0.015	0.079		0.193	0.139	0.137
770	38:3	0.269	0.279	0.003	0.000			0.138	0.020		0.013	0.015			0.014
772	38:2	0.511	0.478	0.309	0.326	0.176	0.195	0.332	0.025	0.114	0.373	0.273	0.228	0.185	0.265
774	38:1	0.092	0.057	0.010	0.038			0.049			0.036	0.089	0.011		0.045

DD13 α AL _{S-4} / β AL: PC acyl chain lengths															
M/Z	PC	Cells, 28 °C							Chromatophores, 28 °C						
		LD001745	LD001748	LD004342	LD004345	LD004330	LD004333	Mean	LD001751	LD001754	LD004348	LD004351	LD004111	LD004114	Mean
678	28:1	0.239	0.100			0.185		0.175	0.161	0.092	0.147	0.046	0.273	0.107	0.138
688	28:0	0.045	0.026	0.233	0.145	0.217	0.185	0.142	0.029		0.227	0.085	0.471	0.318	0.226
690	29:1	0.092	0.163	0.824	0.408	0.670	0.498	0.442	0.183	0.142	0.888	0.662	0.471	0.504	0.475
692	29:0			0.026		0.187		0.106		0.007	0.042				0.024
704	30:1	0.064	0.033	0.019	0.084	0.266		0.093	0.033	0.037	0.008	0.101	0.108	0.102	0.065
706	30:0	0.071	0.042	0.029	0.123	0.094	0.123	0.080	0.031	0.027	0.149	0.092	0.016	0.043	0.060
718	31:1	0.063	0.072		0.068	0.015		0.055	0.013	0.030	0.075	0.087			0.051
720	31:0	0.134	0.086		0.093	0.021		0.083	0.019	0.025	0.108	0.155		0.013	0.064
730	32:2		0.016	0.008	0.081	0.113	0.182	0.080		0.084	0.159	0.078		0.128	0.112
732	32:1	0.732	0.622	0.140	0.172	0.215	0.142	0.337	0.301	0.272	0.276	0.177	0.359	0.231	0.269
734	32:0	0.311	0.337	0.020	0.129	0.049	0.128	0.162	0.134	0.162	0.165	0.141	0.025	0.150	0.129
744	33:2	0.005	0.046			0.025		0.025	0.007	0.012			0.085	0.046	0.038
746	33:1	2.664	2.574	0.224	0.114	0.016	0.028	0.937	0.552	0.508	0.168	0.080		0.004	0.262
748	33:0	0.112	0.095		0.130			0.112	0.011	0.016	0.046	0.085			0.040
756	34:3				0.234			0.234	0.005	0.015	0.662	0.123	0.168	0.020	0.165
758	34:2	1.548	1.466	2.699	2.296	2.683	2.611	2.217	2.362	2.377	2.314	2.444	3.215	2.437	2.525
760	34:1	8.521	8.697	5.031	4.932	6.619	5.355	6.526	6.454	6.320	4.460	4.826	6.401	5.185	5.608
762	34:0	0.609	0.536	0.512	0.392	0.098	0.113	0.377	0.302	0.359	0.476	0.303	0.297	0.427	0.361
772	35:2	0.367	0.373	0.066	0.324	0.046	0.007	0.197	0.234	0.209	0.140	0.284	0.100	0.057	0.171
774	35:1	0.642	0.723	0.544	0.414	0.486	0.495	0.550	0.326	0.341	0.583	0.443	0.266	0.267	0.371
776	35:0		0.053		0.266		0.037	0.119			0.269	0.155		0.050	0.158
782	36:4					0.014		0.014					0.530	0.078	0.304
784	36:3	0.091	0.112	0.005	0.228	0.128	0.128	0.115			0.040	0.012	0.642	0.141	0.209
786	36:2	69.909	69.608	72.952	74.049	74.007	77.286	72.968	75.505	76.090	76.157	74.525	70.281	76.790	74.891
788	36:1	9.189	9.432	8.227	8.332	8.834	8.048	8.677	8.686	8.496	5.253	7.163	11.978	7.952	8.254
790	36:0	0.336	0.453	0.100	0.450	0.339	0.425	0.351	0.345	0.398	0.286	0.094		0.405	0.306
798	37:3	0.208	0.247	0.075	0.135	0.141	0.143	0.158	0.192	0.166	0.158	0.146	0.148	0.150	0.160
800	37:2	3.237	3.131	6.354	6.002	3.349	2.873	4.158	3.202	3.038	7.114	6.933	2.546	2.782	4.269
802	37:1	0.532	0.499	0.894	1.093	0.239	0.362	0.603	0.480	0.464	0.860	0.755		0.428	0.598
806	38:6					0.097		0.097					0.206	0.004	0.105
810	38:4			0.090	0.142		0.106	0.113	0.002	0.002			0.157	0.162	0.081
812	38:3				0.029	0.002		0.015	0.008	0.008			0.414	0.135	0.141
814	38:2	0.248	0.291	0.191	0.248	0.428	0.350	0.293	0.286	0.286	0.231	0.299	0.375	0.316	0.299
816	38:1			0.169	0.090	0.034	0.155	0.112	0.053	0.047	0.002	0.087	0.057	0.202	0.075
818	38:0		0.044	0.012		0.161	0.006	0.056	0.046	0.029	0.006		0.057	0.167	0.061
826	39:3		0.027					0.027	0.039	0.027	0.090	0.067			0.056
828	39:2	0.014	0.034	0.384	0.181	0.483	0.201	0.216	0.039	0.028		0.270	0.209	0.178	0.145
830	39:1	0.018	0.015	0.028	0.053	0.091	0.008	0.036	0.034	0.029	0.208	0.063	0.031	0.073	0.073
832	39:0			0.185	0.067			0.126	0.016	0.012		0.033	0.010		0.017

DD13 α AL _{S-4} / β AL: PE acyl chain lengths															
M/Z	PE	Cells, 28 °C						Chromatophores, 28 °C							
		LD001746	LD001749	LD004343	LD004346	LD004331	LD004334	Mean	LD001752	LD001755	LD004349	LD004352	LD004112	LD004115	Mean
646	29:2												0.110		0.110
648	29:1				0.291			0.291	0.035	0.038					0.037
650	29:0	1.980	2.690	0.321	0.629			1.405	2.787	2.884	1.657	1.557			2.221
662	30:1		0.069	0.340				0.205	0.630	0.699	0.291	0.640	0.032		0.458
664	30:0	6.043	8.393	2.916	1.598	0.162	0.102	3.202	6.937	6.359	4.419	3.898	0.218	0.284	3.686
676	31:1	0.392	0.853	0.243	0.589			0.519	1.929	1.889	1.308	2.060	0.026		1.443
678	31:0	5.218	6.7191	1.105	1.208		0.119	1.913	5.689	5.484	2.497	2.877		0.027	3.315
688	32:2						0.001	0.001	0.181	0.160			0.080		0.140
690	32:1	1.461	2.012	1.024	1.433	0.497	0.567	1.166	2.623	2.714	4.069	3.175	0.282	0.772	2.273
692	32:0	2.891	3.528	0.929	0.825		0.538	1.742	1.761	1.775	1.079	0.922	0.395	0.357	1.048
700	33:3	0.065	0.055					0.060	0.008						0.008
702	33:2	0.006	0.034					0.020	0.135	0.102					0.119
704	33:1	6.269	7.023	1.126	0.869		0.076	3.073	2.388	2.411	1.920	1.714		0.001	1.687
706	33:0	1.265	1.902					1.584	0.564	0.545		0.047			0.385
712	34:4					0.115		0.115							
716	34:2	1.265	1.088	2.385	2.267	1.587	2.689	1.880	1.776	2.034	2.058	1.870	2.392	2.723	2.142
718	34:1	8.773	8.754	7.500	8.094	7.231	8.514	8.144	8.588	8.242	6.816	6.134	8.231	8.234	7.708
720	34:0	1.923	2.184	0.664	0.828	1.038	0.772	1.235	0.760	0.937	0.665	0.781	0.564	0.870	0.763
730	35:2	0.510	0.631		0.295			0.479	0.232	0.210					0.221
732	35:1	1.122	1.236	0.230	0.367	0.888	0.178	0.670	0.414	0.392	0.434	0.307	0.184	0.160	0.315
734	35:0	0.139	0.108					0.123						0.027	0.027
744	36:2	45.539	37.663	66.694	67.138	73.134	72.841	60.502	50.563	51.153	59.131	60.841	73.207	72.813	61.285
746	36:1	13.043	13.125	11.685	11.039	13.229	11.776	12.316	10.861	10.644	11.254	11.294	11.963	12.610	11.438
748	36:0	1.050	0.864	1.040	0.625	0.850	0.597	0.837	0.363	0.539	0.922	0.025	1.241	0.313	0.567
758	37:2	0.788	0.742	1.730	1.590	0.598	0.816	1.044	0.596	0.634	1.237	1.651	0.746	0.638	0.917
760	37:1	0.161	0.170		0.063	0.263	0.063	0.144	0.077	0.028	0.057	0.207		0.119	0.098
770	38:3					0.042		0.042					0.071		0.071
772	38:2	0.156	0.155	0.040	0.245	0.366	0.262	0.204	0.103	0.112	0.186		0.258	0.052	0.142
774	38:1			0.028				0.058		0.055					0.055

DD13 α WT/ β WT _{-20A} : PC acyl chain lengths												
M/Z	PC	LD002221	LD002223	LD002175	LD002177	LD003015	LD003018	LD002985	LD002988	LD004336	LD004339	Mean
678	28:1	0.339	0.242	0.258	0.171		0.209	0.245	0.160	0.323		0.243
688	28:0	0.174	0.097	0.401		0.196	0.015	0.005		0.329	0.317	0.192
690	29:1	0.959	0.486	2.671	0.263	0.512	0.249	0.382	0.194	1.431	1.041	0.819
692	29:0					0.011		0.078				0.044
704	30:1	0.396	0.205	0.640	0.060	0.080	0.094	0.041		0.175	0.249	0.216
706	30:0	0.230	0.037	0.947	0.011	0.198	0.071	0.015	0.006	0.102	0.125	0.174
720	31:0		0.040	0.167							0.052	0.086
730	32:2	0.177	0.086		0.137	0.020	0.069	0.115	0.077	0.126		0.101
732	32:1	0.637	0.407	1.338	0.161	0.277	0.147	0.261	0.130		0.143	0.389
734	32:0	0.171	0.116	0.098	0.094		0.021	0.036		0.013		0.078
744	33:2	0.104								0.007	0.092	0.067
748	33:0									0.093		0.093
756	34:3				0.005							0.005
758	34:2	3.659	3.433	4.609	3.107	2.333	1.859	2.856	2.315	2.767	2.447	2.939
760	34:1	5.289	5.160	4.165	4.228	2.658	2.637	3.075	2.539	3.448	3.157	3.636
762	34:0	0.256	0.272	0.346	0.158	0.011	0.054	0.122	0.062	0.043	0.003	0.133
772	35:2		0.179	0.199	0.113	0.067	0.018	0.055	0.046	0.156	0.149	0.109
774	35:1	0.378	0.176	0.275	0.195	0.161	0.177	0.121	0.116	0.406	0.259	0.226
776	35:0				0.019	0.071		0.003	0.021	0.007	0.032	0.026
782	36:4		0.471	0.160	0.178			0.031				0.210
784	36:3	0.154	0.351	0.107	0.244	0.149	0.042	0.132	0.096	0.206	0.026	0.151
786	36:2	75.928	76.004	71.124	78.728	81.573	82.254	80.741	83.126	80.332	79.892	78.970
788	36:1	6.135	6.360	6.939	6.810	6.176	5.920	5.519	5.124	3.333	4.860	5.717
790	36:0	0.113	0.334	0.445	0.201	0.175	0.337	0.272	0.203	0.400	0.275	0.275
798	37:3	0.383	0.481	0.260	0.423	0.549	0.588	0.164	0.061	0.396	0.432	0.374
800	37:2	1.941	2.592	2.217	2.510	2.873	2.955	3.670	3.772	4.878	5.230	3.264
802	37:1	0.375	0.417	1.141	0.384	0.255	0.362	0.296	0.296	0.347	0.301	0.417
806	38:6	0.356	0.088		0.014							0.152
808	38:5		0.108		0.023							0.066
810	38:4	0.493	0.473		0.539	0.443	0.403	0.216	0.270	0.359	0.153	0.372
812	38:3	0.248	0.401	0.184	0.370	0.126	0.257	0.872	0.812		0.033	0.367
814	38:2	0.537	0.360	0.350	0.424	0.832	0.918	0.388	0.311		0.360	0.498
816	38:1	0.056	0.151	0.052	0.036	0.032	0.090		0.069			0.069
818	38:0	0.202		0.504			0.016	0.050				0.193
826	39:3				0.051	0.073	0.046					0.057
828	39:2	0.064	0.445	0.176	0.302	0.078	0.195	0.203	0.193	0.090	0.250	0.199

DD13 α WT/ β WT _{-20A} : PE acyl chain lengths												
M/Z	PE	LD002222	LD002224	LD002176	LD002178	LD003016	LD003019	LD002986	LD002989	LD004337	LD004340	Mean
650	29:0					0.055						0.055
662	30:1					0.190	0.130					0.160
664	30:0			0.129		0.826	0.259	0.177	0.087	0.053	0.092	0.232
676	31:1	0.054				0.601	0.127			0.182	0.042	0.201
678	31:0					0.582	0.089			0.305	0.296	0.318
688	32:2	0.293			0.071	0.011			0.123			0.125
690	32:1	0.283	0.251	0.314	0.149	0.746	0.204	0.051	0.040	0.299	0.393	0.273
692	32:0	0.001	0.143		0.001	1.482	0.315	0.141	0.027	0.049	0.199	0.262
700	33:3									0.002		0.002
704	33:1	0.126		0.023		0.050		0.042	0.123		0.015	0.063
706	33:0					0.092				0.152		0.122
712	34:4									0.012		0.012
714	34:3						0.032					0.032
716	34:2	1.899	1.971	1.698	2.079	1.608	1.816	1.836	1.896	3.257	2.282	2.034
718	34:1	5.407	5.890	7.866	6.032	3.011	3.591	4.488	3.560	6.116	5.683	5.165
720	34:0	0.768	0.542	0.295	0.442	0.084	0.050	0.422	0.132	0.346	0.435	0.352
730	35:2	0.015		0.340	0.062	0.016	0.103					0.107
732	35:1	0.242	0.148		0.141	0.356	0.198			0.092	0.354	0.219
734	35:0					0.051						0.051
744	36:2	78.700	79.151	76.213	79.239	78.142	82.642	82.270	84.349	78.981	77.159	79.685
746	36:1	11.044	10.663	10.122	10.009	9.472	8.293	9.419	8.171	7.196	10.424	9.481
748	36:0	0.347		0.235	0.375		0.341	0.151	0.451	1.138	0.394	0.429
756	37:3	0.012	0.017		0.028		0.053				0.089	0.040
758	37:2	0.409	0.774	1.233	0.888	0.813	0.755	0.857	0.815	1.312	1.669	0.952
760	37:1	0.011	0.075	0.662	0.042	0.042	0.037	0.131	0.003		0.024	0.114
770	38:3	0.076	0.068		0.021	0.057						0.055
772	38:2	0.194	0.285	0.252	0.418	1.323	0.905	0.238	0.224	0.332	0.263	0.443
774	38:1	0.064	0.023		0.003	0.121	0.059				0.143	0.069

APPENDIX 4

DD13: PC acyl chain lengths						
M/Z	PC	LD000690	LD000692	LD001721	LD001724	Mean
678	28:0	0.941	0.523	0.254	0.119	0.459
688		0.200	0.303	0.127	0.063	0.173
690	29:1	0.088		0.508	0.267	0.288
692	29:0			0.010		0.010
704	30:1	0.088	0.065	0.066	0.040	0.065
706	30:0			0.051	0.024	0.038
720	31:0	0.025		0.001	0.009	0.011
730	32:2	0.142	0.139	0.162	0.204	0.162
732	32:1	0.344	0.300	0.284	0.213	0.285
734	32:0	0.199	0.179	0.108	0.073	0.140
746	33:1	0.023		0.008	0.010	0.014
748	33:0	0.091				0.091
756	34:3			0.103	0.012	0.058
758	34:2	2.752	2.991	2.992	2.706	2.860
760	34:1	7.149	7.230	4.645	4.601	5.906
762	34:0	0.477	0.356	0.120	0.170	0.281
772	35:2	0.057	0.060	0.072	0.086	0.069
774	35:1	0.483	0.424	0.172	0.174	0.313
776	35:0	0.040	0.076		0.011	0.042
782	36:4			0.208		0.208
784	36:3	0.009		0.115	0.089	0.071
786	36:2	74.052	74.662	78.923	80.308	76.986
788	36:1	8.936	8.332	6.475	6.407	7.538
790	36:0	0.200	0.360	0.252	0.288	0.275
798	37:3	0.010	0.088	0.247	0.232	0.144
800	37:2	2.935	2.857	2.920	2.807	2.880
802	37:1	0.260	0.2713	0.426	0.387	0.358
810	38:4	0.021	0.072		0.135	0.076
812	38:3	0.314	0.427	0.029	0.025	0.199
814	38:2	0.072	0.199	0.332	0.302	0.226
816	38:1	0.074	0.042	0.051	0.055	0.056
818	38:0		0.015	0.017	0.022	0.018
828	39:2			0.088	0.111	0.100
830	39:1			0.082	0.019	0.051
832	39:0	0.019	0.030			0.024

DD13: PE acyl chain lengths						
M/Z	PE	LD000689	LD000691	LD001859	LD001861	Mean
648	29:1	0.044				0.044
660	30:2	0.016				0.016
664	30:0	0.346	0.852	0.050		0.416
676	31:1	0.388	0.455			0.422
688	32:2	0.030	0.049	0.105	0.137	0.080
690	32:1	0.085	0.217	0.267	0.207	0.194
692	32:0			0.266	0.242	0.254
700	33:3	0.517	0.481			0.499
702	33:2		0.050			0.050
704	33:1	0.156	0.410	0.019		0.195
706	33:0		0.040			0.040
712	34:4	0.231	0.260			0.245
714	34:3	0.237	0.337			0.287
716	34:2	2.871	2.495	2.521	2.532	2.605
718	34:1	7.547	6.635	7.195	6.981	7.090
720	34:0	0.744	0.904	0.400	0.402	0.612
730	35:2		0.051	0.030	0.061	0.048
732	35:1	0.975	0.317	0.207	0.199	0.424
734	35:0			0.010		0.010
744	36:2	75.316	75.004	77.328	78.092	76.435
746	36:1	10.321	11.106	9.957	9.616	10.250
748	36:0	0.652	0.335	0.502	0.237	0.431
758	37:2	0.463	0.565	0.700	0.819	0.637
760	37:1	0.128	0.026	0.093	0.101	0.087
770	38:3	0.058	0.021	0.023	0.021	0.031
772	38:2	0.134	0.022	0.221	0.246	0.156
774	38:1	0.013		0.026	0.018	0.019

DG2 WT: PC acyl chain lengths											
M/Z	PC	Cells, 28 °C					Chromatophores, 28 °C				
		LD002242	LD002244	LD002704	LD002707	Mean	LD002246	LD002248	LD002710	LD002713	Mean
678	28:1	0.372	0.268		0.063	0.234	0.468	0.215	0.309	0.153	0.286
690	29:1	0.706	0.461	0.250	0.100	0.379	0.379	0.360	0.496	0.095	0.332
692	29:0	0.041	0.041	0.036	0.023	0.035	0.041	0.039	0.018	0.031	0.032
704	30:1	0.179	0.191	0.006	0.014	0.098	0.170	0.158	0.078	0.016	0.106
706	30:0	0.124	0.133	0.034		0.097	0.121	0.115	0.002		0.079
718	31:1	0.118	0.086			0.102	0.102	0.057			0.080
720	31:0	0.092	0.060	0.094		0.082	0.055	0.041			0.048
730	32:2	0.099	0.096	0.038	0.083	0.234	0.163	0.059	0.050	0.091	0.091
732	32:1	0.325	0.286	0.166	0.066	0.211	0.386	0.274	0.267	0.129	0.264
734	32:0	0.138	0.216		0.013	0.122	0.471	0.227			0.349
744	33:2	0.034	0.082			0.058	0.043	0.049			0.046
746	33:1	0.172	0.089		0.009	0.090	0.137	0.111			0.124
748	33:0	0.071	0.049			0.060	0.053	0.045			0.049
756	34:3	0.060	0.031	0.013		0.035	0.090	0.053			0.071
758	34:2	2.423	2.406	2.668	2.461	2.489	2.643	2.204	2.182	2.113	2.286
760	34:1	6.224	7.303	3.890	3.486	5.226	6.589	7.074	3.781	3.373	5.204
762	34:0	0.235	0.352	0.155	0.106	0.212	0.314	0.414		0.167	0.298
772	35:2	0.264	0.183	0.455	0.196	0.274	0.225	0.186	0.249	0.162	0.286
774	35:1	0.549	0.432	0.793	0.149	0.481	0.882	0.746	0.206	0.151	0.496
776	35:0	0.130				0.130			0.061		0.061
784	36:3			0.045	0.128	0.086			0.039	0.028	0.033
786	36:2	74.545	73.753	80.084	81.205	77.397	71.309	71.776	80.643	81.887	76.404
788	36:1	7.603	8.279	4.918	5.120	6.480	9.220	8.855	4.631	4.985	6.923
790	36:0	0.231	0.184	0.376	0.423	0.303	0.115	0.298	0.433	0.290	0.284
798	37:3	0.463	0.679	0.435	0.455	0.508	0.301	0.178	0.581	0.636	0.424
800	37:2	2.793	3.079	3.211	3.329	3.103	3.385	3.864	3.282	3.159	3.423
802	37:1	0.489	0.256	0.350	0.344	0.360	0.316	0.522	0.348	0.216	0.350
810	38:4	0.892	0.712	0.433	0.599	0.659	0.665	0.621	0.345	0.564	0.549
812	38:3	0.288	0.156	0.570	0.677	0.423	0.353	0.274	0.313	0.286	0.306
814	38:2	0.299	0.326	0.412	0.453	0.372	0.534	0.408	0.466	0.419	0.457
816	38:1	0.076	0.089	0.017		0.061	0.169	0.087		0.013	0.090
818	38:0		0.113	0.012		0.062	0.157	0.109			0.133
826	39:3	0.218	0.309	0.004	0.037	0.142	0.209	0.247	0.073	0.111	0.160
828	39:2	0.733	0.174	0.529	0.428	0.466	1.030	0.976	1.132	0.851	0.997
830	39:1	0.210	0.120	0.101	0.006	0.109	0.039	0.129		0.054	0.074
832	39:0	0.208	0.099			0.153	0.201	0.037	0.046		0.095

DG2 WT: PE acyl chain lengths											
M/Z	PE	Cells, 28 °C					Chromatophores, 28 °C				
		LD002243	LD002245	LD002705	LD002708	Mean	LD002247	LD002249	LD002711	LD002714	Mean
688	32:2				0.088	0.088					0.000
690	32:1	0.380	0.202			0.291	0.556	0.568			0.562
692	32:0	0.538	0.326			0.432	0.912	0.676	0.035	0.053	0.419
704	33:1		0.166			0.166					0.000
716	34:2	2.825	2.018	1.609	2.109	2.140	1.753	1.912	2.155	2.009	1.957
718	34:1	9.362	8.021	4.637	5.161	6.795	10.926	10.138	4.597	4.472	7.533
720	34:0	0.954	0.364	0.537	0.232	0.521	1.347	1.246	0.317	0.111	0.755
730	35:2	0.252	0.112			0.182	0.076	0.063		0.011	0.050
732	35:1	1.114	0.482	0.087	0.106	0.447	0.860	1.340		0.045	0.748
734	35:0					0.000	0.123				0.123
744	36:2	72.115	76.280	83.852	82.750	78.749	68.062	70.319	82.359	84.079	76.205
746	36:1	9.458	9.446	7.153	7.483	8.385	12.728	11.522	8.183	7.762	10.049
748	36:0	0.725	0.578	0.015	0.456	0.443	0.300	0.388	0.507		0.398
756	37:3	0.114	0.081	0.071		0.089			0.099		0.099
758	37:2	1.068	1.082	1.265	1.133	1.137	1.577	1.323	1.081	1.018	1.250
760	37:1		0.032	0.066	0.166	0.088	0.060	0.054	0.002	0.015	0.033
770	38:3	0.071		0.075		0.073					0.000
772	38:2	1.026	0.811	0.513	0.349	0.675	0.565	0.442	0.425	0.174	0.401
774	38:1					0.000	0.095	0.025			0.060

APPENDIX 4

DG2 α WT/ β WT _{-20A} : PC acyl chain lengths						
M/Z	PC	LD002233	LD002236	LD004186	LD004189	Mean
678	28:1	0.264	0.191		0.191	0.215
688	28:0	0.279	0.382			0.331
690	29:1	1.114	0.841	0.766	0.350	0.768
692	29:0	0.324			0.010	0.167
704	30:1	0.312	0.044	0.010		0.122
706	30:0	0.081	0.104			0.092
732	32:1	0.016	0.254	0.069	0.183	0.130
734	32:0	0.129	0.100	0.039	0.020	0.072
744	33:2		0.011	0.140	0.373	0.175
746	33:1	0.258	0.317	0.069		0.215
748	33:0	0.171	0.077	0.039	0.116	0.101
756	34:3	0.024		0.006		0.015
758	34:2	4.356	2.639	2.363	2.027	2.846
760	34:1	5.548	4.801	2.930	4.109	4.347
762	34:0		0.426	0.889	0.403	0.572
772	35:2	3.444	3.693	2.657	2.981	3.194
774	35:1	6.590	6.806	7.523	5.936	6.714
776	35:0	0.218		0.307	0.251	0.258
782	36:4	0.027	0.034			0.031
784	36:3	0.146	0.157	0.055		0.119
786	36:2	57.731	62.159	57.369	66.725	60.996
788	36:1	5.588	4.727	11.189	3.862	6.341
790	36:0	0.549	0.082	0.236	0.158	0.256
798	37:3	0.210	0.480	0.927	1.323	0.735
800	37:2	7.009	7.008	7.158	7.944	7.280
802	37:1	0.800	0.988	2.207	1.003	1.249
806	38:6	0.058				0.058
808	38:5			0.025	0.027	0.026
810	38:4	1.679	1.322	0.930	0.637	1.142
812	38:3	0.869	0.315	0.450	0.150	0.446
814	38:2	0.237	0.476	0.355	0.235	0.326
816	38:1	0.091	0.203	0.281	0.274	0.212
818	38:0	0.197		0.056		0.215
826	39:3	0.285	0.126			0.205
828	39:2	1.398	1.238	0.620	0.005	0.815
830	39:1				0.003	0.003

DG2 α WT/ β WT _{.20A} : PE acyl chain lengths						
M/Z	PE	LD002234	LD002237	LD004187	LD004190	Mean
664	30:0			0.451		0.451
690	32:1		0.180			0.180
692	32:0	0.008	0.192	0.287	0.195	0.171
704	33:1	0.259	0.462	1.082	0.668	0.618
706	33:0	0.174	0.207	0.336	0.610	0.332
716	34:2	2.607	1.468	2.064	2.086	2.056
718	34:1	6.972	7.310	5.691	6.880	6.713
720	34:0	0.562	0.963	2.242	1.283	1.262
730	35:2	1.808	2.567	2.546	2.980	2.476
732	35:1	7.989	9.242	14.087	12.499	10.954
734	35:0	0.450		1.087	0.571	0.703
744	36:2	69.925	65.822	56.872	59.424	63.010
746	36:1	4.518	7.333	8.849	8.546	7.312
748	36:0	0.406	0.384	1.164	0.429	0.596
756	37:3	0.307	0.153	0.164	0.210	0.208
758	37:2	3.356	3.006	1.815	2.971	2.787
760	37:1	0.396	0.330	1.192	0.648	0.641
772	38:2	0.179	0.381			0.280
774	38:1	0.084				0.084

LH2 WT in micelles: PC acyl chain lengths								
M/Z	PC	LD002133	LD002135	LD003991	LD003994	LD003997	LD004000	Mean
678	28:0	0.609		1.429	0.229			0.756
690	29:1			4.267		1.098	1.092	2.152
692	29:0		0.008			0.058		0.033
704	30:1		0.189					0.189
706	30:0		0.556	2.943		0.234		1.244
732	32:1					0.321		0.321
734	32:0			0.352	0.658			0.505
758	34:2	8.602	8.484	2.998	3.482		1.371	4.987
760	34:1	0.618	4.693	9.721	11.694	4.853	6.574	6.359
772	35:2						0.264	0.264
774	35:1			4.165		2.858	1.667	2.897
776	35:0	1.192						1.192
786	36:2	79.965	75.525	54.131	55.584	55.675	54.066	62.491
788	36:1	4.949	2.520	9.207	13.915	19.418	19.746	11.626
790	36:0		0.370	3.363			0.811	1.515
798	37:3				1.832		0.257	1.044
800	37:2	3.022	6.531	6.170	5.970	11.961	5.900	6.592
802	37:1	0.265		0.110	3.873	0.396	1.406	1.210
810	38:4					0.741		0.741
812	38:3				0.742	0.348	2.111	1.067
814	38:2	0.778	1.124		0.596		1.846	1.086
816	38:1			0.794				0.794
818	38:0			0.353				0.353
828	39:2				0.061			0.061

LH2 WT micelles: PE acyl chain lengths								
M/Z	PE	LD002134	LD002136	LD003992	LD003995	LD003998	LD004001	Mean
664	30:0			1.120				1.120
678	31:0						1.834	1.834
688	32:2				0.054			0.054
692	32:0				1.885			1.885
700	33:3	1.087						1.087
716	34:2	0.649	2.251	5.628	0.088	0.536		1.830
718	34:1	8.577	2.102	7.058	7.961	8.757	6.576	7.786
720	34:0			3.437	4.603	1.217	4.375	3.408
730	35:2						2.216	2.216
732	35:1			2.073	0.564	1.111	1.619	1.342
734	35:0				0.263			0.263
744	36:2	67.778	81.494	56.313	48.823	50.017	49.761	59.031
746	36:1	13.455	13.409	13.221	10.336	12.190	13.553	12.694
748	36:0	1.335	1.833	2.722	0.802	0.508	5.659	2.143
756	37:3						0.174	0.174
758	37:2	6.961		4.772	1.678	1.137	4.056	3.721
774	38:1	1.495		2.321			0.178	1.331

DD13 α WT/ β WT _{-20A} in micelles: PE acyl chain lengths						
M/Z	PE	LD002887	LD002890	LD003122	LD003131	Mean
700	33:3				2.039	2.039
702	33:2			2.663		2.663
716	34:2		1.023	0.300		0.662
718	34:1	2.084	5.080	7.575	4.163	4.725
732	35:1		0.283	0.879		0.581
744	36:2	71.165	75.032	67.946	70.867	71.252
746	36:1	18.102	14.898	16.752	14.245	15.999
758	37:2			0.609	3.690	2.149

DD13 WT cells: temperature experiment (PC)									
M/Z	PC	28 °C, 28 hour		30 °C, 39 hour		32 °C, 49 hour		34 °C, 27 hour	
678	28:1	0.100	0.104	0.644	1.146	0.673	0.372	0.379	0.204
688	29:2				0.078	1.651	0.275	0.163	0.088
690	29:1	0.594	0.228	0.058	0.147	0.196	0.066	0.307	0.175
692	29:0		0.005	0.061	0.057	0.118	0.078	0.062	0.089
704	30:1	0.110	0.042	0.088	0.214	0.253	0.131	0.095	0.094
706	30:0	0.024		0.063	0.136	0.072	0.067	0.064	0.044
718	31:1			0.027	0.081	0.228	0.137	0.060	0.024
720	31:0	0.013		0.099	0.141	0.220	0.158	0.040	0.029
730	32:2	0.020	0.090	0.074	0.214	0.373	0.173	0.278	0.239
732	32:1	0.301	0.135	0.221	0.156	0.336	0.409	0.400	0.256
734	32:0	0.092		0.140	0.109	0.371	0.194	0.263	0.151
744	33:2			0.002	0.059	0.220	0.069	0.023	0.024
746	33:1			0.099	0.058	0.710	1.188	0.085	0.029
748	33:0			0.144	0.102	0.269	0.031	0.051	0.026
758	34:2	3.113	3.539	2.286	2.288	3.349	3.056	2.565	2.618
760	34:1	3.720	2.990	3.488	3.395	4.686	4.105	6.890	7.014
762	34:0	0.109	0.095		0.119		0.259	0.289	0.315
772	35:2	0.086	0.127	0.115	0.131	0.032	0.387	0.809	0.436
774	35:1	0.279	0.177	0.356	0.238	0.399	0.454	0.341	0.394
780	36:5	0.088						0.103	0.007
782	36:4	0.069	0.050					0.069	0.005
784	36:3	0.055	0.069					0.123	0.163
786	36:2	78.661	81.040	81.117	80.505	74.905	77.381	74.441	75.338
788	36:1	6.008	5.755	5.794	6.878	6.388	5.417	8.946	8.744
790	36:0	0.162	0.205	0.546	0.118	0.387	0.344	0.250	0.326
798	37:3	0.353	0.345	0.480	0.377			0.300	0.302
800	37:2	3.530	3.351	3.007	2.742	4.938	4.444	2.004	1.790
802	37:1	0.351	0.238	0.402		0.570	0.562	0.467	0.405
806	38:6	0.350						0.014	0.019
810	38:4	0.767	0.310					0.257	0.201
812	38:3	0.151	0.111					0.450	0.460
814	38:2	0.406	0.398	0.504	0.545	0.811	0.257	0.490	0.391
816	38:1	0.111	0.030					0.145	0.094
818	38:0		0.003					0.105	0.051
826	39:3		0.069					0.080	0.033
828	39:2	0.253	0.267					0.181	0.167
830	39:1	0.057						0.056	0.040
832	39:0		0.002					0.085	0.060

APPENDIX 4

DD13 WT cells: temperature experiment (PE)									
M/Z	PE	28 °C, 28 hour		30 °C, 39 hour		32 °C, 49 hour		34 °C, 27 hour	
648	29:1			0.019	0.151	0.029	0.023		
662	30:1			0.032	0.025	0.052	0.057		
688	32:2	0.010	0.150	0.141	0.235	0.183	0.285		0.071
690	32:1	0.201	0.054	0.143	0.197	0.380	0.279	0.148	0.223
692	32:0	0.069	0.076	0.355	0.319	0.437	0.501	0.315	0.399
706	33:0					0.014	0.028		
716	34:2	2.703	2.254	2.167	1.982	2.523	2.963	2.094	2.101
718	34:1	5.572	5.412	6.304	5.993	7.684	8.302	10.463	10.132
720	34:0	0.124	0.355	0.655	1.736	0.885	0.731	0.617	0.892
730	35:2			0.134	0.019	0.086	0.101		
732	35:1	0.246	0.241	0.273	0.450	0.184	0.263	0.388	0.335
734	35:0					0.028	0.022		
744	36:2	80.253	80.046	79.023	77.386	75.338	74.584	72.302	72.094
746	36:1	9.101	9.778	9.306	10.033	10.337	10.071	12.327	12.205
748	36:0	0.493	0.265	0.446	0.379	0.522	0.528	0.331	0.547
756	37:3		0.019	0.037		0.118	0.107		0.004
758	37:2	1.038	1.043	0.729	0.782	0.676	0.586	0.710	0.604
760	37:1		0.113						0.090
770	38:3					0.014	0.014		0.010
772	38:2	0.176	0.195	0.573	0.544	0.320	0.338	0.305	0.290
774	38:1			0.092	0.057	0.021	0.051		0.004

CURRICULUM VITAE

Personal data

Family name: Kwa
First name: Lee Gyan
Home address: 5499C Limbongan 75200 Melaka, Malaysia
Date of birth: 30.12.1975

Education

Jan 2002- Mar 2007 Post-graduate study in the Ludwig-Maximilians-University, Department of Biology I, Botanic, Munich, Germany

Oct 1998- Jul 1999 Master degree in Agricultural Development, University of Reading, United Kingdom

Sept 1995- Jul 1998 Bachelor of Science (Honours) in Biotechnology and Microbiology, University of Sheffield, United Kingdom

1989-1994 Secondary School, Melaka, Malaysia

Publications

Kwa L.G., Garcia-Martin A., Vegh A.P., Strohmann B., Robert B., Braun P. (2004) Hydrogen bonding in a model bacteriochlorophyll-binding site drives assembly of light-harvesting complex. *J. Biol. Chem.* 279, 15067-15075.

Braun P., Gebhardt R., Kwa L.G., Doster W. (2005) High pressure near infrared study of mutated light-harvesting complex 2. *Braz. J. Med. Biol. Res.* 38, 1273-1278.

Garcia-Martin A., Kwa L.G., Strohmann B., Robert B., Holzwarth A.R., Braun P. (2006) Structural role of (bacterio)chlorophyll ligated in the energetically unfavourable β -position. *J. Biol. Chem.* 281, 10626-10634.

Garcia-Martin A., Kwa L.G., von Jan M., Hunter N.C., Braun P. (2006) Assembly of model bacteriochlorophyll proteins in the native lipid environment. In *Chlorophylls and Bacteriochlorophylls: Biochemistry, Biophysics, Functions and Applications*, Vol. 25, (Grimm B., Porra R.J., Rüdiger W., Scheer H. Eds.), pp 387-396. Springer, Dordrecht, The Netherlands.

Kwa L.G., Wegmann D., Brügger B., Wanner G., Braun P. Mutation of a single residue, glutamate β 10, alters protein-lipid interactions of light-harvesting complex 2. In preparation.

Eidesstattliche Erklärung

Hiermit versichere ich, dass ich die vorliegende Arbeit selbständig verfasst und nur unter Verwendung der angegebenen Hilfsmittel und Quellen angefertigt habe. Ich versichere ferner, dass ich die vorliegende Arbeit nicht schon als Doktor-, Magister- oder Diplomarbeit bei einer anderen Hochschule eingereicht habe.

München, 2007

Lee Gyan KWA